THE UNIVERSITY OF QUEENSLAND

AUSTRALIA

Manufacture and Characterisation of Short Fibre Biocomposites

Angelica Maëlle Delphine LEGRAS

M. Sc.

A thesis submitted for the degree of Doctor of Philosophy at

The University of Queensland in 2016

School of Mechanical and Mining Engineering

Abstract

In response to environmental concerns, the composites industry is showing a growing interest in natural fibre biocomposites as an alternative to wood plastic composites and glass fibre thermoplastics. Albeit many years of research, the potential of these new materials has not being reached and the properties obtained are too often lower than expected. A main reason for this is because the natural fibre properties are variable and poorly characterised, and inefficient traceability makes it difficult to grade the fibres. When it comes to biocomposite manufacturing, short plant fibre composites have attracted the interest of the thermoplastic compounding industry but only a few companies have mastered the compounding step. Too often, the extruder is treated as a "black box" and the critical processing parameters have not yet been identified. As a result, the full potential of extrusion process for biocomposites is not exhausted.

This research aimed to generate a better understanding of bast fibre surfaces, their interaction with the matrix and to optimise the extrusion process for short fibre biocomposites. New generation in-lens Scanning Electron Microscopy (SEM) and X-ray Photoelectron Spectroscopy (XPS) provided quantitative information of the first ten nanometres of the fibre surface with high precision, and Inverse Gas Chromatography (IGC) enabled the determination of natural fibre surface energy. Combined, XPS, in-lens SEM and IGC offered a unique complementarity to unravel natural fibre surface properties. In particular, the results achieved provided key complementary information about the nature of the chemical groups present at the fibre surface and showed clear evidence of the effect of fibre treatment on the surface properties. Field retting and water washing were insufficient to remove lignins, pectins and waxes from flax and kenaf fibre surface. Alkaline treated fibres had a cleaner but rough surface still partially covered with an amorphous layer rich in lignins and waxes. Surface energy profiles obtained by IGC also revealed a change in polarity and the distribution of the energetic active sites post treatment. In addition, the critical parameters to determine the BET surface area values with IGC were identified and a protocol applicable to natural fibres was proposed.

The series of extrusion trials brought new insights into the feasibility of large scale biocomposite extrusion. Statistical analysis showed a significant interdependence between all factors and particularly between the screw speed and the screw design. At both laboratory scale and

medium scale, fibre content was the dominant factor for the tensile strength and elastic modulus whilst screw speed and screw design affected to a lower degree the tensile properties. The fibre surface properties and fibre length distribution were also determinant for the biocomposite properties. For instance, the alkaline treated fibre reinforced polypropylene composites underperformed compared to the water washed fibre polypropylene composites although the former had a surface more energetically homogeneous and less polar. It is assumed that the higher fibre aspect ratio of the water washed fibres and their homogeneous fibre length distribution largely contributed to increase the composite performance.

Finally, extrusion at industrial scale has been successfully performed and represents a major achievement of the thesis. However, significant amount of porosity was noticed in the extruded samples throughout the trials and further work is required to overcome this issue. Whilst the porosity detected in the samples questions the industrial-usefulness of some of the results, the contribution of this thesis to the development of natural fibre compounding capability at The University of Queensland and collaborating local industries was immense. The methodology and the lessons learned will undoubtedly be used to further optimise the extrusion process and produce better biocomposite materials.

Declaration by author

This thesis is composed of my original work, and contains no material previously published or written by another person except where due reference has been made in the text. I have clearly stated the contribution by others to jointly-authored works that I have included in my thesis.

I have clearly stated the contribution of others to my thesis as a whole, including statistical assistance, survey design, data analysis, significant technical procedures, professional editorial advice, and any other original research work used or reported in my thesis. The content of my thesis is the result of work I have carried out since the commencement of my research higher degree candidature and does not include a substantial part of work that has been submitted to qualify for the award of any other degree or diploma in any university or other tertiary institution. I have clearly stated which parts of my thesis, if any, have been submitted to qualify for another award.

I acknowledge that an electronic copy of my thesis must be lodged with the University Library and, subject to the policy and procedures of The University of Queensland, the thesis be made available for research and study in accordance with the Copyright Act 1968 unless a period of embargo has been approved by the Dean of the Graduate School.

I acknowledge that copyright of all material contained in my thesis resides with the copyright holder(s) of that material. Where appropriate I have obtained copyright permission from the copyright holder to reproduce material in this thesis.

Publications during candidature

Journal Paper

1. A. Legras, A. Kondor, M. T. Heitzmann and R. W. Truss, *Inverse gas chromatography for natural fibre characterisation: Identification of the critical parameters to determine the Brunauer–Emmett–Teller specific surface area*, Journal of Chromatography A 1425 (2015): 273-279.

Peer-reviewed Conference Papers

1. A. Legras, R. W. Truss, C. Chaleat and M. T. Heitzmann, *A practical toolbox to overcome the multiple challenges of biocomposites extrusion*, Australasian Composites Conference, 2015, Gold Coast, Australia.

2. A. Legras, R. W. Truss, S. Rao, D. Bhattacharyya, N. Soatthiyanon, A. Crosky and M. T. Heitzmann, *Optimisation of the twin-screw compounding process for short fibre biocomposites*, Australasian Composites Conference, 2014, Newcastle, Australia.

3. M. T. Heitzmann, A. M. Ali, A. Legras, L. J. Vandi and J. Milne, *Hemp hurd flour as an alternative low cost filler in wood plastic composites*, Second International Conference on Performance-based and Life-cycle Structural Engineering, 2015, Brisbane, Australia.

Publications included in this thesis

1. A. Legras, A. Kondor, M. T. Heitzmann and R. W. Truss, *Inverse gas chromatography for natural fibre characterisation: Identification of the critical parameters to determine the Brunauer–Emmett–Teller specific surface area*, Journal of Chromatography A 1425 (2015): 273-279 - incorporated in Chapter 4 as Section 4.1.

Contributor	Statement of contribution
A. Legras	Designed experiments (100%) Wrote the paper (100%)
A. Kondor	Edited paper (30%)
M. T. Heitzmann	Edited paper (10%)
R. W. Truss	Edited paper (60%)

Contributions by others to the thesis

Chapter 3

Ron Rasch (Centre for Microscopy & Microanalysis, The University of Queensland) performed the Scanning Electron Microscopy analysis which led to the results presented in Section 3.2.

Dr. Barry Wood (Centre for Microscopy & Microanalysis, The University of Queensland) performed the X-Ray Photoelectron Spectroscopy measurements and significantly contributed to the interpretation of the high resolution spectra presented in Section 3.3.

Chapter 4

Dr. Anett Kondor (Surface Measurement Systems) provided guidance in Inverse Gas Chromatography and assisted in interpreting the data presented in Section 4.1 and 4.2.

Chapter 5

Mercedes Alcock (Composites Innovation Centre) did the Single Fibre Tensile Testing and provided the raw data, which led to the tensile properties shown in Figure 5.6.

Dr. Celine Chaleat, John Milne (Centre for High Performance Polymers, The University of Queensland) and Dr. Michael T. Heitzmann (Composites Group, The University of Queensland) largely contributed in performing the series of extrusion trials and injection moulding presented in Section 5.3 and 5.5.

Dr. Lin-P'ing Choo-Smith (Composites Innovation Centre) performed the X-Ray Diffraction analysis presented in Section 5.3 and significantly contributed to the data interpretation.

Dr. Hayder Salem (The University of British Columbia) performed the fibre dimensional analysis with the Fibre Quality Analyser, which led to the fibre length distribution profiles presented in Section 5.3.

Dr. Chad Ulven (North Dakota State University) organised Micro Computed Tomography of extruded compounds shown in Figure 5.15 and Figure 5.11.

Dr. Luigi J. Vandi (Composites Group, The University of Queensland) organised the Thermogravimetric Analysis presented in Section 5.3 and assisted with the data interpretation.

Benjamin Ziegelaar (undergraduate student, The University of Queensland) assisted in the laboratory scale extrusion trials described in Section 5.2.

Statement of parts of the thesis submitted to qualify for the award of another degree

None.

Acknowledgements

To the Cooperative Research Centre for Advanced Composite Structures (CRC-ACS) and The University of Queensland for funding my research and giving me the opportunity to travel within Australia and to North America for experimental work and conferences.

To Rowan W. Truss, my Principal Advisor, for your guidance and often thought provoking feedback which guided me in my research and led me down to the right path. Your experience and knowledge enabled us to bring new perspectives into the field and I really enjoyed our endless debates on the complexity of *natural fibres*. Thank you for supporting me and encouraging me all the way along. You helped me bringing this journey to the finish line and I am deeply grateful for your advice and patience in the process.

To Michael T. Heitzmann, my mentor and Scientific Advisor, for your guidance and inspiration throughout. This biocomposite success story would not be, without your unfailing motivation and creativity. You taught me a lot and showed me new perspectives. You also gave me the opportunity to extend this journey beyond Australia and offered me one of the greatest challenge of these years; a ticket to Winnipeg. Thank you Michael, it has been a pleasure to work with you and I am looking forward to further collaboration in the future.

To the FibreCITY team, Lin-P'ing Choo-Smith, Mercedes Alcock, Jennifer Bell, Frank Wheeler, Simon Potter, Sean McKay and Co. from the Composites Innovation Centre in Winnipeg, and to Anett Kondor from Surface Measurement Systems. I am indebted for your warm welcome and generous assistance in the research on Inverse Gas Chromatography. Winnipeg has been a unique adventure that opened new opportunities beyond the PhD.

To the colleagues from the Centre for High Performance Polymers, Celine Chaleat and John Milne who helped me in designing many of the extrusion trials in the laboratory. Thanks for your time and guidance, the much of the success of biocomposite extrusion is attributable to your assistance. Acknowledgements and thanks also go to the colleagues from Eagle Farm, Lance McGarva and Doug Holliday and to the CRC-ACS P1.1 team, especially the fellows from the University of Auckland and from the University of New South Wales.

To Ron Rasch and Dr. Barry Wood (Centre for Microscopy and Microanalysis, The University of Queensland), for your expertise and all the time you dedicated to my experimental work on the surface characterisation.

To the UQ Composites Group, Martin Veidt, Amandeep Virk, Luigi, Philippe, Simon, Hannes, Mitch and Co. It was a pleasure to work with you in such a nice atmosphere. Thanks for your advice and, most of all, thank you for the positive energy you all brought to the team.

To my extended family, alias all the UQ fellows that shared with me many hours in this amazing campus. Special dedication to Mingyuan, Jenny, Liliana, Maria Clara, Mauricio, Hugh, Sandeep, Simon, Alex. We shared much more than scientific discussions and for sure our paths will cross again in the future. You were the best adopted family one could imagine and I cannot fully express here how much you gave me.

To my housemates Fred and Hayley, it was a pleasure to reach home everyday and find these two happy faces. Thank you for making every day a great one, thank you for your patience, help and advice in this Australian journey. Cricket101 was an appetizer to the Australian life, we have more to share in the future.

To the EEIGM family, Pauline, Elise, Lucie, Stephane, Jo., Maxime and Co. Thank you for your support, your respective journeys have been enriching and motivating.

To the French community, in particular the Pisasale family, Vanessa & Chris and Nathalie & Luigi. You took me under your wings when I landed in Brisbane and you have always been there to help me. Thank you for your kindness and support.

To *Sensei* Sinn Chew and all the karate mates, you taught me more than Okinawa Goju-Ryu Karate. In the Dojo I found respect, relief and a place to breath away. I am looking forward the next Katas and sparring sessions. See you on the Dojo.

To *el Argentino*, Juan Pablo, you were the best "collateral damage" of this journey... Thank you for your encouragement and ongoing support beyond the borders, especially during thesis writing. Your happiness and philosophy of life inspire me, you took my breath away. I am ready for our next challenge, see you there.

Finally, and above all, thanks to my family for their endless support all these years. Beyond Spain, Sweden, Germany and Australia, you have always been there for me. I am immensely grateful for all the love and encouragement you have given me.

This thesis was accomplished with the important life ingredients you have all instilled in me,

Thank You.

Keywords

natural fibres, biocomposites, surface analysis, inverse gas chromatography, extrusion, compounding

Australian and New Zealand Standard Research Classifications (ANZSRC)

ANZSRC code: 091202, Composite and Hybrid Materials, 100%

Fields of Research (FoR) Classification

FoR code: 0912, Materials Engineering, 100%

Science is a way of thinking much more than it is a body of knowledge.

C. Sagan

Contents

List of Figures

List of Tables

Abbreviations

AB	**A**cid **B**ase
AFM	**A**tomic **F**orce **M**icroscopy
ANOVA	**AN**alysis **O**f **VA**riance
ASTM	**A**merican **S**ociety for **T**esting and **M**aterials
BE	**B**inding **E**nergy
BCA	**B**uilding **C**ode of **A**ustralia
BET	**B**runauer **E**mmett **T**eller
BSE	**B**ack **S**catter **E**lectron
CACM	**C**entre for **A**dvanced **C**omposite **M**aterials
CI	**C**rystallinity **I**ndex
CIC	**C**omposites **I**nnovation **C**entre
CMM	**C**entre for **M**icroscopy and **M**icroanalysis
CoM	**C**entre of **M**ass
^{13}**CNMR**	^{13}**C** **N**uclear **M**agnetic **R**esonance
CRC-ACS	**C**ooperative **R**esearch **C**entre for **A**dvanced **C**omposite **S**tructures
CT	**C**omputed **T**omography
EDX	**E**nergy **D**ispersive **X**-Ray spectroscopy
ESEM	**E**nvironmental **S**canning **E**lectron **M**icroscopy
ETI	**E**xtrusion **T**echnology **I**nternational
FE-SEM	**F**ield **E**mission - **S**canning **E**lectron **M**icroscopy
FID	**F**lame **I**onisation **D**etector
FQA	**F**ibre **Q**uality **A**nalyser
FTIR	**F**ourier **T**ransform **I**nfra **R**ed Spectroscopy

FWHM	**F**ull **W**idth **H**alf **M**aximum
HDPE	**H**igh **D**ensity **P**oly**E**thylene
IGC	**I**nverse **G**as **C**hromatography
KK60	**K**ohn **K**aen **60**
L/D	**L**ength to **D**iameter ratio
LW	**L**ifshitz- **W**and der Waals
MAPP	**M**aleic **A**nhydride **P**oly**P**ropylene
MFI	**M**elt **F**low **I**ndex
NFCs	**N**atural **F**ibre **C**omposites
NIST	**N**ational **I**nstitute of **S**tandards and **T**echnology
O/C	**O**xygen to **C**arbon ratio
PE	**P**oly**E**thylene
PEMA	**P**oly**E**thylene **M**aleic **A**nhydride
PP	**P**oly**P**ropylene
PVC	**P**oly**V**inyl **C**hloride
RH	**R**elative **H**umidity
SE	**S**urface **E**nergy
SEA	**S**urface **E**nergy **A**nalyser
SEI	**S**econdary **E**lectron **I**mage
SEM	**S**canning **E**lectron **M**icroscopy
SFFT	**S**ingle **F**ibre **T**ensile **T**esting
TGA	**T**hermo **G**ravimetric **A**nalysis
TTL	**T**hrough **T**he **L**ens
UED	**U**pper **E**lectron **D**etector
WPCs	**W**ood **P**lastic **C**omposites
XPS	**X**-Ray **P**hotoelectron **S**pectroscopy
XRD	**X**-**R**ay **D**iffraction

To my grandma Alice

Chapter 1

Introduction

1.1 Background & Motivations

Over the past few decades, considerable efforts have been made to develop alternatives to synthetic polymer composites. Tightening of the environmental directives across the globe is putting pressure on many industries to become more sustainable. At the same time, there is a drive to create new markets for natural products and this has opened new fields of research. In order to tackle such environmental issues and respond to an ever-increasing demand, natural fibres, which by definition embody eco-friendly raw products, appear as potential candidates.

Plant fibre composites have been deemed potential substitutes for traditional materials as well as replacements for other materials, in particular glass filled/reinforced plastics, Wood Plastic Composites (WPCs) and timber. It is well established that some natural fibres possess interesting physico-mechanical properties and, for instance, have an elastic modulus that compares well to E-glass [Summerscales et al., 2010]. Their sustainability and high Young's Modulus per unit mass are the main advantages when compared to synthetic reinforcement elements [Mohanty et al., 2001]. The combination of low cost, low carbon footprint and good tensile properties makes plant fibres attractive as a reinforcement element in a plastic matrix for high volume commodity products.

WPCs have already gained significant share replacing timber as a building product. Due to the large demand for timber, this resource is becoming increasingly sparse and expensive. In many applications, plant fibre composites also have the potential to substitute timber. Plant fibre biocomposites perform typically better than WPCs and yield (per area/per annum) is higher for the common bast fibre producing plants [Grigoriou and Ntalos, 2001]. This makes bast fibres attractive as replacement for wood fibres as fillers in commodity thermoplastics.

Despite many years of research, Natural Fibre Composites (NFCs) have not yet made it into the market and research projects often stagger at up-scaling. Actual performance of NFCs remains average compared to thermoplastics and sometimes underperform in tensile strength [Sobczak et al., 2012]. Major issues persist along the value chain of NFCs, creating multiple challenges for the industries involved and limiting the uptake of plant fibre composites. This is due to the fact that the route to manufacture NFCs is complex and involves multiple variables (see Figure 1.1).

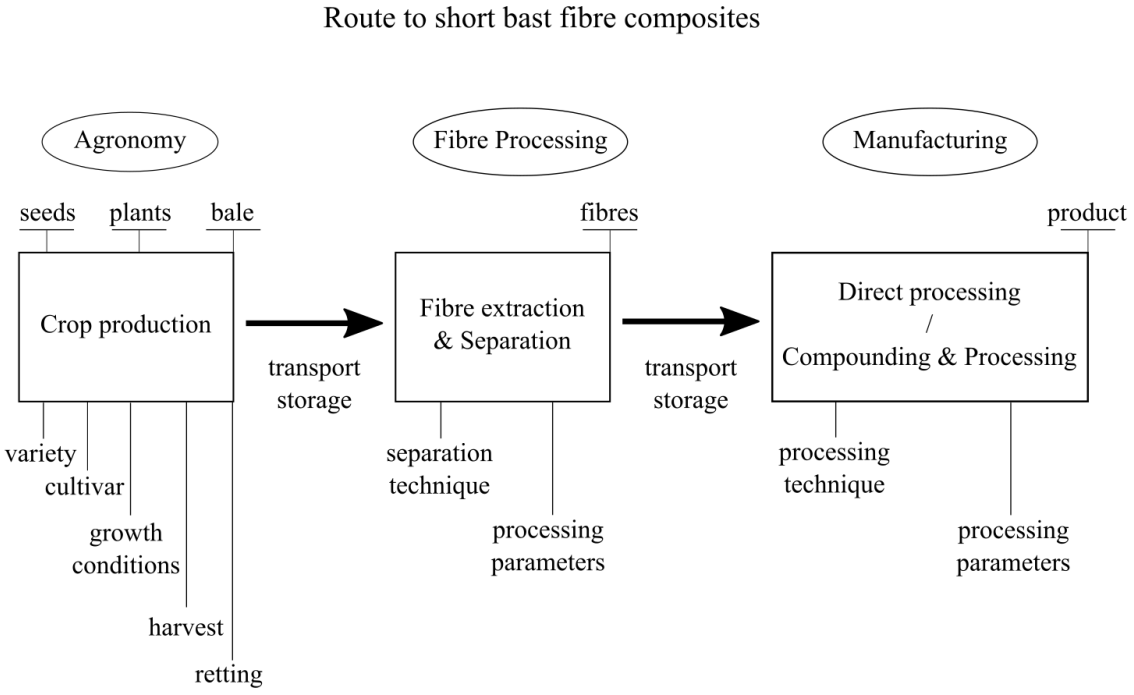

Figure 1.1: Chart representing the route to short bast fibre biocomposites

Many factors influence the properties and quality of the fibres during crop production; the choice of cultivar, the growth conditions and the harvesting period and technique. Post harvest retting, fibre separation and fibre extraction are also critical stages that affect the fibres' length

and the fibres' surface properties [Akin, 2012]. In addition, short natural fibre composites are manufactured by direct processing or via compounding and processing. Each technique involves specific processing variables that need to be adjusted for maximal product performance. Between each stage, the transport and storage conditions can also affect the fibre quality. For instance, moisture uptake and biodegradation are of major concern as natural fibres have high hygrothermal sensitivity.

Too often, traceability during the fibre production, the fibre processing and the product manufacturing is lacking or, when it exists, is insufficient. Consequently, systematic correlation between the composite performance and the fibre properties is often not possible. In particular, many research studies have focused on process optimisation while working with fibres that were poorly characterised; with little information on the fibre cultivar, the size distribution,the degree of separation and on the surface properties. However, the performance of short fibre reinforced composites strongly depends on the quality of the fibre/matrix interface, which in turn is closely related to the fibre surface physico-chemical structure. This makes scale-up to industrial production problematic. It seems necessary to bridge the gap between the fibre producers and the product manufacturers so that one can relate the fibre processing effects with the biocomposite properties to maximise the overall performance. Optimisation of the compounding process for short fibre biocomposites and investigation of the feasibility of large scale production should also be performed to launch short fibre biocomposites on the market.

1.2 Scope and Objectives

This PhD project was part of project P1.1 "Plant Fibre Biocomposites"of the Cooperative Research Centre for Advanced Composite Structures (CRC-ACS). The overall aim of this project was to develop technology for increased adoption of plant fibre biocomposites, to provide information and guidelines to the Australian composites industry enabling them to increase usage of sustainable composites, and to develop new composites based on thermoset, thermoplastic and/or biopolymer matrices. The project consists of two major work packages. One work package was focused on developing design guide lines for biocomposites, whilst work package two was focused on the development of a thermoplastic short plant fibre composite. This PhD

project forms an essential part of work package two. The objective of work package two was defined in the CRC-ACS participant agreement as follows:

"Short fibre composite products, with fibres from plant sources, will be developed with an aim of producing building products compliant (or compliant in the future) with the Building Code of Australia (BCA). Short fibres from candidate bast fibres (a minimum of kenaf and hemp) will be extracted using different physical and chemical methods, allowing the production of reinforcing biofibre with maximised performance and competitive cost. Fibre lengths studied will encompass short fibres (less than 5 mm) through to nanocellulose. Where a suitable method is identified, extraction of plant product will be extended to the core to allow manufacture of low-cost products. Candidate materials will undergo an optimised compounding process for subsequent extrusion (optionally also for injection moulding and/or rotomoulding) to enable maximised retained aspect ratio (above ten), optimised dispersion of reinforcing material, and treatment system optimisation to enhance properties such as toughness, creep and elongation to failure. Compounded materials will be manufactured by extrusion into structural shapes and benchmarked against equivalent wood composites and manufactured products. Benchmarking may include dry and wet mechanical properties, tensile, compression, flexural, impact and creep properties. Demonstration of semi-structural or structural components will be undertaken, with the aim of producing product compliant with the BCA."

This thesis focused on key aspects of biocomposite development for industrial application that is the triad of natural fibre properties, the techniques for natural fibre grading and the extrusion process (ref Figure 1.2). Main objectives of the thesis were to:

• Characterise natural fibres with advanced surface techniques to resolve the chemistry and physical properties of the fibres' surface. These techniques include Scanning Electron Microscopy (SEM), X-ray Photoelectron Spectroscopy (XPS) and Inverse Gas Chromatography (IGC).

• Optimise the extrusion process: investigate the effects of processing variables on the final product performance and study the feasibility of large volume production by up-scaling.

• Establish a correlation between the fibre properties and the composite properties with respect to the fibres' surface characteristics and the processing variables.

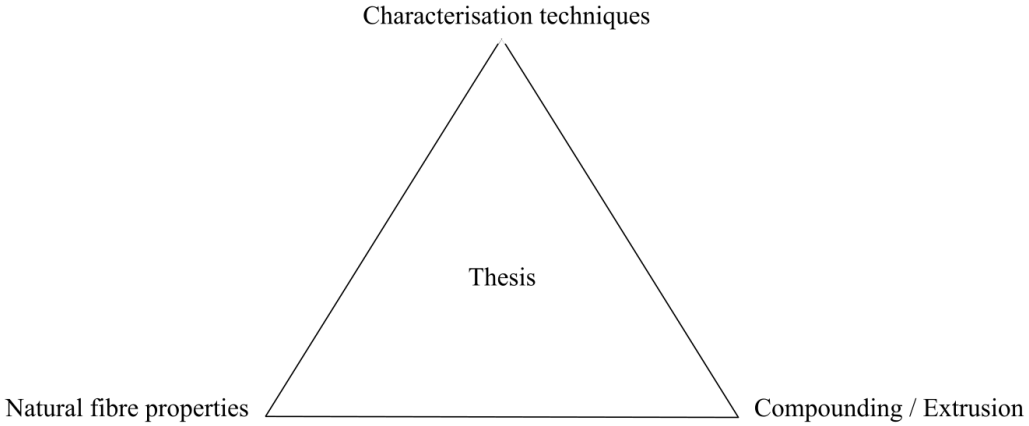

Figure 1.2: Triad of natural fibre properties, characterisation techniques and extrusion

1.3 Thesis Outline

In this thesis, **Chapter 1** introduces the general background and identifies the specific issues that need to be addressed to expand short fibre biocomposites to the industrial market. It also outlines the scope of research and the main objectives. **Chapter 2** provides an overview of the previous work on natural fibre composites, focusing on the overall performance of short fibre biocomposites. A review of the current state-of-the-art in natural fibre surface characterisation is also presented. The last section of this chapter outlines the current challenges to biocomposites extrusion. In **Chapter 3**, the results of XPS and SEM are reported with critical analysis and discussions. **Chapter 4** introduces Inverse Gas Chromatography as a potential technique for fibre surface energy characterisation. The first section investigates the capability to determine the specific surface area of bast fibres with IGC and the second section describes the methodology for natural fibre surface energy determination. A couple of case studies are presented with discussions. The optimisation of twin-screw extrusion process for biocomposites is presented in **Chapter 5**. Finally, **Chapter 6** summarises the main findings of the thesis and suggests future works for the development of short fibre biocomposites.

Chapter 2

Literature Review

2.1 Natural Fibre Composites: general background

Natural fibre composites is a broad and rapidly developing area of materials science. Several publications provide a complete histology of natural fibres and their applications. Bledzki and Gassan [1999] provided a state of the art review on natural fibre composite research and development until the late 90s. Faruk et al. [2012] produced later an updated review on the latest progresses from 2000 till 2010. Both manuscripts provide a clear and concise understanding of what natural fibre reinforced composites are made of, how they are manufactured and how they perform. The aim of this section is to give a general overview and to introduce short fibre biocomposites which is the main theme of this work.

2.1.1 Natural fibres and biocomposites

The denomination "Natural Fibre Composite"(NFC) relates to any material that contains one type of biofibre (or more) and a matrix component. The commonly accepted hierarchy in the field of NFCs begins with "bio-based composites"at the top, beneath this biocomposites (also called eco-composites) refer to any material containing a "bio"component and composites that are fully "bio"are usually categorised as "green composites"[Mohanty et al., 2005]. The following discussion focuses on composites reinforced with plant fibres.

Chapter 2

Natural fibres refer to vegetal fibres, fibres produced from biomass, mineral fibres and animal fibres. Plant fibres are extracted from plants grown specifically (primary plants) or for other purpose (secondary plants). In the latter case, the fibres are usually a by-product and sometimes considered as agri-waste. There are multiple ways to classify plant fibres (taxonomy, cellulose content, application etc.), the most common is the botanical hierarchy illustrated in Table 2.1. Six major groups include fibres extracted from plant stems (bast and core fibres), from leaves or seeds, grass fibres and reeds and wood fibres.

TABLE 2.1: Botanical classification of plant fibres [Pickering, 2008]

Bast	Leaf			Seed			Core	Grass	Other
		Fibres	Pod	Husk	Fruit	Hulls			
Hemp	Pineapple	Cotton					Kenaf	Wheat	Wood
Ramie	Sisal		Kapok				Jute	Oat	Roots
Flax	Agava		Loofah				Hemp	Barley	Galmpi
Kenaf	Henequen		Milk weed				Flax	Rice	
Jute	Curaua			Coir				Bamboo	
Mesta	Banana				Oil palm			Bagasse	
Urena	Abaca					Rice		Corn	
Roselle	Palm					Oat		Rape	
	Cabuja					Wheat		Rye	
	Albardine					Rye		Esparto	
	Raphia							Sabai	
								Canary Grass	

Both biobased and petroleum-based polymers are common matrices for biocomposites applications. Petrochemical plastics represent a vast majority of the matrices used for NFCs with commodity thermoplastics (polyolefins, polystyrene, polyvinyl chloride) and thermosets (polyester, epoxy, vinyl esters) being extensively applied. Popular biopolymers include cellulose polymers, starch polymers, corn-derived polymers (polylactic acid) and protein and vegetable oil-based polymers. Note that biobased polymers may not all be biodegradable and some petroleum-derived polymers are biodegradable. For instance, soy oil-based resins and biobased polyolefins

are non biodegradable polymers. Poly(ε-caprolactone) and aliphatic polyesters are common examples of petrochemical biodegradable polymers. The ISO definition states that a biodegradable plastic may be defined as a compound that undergoes "a significant change in its chemical structure under specific environmental conditions resulting in a loss of some properties that may vary as measured by standard test methods appropriate to the plastic and the application in a period of time that determines its classification. The change in the chemical structure results from the action of naturally occurring microorganisms."[Müller, 2005]. Biodegradability depends on the compound chemical structure and the environment. Some biocomposites may be 100% biobased (in that case they are called green biocomposites) and partially or completely biodegradable. For instance, Wood/PLA compounds are green composites completely biodegradable whilst products made of flax fibres embedded in biobased polyethylene are partially biodegradable only. Satyanarayana et al. [2009] published an extended review that provides a clear insight on biodegradable composites based on lignocellulosic fibres.

Finally, hybrid biocomposites combine biofibres with a polymer matrix. The latter can be biobased, petroleum-derived or a blend of both. Combinations of biobased and petrochemical polymers have been of particular interest as they offer interesting cost-performance properties and provide a compromise between fully fossil-based plastic matrices and 100% biobased materials, for instance by limiting the moisture absorption or increasing the impact strength [Mohanty et al., 2005]. Hybrid biocomposites may be the way to foster the implementation of NFCs in industrial applications. An overview of the NFC types and their related compounds is shown in Figure 2.1.

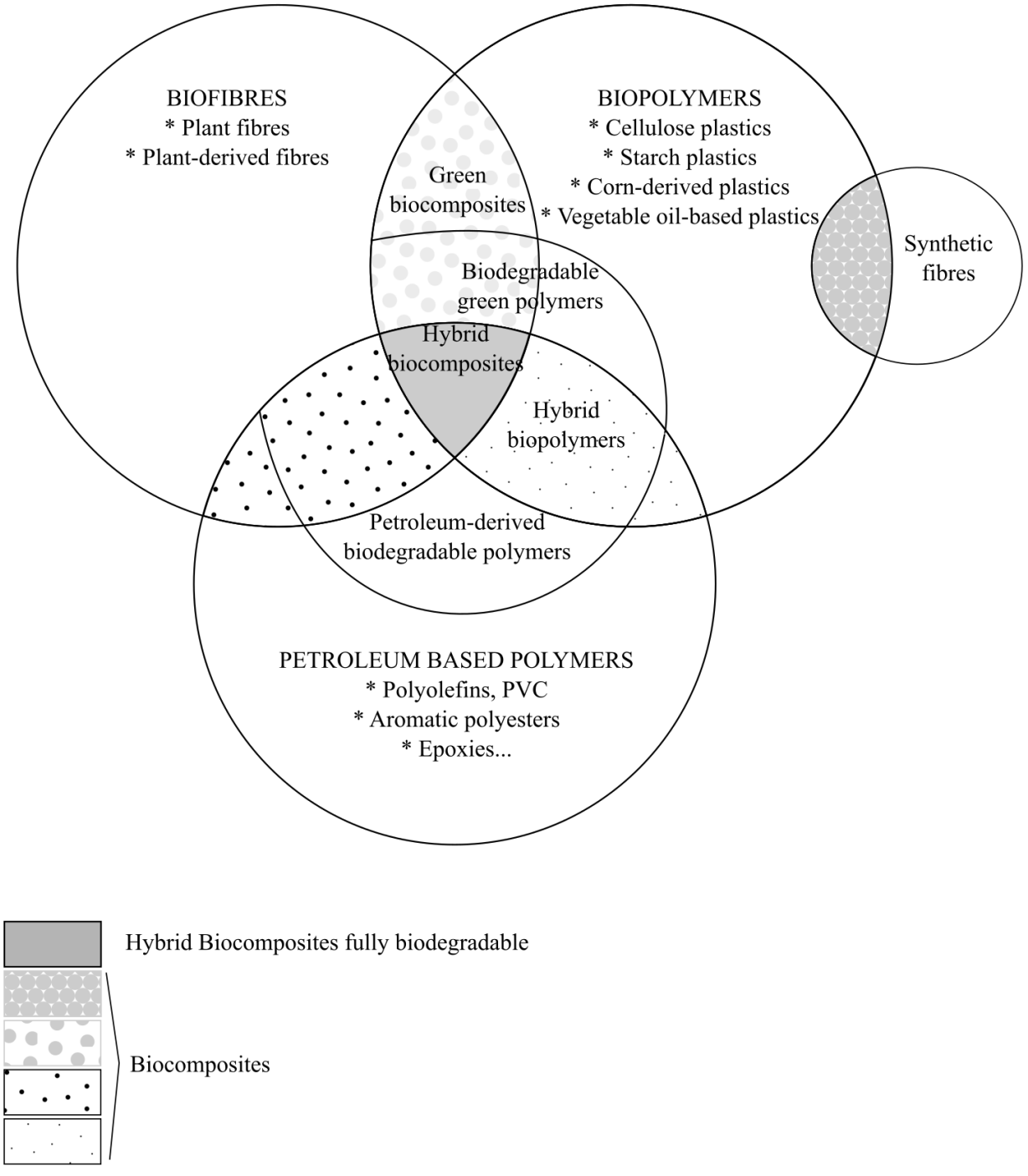

Figure 2.1: Natural fibres, Biopolymers and Biocomposites

2.1.2 Performance & properties

2.1.2.1 Natural fibre properties

Plant fibres, contrary to synthetic fibres, do not have standardised properties but rather their properties spread over a large range. The mechanical properties of plant fibres depend on the species, the growth conditions, time of harvest and the fibre location in the stem [Ayre et al., 2009, Charlet et al., 2007, Duval et al., 2011, Mediavilla et al., 2001, Satyanarayana et al., 2007]. Natural fibre mechanical properties also depend on the retting process [Akin et al., 2001, Paridah et al., 2011, Stuart et al., 2006] and the extraction and separation techniques [Dupeyre et al., 1998]. These processes also likely induce potential damage to the fibres [Hänninen et al., 2012]. Finally, testing procedures are another source of discrepancy in the data [Mukherjee and Satyanarayana, 1986]. For instance, the tensile performances vary with the specimen length as the probability of sampling defects increases with increasing fibre length [Defoirdt et al., 2010, Fidelis et al., 2013, Virk et al., 2009]. All the parameters mentioned above explain why values published in literature vary to a considerable extent. An attempt to provide typical specific modulus values for common plant fibres is given in Figure 2.2.

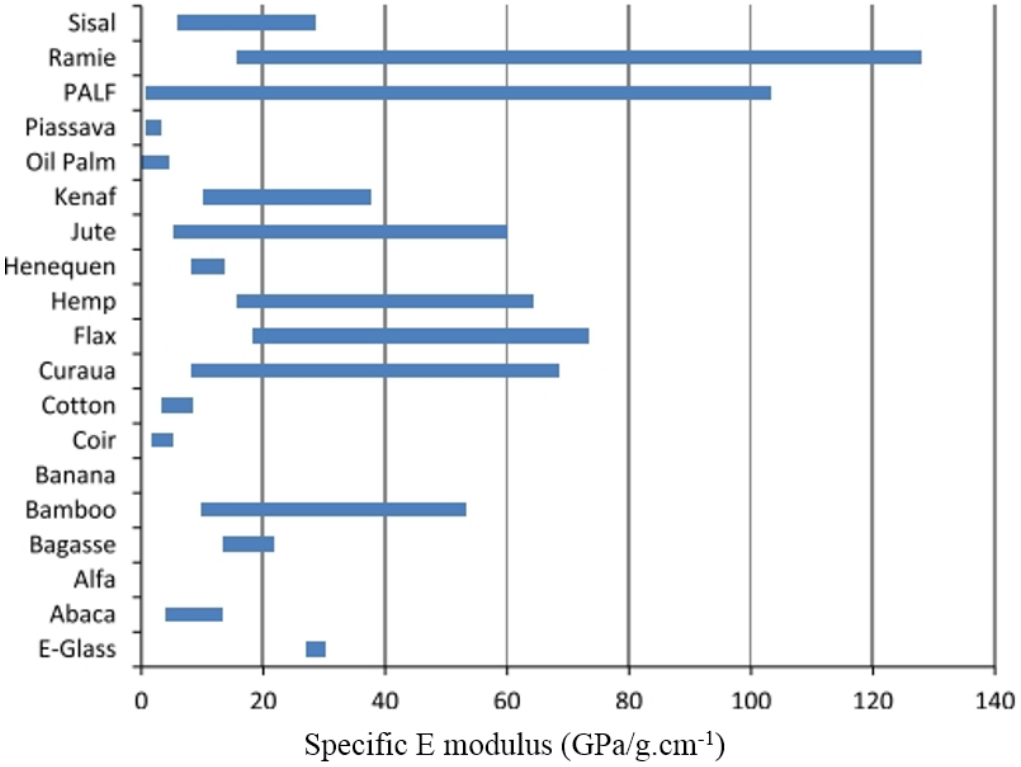

Figure 2.2: Ranges of specific Youngs' Modulus values for natural fibres and glass fibres [Dittenber and GangaRao, 2012]

2.1.2.2 NFCs properties

A majority of studies on NFC performances focus on the tensile properties whilst impact, shear, compression and flexural responses are less frequently investigated [Anderson, 2008, Arbelaiz et al., 2005, Herrera-Franco and Valadez-Gonzalez, 2005, Thumm and Dickson, 2013]. This section gives an overview of the tensile and impact properties one can expect from short plant fibre reinforced thermoplastics.

Tensile behaviour Introduction of short fibres in thermoplastic matrix increases the stiffness due to the fibre's high elastic moduli. However, composite failure is usually more brittle compared to the neat polymer and tensile strength tends to be similar or slightly reduced. Lower strain at break and reduced strength are due to the composite microstructure and is directly related to the constituents, the composition and manufacturing process. For instance, voids, weak interfacial interactions and poor fibre dispersion act as defects and stress concentration

points that induce failure. Under tensile load, composites with efficient stress transfer show higher strength, higher stiffness and lower strain at break than those with a weak interface. A review of the literature on tensile performance of short fibre thermoplastic biocomposites is given in Figure 2.3. As shown in the graphs, there is an approximately linear increase in stiffness with increasing fibre content till ca. 40 wt.%. Adding more than 40 wt.% fibre is less efficient and the performance seems to reach a plateau. Efficient and homogeneous dispersion is indeed difficult to achieve at higher fibre load and fibre agglomerates become potential stress concentration zones. The data scattering in Figure 2.3 also reflects how the coupling agent, the manufacturing process and the fibre treatment affect the biocomposite stiffness. Tensile strength is much more difficult to improve and in many cases the performance equal the matrix performance, or in some cases degrades the matrix performance (Figure 2.3).

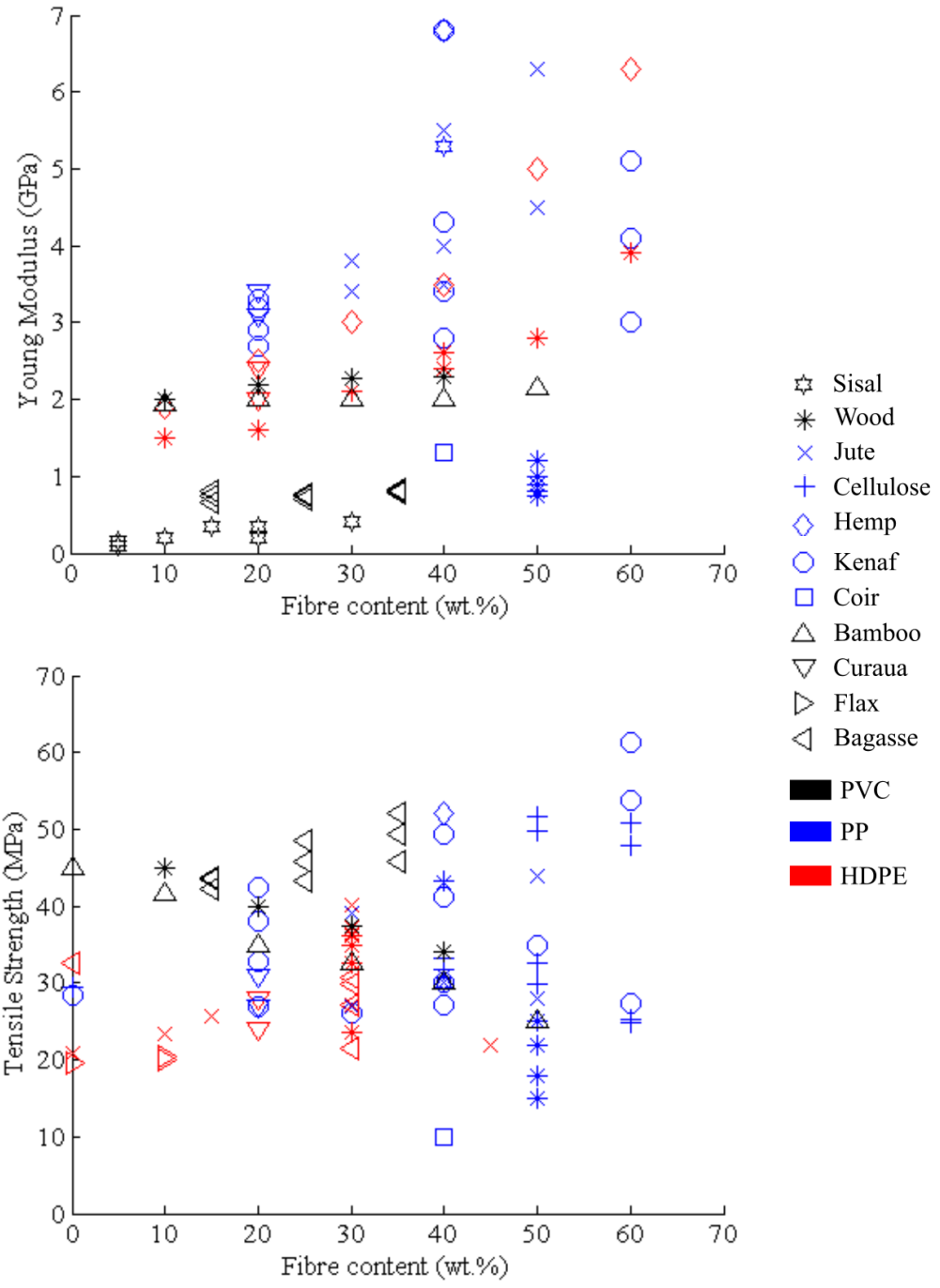

Figure 2.3: Performances of natural fibre thermoplastics (see references in Appendix A)

Impact strength NFCs response to impact stress has been less studied than the tensile properties and the mechanisms remain poorly understood [Bledzki and Gassan, 1999, Sobczak et al., 2012]. The published literature shows inconsistent results. In many cases, addition of fibres to the matrix reduced the impact strength [Huda et al., 2008, Lei et al., 2007, Xu et al.,

2008, Zheng et al., 2007] but some authors reported an improvement in impact properties [Karnani et al., 1997, Rahman et al., 2010]. The fibre type also influence the impact properties [Pavithran et al., 1987].

From a micromechanics point of view, adding short fibres to the polymer induces specific failure modes, namely fibre-matrix interface failure, fibre fracture and fibre pull-out. These can increase the energy dissipation but the deformation mechanisms and strain at break strongly depend on the quality of the interface. Fibre load and fibre length are also critical [Bengtsson et al., 2007, Rana et al., 2003]. Impact strength usually increases with fibre load till a threshold where good dispersion may be difficult to achieve and fibre agglomerates become potential defects [Mohanty et al., 2006, Thwe and Liao, 2003]. Impact strength increases with increasing fibre length but the evolution profile closely depends on the interfacial shear strength and the critical fibre length (this will be detailed in the next paragraph). Note that fibre length may also affect the dispersion of the fibres in the matrix hence its influence is difficult to quantify. Efficient coupling agents that strengthen the interface also tend to improve the impact properties [Bledzki and Gassan, 1999, Mohanty et al., 2004]. Finally, NFCs have lower impact strength than Glass Fibre Reinforced Plastics (GFRPs) because natural fibre tensile strengths fall below those of glass fibres and hence fibre fracture occurs earlier i.e. at lower strain [Sobczak et al., 2012, Wambua et al., 2003].

Main factors for biocomposite performance Like in traditional short fibre composites, the compound mechanical properties depends on multiple variables. Fibre length is a major criteria for mechanical properties. The concept of critical fibre length established by Cox [1952] and Kelly and Tyson [1965] is well accepted for short synthetic fibre reinforced polymers. The authors modelled the micromechanics of short fibre composites with a shear-lag mechanism and defined the minimum fibre length required for the fibres to carry maximal shear stresses so that the composite fails by fibre fracture rather than by shear failure at the interface [Bowyer and Bader, 1972]. The critical fibre length l_c is defined as:

$$l_c = \frac{\sigma_f d_f}{2\tau_m} \tag{2.1}$$

with σ_f the tensile strength of the fibre, d_f the fibre diameter and τ_m the shear strength of the interface, which is usually considered as the matrix shear strength. Equation 2.1 also shows how the fibre aspect ratio and the fibre/matrix adhesion limit the reinforcement effect; low aspect ratios or poor adhesion restrict the fibre reinforcement for any given length. On the other hand, for a given [fibre, matrix] system with fixed aspect ratio and interface shear strength, increasing fibre length results in better properties (Figure 2.4). Figure 5 also highlights how the composite stiffness is readily improved even with very short fibres (<0.5 mm) compared with tensile strength and toughness. This is because stiffness mainly relies on strain transfer between the fibres and the matrix. Stiffness is measured in the elastic behaviour of the composite and is barely sensitive to the ultimate tensile strength of each component.

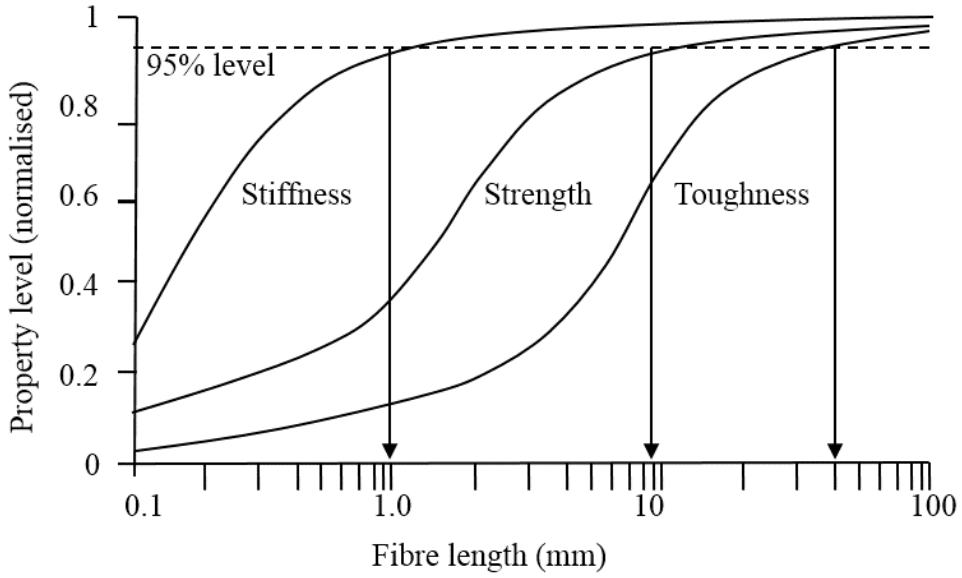

Figure 2.4: Prediction of tensile and impact performance with respect to fibre length for fibre reinforced thermoplastic composites (adapted from Thomason and Vlug [1996])

However, the model of critical fibre length assumes a perfect interface (i.e. full stress transfer from the matrix to the fibres) and elastic behaviour, which might not be realistic for natural fibre composites. Given the complexity of the fibre/matrix interface, the variability in the fibre dimension and the large range of properties, estimation of a single critical length for natural

fibre composites is questionable. One can have the ideal [fibre, matrix] components but the composite properties will not reach high performance unless the interface is efficient.

Fibre content and fibre orientation are also main factors for biocomposite performance. Optimal condition is when the fibres are oriented along the load direction while increasing angles reduce the transferred load. Actually, most of the short fibre reinforced thermoplastics have 2D or 3D randomly oriented fibres and therefore fibre orientation is usually not considered as a variable one can control. Fibre content is much easier to control and largely affects the overall mechanical properties (Figure 2.4, Figure 2.3). Theoretically, the higher the fibre content the better the reinforcement but actual performance is limited by the manufacturing process. Natural fibres are indeed more challenging to process than traditional synthetic fibres and it is difficult to achieve homogeneous dispersion at high fibre load. This will be discussed later in the chapter.

Finally, long term performance and durability are crucial for NFCs and constitute the major concerns for their applications. Exposure to humidity, temperature and weathering (UV radiation) reduce the product performance [Espert et al., 2004, Pickering, 2008]. Natural fibres degrade easily under environmental conditions, which is an advantage for material disposal but also a challenge for the compound durability. UV-absorber, anti-fungi and other additives are usually introduced during the manufacturing process to slow down the degradation mechanisms and better control the degradation rate over the product lifetime [Kamdem et al., 2004, Xie et al., 2010].

2.2 Natural Fibre Characterisation

This section reviews firstly the complexity of natural fibre structure and surface properties. The second part discusses the challenges to characterise the surface of bast fibres with traditional techniques. The third part introduces Inverse Gas Chromatography as a novel promising technique.

2.2.1 Surface properties

2.2.1.1 Natural fibre structure

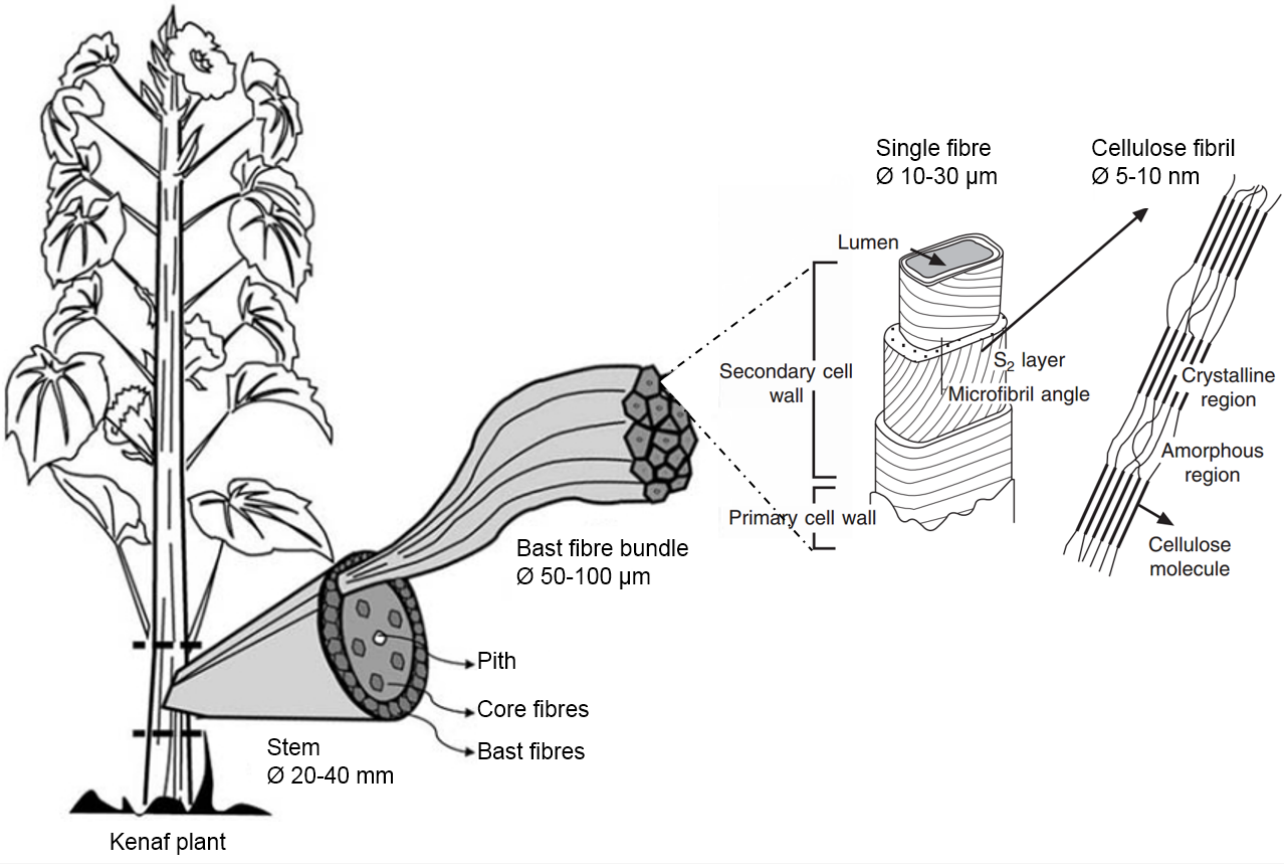

Figure 2.5: Structural hierarchy in kenaf plant (modified from Khalil et al. [2013] and Baillie [2004])

Chapter 2

Note nomenclature: a single fibre is frequently called macrofibril, cell wall or technical fibre. The cellulose fibril is also called microfibril or elementary fibre. For the sake of clarity, the terms single fibre and cellulose fibril are used in the document.

Plants exhibit a multiscale hierarchical structure that reflects the outstanding complexity of nature (Figure 2.5). Bast fibres are located in the outer layer of the plant stem, between the bark (cuticle/epidermis and bark parenchyma cells) and the phloem (see illustration in Gorshkova et al. [2000]). Bast fibres represent ca. 30-40% of the stem. In that area, single fibres gather in bundles of variable sizes depending on the plant variety and its maturity (typically 50-100 μm in kenaf stem and 100-300 μm in flax). A single fibre, so called bast fibre, has a complex 3D microstructure with three membranes enclosing the lumen: the primary cell wall, the secondary cell wall (S_1, S_2 and S_3) and the plasma membrane. Each membrane consists of cellulose fibrils embedded into a matrix of hemicellulose and lignin and also contains pectins, proteins, waxes and other extractives. The chemical composition and the molecular arrangement vary between the layers and fluctuate with the fibre location in the plant stem. For instance, the density of cellulose crystals and the chain orientation vary within the different layers. The primary wall contains fibrils dispersed with no proper orientation whilst in the secondary wall the cellulose chains gather into bundles that follow to a certain degree the fibre axis. The arrangement in the latter makes it more dense than in the other layers. The tertiary wall has the lowest content of cellulose and poor chain orientation [O'Sullivan, 1997]. The average composition for common bast fibres is given in Table 2.2.

TABLE 2.2: Average chemical composition of common bast fibres [Bledzki and Gassan, 1999, Dittenber and GangaRao, 2012, Faruk et al., 2012, Mohanty et al., 2005, Satyanarayana et al., 2009]

	Chemical composition (wt.%)				
Fibre	cellulose	hemicellulose	lignin	pectins	waxes
Flax	62-72	17-21	2-5	1.8-2.3	1.5-1.7
Hemp	68-78	15-22	4-10	0.9	0.8
Jute	59-72	12-20	12-13	0.2-0.4	0.5
Kenaf	31-72	20-22	8-19	3-5	
Ramie	69-85	13-17	0.5-0.7	1.9	0.3

2.2.1.2 Natural fibre surface properties

The type of cellulose, the cellulose content, the orientation of the cellulose fibrils in the cell walls (microfibril angle) and the crystallinity determine the mechanical properties [Baley, 2002, Bledzki and Gassan, 1999]. On the other hand, the capability to form a strong interface with polymer matrices closely depends on the surface chemistry. Natural fibres as an entity absorb water and contain numerous hydrophilic components (cellulose, hemicellulose), which raises two major issues. First, the fibres have high moisture uptake that compromises their dimensional stability (swelling) and increases the risk of degradation. It also challenges the biocomposite stability and long term performances. Secondly, the polarity of the polymers on the surface of natural fibres can produce severe incompatibility with non-polar matrices. Fibre wetting is therefore difficult to achieve. This inherent incompatibility should be overcome to get a strong interface in the compound.

Note that the concept and the definition of surface for natural fibres is complex because the nature of the surface depends on which "layer"is exposed, which in turn depends on the extraction process and the post-processing steps, since these affect different levels of the fibre structure [Le Duigou et al., 2012, Zafeiropoulos et al., 2002]. Depending on the surface exposed, natural fibres may be more or less hydrophilic and more or less polar.

Common approaches to enhance the fibre/matrix interface involve fibre surface modification (via chemical treatment, physical modification or grafting), use of coupling agents (fibre or matrix) or use of compatibilisers. Bledzki et al. [1996], George et al. [2001], Keener et al. [2004], Li et al. [2007] and John and Anandjiwala [2008] successively published reviews on the common treatments applied to bast fibres. These documents describe the mechanisms and summarise the main effects associated with the treatments. Actually, many studies showed sparse and inconsistent results. No clear trends could be established so far on the effects of these surface modification methods, but rather a general state of confusion and recurrent contradictions exist.

There are various explanations for these contradictions:

• Samples differ by their origin and processing history hence it is difficult to establish direct comparison and cross-correlation between studies. For instance, treatment may be applied to

the fibres before the final processing stage and therefore loses efficiency due to separation of the bundles.

• Poor information on the fibre samples challenges data interpretation. Too often, an assumption is made on the fibre specimen history. For example, in comparing flax samples, retted and non retted, the latter fibre surface likely contains epidermal tissues. The nature of these samples is quite different so a direct comparison would be inappropriate. As mentioned earlier, this is more a problem of communication and a lack of traceability rather than a scientific issue.

• The methods used to analyse natural fibre surfaces. Characterisation of natural fibre surface is complex because of the numerous components present on the surface. Appropriate methods and strategy should be used to investigate these materials. This will be discussed in the next section.

2.2.1.3 Surface characterisation techniques

Scanning Electron Microscopy (SEM) has been widely used to analyse natural fibre surface topography and particularly to compare fibres before and after treatment [Baley et al., 2006, Bismarck et al., 2001, Edeerozey et al., 2007, Sreekala et al., 2000]. A typical series of SEM images is shown in Figure 2.6. The SEM micrographs reveal distinct topographies between the treated fibres, which highlight the different effects of fibre treatment on the sisal fibres' surface. Environmental Scanning Electron Microscopy (ESEM) is another type of SEM that allows imaging of fibres in their natural state without being dehydrated (no vaccuum, no sample coating) [Donald, 2003]. This technique has a potential interest to study natural fibres but few works have been published so far [Liu et al., 2004, Lu et al., 2008]. A novel generation of SEM (field emission SEM) is being developed that achieves good resolution at low acceleration voltages thanks to a specific "in-lens"detector configuration [Liu, 2000]. This technique allows imaging of the very near fibre surface (ca. tens of nanometers) and contrast mapping at low atomic number [Rasch et al., 2014, Truss et al., 2015, Trygg and Fardim, 2011].

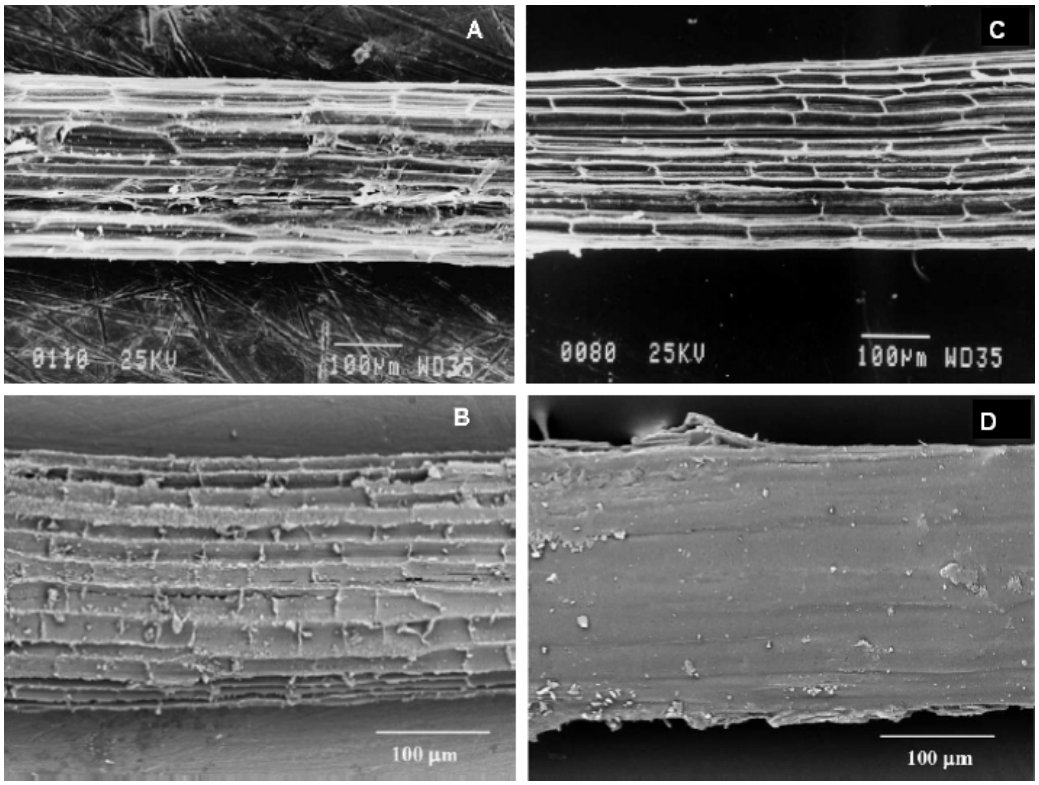

Figure 2.6: SEM images of raw sisal fibre (A) and sisal fibres after various chemical treatments: immersion in resorcinol/hexamethylenetetramine aqueous solution (B), mercerisation (C) and mercerisation followed by immersion in resorcinol/hexamethylenetetramine aqueous solution (D) (modified from Martins et al. [2006])

Atomic Force Microscopy (AFM) has been used to a lesser extent to evaluate the fibre surface roughness [Gustafsson et al., 2003, Koljonen et al., 2003, Le Duigou et al., 2012]. AFM provides 3D topography and has higher resolution than SEM (typically <1 nm and 10 nm respectively) but a much smaller analysis window (ca. factor 100). SEM is usually preferred to visualise various fibres at a time. AFM is also more complicated to operate than SEM, is a sensitive technique but time consuming. On the other hand, AFM allows force mapping (elastic forces, adhesion forces) but few works have been published on these applications for natural fibres [Guhados et al., 2005, Le Troëdec et al., 2011].

Fourier Transform Infrared Spectroscopy (FTIR) and X-ray Photoelectron Spectroscopy (XPS) are commonly applied to characterise natural fibre surfaces [Felix and Gatenholm, 1991, Sgriccia et al., 2008, Tserki et al., 2005, Valadez-Gonzalez et al., 1999]. FTIR gives semi-quantitative information of the chemical groups present on the fibre surface (the absorbance spectra are compared to a reference spectrum), is easy to operate and it is also relatively straightforward

to interpret data. After many years of research, the absorption bands of the main components (cellulose, hemicellulose, lignins) have been identified and reference data are available [Morán et al., 2008, Nelson and O'Connor, 1964b, Oh et al., 2005b, Yang et al., 2007]. XPS provides quantitative information of the very near surface composition (first 10 nm) based on the analysis of peak shifts in the binding energy spectra. Wood pulp and cellulose fibres have been extensively studied [Andresen et al., 2006, Dorris and Gray, 1978a, Johansson, 2002, Johansson and Campbell, 2004, Johansson et al., 1999]. However, data analysis is challenging for complex surfaces typical of natural fibres. The accuracy of peak fitting and identification of chemical groups have been discussed by multiple authors [Artyushkova, 2010, Johansson et al., 2004, McIntyre et al., 1981].

Average chemical composition of natural fibres has also been studied by Carbon-13 Nuclear Magnetic Resonance (^{13}CNMR) and particularly the identification of aromatic compounds in lignins [Froass et al., 1998, Martínez et al., 2008, Seca et al., 1998]. ^{13}CNMR is a powerful technique to decipher the chemistry of natural fibres but it reflects the overall chemical composition rather than the surface chemistry (samples are dissolved in solution). Data interpretation also remains difficult due to the complexity of the technique [Mansfield et al., 2012].

Finally, characterisation of the crystalline structure and estimation of the degree of crystallinity of cellulose fibrils in plants have been performed with X-Ray Diffraction (XRD), Fourier Transform Raman Spectroscopy, FTIR and ^{13}CNMR [He et al., 2007, Nelson and O'Connor, 1964a, Newman and Hemmingson, 1990, Oh et al., 2005a, Zuluaga et al., 2009]. XRD is usually preferred because it is more direct than the other techniques and it provides quantitative information (calculation of the Crystallinity Index (CI)) but data interpretation remains difficult [Park et al., 2010].

Each of the techniques aforementioned has its own specific variables: analysis depth, sensitivity and sampling area. The concept of "surface"is therefore relative to the method chosen for characterisation. For fibre grading at large scale, other criteria should also be considered when selecting a characterisation technique such as the resources necessary to run an experiment (time, funds, personnel, consumables) and the complexity to run and interpret experimental data. The latter depends on whether the technique is well established for natural fibres and if

consistent databases are available. A comparison of the techniques reviewed in this section is given in Table 2.3.

2.2.1.4 IGC: a novel technique to characterise natural fibre surfaces

The fibre surface chemistry, its adsorption capacity as well as its wettability and dispersability in a matrix correlate with the fibre surface energy values and depend also on the accessible surface area. The surface energy is directly related to the thermodynamic work of adhesion. The surface energy provides information on the intermolecular forces that can occur at the fibre surface. These combine long range Van der Waals forces and short range chemical forces, also known as dispersive and polar forces respectively. The nature of these interactions and their intensity also depend on the accessible surface area.

Traditional methods used to determine the fibre surface energy involve the measurement of contact angles. Various approaches reviewed by Williams [2015] and Heng et al. [2007] provide methods for measuring droplet angles to calculate the fibre surface tension. The most common are the Young model, the Fowkes and extended Fowkes (Owens & Wendt) approaches and the Van Oss et al. model. Capillary rise, Wilhelmy plate and sessile drop are common methods and numerous studies have been published on natural fibres [Collins, 1947, Rong et al., 2002, Shen et al., 2004]. Although these techniques are excellent on flat surfaces, natural fibre's porous structure and heterogeneous surface properties challenge the accuracy and the validity of the experimental data [Pietak et al., 2007]. These methods are based on liquid-solid interactions where swelling and dissolution may occur and skew the data.

Inverse Gas Chromatography (IGC) is an alternative tool to study surface energies. Briefly, the gas probe molecules are transported by the carrier gas and injected into the chromatography column containing the sample at defined conditions of pressure and temperature. Adsorption followed by desorption occur at the sample surface and an elution peak results (Figure 2.7). The study of the thermodynamic quantities from sorption equilibrium enables to determine the surface energy components of the material under investigation. It is a versatile technique to characterise samples of any shape, as long as the specimen can be packed in the column and molecular interactions can occur. IGC exists since the early 50s and it has been applied

Table 2.3: Comparison of common surface characterisation techniques

	AFM	^{13}C NMR	FTIR	SEM	XPS	XRD
Analysis area	20 μm x 20 μm	in solution	2 μm x 2 mm	200 μm x 200 μm	300 μm x 700 μm	single fibre, bundles
Analysis depth	<1 nm (first atomic layers)	in solution	<10 μm in Attenuated Total Reflectance mode	5-15 nm (topography) 250-400 nm (contrast mapping) 1-5 μm (X-rays)	2-10 nm	variable (depends on X-ray wavelength, angle of incidence and sample surface)
Topography	3D high resolution force mapping (stiffness, adhesion)	/	/	high resolution contrast mapping	/	/
Chemical composition	/	quantitative	relative	elemental composition (X-rays)	quantitative	elemental composition of crystalline elements
Cellulose crystallinity	/	quantitative CI	relative CI	/	/	quantitative CI crystalline structure
Pros & Cons						
Fibre sample	-	/	+	+	+	+
Size analysis area	-	/	+	-	+	-
Time experiment	- -	- -	+	+	-	+
Resources required	-	-	+	+	- -	+
Data interpretation	+	- - -	-	-	- -	CI +, structure -

CI: Crystallinity Index

mostly to pharmaceutical industry [Mohammadi-Jam and Waters, 2014], for characterisation of zeolites [Aşkin and Bilgiç, 2005, Eva Díaz, 2004] and carbon nanostructures [Papirer et al., 1999] but IGC has not been well established yet for natural fibre characterisation.

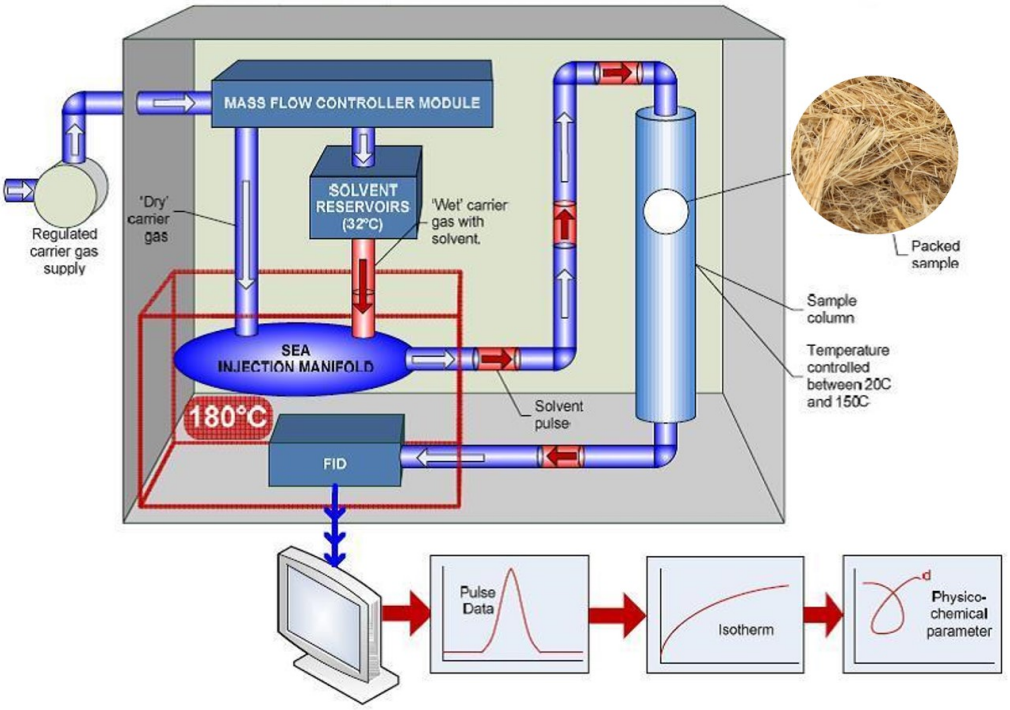

Figure 2.7: IGC Surface Energy Analyser (modified image supplied by Surface Measurement Systems)

Gamelas [2013] published an extended review on the characterisation of natural fibres with IGC that introduces the theoretical approaches to determine both dispersive and specific energy components of plant fibres and discusses the main findings up to the present. This review provides a solid insight into IGC investigations of natural fibres. The following paragraphs summarise the main results published in the literature.

Cellulose fibres and wood fibres have been the most studied because of its relevance to the pulp and paper industry. For instance, Dorris and Gray [1979, 1980] pioneered that area with their work on cotton paper and thermomechanical wood pulp. They developed novel calculation methods to determine the London dispersive component of the surface free energy in the Henry's law region of the adsorption isotherm where only London forces interactions occur between the adsorbent (the fibre) and the adsorbate (the solvent). The London dispersive components were

estimated at 50 $mJ.m^{-2}$ and 39 $mJ.m^{-2}$ for the cellulose paper and the wood fibres respectively. Since then, their approach has been widely used to determine the dispersive surface energy component of natural fibres. Other studies on various type of cellulose (cotton, hardwood cellulose, cellulose powder etc.) reported values between 40 $mJ.m^{-2}$ and 50 $mJ.m^{-2}$ [Belgacem et al., 1995, Tshabalala, 1997, Tze et al., 2006].

It would seem appropriate here to explain in further detail why the dispersion of surface energy is of interest and how this is specifically of importance to bio-based composites since polar forces are not mentioned here.

More recently, IGC has been applied to bast fibres. A review of the literature shows that the data obtained range from ca. 35 $mJ.m^{-2}$ to 45 $mJ.m^{-2}$ i.e. slightly lower values than those of cellulose fibres [Gamelas, 2013]. Mills et al. [2008] attributed these values to the lower cellulose content and higher lignin and hemicellulose content in bast fibres compared with cellulose fibres but no clear trend was established and energy values differed considerably within the same fibre varieties. For instance, the energy dispersive component of hemp at 40°C varied between 36 $mJ.m^{-2}$, 38 $mJ.m^{-2}$ and 41 $mJ.m^{-2}$, that of sisal was estimated at 38 $mJ.m^{-2}$, 41 $mJ.m^{-2}$ and 49 $mJ.m^{-2}$ and that of flax at 35 $mJ.m^{-2}$ and 43 $mJ.m^{-2}$ [Gulati and Sain, 2006, Heng et al., 2007, Mills et al., 2008, Ramires and Frollini, 2012].

As expected, energy values changed substantially with temperature although the evolution was non uniform. Mills et al. [2008] studied the evolution of dispersive energy with temperature for various fibres and found that hemp, flax and kenaf energy decreased with increasing temperature from 43.1 $mJ.m^{-2}$, 42.7 $mJ.m^{-2}$ and 43.1 $mJ.m^{-2}$ at 20°C to 35.9 $mJ.m^{-2}$, 34.9 $mJ.m^{-2}$ and 36.9 $mJ.m^{-2}$ at 40°C respectively. However, jute, abaca and sisal showed higher energy values at higher temperature: 40.2 $mJ.m^{-2}$, 35.8 $mJ.m^{-2}$ and 35.5 $mJ.m^{-2}$ at 20°C and 43.5 $mJ.m^{-2}$, 36.2 $mJ.m^{-2}$ and 41.2 $mJ.m^{-2}$ at 40°C respectively.

IGC has also been used to study the effect of fibre processing and chemical treatment on the surface energy. Heng et al. [2007] found that flax fibres dew retted in the field had higher energy values than fibres separated with industrial washing or by steam explosion treatment (45.4 $mJ.m^{-2}$ versus 35.5 $mJ.m^{-2}$ and 31.6 $mJ.m^{-2}$ respectively). Cordeiro et al. [2011a] studied the effect of alkali treatment and zein treatment on various fibres and a majority

of samples showed a decrease in dispersive energy values after treatment (flax, hemp, kenaf, agave and sisal) although some fibres were outliers (pineapple). The authors extended their study to wood and bagasse fibres and observed a similar scenario: eucalyptus and bagasse fibres displayed lower energy values after treatment (respectively 43.2 $mJ.m^{-2}$ and 44.2 $mJ.m^{-2}$ before treatment vs. 42.7 $mJ.m^{-2}$ and 42.8 $mJ.m^{-2}$ after treatment) whereas spruce and wheat showed higher energy (respectively 41.6 $mJ.m^{-2}$ and 45.1 $mJ.m^{-2}$ before treatement vs. 44.2 $mJ.m^{-2}$ and 48.8 $mJ.m^{-2}$ after treatement) [Cordeiro et al., 2012]. Ashori et al. [2012] also observed different behaviours on cotton fibres, tobacco fibres and other natural fibres after alkali treatment. Besides, Pommet et al. [2008] observed a slight decrease in energy for both hemp and sisal fibres treated in bacterial cellulose medium (2% and 9% respectively) but an increase in energy by 50% and 62% respectively when the fibres were pretreated in alkali solution.

Overall, no general trends could be established so far on the surface energy values of bast fibres due to the variety of the results obtained. This is likely because IGC has only been recently applied to natural fibres and a lot still needs to be done to better understand the thermodynamic phenomena involved. The current status of IGC for natural fibre surface characterisation can be summarised as follow:

• Few IGC studies have been performed on bast fibres hence only small data sets are available. Given the various fibre types and their wide range of properties, more experimental work should be conducted in order to extend the existing database and, when possible, to establish trends between the fibre types and their surface properties.

• Most of the studies on natural fibres have been performed in different conditions (temperature, relative humidity), with different solvents and using various calculation procedures. The lack of information and details of experimental procedures make it difficult to compare and validate data. Moreover, the large variability of natural fibre properties and their complexity compared to synthesised and well designed man made materials means that a systematic study of the common procedures and models implemented in IGC is required to assess its capabilities as a technique to characterise natural fibre surfaces.

• IGC requires the specific surface area to determine the surface energy, especially as this can depend on surface coverages. Usually, the specific surface area is determined by the Brunauer

Emmett Teller (BET) method which uses nitrogen sorption [Bismarck et al., 2002, Livingston, 1949] or krypton [Beebe et al., 1945, Rosenberg, 1956], for surface areas below 0.5 $m^2.g^{-1}$ where the nitrogen shows limitations [Sing, 2001]. These techniques involve extreme conditions of high vacuum at low temperature (77K) under which the fibre properties are likely to change and thus the BET surface area. An alternative and preferred technique for measuring the BET surface area of low surface natural fibres would be to use IGC at room temperature. Some authors determined the BET area values of bast fibres with IGC but none questioned the influence of experimental conditions on the measured specific surface areas [Ashori et al., 2012, Cordeiro et al., 2012]. For instance, the solvent choice and the effect of sample packing have not been investigated. Whether these experimental conditions influence the thermodynamic behaviour of the molecules in the column and hence lead to different BET values should be considered. Lee and Luner [1993] already raised this issue when studying the adsorption isotherms of alkanes on cellulose and suggested further investigation but not much has been done since then.

• Traditional IGC is performed at infinite dilution which means that only the higher energetic sites interact with the solvent molecules and therefore single surface energy values will be similar even though the fibre surface is heterogeneous [Williams, 1994]. Natural fibre surfaces present chemical heterogeneities (functional groups, degree of crystallinity) and physical heterogeneities (porosity, asperities etc.) hence the energy values are expected to vary along the surface. Mapping the surface energy heterogeneity profile would be more representative of natural fibre surface and constitutes a new area of research to explore. The new generation of IGC equipment enable experiments with finite dilution which opens new opportunities for natural fibre surface characterisation [Rudzinski and Everett, 2012, Thielmann, 2004, Ylä-Mäihäniemi et al., 2008].

2.3 Compounding Short Fibre Biocomposites

Twin-screw extrusion is one of the key processes used both in the compounding stage and production stage for short fibre reinforced thermoplastics. Despite the importance of this process, all too often the extruder is treated as a "black-box" with temperature and screw-speed being the main parameters controlled [Beaugrand and Berzin, 2013, Chevali and Ulven, 2012, Oksman et al., 2003]. By neglecting aspects such as the screw configuration, feeding location or feeding strategy, the full potential of the extruder is not exhausted. While the importance of these aspects is widely acknowledged for the compounding of traditional filled/reinforced thermoplastics [Giles Jr et al., 2004, Villmow et al., 2010, Wang et al., 2004], the effects of screw design and feeding location in the compounding of biofibres have not received a great deal of attention. When these aspects have been considered, findings showed a strong relationship between these and the composite performance but no general trends could be established because the results were rather inconsistent and the studies involved different processing variables [Keller, 2003, Santos et al., 2007, Zhang et al., 2012].

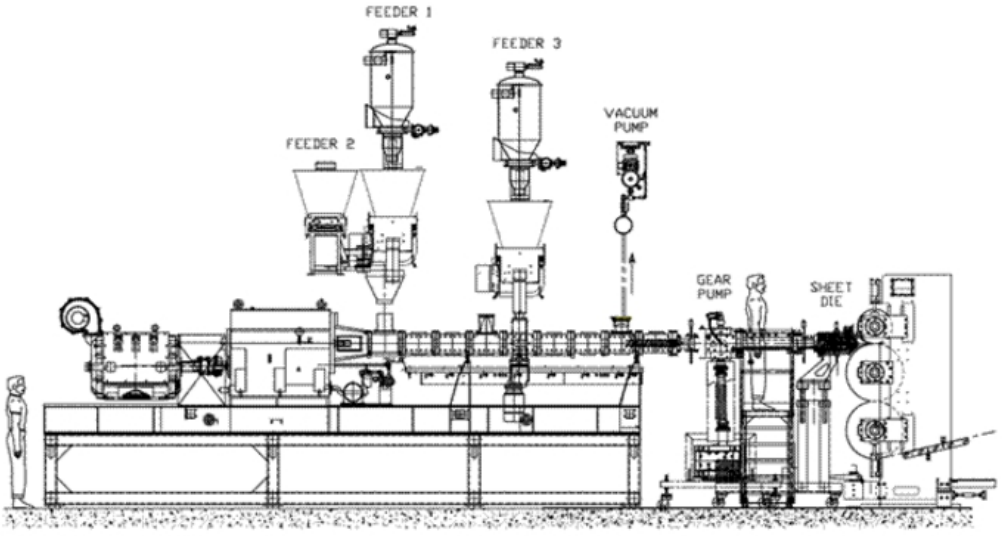

Figure 2.8: Twin-screw extrusion sheet line with downstream side feeding (www.leistritz-extrusion.com)

Understanding the twin-screw compounding process of plant fibre composites is one of the key steps on the route to a viable commercial product. It is necessary to relate the processing variables with the composite microstructure in order to optimise the final product performance.

Multiples authors showed that the processing variables affect the final properties of the extruded compound [Carneiro et al., 2000, Siaotong et al., 2010, Sombatsompop and Panapoy, 2000]. Development and optimisation of extrusion process for biocomposites also require specific challenges to be tackled that arise when working with natural fibres:

• Feeding the fibres into the barrel is a main issue because of their low density and fluffiness. Feeding masterbatches is difficult because the blend tends to separate. Side-feeding the fibres is also challenging as these tend to bridge in the hopper, which generates inconsistent feeding into the barrel.

• It is necessary to control the humidity in the barrel as natural fibres have high moisture uptake and moisture release during processing induces porosity in the final product unless efficient venting is maintained. The vacuum systems should be positioned according to the screw design and in particular the location of the kneading blocks [Giles Jr et al., 2004]. Monitoring the fibre humidity content during storage also helps to reduce moisture release.

• Natural fibres have low thermal degradation that requires the temperatures in the barrel to stay below 180°C- 200°C [John and Anandjiwala, 2008, Mohanty et al., 2001]. However, the temperature profile in an extruder is complex and results from multiple mechanisms. The materials, the extruder configuration (screw design, barrel length to weight ratio, venting and cooling zones) and the processing conditions (screw speed, barrel temperature, torque, residence time) determine the melt temperature profile in the barrel. The extruder should be configured to achieve efficient mixing and fibre dispersion without degradation of the fibres.

• Last but not least, characterisation of biocomposites may be arduous especially analysing fibre dispersion in the matrix. Estimation of the fibre length distribution is difficult as well because traditional techniques applied to synthetic fibre composites involve burning the matrix [Bowyer and Bader, 1972, Fu et al., 2000]. This method is obviously not applicable to natural fibre composites. X-Ray Micro Computed Tomography (μ-CT) enables 3D visualisation of short fibre composites and has made significant progress in the last decades [Shen et al., 2004, Stock, 1999] but few works have been published on natural fibres composites [Alemdar et al., 2008, Chinga-Carrasco et al., 2013, Etaati et al., 2014]. Limitation in resolution (typically 1μm to 5μm) and low contrast between natural fibres and thermoplatics render the analysis

difficult [Virk et al., 2010]. New generations of X-Ray nanotomographs enable higher resolution (<400nm) but these are expensive and few research laboratories own such apparatuses. Finally, image processing and quantification are complex [Miettinen et al., 2012].

When it comes to large scale production of biocomposites, only a few companies have mastered the compounding step and are selling commercial biocomposite compounds (c2renew, Automotive Performance Materials (NAFILean technology), Greencore). A major reason is the many challenges upstream of the extrusion process with which manufacturers are typically unfamiliar. Numerous research programs are conducted in Europe, Canada, South America and in other countries with an interest in this part of the bio-economy (BioStruct, UltraFibre, Naturtruck etc.). The majority of investigations have not made it past the laboratory scale. Studies are performed with small to medium extruders and usually focus on one aspect rather than on the overall production process. A complete production process also encompasses the management of material supply, storage, material preparation in large volumes and last but not least, extrusion on a large scale i.e. with large throughput. Handling big volumes of natural fibre is complicated because of their important volume to weight ratio and high sensitivity to humidity. The scale-up process is challenging, particularly for research groups with limited facilities, but this procedure is *sine qua non* for commercialisation of short fibre biocomposites. It is necessary to study the feasibility of the biocomposite extrusion at a large scale to identify the specific needs and issues that arise. Resultant information should be transmitted to the manufacturers so that extrusion production lines become competitive and biocomposites are implemented progressively into the market.

Chapter 3

Surface Characterisation

This chapter lays out firstly the materials used throughout the thesis and gives a brief overview of the effects of alkaline treatment on natural fibre properties. The second section presents the Scanning Electron Microscopy (SEM) analysis, with a comparison between the surface properties of natural fibres as received and post chemical treatment. Surface analysis by X-ray Photoelectron Spectroscopy (XPS) follows in the third section. The latter investigates the effect of fibre processing on the oxygen to carbon ratio and further analyses the fibre surface chemistry by peak fitting the high resolution spectra.

3.1 Materials

The purpose of this study was to develop and validate the capability of various experimental techniques to characterise natural fibre surfaces and, in particular, to analyse the effect of fibre processing on the surface properties. As mentioned in the previous chapters, there is a large variability of fibre properties between species and genera and as result of fibre growth conditions and processing. Since the focus of this work was on commercial exploitation of natural fibres, it was important to select fibres readily available and processed via standard methods at industrial scale to ensure traceability and reliable supply. Various types of fibres were used so that the experimental data could be representative and to enable cross comparisons. Three main varieties of bast fibres were tested: flax, kenaf and hemp. Various samples of each variety were

provided by different suppliers and in variable amounts. Cellulose fibres and a batch of cellulose pellicles produced by bacteria were also integrated to the test matrix as a reference for Inverse Gas Chromatography (IGC) and XPS. The information available regarding the fibre origins and processing steps were sometimes unfortunately incomplete among the samples. The data provided by the suppliers are reported in the following paragraphs and summarised in Table 3.1 and Table 3.2.

A Canadian linseed flax and a Chinese linen flax (varieties unknown) were supplied by Composites Innovation Centre (CIC), Winnipeg, Canada. The latter had been previously water retted while the linseed flax (unretted) had been mechanically decorticated by a lab scale scutching machine (Alcock et al. [2012]). Two kenaf samples from different origins were used: a Thai kenaf and a variety of kenaf grown in the USA. Engage Eco Product Co. Ltd (Wattana, Thailand) supplied batches of Thai kenaf variety Kohn-Kaen 60 (KK60). The fibres were locally ribbon retted for 2-3 weeks in local waterways, rinsed and dried before shipping. The other kenaf sample was supplied by Ecofibre Industries Operations Pty Ltd. (EIO), grown in Mississippi (USA) and retted (retting process unknown). Finally, a non-woven hemp mat (variety unknown) was supplied by CIC. All the samples mentioned previously were considered and labelled "as received"as per the conditions at delivery.

BioMid cellulose fibres were supplied by ENC International (South Korea). BioMid is a cellulose-based continuous filament produced from a dry-jet-wet spinning process. The feedstock is a mixture of softwood and hardwood chips, a by-product from the wood pulp and paper industry. The cellulose is extracted from the biomass and then injected through a spinneret. Cellulose films generated by *G. Xylinus* bacterial activity were used as a second reference material. *G. Xylinus* bacteria cultivated in a specific medium (Hestin and Schramm liquid medium) can produce cellulose in a similar way to plants. In the process, bacterial cellulose pellicles are extracted from the gel grown during fermentation, then washed to remove the extra bacteria and polymers and stored in a biocide solution (Dolan [2014]). This biomimetic system has been largely used to model plant cell wall mechanics (Iguchi et al. [2000], Mikkelsen and Gidley [2011]). The samples were provided by G. Dolan (ARC Centre of Excellence in Plant Cell Walls, The University of Queensland, Australia). Both BioMid and cellulose film were expected to be

pure cellulose and were hence considered as reference materials. The sample used in the study are summarised in Table 3.1.

TABLE 3.1: Samples used in the study

Sample	Supplier	Variety
Kenaf	Engage Eco Product Co. Ltd.	Thai cultivar KK60
Kenaf	Ecofibre Industries Operations Pty Ltd.	US cultivar
Linseed flax	Composites Innovation Centre	Canadian cultivar
Linen flax	Composites Innovation Centre	Chinese cultivar
Hemp	Composites Innovation Centre	unknown
Bacterial Cellulose	ARC Centre of Excellence in Plant Cell Walls	Cellulose produced by *G. Xylinus* culture
Cellulose BioMid	ENC International	Hardwood and softwood shives

As mentioned in Chapter 2, post-processing is necessary to extract the bast fibres from the plant stem and to remove extractives, lignins and pectins from the fibre surface. In this study, some samples "as recieved"were further water washed and chemically treated while others were mechanically processed. The flax and hemp fibres were treated by CIC and the kenaf (KK60) fibres were treated and post-processed on site by Engage Eco Product before shipping to Australia.

The flax, hemp and kenaf KK60 fibres were alkaline treated at different concentration in a more or less aggressive environment. Both linseed and linen flax received a "gentle"treatment (1% w/v NaOH at 78°C) compared to the hemp mat (10% w/v NaOH at 78°C). Kenaf KK60 was soaked in a solution of 1% w/v sodium hydroxide with sodium metasilicate pentahydrate ($Na_2SiO_3.5H_2O$) at 70°C. This is a standard wood treatment to extract lignin, similar to the Kraft process [Blount, 1977]. Kenaf KK60 received the most "aggressive"treatment compared to hemp and flax respectively. Finally, EIO processed the kenaf fibres using a high velocity airmill "Aximill", a system developed by the company (Morrison and Andre, 2005). The processing details, when available, are summarised in Table 3.2.

TABLE 3.2: Details on the treatments applied to the fibre samples

Sample	As received	Water washed	Post-Processed
Linseed flax	Non retted, mechanically decorticated by scutching	/	1. Scutched 2. Soaked: 1% w/v NaOH in ethanol solution (95%), at 78°C 3. Washed, oven dried at 80°C for 24 h
Linen flax	Water retted	/	Same treatment as linseed flax
Hemp mat	No data	1. Soaking in distilled water for 24 h at RT 2. Washed, air dried for 48 h	1. Water washed 2. Soaked: 10% w/v NaOH at 60°C for 2 h 3. Washed till pH=7, air dried for 48 h
Kenaf KK60	Water retted 2-3 weeks in local waterways	1. Water retted 2. Washed, dried and hammer milled	1. Water retted 2. Soaked in a alkaline solution (1% w/v NaOH, sodium metasilicate pentahydrate) at 70°C for 40 min 3. Washed, dried and hammer milled
Kenaf EcoFibre	No data	/	Mechanically processed by high velocity airmill

The following paragraphs describe the physico-chemical modifications induced by alkaline treatment on natural fibres in order to better understand the effect on the surface properties of the fibres studied and to help with the interpretation of experimental data.

Alkaline treatment, also called mercerisation, is an old process developed by John Mercer (UK) in the early 19th century to modify cellulose fibres, particularly cotton in the textile industry. The standard definition established in the ASTM D1965 refers to "the process of subjecting a vegetable fibre to an interaction with a fairly concentrated aqueous solution of a strong base, to produce swelling with resultant changes in the fine structure, dimension, morphology and

mechanical properties". This technique has been developed, applied and improved for cotton textiles. The physico-chemical transformations happening through mercerisation are fairly well understood for cotton fibres and the process has been optimised to tailor the fibre properties. The effects of mercerisation on cotton fibres have been expansively reviewed [Ugbolue, 1990, Warwicker and Hallam, 1970] and will not be detailed here. The main effects on mechanical properties are: an increase in tensile strength, a better elasticity and a higher strain at break. Cotton fibres also gain in lustre and uniformity due to the changes in the cross-section (they get more circular), to a better surface homogeneity and untwisting of the cellulose fibrils [Ugbolue, 1990].

A brief overview of the effects of alkaline treatment on cellulose fibres may help to interpret the mechanisms that occur on bast fibres. Soaking cellulose fibres in highly concentrated alkali medium induces swelling that further leads to shrinkage and molecular chain reorientation upon removal of the swelling agent. Another important structural change is the transformation of cellulose I into cellulose II [Ugbolue, 1990]. The polymorphs have slightly dissimilar crystallographic structures but the main difference is the way the cellulose chains are packed. These lie parallel to each other in cellulose I and anti-parallel in cellulose II [O'Sullivan, 1997]. In the latter configuration, the chain elastic modulus is slightly lower compared to the E modulus in native cellulose [Kroon-Batenburg and Kroon, 1997] but the effect of molecular orientation and fibre shrinkage predominate and the overall tensile properties increase [Zeronian et al., 1990].

Unlike cotton fibres that are made of ca. 90% cellulose, bast fibres contain multiple components and the overall effect of alkali treatment results from the effects on the cellulose fibrils and on the non-cellulosic constituents i.e. hemicellulose, lignins, pectins, waxes and other extractives present on the fibre surface. Consequently, immersion of bast fibres in alkali medium involves various adjunct mechanisms. It is assumed that the non cellulosic matrix [hemicellulose + lignin] is partially dissolved and so the cellulose chains pack more densely i.e. the crystallinity index increases [Bledzki and Gassan, 1999, Lefeuvre et al., 2015, Sharma et al., 1995]. This phenomenon also increases the Youngs' modulus. Gassan and Bledzki [1999a] claimed that reduction of the non cellulosic matrix, on the other hand, weakens the stress transfer to the cellulose fibrils i.e. it reduces the stress development in the fibres under tensile load. The authors mentioned that removal of lignins also affects the middle lamella because some microvoids

collapse as the lignins dissolve. This results in higher degree of plasticity and higher strain at break.

There seems to be a compromise between improving the tensile strength and strain at break and decreasing the elastic moduli, the resultant effects depending on the treatment conditions [Bledzki et al., 2004, Gassan and Bledzki, 1999a, Goda et al., 2006, Mukherjee et al., 1993, Ray et al., 2001]. Unfortunately, reviewing the literature is confusing because publications report inconsistent results. Actually, improved properties may be obtained when the treatment intensity is balanced to be efficient enough without degrading the tissues. Considering that bast fibres have a complex physico-chemical structure that varies between the species and depends as well on the fibre processing history, it is very difficult to understand and dissociate the mechanisms occurring during alkali treatment (and any other treatment) on different natural fibres. This likely explains why the results published in literature are inconsistent, poorly understood and no general claim could be established so far with confidence.

3.2 Scanning Electron Microscopy

Conventional SEM involves high accelerating voltage (typically 10 kV for natural fibre imaging) and standard detectors positioned below the lens. This configuration requires coating of the samples to avoid charging effects, which limits the capability to observe good contrast between organic samples that have low atomic numbers. In addition, high energetically charged electrons travel more than 100 nm through the surface and therefore the signal provides information from below the surface more than the very near surface.

A new generation of Field Emission (FE) SEM has been developed lately with detectors located in the column, commonly named “in-lens”, “upper”or “Through The Lens”(TTL) detectors (Figure 3.1). This specific configuration allows low voltage imaging of uncoated organic samples when operating in certain conditions to achieve dynamic charge balancing [Joy and Joy, 1998]. Under these conditions, it is possible to obtain good contrast even at low atomic number, which offers a considerable advantage for natural fibre characterisation compared to conventional SEM. The electron beam in low voltage SEM has a short depth of penetration and therefore the signal

provides information from about the first 10 nm to 20 nm and reflects the very near surface properties [Goldstein et al., 2012]. The benefits of working at low voltage also come with a few drawbacks: low resolution signal implies high signal-to-noise ratio and difficulty in focusing. Imaging is more challenging and requires a slow scan rate.

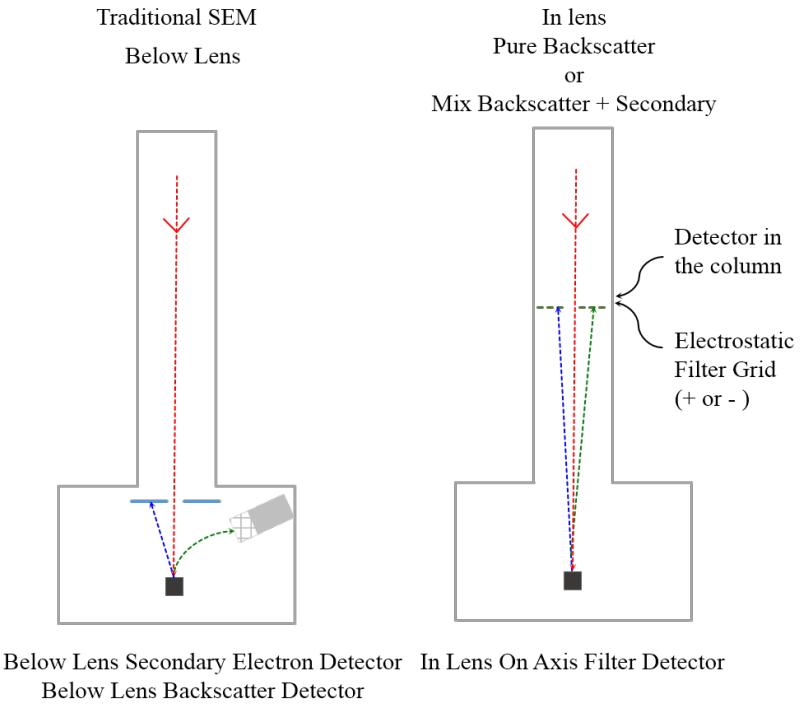

Figure 3.1: Conventional SEM with below lens SE detector and new generation FE-SEM with in-lens on axis filter detector (adapted from [Stricher, 2012])

The linseed flax (as received, alkaline treated) and the kenaf KK60 (as received, water washed and alkaline treated) were imaged with a JEOL JSM7001 FE-SEM. This SEM has an in-lens detector with a metallic grid placed above the latter that enables pure Backscatter Electron (BSE) or a combination of SE and BSE signals [Asahina et al., 2012]. The specimens were uncoated and imaged at 1.4 kV accelerating voltage with both the conventional below-lens SE detector and the JEOL in-lens on-axis Upper Electron Detector (UED). The bias filter was -200 V for the BSE mode. The micrographs obtained are shown in the following paragraphs with discussions.

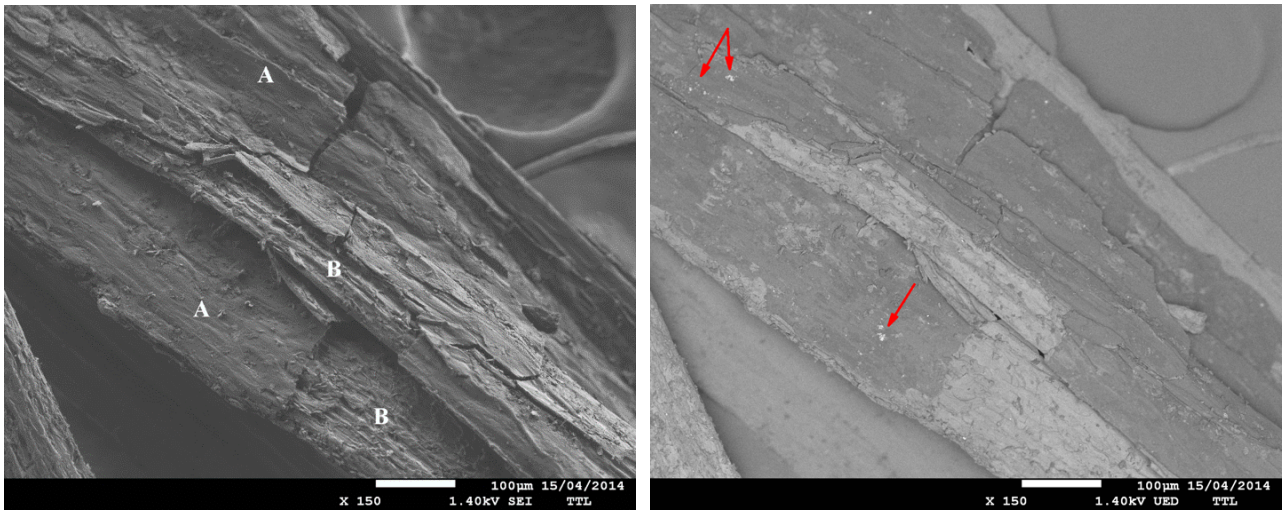

(a) (b)

Figure 3.2: SEM micrographs of flax fibres as received imaged with conventional SE detector (a) and UED detector filtering backscattered electrons (b)

The Secondary Electron Images (SEI) of the flax fibres as received show that the fibre surface was rough and contained multiple layers (Figure 3.2a). The top layer (label A) was likely the cuticle/epidermis layer, which was expected to be seen as these fibres were non retted. Dust particles and traces of epidermal particles were scattered over the outer layer surface, likely projected during scutching. The outer layer was fragmented during mechanical scutching in some areas (bottom centre and middle right of the fibre) and made visible the bast fibre bundles underneath (label B) but most of the fibre surface remained coated with a mixture of amorphous like materials, probably lignins, lipids, pectins and extractives.

Micrographs obtained with UED detector filtering the BSE reveal a clear contrast between the outer layer and the layer underneath (Figure 3.2b), with boundaries corresponding to the fragmentation pattern identified on the topographical SEI. This suggests a significant difference in the chemical composition between both layers, due to the presence of polymeric components of various average atomic numbers [Rasch et al., 2014, Truss et al., 2015]. Bast fibres contain cellulose, hemicellulose, pectins, lignins and other extractives, and each component has a specific oxygen content and average atomic number, which explains the contrast observed with BSE imaging. Cellulose has a theoretical oxygen to carbon (O/C) ratio of 0.83, hemicellulose and pectins have similar O/C given their chemical structure, pure lignins O/C averages 0.33 and

extractives have lower O/C values [Dorris and Gray, 1978a]. A scale based on the O/C ratio of each component gives the following increasing brightness sequence using the UED BSE imaging:

Extractives <Lignins <Cellulose, hemicellulose, pectins <Inorganic particles

Some spots appear much brighter than other components of the outer layer (indicated with arrows). These were likely inorganic particles from the plants such as mineral silicates. Rasch et al. [2014] observed similar features on flax fibres and performed Energy Dispersive X-Ray (EDX) analysis that confirmed traces of Si, Al, Mg, K and O in various samples. Truss et al. [2015] also identified silica, particles rich in Ca and particles rich in Si, Al, Mg, K and O on the surface of hemp fibres.

SEM imaging was performed on the fibres post alkaline treatment (Figure 3.3). The individual flax fibres can be clearly distinguished on the SEI image of the alkaline treated fibres (Figure 3.3a and 3.3b). The chemical treatment removed most of the cuticle/epidermis layer, revealing the fibres located underneath. Although fibre separation was obvious, the outer layer was still visible in some cases in the background (label A). The regular patterns transverse to the fibre axis were nodes and kinks (indicated with arrows 1). The bast fibres were still covered by scattered patches of an amorphous like substance adhering to the fibre surface that was probably a mixture of lignins remaining on the surface (indicated with arrows 2). It is common to observe residual lignin particles adhering to the fibre surface after chemical treatment [Edeerozey et al., 2007, Gassan and Bledzki, 1999b, Stuart et al., 2006].

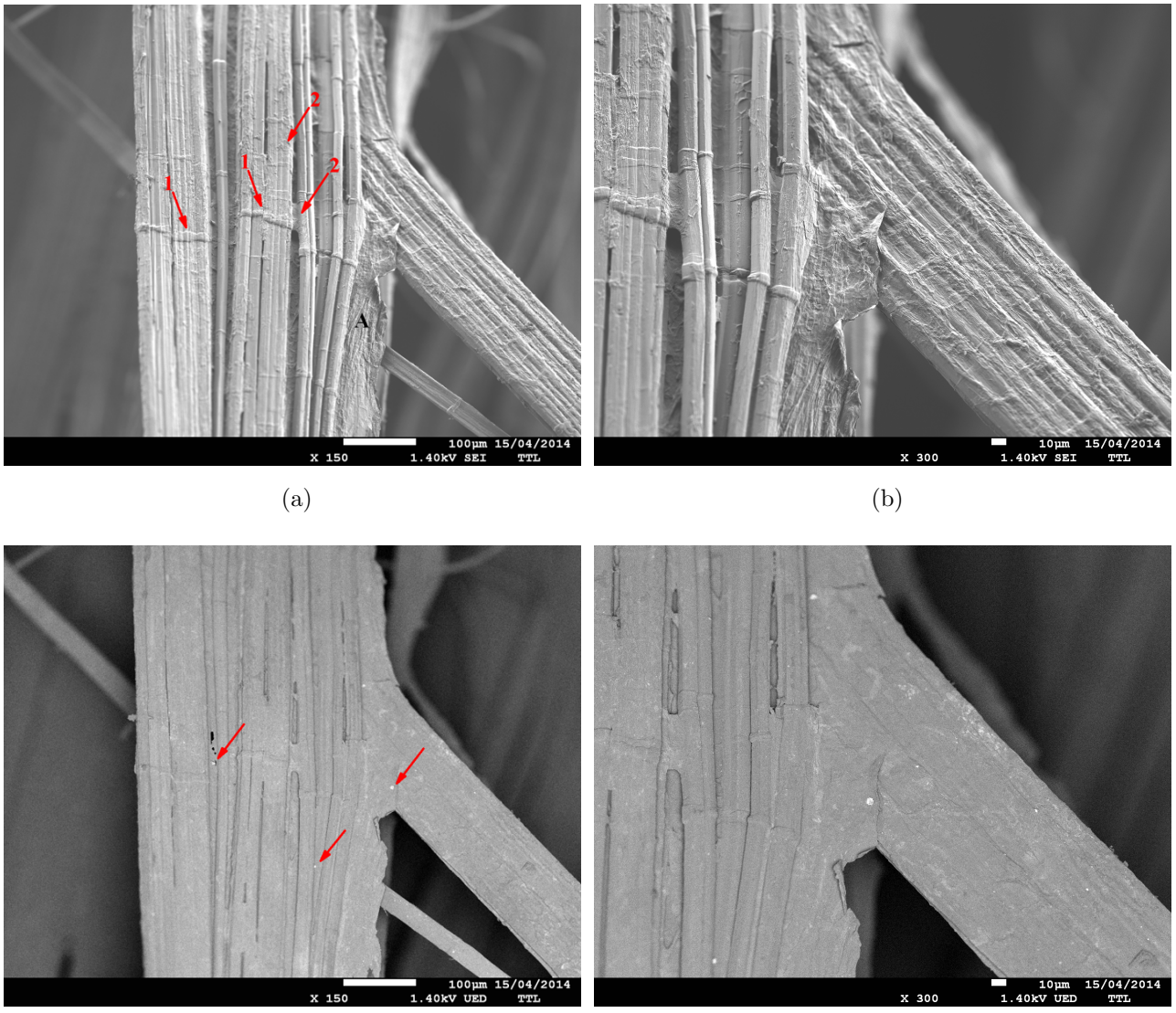

(a) (b)

(c) (d)

Figure 3.3: SEM micrographs of flax fibres alkaline treated imaged with conventional SE detector (a), (b) and UED detector filtering backscattered electrons (c), (d)

The UED BSE images of the alkaline treated fibres have low contrast (illustrated in Figure 3.3c and 3.3d), meaning that the fibre surfaces were much more homogeneous than in their as received state (Figure 3.2b). Some spots appeared slightly darker than the background fibre surface, which supports the hypothesis that these were a mixture of lignins remaining on the surface after treatment. A few bright spots were also still visible, most likely residual inorganic compounds (indicated with arrows).

Another series of experiments was performed with kenaf fibres to validate the capability of the TTL FE-SEM technique to observe the effect of chemical treatment on the fibre surface. Examples of the images obtained are given below with discussions.

The kenaf fibres as received were covered with an amorphous layer and scattered with adhering particulates, likely inorganic components (Figure 3.4a). Epidermal hairs and stomata were also visible on the surface (indicated with arrows). These are typical features of the epidermal tissue and suggest that the fibres, although water retted, were still covered with epidermal tissues. This was expected as the fibres were water retted in the field without further decortication processing. In this case, water exposure solely was insufficient to remove lignins, pectins and waxes from the bast fibre surfaces.

Three levels of contrast can be seen on the BSE images (Figure 3.4b). The sticky agglomerates observed on the SE image appeared as bright spots on the BSE image, suggesting these were inorganic compounds similar to those observed previously on flax fibres (Figure 3.2b). The two other levels of contrast are less obvious: the fibre surface was relatively homogeneous but some spots appeared darker than the background surface (indicated with arrows). The latter were probably traces of extractives un-dissolved during water retting. The fibre surface was most likely a mixture rich in lignins and waxes. The epidermal hairs could barely be distinguished from the background layer, suggesting these had a similar chemical composition to the surface layer. This is consistent with the hypothesis that the fibre surface layer contains mostly lignins and waxes compounds rather than cellulose and hemicellulose (in that case, the epidermal hairs would have appeared darker than the surface layer).

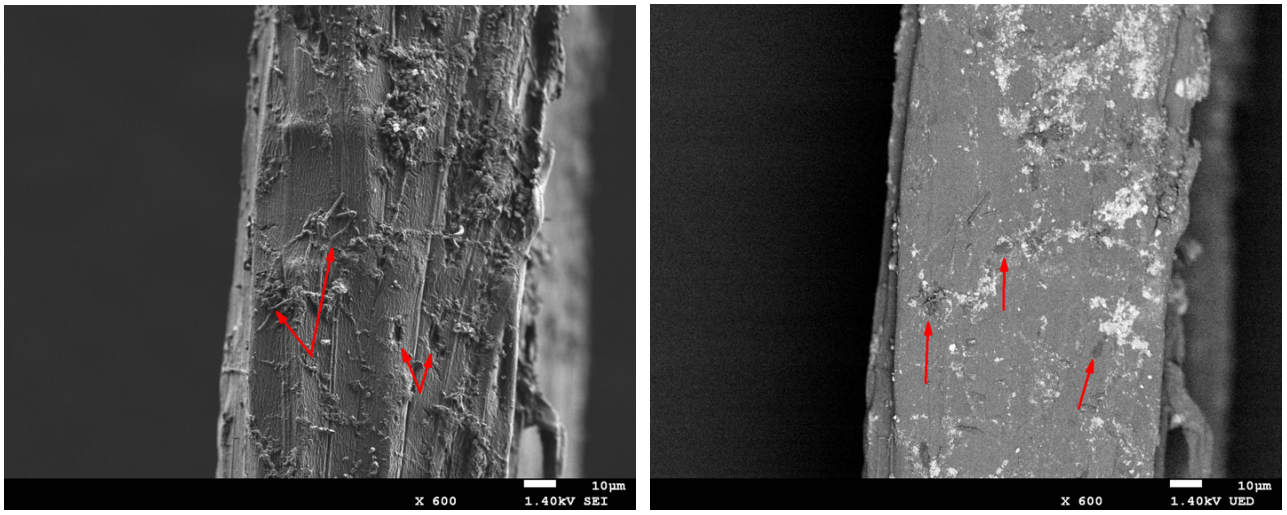

(a) (b)

Figure 3.4: SEM micrographs of kenaf fibres as received imaged with conventional SE detector (a) and UED detector filtering backscattered electrons (b)

The kenaf water washed fibres were then rinsed, dried and hammer milled. The resulting fibres were much cleaner than the previous batch and appeared relatively smooth (Figure 3.5a). Few traces of epidermal hairs and cuticle particulates could be seen but small particulates were still visible all over the surface. These seemed to be loosely attached to the fibre surface and were most likely inorganic materials deposited during the water wash process or projected when the fibres were milled. The particle features could be identified on the BSE images as they appeared much brighter than the other elements (Figure 3.5b). There was no other major contrast in the pictures except these spots, assuming the fibre surface was relatively homogeneous in terms of chemical composition. The surface layer was probably rich in lignins and waxes i.e. of similar composition to that of the background layer observed in the previous batch (Figure 3.4b). Both batches underwent water exposure only and hence the fibre surfaces were expected to be alike.

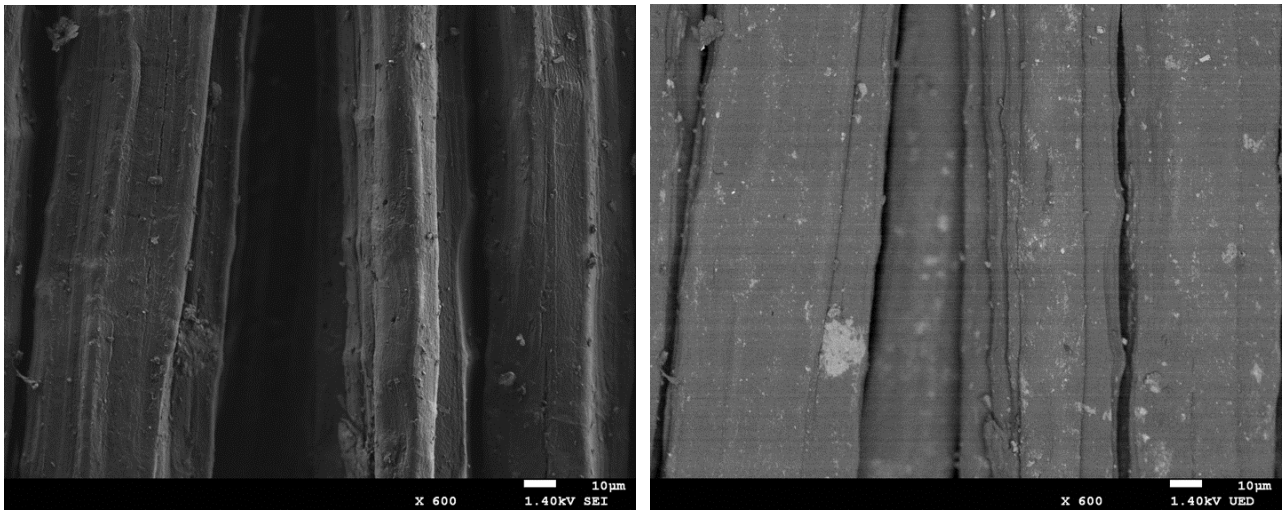

(a) (b)

Figure 3.5: SEM micrographs of kenaf fibres water washed imaged with conventional SE detector (a) and UED detector filtering backscattered electrons (b)

The third batch of kenaf fibres was water retted and then chemically treated by immersion in an alkaline solution with sodium metasilicate pentahydrate (see details in Table 3.2). SE images of the chemically treated fibres show that the outer surface layer was degraded during the process and individual fibres appeared underneath (Figures 3.6a). Although some areas were still covered with the amorphous substance layer (label A), the chemical treatment removed most of it. Note that the cover layer seemed to have been dissolved in certain zones more than others, which created a pattern. This phenomenon has been previously observed in other studies [Alvarez and Vázquez, 2006, Arsène et al., 2013, Martins et al., 2006].

The pattern was also visible on the BSE images, as illustrated in Figure 3.6b. Various levels of contrast can be seen in these micrographs. The background surface was slightly brighter than the pattern layer, confirming that the amorphous layer is rich in lignins and waxes and the surface underneath contains more cellulose, hemicellulose and pectins. This is consistent with the observations made earlier on the kenaf water retted and water washed fibre samples (Figures 3.4 and 3.5). The few bright spots visible on the surface were probably remnants of inorganic compounds deposited during the treatment, as observed in the water washed batches. A couple of dark spots were also visible on some fibres (indicated with arrows), likely traces of extractives.

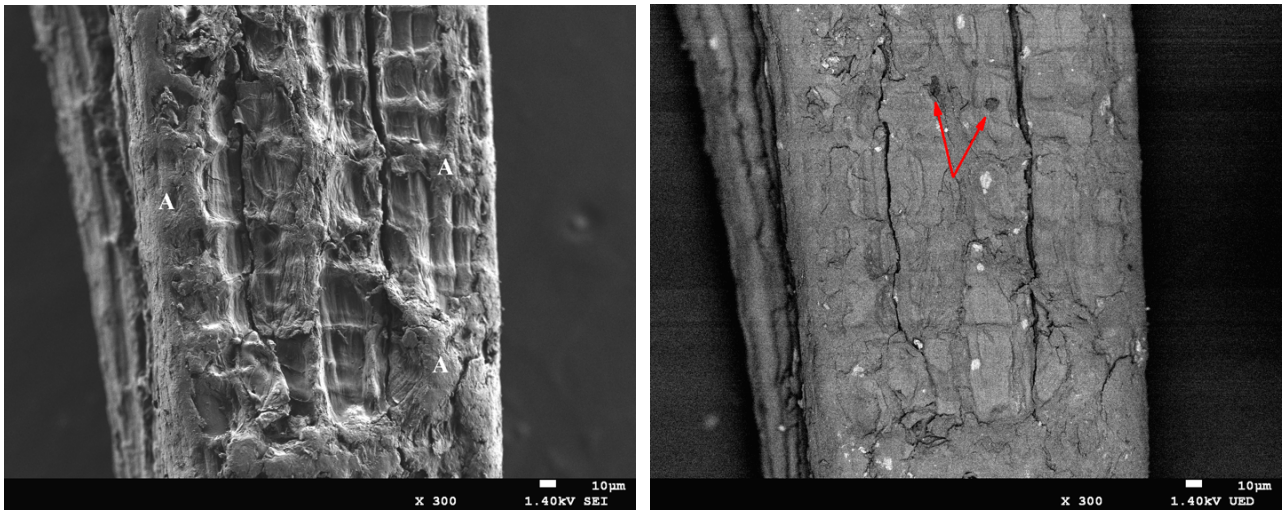

(a) (b)

Figure 3.6: SEM micrographs of kenaf fibres alkaline treated imaged with conventional SE detector (a) and UED detector filtering backscattered electrons (b)

This series of experiments performed with the new generation of FE-SEM with TTL BSE detectors demonstrated the capability to obtain good contrast between low atomic number polymeric species as well as fine topography of the very near surface. The SE and BSE images of flax and kenaf fibre samples showed clear evidence of the effect of chemical treatment on the fibre surface properties. Specific UED BSE images provided complementary information to interpret the physico-chemical mechanisms that occur on bast fibre surfaces during processing. Further experiment on XPS is needed to identify the nature of the compounds and to quantify the elemental chemical composition. This will be explored in the following section.

Chapter 3

3.3 X-Ray Photoelectron Spectroscopy

3.3.1 Theroretical background

X-Ray Photoelectron Spectroscopy (XPS) is a high resolution analysis technique to investigate the surface chemical composition of materials. XPS is nondestructive and provides high precision information ($\pm 10\%$ relative) on a small surface area (ca. 300 μm by 700 μm). Briefly, the sample under investigation is irradiated with X-Ray photons in a ultra-high vacuum chamber ($< 1 \times 10^{-8}\ Torr$). X-Rays interact with the core electrons of the material and some of these undergo elastic scattering (Figure 3.7). The emitted electrons have a kinetic energy E_k given by:

$$E_k = h\nu - E_b - \phi \tag{3.1}$$

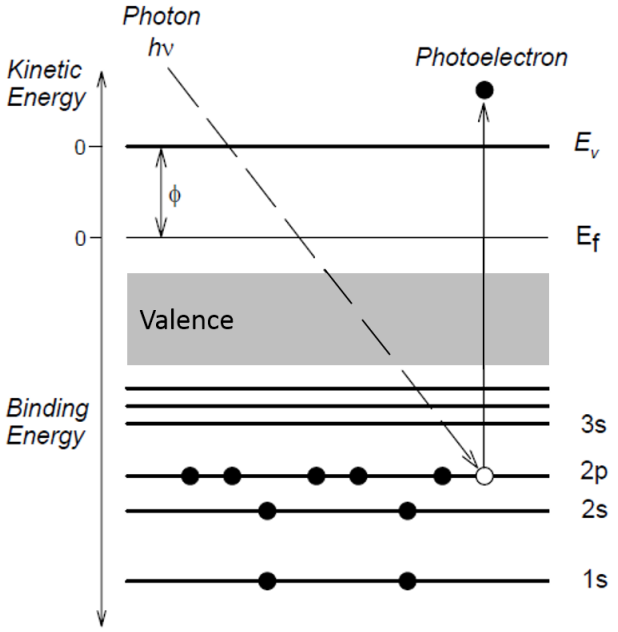

Figure 3.7: Photoelectron scattering induced by X-Ray illumination

where $h\nu$ is the photon energy, E_b the binding energy of the atomic orbital from where the electron is ejected and ϕ the work function of the spectrometer. The XPS spectrum gives the intensities of the photoelectrons (counts per second) as a function of the binding energy

E_b (eV). As the binding energy is specific to each element, it is possible to determine which atoms are present in the sample surface by measuring the kinetic energy of the photoelectron. The position and intensity of the peaks provide information on the chemistry (oxidation state) and quantitative elemental composition (>0.1 atom %) for all elements, except hydrogen and helium [Dorris and Gray, 1978b].

In XPS, the emitted photons electrons have low kinetic energy and so only those from the very near surface escape and can be detected. In other words, XPS data is representative of the near sample surface only. Hence, this technique is of particular interest for natural fibres because it involves the chemical groups that will interact directly with the polymer matrix. For comparison, XPS analysis samples ca. 2-10 nm in depth (ca. 30 first atomic layers) vs. 1-5 μm for Energy Dispersive X-ray Spectroscopy (EDX). EDX data give chemical analysis of a deeper volume that may have considerably different chemistry than the first atomic layers.

XPS analyses on natural fibres were originally performed on wood fibres and cellulose paper in the late 70s, driven by the pulp and paper industry. Dorris and Gray [1978a,b], Gellerstedt and Gatenholm [1999], Laine et al. [1994] pioneered XPS analysis with their works on wood pulps and paper. Since then, numerous studies were published on natural fibre characterisation by XPS [Johansson et al., 2004, Östenson et al., 2006, Rasch et al., 2014, Truss et al., 2015, Zafeiropoulos et al., 2003]. However, it remains difficult to establish the elemental composition and to quantify the compounds present on the fibre surface because the reference values for chemical composition found in the literature are based on dry matter and hence represent the average chemical composition of the fibre (primary wall, secondary walls, inner membrane). The fibre surface chemistry contains other specific groups (pectins, lignins, waxes, extractives) and therefore the average composition may be non representative and constitutes a poor reference for XPS analysis. It is also particularly challenging to build models for natural fibres because the elemental proportions vary between the fibre genera and species and also within a sample. All the reasons aforementioned suggest that XPS data interpretation for natural fibres is particularly problematic and should be based on the analysis of multiple specimen per sample rather than a singular specimen in order to have good confidence in the data.

3.3.2 Experimental

Two varieties of flax (linseed and linen flax), two types of kenaf (Ecofibre, KK60) and one variety of hemp were characterised by XPS. The main purpose was to check if similarities (atomic composition, oxygen to carbon ratio) could be detected between fibres from multiple varieties and different species. XPS was also performed on the fibres after treatment to assess the effect of post-processing and to compare their efficiency. In addition, both cellulose samples (BioMid® and bacterial cellulose) were characterised and used as reference materials. A minimum of three runs and up to 11 runs were performed on each sample to ensure average representative values. A summary of the test matrix is presented in Table 3.3. Survey scans were performed on all specimens and kenaf KK60 were further characterised with high resolution scans.

Table 3.3: Samples studied by XPS

Sample	As recieved	Processed
Bacterial cellulose	/	/
Cellulose BioMid®	/	/
Linen flax	Water retted	Scutched + alkaline treated (gentle)
Linseed flax	Non retted, scutched	Scutched + alkaline treated (gentle)
Kenaf Ecofibre	No information	Mechanically processed by high velocity air mill (Aximill)
Kenaf KK60	Water retted	Water washed + alkaline treated (aggressive)
Hemp	No information	Water washed + alkaline treated (gentle)

The specimen were characterised with an XPS Kratos Axis ULTRA at the Centre of Microscopy and Microanalysis (CMM). The X-Ray source was monochromatic Al Kα. The advantages of using an X-Ray monochromator rather than a conventional source (achromatic) include a reduced background, better resolution and no satellite peaks. The binding energy steps for survey scan and high resolution scan were 1 eV and 0.05 eV respectively. The analyser pass energy (intensity resolution) was 160 eV for survey scans and 20 eV for high resolution

scans. The fibre samples were mounted on a bar (see Figure 3.8) and loaded under vacuum overnight to reach Ultra High Vacuum (UHV) conditions ($< 1 \times 10^{-8}$ $Torr$). These vacuum conditions are necessary to detect electrons, avoiding scattering of the photoelectrons from residual gases between the detector and the sample surface. Conditioning the sample overnight enables to eliminate residual water molecules that adsorbed on the chamber walls. Data analysis was performed with CasaXPS v.2.3.12 and the Kratos Library to identify the elements. The correction factor was 2.8 eV. The calibration for peak fitting was set up for C-C bond at 285 eV.

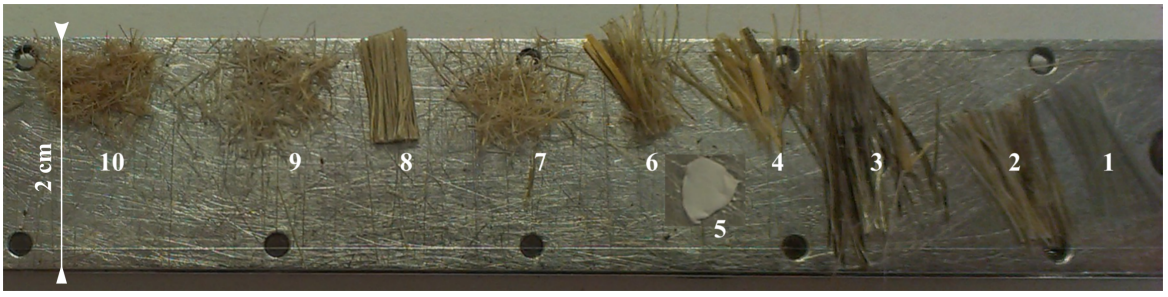

Figure 3.8: Samples mounted for XPS analysis. 1: BioMid®, 2, 3: linen flax as received, NaOH treated, 4,6: linseed flax as received, NaOH treated, 5: bacterial cellulose, 7: kenaf Aximilled, 8, 9, 10: kenaf Engage as received, water washed, NaOH treated

3.3.3 Results and discussions

Three levels of discussions are presented below. Firstly, the analysis based on the data from survey scans is presented to compare the O/C ratios of multiple fibres, as received and post treatment. The second part discusses the evolution of O/C ratio of hemp and kenaf fibres at different stages. Finally, an analysis of the high resolution scans of kenaf KK60 is presented to identify the chemical groups and discuss the evolution of the surface composition due to chemical treatment.

The average chemical compositions and the O/C ratio of the fibre samples are listed in Table 3.4 and illustrated in Figure 3.9.

TABLE 3.4: Chemical compositions of the sample surfaces obtained by survey scans

Sample	C	O	N	Ca	O/C	Trace others
Cellulose theoretical					0.83	
Bacterial cellulose	57.5	42.2	0.4		0.73	N
Cellulose BioMid®	75.5	23.4	0.8		0.31	Ca, Na
Linen flax as recieved	85.7	13.0	1.1		0.15	Ca
Linen flax NaOH treated	72.1	24.7	2.3	0.9	0.34	
Linseed flax as recieved	81.6	16.6	1.9		0.20	
Linseed flax NaOH treated	69.2	26.1	3.3	1.4	0.38	Ca
Kenaf Ecofibre as recieved	76.5	19.8	3.8		0.26	
Kenaf Ecofibre Aximilled	72.0	25.3	2.2		0.35	Ca, Mg
Kenaf KK60 as recieved	76.4	21.1	2.4	Traces	0.28	Ca, Si
Kenaf KK60 water washed	72.3	24.5	2.1	Traces	0.34	Ca, Si, Al
Kenaf KK60 NaOH treated	66.4	29.0	1.8	Traces	0.44	Ca, Si,Na
Hemp as recieved	72.9	23.3	3.8	Traces	0.32	
Hemp water washed	71.9	25.4	2.7	Traces	0.35	
Hemp NaOH treated	65.5	32.4	1.8	Traces	0.49	

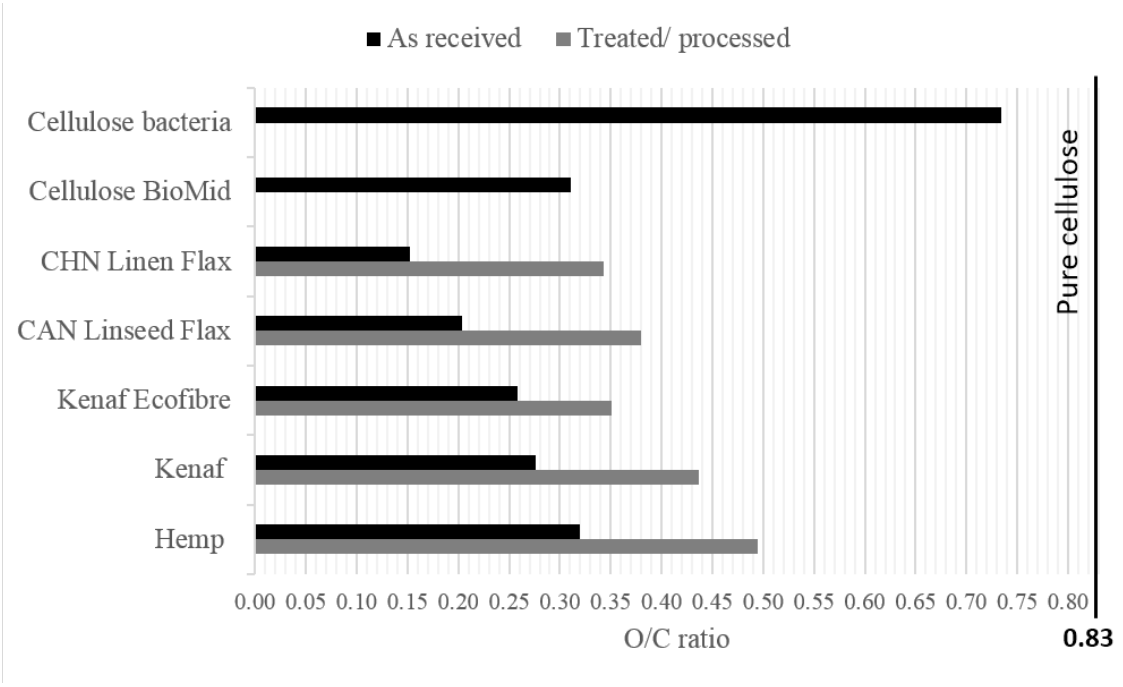

Figure 3.9: O/C ratios of the fibre samples as received and after treatment

Firstly, the O/C ratios obtained from the fibres as received were far lower than the O/C ratio of pure cellulose (0.83), indicating that the fibre surfaces contained several components other than cellulose. This was expected, given the composition of bast fibres, and the values obtained agree well with XPS data found by previous authors. Sgriccia et al. [2008] observed higher O/C ratio for kenaf fibres (0.45) than for hemp (0.27) and flax fibres (0.19). Tserki et al. [2005] reported similar O/C values for hemp (0.26) and slightly higher values for flax (0.24) but other authors reported low O/C values for flax fibres. Stricher [2012] analysed flax LINEO® fibres and estimated an O/C of about 0.19 and Csiszár et al. [2013] found O/C of 0.16. Zafeiropoulos et al. [2003] studied green flax and dew retted flax with XPS and found O/C ratios of 0.22 and 0.25 respectively. The authors claimed that these low O/C values resulted from a surface rich in waxes and lignins.

Cellulose BioMid® surface displayed a ratio O/C of 0.31 that is far from the theoretical ratio of pure cellulose. The surface seemed rather similar to kenaf and hemp (both are produced also at industrial scale) with a O/C ratio of 0.28 and 0.32 respectively. The cellulose paper-like surface produced from bacteria showed an average O/C ratio of 0.73 that is much closer to pure cellulose. Dorris and Gray [1978b] and Andresen et al. [2006] found similar values on XPS analysis of cellulose fibres from filter paper (0.79 to 0.83 and 0.74 respectively). In the current study, a set of three cellulose samples from different production batches have been analysed and showed similar values from 0.70 to 0.75, hence the average value was assumed to be representative. A possible sample contamination with carbon may have induced the slightly lower values than that of pure cellulose and is often observed on cellulose samples [Johansson and Campbell, 2004]. Traces of nitrogen were detected in one of the specimen, which suggested residual bacteria on the sample surface. Bacteria contain multiple intracellular organic molecules including proteins, made from chains of amino acids that contain amine groups [Carpita and Gibeaut, 1993, Cosgrove, 1997].

Fibres subjected to milling have seen their O/C ratio increased by ca. 35% that could be explained by the fibre breaking and defibrillation. In an Aximill, the fibres are exposed to high velocity air flow that generates two reverse cyclones leading the fibres bundles to break and separate as they impact each other and the chamber wall. The epidermal tissues and cuticle attached to the fibres were also likely removed during dry milling. These epidermal tissues had low O/C ratio, which explains the increase in O/C observed after the Aximilling process. This

mechanical process seemed to have less impact on the fibre surface properties than the alkaline treatments. The O/C ratio increased by 50% minimum after alkaline treatment and by 35% only after the Aximilling process. However, the comparison between both processes should be done with caution. The surface may have been modified to different levels (depth) and in various aspects; not only chemically but structurally (surface roughness, degree of separation) and a comparison based on survey scan only could be misleading.

The effect of alkaline treatment on O/C ratio was clear for all specimens: O/C increased considerably by more than 50% on hemp fibres and up to 125% on flax fibres. It would be incorrect to compare directly the chemical compositions between the specimens because the alkaline treatments applied were different. Kenaf KK60 fibres were subjected to an aggressive treatment with sodium silicate and caustic soda while the flax fibres were immersed in a more gentle alkaline solution. Hemp fibres were treated with an intermediate alkaline solution. This will be discussed in detail later.

At this level, based on survey scan data, interpretation of the chemical composition evolution is anything but straightforward because the mechanisms involved may be different and might still result in similar O/C values (linen flax and kenaf Ecofibre for example).

The highest O/C ratio increase has been observed on the flax fibre specimens, with an augmentation of 90% and 125% for the linseed and the linen flax respectively. The variability between the two types of flax subjected to same treatment is of particular interest. This could be related to the fibre properties in their as received state: both fibre surfaces showed different O/C ratios (0.15 for linen flax vs. 0.20 for linseed flax). This was expected as flax grown for seeds and linen flax go through different cultivation routes. Linseed flax culture maximises seed yield hence harvest occurs at full seed maturity whereas flax linen is harvested earlier for optimal fibre quality [Bismarck et al., 2005]. Bast fibre structure and chemical composition are closely related to plant maturity and the linseed and linen flax fibre surfaces differ in both chemistry and physical structure [Akin, 2012]. Also, linseed flax stems are thicker and more difficult to extract than flax linen stems. In our study, the linseed flax fibres were unretted and extracted by hammer mill. This mechanical process is aggressive on the fibres and likely induced kinks that act as stress concentration points and are preferential sites for chemical reaction [Hänninen et al., 2012]. Unretted fibres likely contain more pectins, waxes and non-cellulosic molecules

than the water retted fibres [Akin, 2012]. For all the reasons aforementioned, it was expected that alkaline treatment may alter the fibres in different ways. Note that the O/C ratio of linseed flax sample as received was lower than the O/C values usually attributed to fibres rich in lignin (at maturity) which range around 0.30 or above [Johansson, 2002]. Morvan et al. [2003] previously questioned the amount of lignin and its location in flax fibre walls. The O/C ratio observed in this study suggests the predominance of extractives and pectins on the surface as the fibres were not retted. Extractives are indeed much richer in carbon than polysaccharides and have lower O/C ratios. For instance, Laine et al. [1994] found O/C values of about 0.12 in wood pulp.

Note that these observations are not exclusive to this study but can be extended to the discussions about natural fibre treatment analysis in general: it does not make sense to compare composition values and O/C ratios without minimal amount of information on the sample (variety, growing conditions, harvest, retting, post- processing). A proper traceability brings clues to avoid incoherent assumptions and to support data interpretation.

3.3.3.1 Effect of water wash and alkaline treatment on kenaf and hemp fibres

Figure 3.10 shows the survey scan spectra of kenaf and hemp fibres at different stages; as received, water washed and alkaline treated. The overlays highlight the specificities of each spectra to detect the presence of singular elements. It is preferable to compare the spectra with the peak ratios rather than the peak amplitudes because the base line varies between the runs and so does the signal intensity. The latter depends to some degree on the sample surface profile, which is particularly true for natural fibres specimens that lay down in bundles like a nest on the XPS stage.

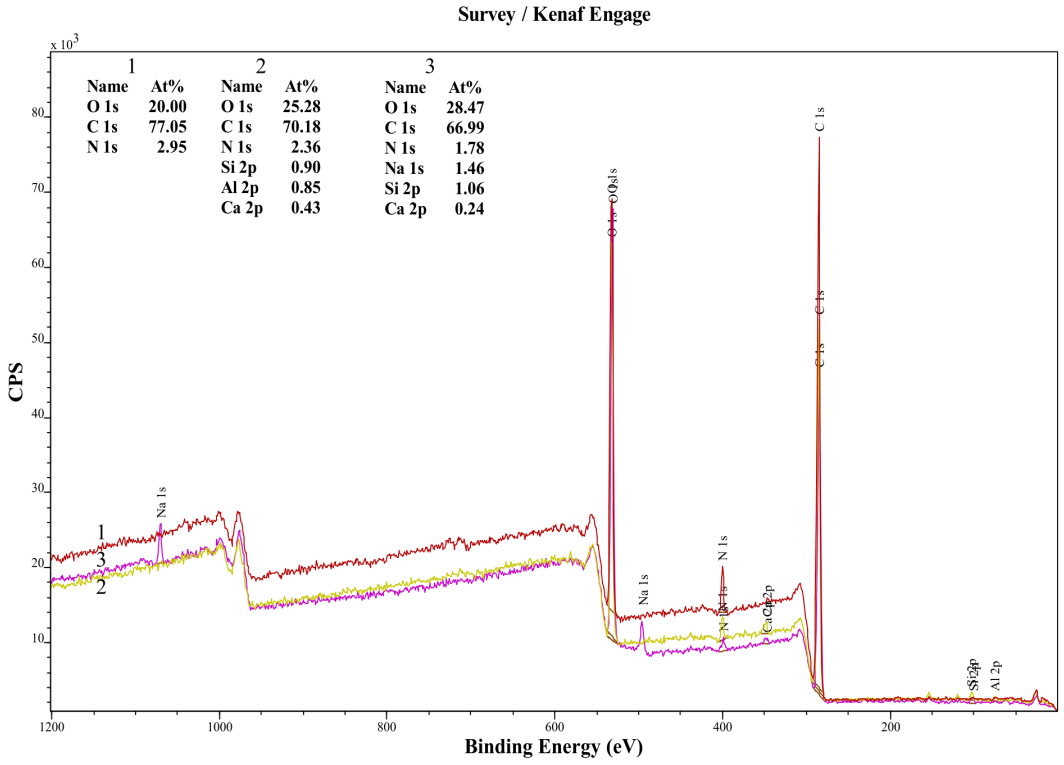

(a)

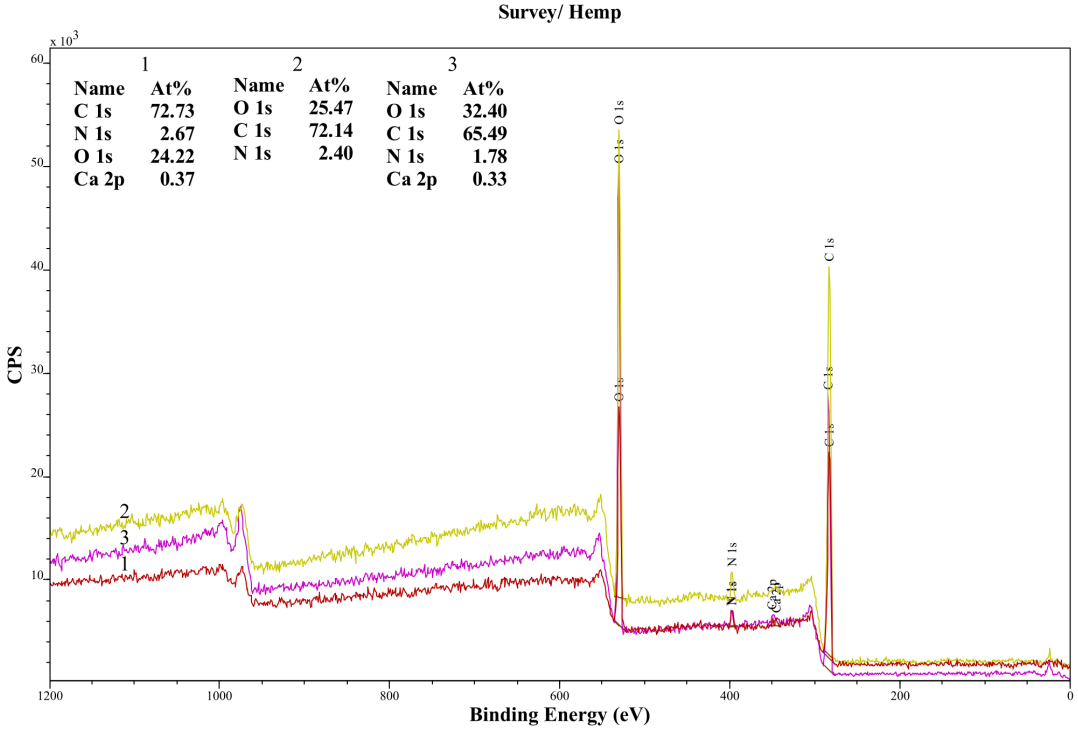

(b)

Figure 3.10: Survey scans of (a) kenaf and (b) hemp fibres at different stages: 1. As received, 2. Water washed and 3. Alkaline treated

No traces of silica, calcium or aluminium were detected in the specimen of kenaf as received showed in Figure 3.10a but multiple runs were performed and these elements appeared in traces in other samples (four specimens from 11). Two of the hemp fibre samples also showed traces of calcium. Calcium can play a key role in the bast fibre structure: calcium molecules cross-link the non-methoxylated carboxyl groups of the glucose acids in pectin to form stable bridges between the pectin molecules [Preisner et al., 2014, Sakai et al., 1993]. Calcium could also be present as calcium carbonate, oxylate, or it could come from aluminosilicates; these compounds are present in plant soils and traces are usually found in plant composition [Curtis N., 1998]. The small amount (ca 1.5 at.%) of sodium detected in the alkali treated fibres was assumed to be a residue from the chemical treatment even though the fibres had been washed. XPS is very sensitive to sodium; Na 1s has a relative sensitivity factor six times higher than C1s (Kratos library Relative Sensitivity Factors in CasaXPS) therefore a very small amount of sodium will be obvious in the spectrum. The alkaline treatment applied to the hemp fibres included water washing till neutral pH and thus no trace of sodium was expected.

The evolution of the O/C peak ratio after water wash and alkaline treatment is an indicator to gauge the effect of chemical treatment. Figure 3.11 shows the ratios of kenaf Engage and hemp fibres at different stages. After water wash, hemp and kenaf fibre surface O/C ratios slightly increased by 10% and 20% respectively. Immersion in water could have removed the cuticle material (low O/C), pectins (high O/C due to glucose rings) and some proteins (low O/C due to long carbon chains) from the fibre surface but was unlikely to affect lignin. Evolution of the O/C ratios results from the combination of these mechanisms and it is difficult to distinguish which one was dominant. The gentle increase in O/C ratio reflects these phenomena, as species with low O/C and high O/C were removed, and might not be a signature for more cellulose established on the surface. These results agree well with the SEM analysis (ref section 3.1): the water washed kenaf fibre surface was still rich in lignin and waxes and poor in cellulose (Figure 3.5). Truss et al. [2015] performed TTL SEM analysis on the hemp fibres and also observed that the water washed fibre surface was still rich in lignin and extractives.

Note that the trend is coherent with the treatment intensity: the kenaf fibres have been soaked for up to three weeks whilst the hemp fibres were immersed in water for 24 h only. Fibre separation and degradation mechanisms occur with time i.e. the longer the fibre are soaked,

the more they tend to separate, facilitating the biodegradation of the components [Paridah et al., 2011].

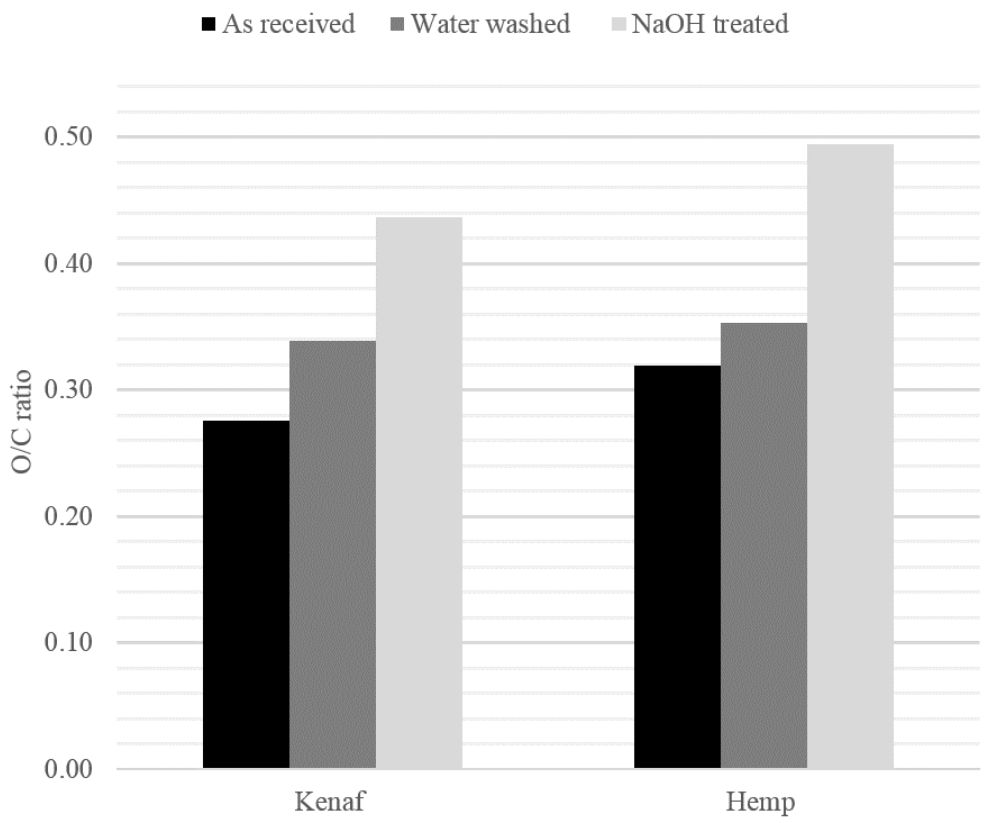

Figure 3.11: Evolution of O/C ratios of kenaf KK60 and hemp fibres after treatment

After alkaline treatment, the O/C ratio increased by 53% for hemp sample and by 57% for kenaf sample, compared to the as received stage. The alkaline treatment applied to the kenaf batch contained sodium metasilicate and caustic soda whilst the hemp batch was immersed in a solution based on NaOH only, but at higher concentration. Kenaf fibres were soaked for 40 min at 70°C and hemp fibres were immersed for 2 h at 60°C (see Table 3.2). Both alkaline solutions were then assumed to be of equivalent degree and lead to a similar increase of the O/C ratio by ca. 50%. Such an increase of the O/C ratio suggests more cellulose on the fibre surface (highest O/C of 0.83) and less amorphous substances that have lower O/C than cellulose i.e. lignins, waxes, extractives etc. This assumption is consistent with the SEM observations that revealed surfaces with proportionally more cellulose compared to the as received and water washed fibre surfaces, for both the kenaf and hemp fibres (see section 3.1 and the results from Truss et al. [2015]). However, the O/C ratios were still much lower than the theoretical value of cellulose:

hemp fibres had an O/C of 0.49 and kenaf 0.44 compared to 0.83 for pure cellulose. This agrees as well with the SEM results that showed in both cases the alkaline treated fibre surfaces were still rich in lignins and extractives.

It is worth noting that a comparison based solely on the O/C ratio absolute values could be misleading. For instance, both water washes seemed to produce the same effect on the fibres (hemp O/C ratio reached 0.35 and kenaf O/C ratio was 0.34 after water wash) and alkaline treatment seemed to be more efficient on hemp than on kenaf (final O/C was 0.49 and 0.44 for hemp and kenaf respectively). However, as mentioned previously, discussions based on the O/C values only should be treated with caution because similar O/C can be obtained from different surface chemistries. Information on the fibre as received (origin, processing) and details on the chemical treatments largely helped to interpret the data. For a better understanding of the fibre surface chemistry and to validate the assumptions made, further analysis with high resolution scans is needed.

3.3.3.2 High resolution scans

High resolution scans were performed over the main elements of interest to study their "chemistry" and deduce which chemical functional groups were present on the sample surface. These scans give information on the chemical shift; the change in Binding Energy (BE) of a core electron due to a change in chemical bonding of that electron. Core binding energies are determined by the electrostatic interactions between the core and the nucleus. Binding energies are reduced or increased depending on whether a valence electron charge is withdrawn or added respectively. Hence, for each element, secondary peaks appear at specific binding energies corresponding to different chemical bonding. These peaks can be dissociated from each other and identified by peak fitting the XPS spectra.

In practice, the XPS spectra is fitted with a series of single peaks positioned so that the sum envelope fits the experimental curve. Each single peak can be (and should be) attributed to a chemical bonding by identification with the corresponding element BE. References for C1s, O1s and N1s binding energies can be found in the literature (Beamson and Briggs [1992], Ratner and Castner [2009]) and a large database established by the National Institute of Standards

and Technology (NIST) is available online (srdata.nist.gov). Note that the chemical shifts may vary slightly depending on the chemical environment of the atoms i.e. in complex molecules. This is particularly true for natural fibre surfaces as these contain various polysaccharides and other extractives components that comprise aromatic groups. A comprehensive peak fitting of the main elements (C, O and N) should provide key information to identify which functional groups are present (or not) on the sample surface.

Peak fitting is powerful but it is a difficult task since peak deconvolution must be fastidious to be correct (Artyushkova [2010]). Peak fitting can have shallow minima so several options may have similar goodness of fit. However, peak shapes and widths are not arbitrary but rather follow models built on physics (Gaussian- Lorentzian shape etc.). Hence, specific rules and criteria apply to ensure the curve fit is coherent, reproducible and as accurate as possible. Four essential rules have been established (Artyushkova [2010], Beamson and Briggs [1992]):

• All peaks within the same element should have the same ($\pm$ 0.2 eV) Full Width Half Maximum (FWHM). In complex molecules, tolerance up to $\pm$ 0.5 eV may be justified.

• When comparing multiple samples from the same specimen (for instance fibres before and after treatment), the reference sample is first curve fitted and the other spectra are fitted following the same constraints. The BE and FWHM should be constrained to $\pm$ 0.2 eV. New peaks are added if necessary.

• If there is no reference sample, one sample is taken as a reference and the other spectra are curve fitted with the constraints mentioned above.

• Cross correlation between the elements is a key indication to verify that the deconvolution is coherent. For example, if the peak representative of C-N=O bond is identified in the C1s spectrum, it should be present as well in N1s and O1s spectra.

The following case study focuses on the kenaf fibre samples. High resolution scans were performed on C, O and N. Peaks were curve fitted with CasaXPS software according to the criteria mentioned previously (BE, FWHM). The alkaline treated fibre sample was taken as a reference assuming that it would be the "simplest" among the three samples because the peaks were sharp and distinct. The peak fitting model was then applied to the water washed fibre sample

and the fibres as received. The C1s spectra of kenaf KK60 fibres alkaline treated is presented in Figure 3.12.

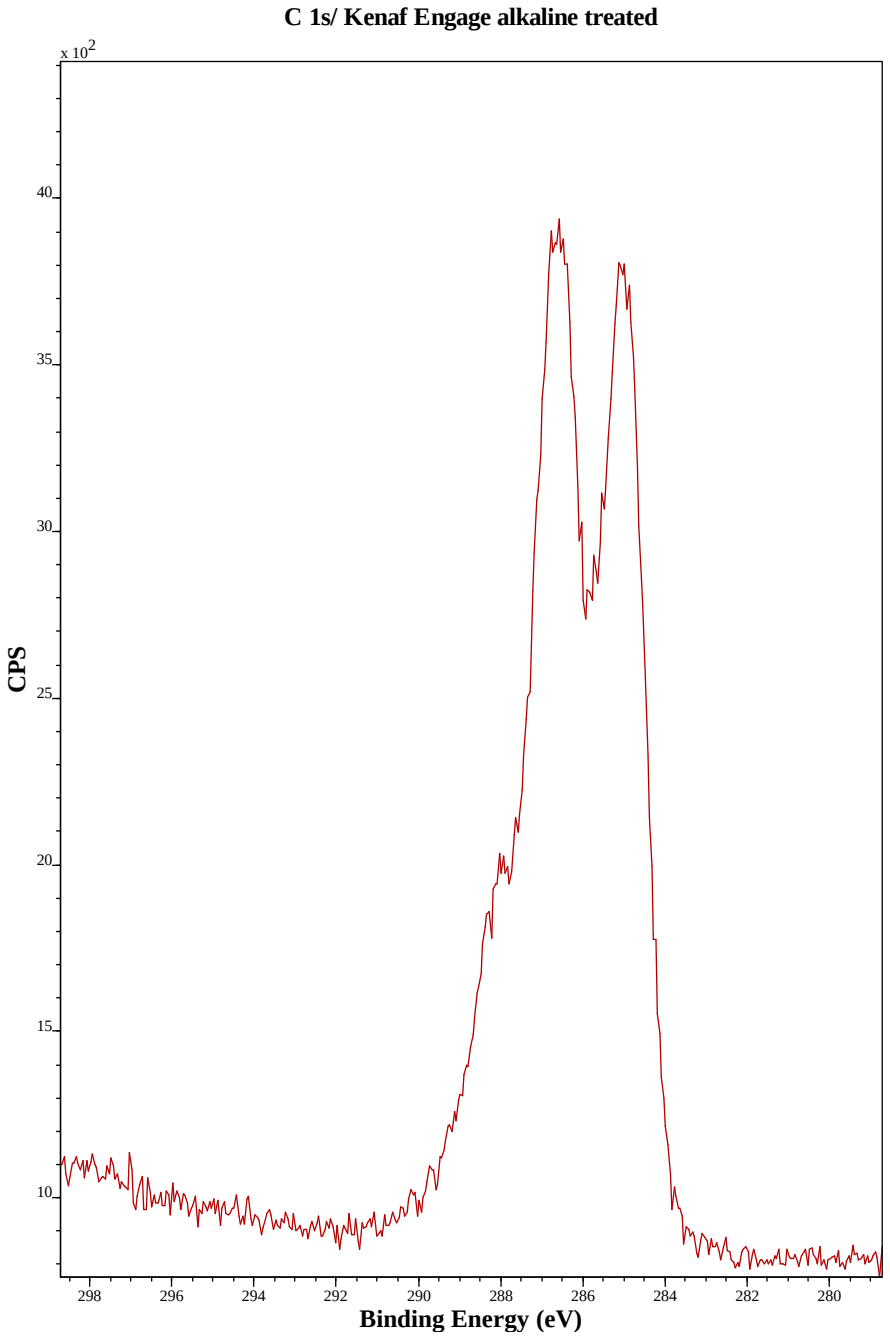

Figure 3.12: C1s spectra for kenaf fibres alkaline treated

Listing the chemical groups likely to exist on the fibre surface is useful to build up a coherent peak fit model. The kenaf fibre surface was assumed to contain cellulose, hemi cellulose, pectins, lignins, fatty acid and water. The function carboxyl, ester and amide present in pectin as well as the functional groups from lignins were expected to be seen on the XPS spectra.

Cellulose is a linear chain of repeated polysaccharide units of D- anhydroglucocypranose. The molecular structure is shown in Figure 3.13. There are two types of carbon bonding in cellulose: carbon bonded to a single O (labelled 1) and carbon bonded to two non-carbonyl oxygen atoms (labelled 2). Beamson and Briggs [1992] and Briggs and Beamson [1992] analysed pure cellulose (Whatman filter paper) and came up with BE of 286.53 eV - 286.73 eV and 287.86 eV - 288.06 eV respectively. Pure cellulose XPS spectrum theoretically contains only these two peaks but a third peak from C-C bond usually appears due to sample contamination and impurity [Johansson and Campbell, 2004]. The oxygen spectrum consists of two peaks at 532.93 eV (corresponding to OH, labelled 1) and 533.51 eV (corresponding to C-O-C, labelled 2).

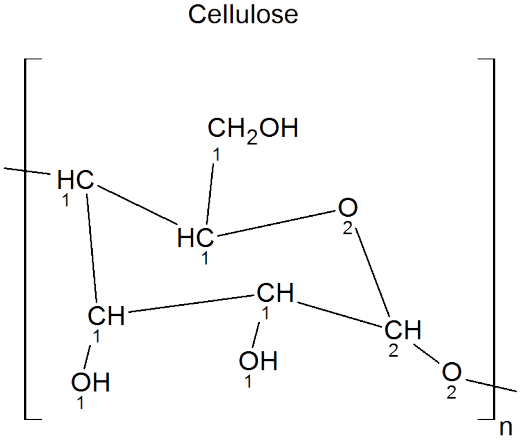

Figure 3.13: Cellulose structure

Hemicellulose is a branched chain of multiple polysaccharides. Its bonding structure is similar to cellulose but the functional groups vary between the different types of sugar. Gutiérrez Suárez et al. [2010] and Neto et al. [1996] studied the chemical composition of hemicellulose in kenaf plants and claimed that kenaf bark hemicellulose (i.e. where the bast fibres are located) was particularly rich in xylose (a pentose with five carbon atoms). Xylose contain numerous hydroxyl group substitutions so a large peak at OH binding energies (286.47 eV - 286.73 eV for C1s and 532.74 eV - 533.09 eV for O1s) may appear on high resolution spectra of a sample surface rich in hemicellulose [Beamson and Briggs, 1992].

Pectins's structure is similar to hemicellulose but contain random sequences of three functional substitutions, as shown in Figure 3.14. The carboxyl, amide and ester substitutions should give specific peaks in the XPS high resolution spectra. The C1s chemical shift associated to carboxyl substitution should be observed at 289.18 eV - 289.26 eV. Amide functional group induces chemical shifts at 287.97 eV - 288.59 eV and ester substitution should be seen at 286.12 - 286.98 eV with a secondary peak at ca. 285.4 eV (carbon bonded to C=O) [Beamson and Briggs, 1992].

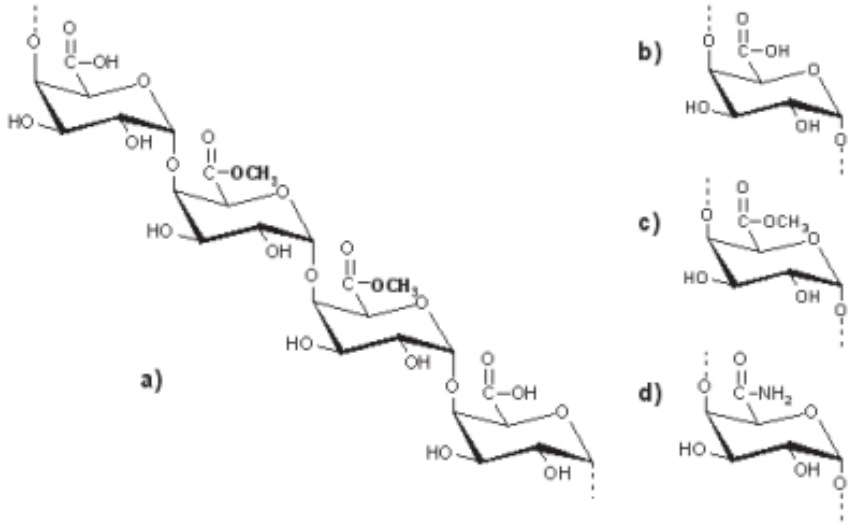

Figure 3.14: a) repeating segment of pectin molecule and functional groups b) carboxyl, c) ester and d) amide in pectin chain [Sriamornsak, 2003]

Lignin(s) is a complex polymer whose structural composition varies in each plant species. Lignin is built up from three monolignol precursors (phenylpropane units) that react via enzyme-initiated dehydrogenative polymerisation [Santos et al., 2013]. The three building blocks are p-coumaryl, coniferyl and sinapyl alcohols (Figure 3.15). The proportion of each structural block varies between plant species, making lignin a complex random network polymer. Lignin is classified into three families depending on the phenylpropane unit ratios: guaiacyl(G) lignin comprised mostly coniferyl groups, guaiacyl-seringyl (G-S) lignin is a copolymer of coniferyl and sinapyl alcohol and H-lignin contains mostly p-coumaryl alcohol units. G-lignin is dominant in softwoods (gymnosperms) and G-S lignin in hardwoods (angiosperms). Both

softwoods and hardwoods contain small amount of H-lignin but this third type of lignin is mainly found in grass plants (graminaceous).

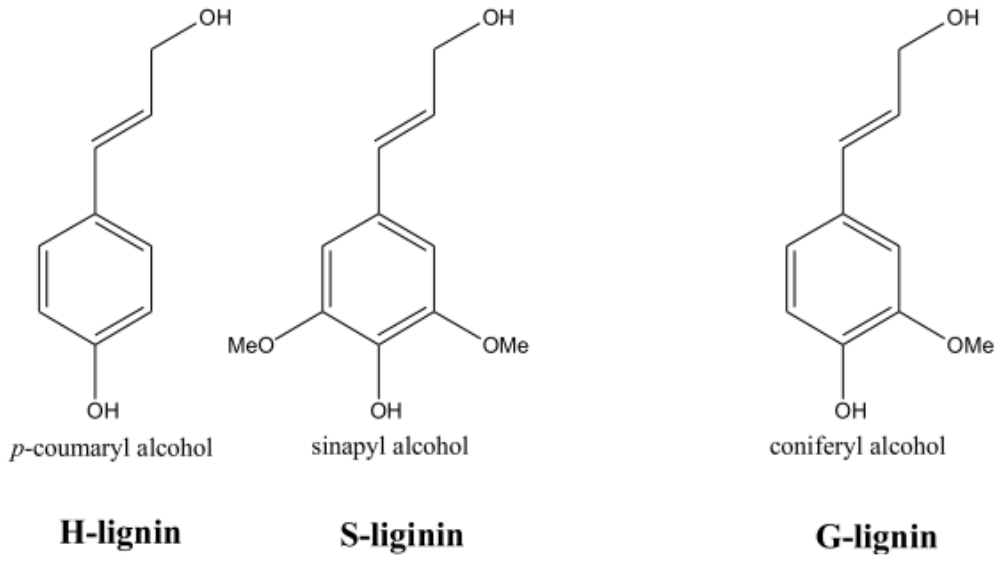

Figure 3.15: The three types of monolignols responsible for lignin synthesis: p-coumaryl alcohol, sinnapyl alcohol and coniferyl alcohol (adapted from Santos et al. [2013])

Bast fibres belong to the angiosperms group and various authors reported that kenaf lignins present similarities with hardwood lignins that has a high S:G ratio i.e. a dominant methoxy substitution on the aromatic rings [Neto et al., 1996, Ralph et al., 1995]. During polymerisation, numerous linkages occur randomly between the phenylpropane units creating a large network with a complex and unique three dimensional structure. As listed in Table 3.5 and illustrated in Figure 3.16, the predominant linkages in hardwood lignins are aryl ethers (β-O-4) and 5-5 linkage, with a majority of β-O-4 linkage (60%). Based on these findings, these types of ether linkages are expected to be seen on the spectra.

TABLE 3.5: Predominant linkages in lignins in softwood (SWD) and hardwood (HWD) (from Santos et al. [2013])

Linkage type	Dimer structure	%Linkage SWD	%Linkage HWD
β-O-4	Arylglycerol β-aryl ether	45-50	60
5-5	Biphenyl and Dibenzodioxocin	18-25	20-25
β-5	Phenylcoumaran	9-12	6
β-1	1,2-Diaryl propane	7-10	7
α-O-4	Phenylpropane α-aryl ether	6-8	7
4-O-5	Diaryl ether	4-8	7
β-β	β-β-linked structures	3	3

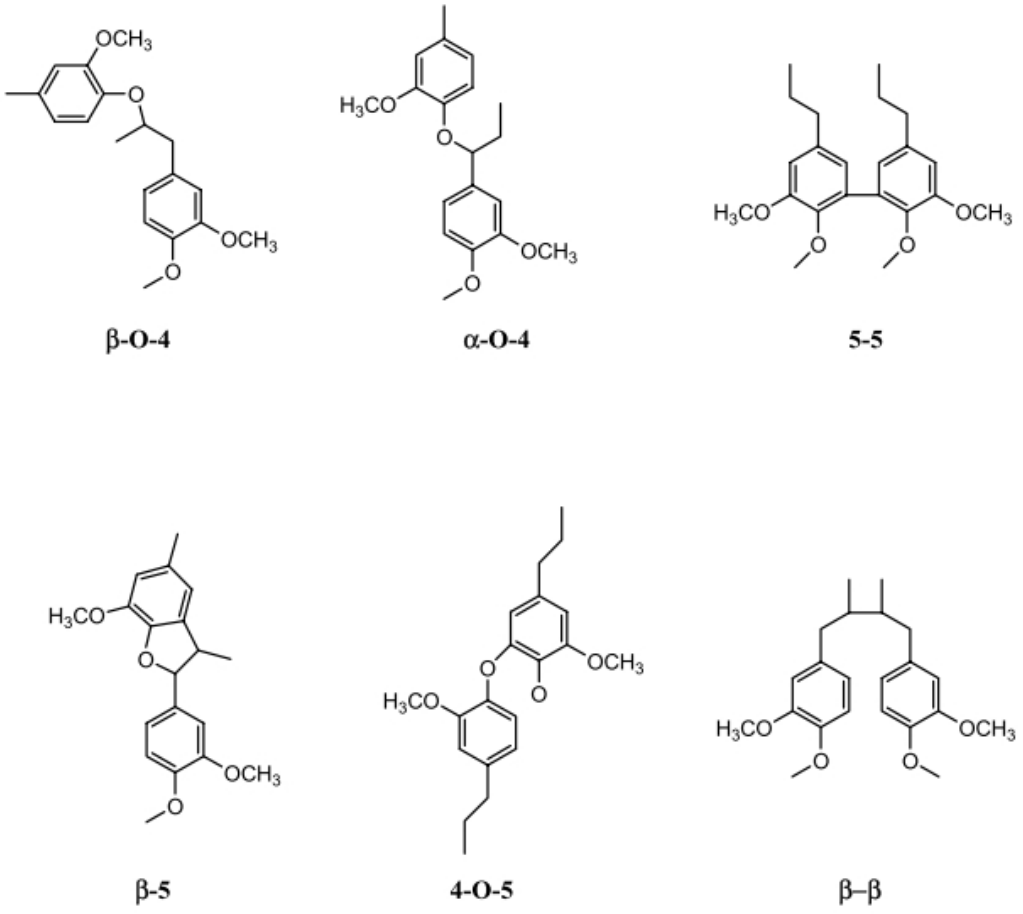

Figure 3.16: Common phenylpropane linkages in lignins (adapted from [Chakar and Ragauskas, 2004])

In addition to the main constituents mentioned above, bast fibres usually contain lipophilic extractives and more particularly waxes and fatty acids, as shown in Table 3.6 and illustrated in Figure 3.17. As it can be seen in Figure 3.17, these compounds have a long carbon chain backbone with terminal groups and some functional groups on the backbone. Hence extractives would generate a strong C-C peak in the XPS spectra (ca. 285 eV) and also some satellite peaks due to the functional groups (hydroxyl, carbonyl, ether etc.).

TABLE 3.6: Composition of lipophilic extractives in bast fibres (adapted from Gutiérrez Suárez et al. [2010])

	Flax	Hemp	Kenaf	Jute
n-alkanes	27	43	27	5
fatty alcohols	220	2	13	13
n-aldehydes	371	25	1	-
fatty acids (**A**)	552	78	33	13
ω-hydroxyfatty acids	-	-	-	3
α-hydroxyfatty acids	11	9	-	10
free sterols/triterpenols	92	36	5	4
sterols/triterpenols esters	6	7	1	-
sterols glycosides	5	13	¡1	1
steroid hydrocarbons	14	30	2	2
steroid/triterpenoid ketones	33	27	4	3
ester waxes (**B, C, D, E**)	284	17	30	20

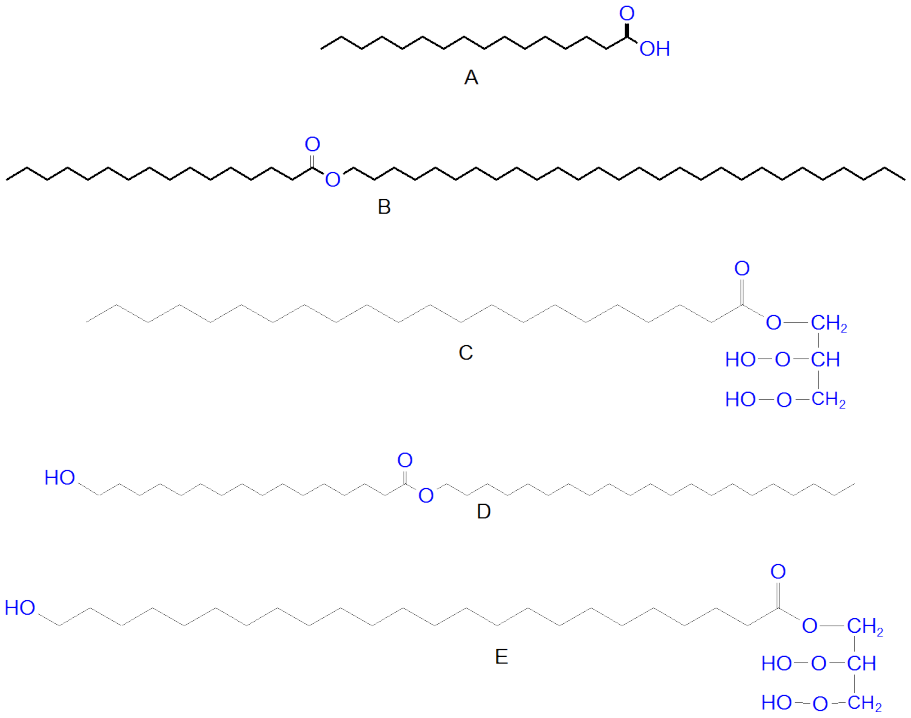

Figure 3.17: Chemical structure of compounds representing the main lipophilic extractives present in bast fibres: A, palmitic acid; B, octacosyl hexadecanoate; C, 1-monodocosanoylglycerol; D, docosanyl, 16-hydroxyhexadecanoate; E, 1-mono(24-hydroxytetracosanoyl)-glycerol (modified from Gutiérrez Suárez et al. [2010])

The procedure applied to curve fit the spectra and identify the chemical bonds present is summarised below:

• The region considered for deconvolution was defined with a linear background type.

• XPS spectra was curve fitted with line shapes of type Gaussian-Lorentzian product function GL(n) with n = 30 (if n=0, pure Gaussian line and if n=100, pure Lorentzian line).

• Constraints were specified for FWHM for each element: 1.2 ± 0.3 eV for C1s, 1.6 ± 0.2 eV for O1s and 1.5 ± 0.2 eV for N1s.

• Deconvolution peaks were positioned so that the residual Standard Deviation of the sum envelope was below 1 for C1s and below 1.4 for O1s and N1s.

• Calibration was done with C-C (Carbon with a single bond) reference at 285 eV.

• Each single peak was attributed to a specific chemical bond by identification with reference to published in the literature (Beamson and Briggs [1992], Ratner and Castner [2009]) and the NIST database.

• Cross-correlation between N, C and O was performed to check the peak fitting model

3.3.3.3 Peak fitting and identification of functional groups in kenaf fibres

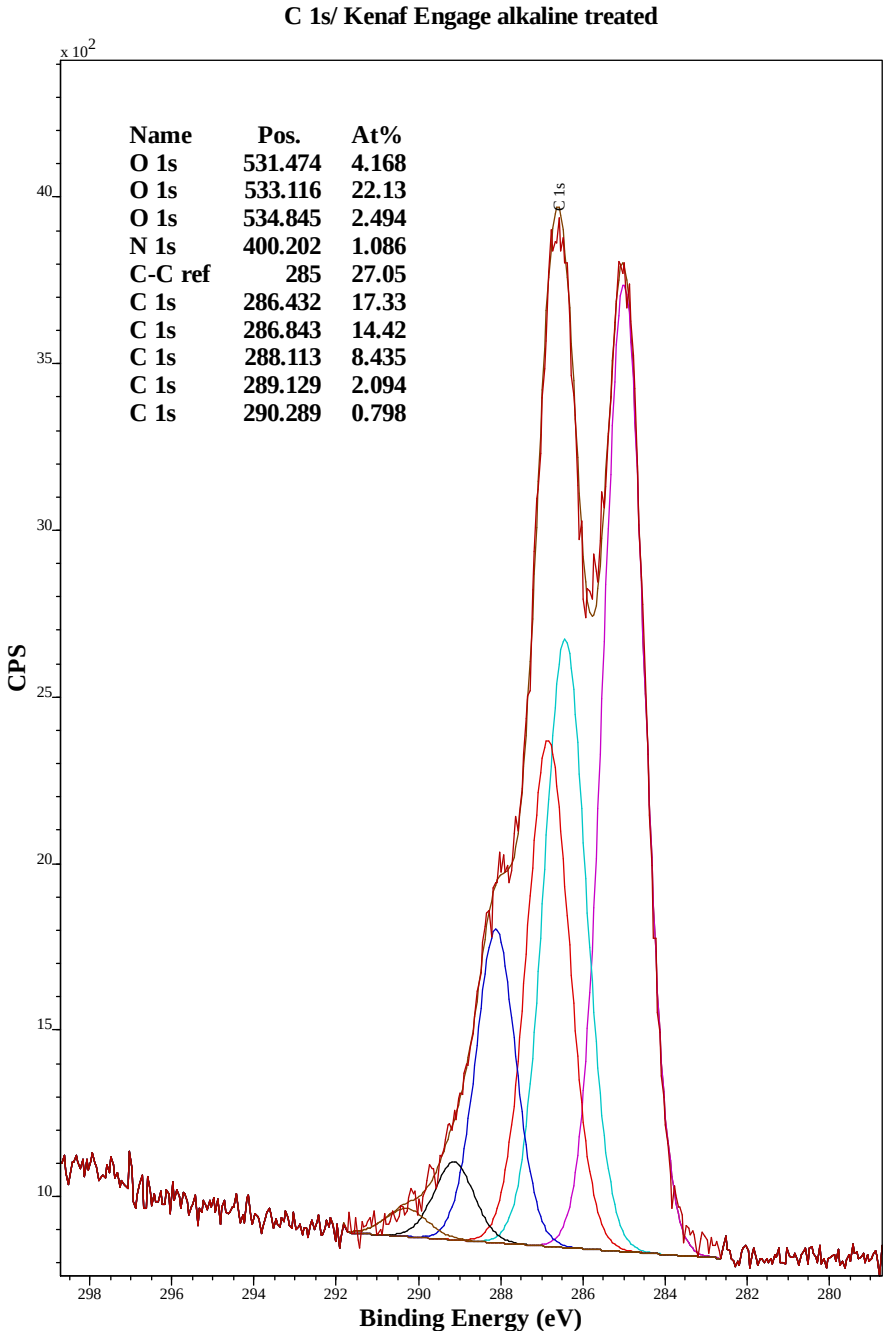

Figure 3.18: C1s spectra curve fitting for kenaf alkaline treated fibre sample

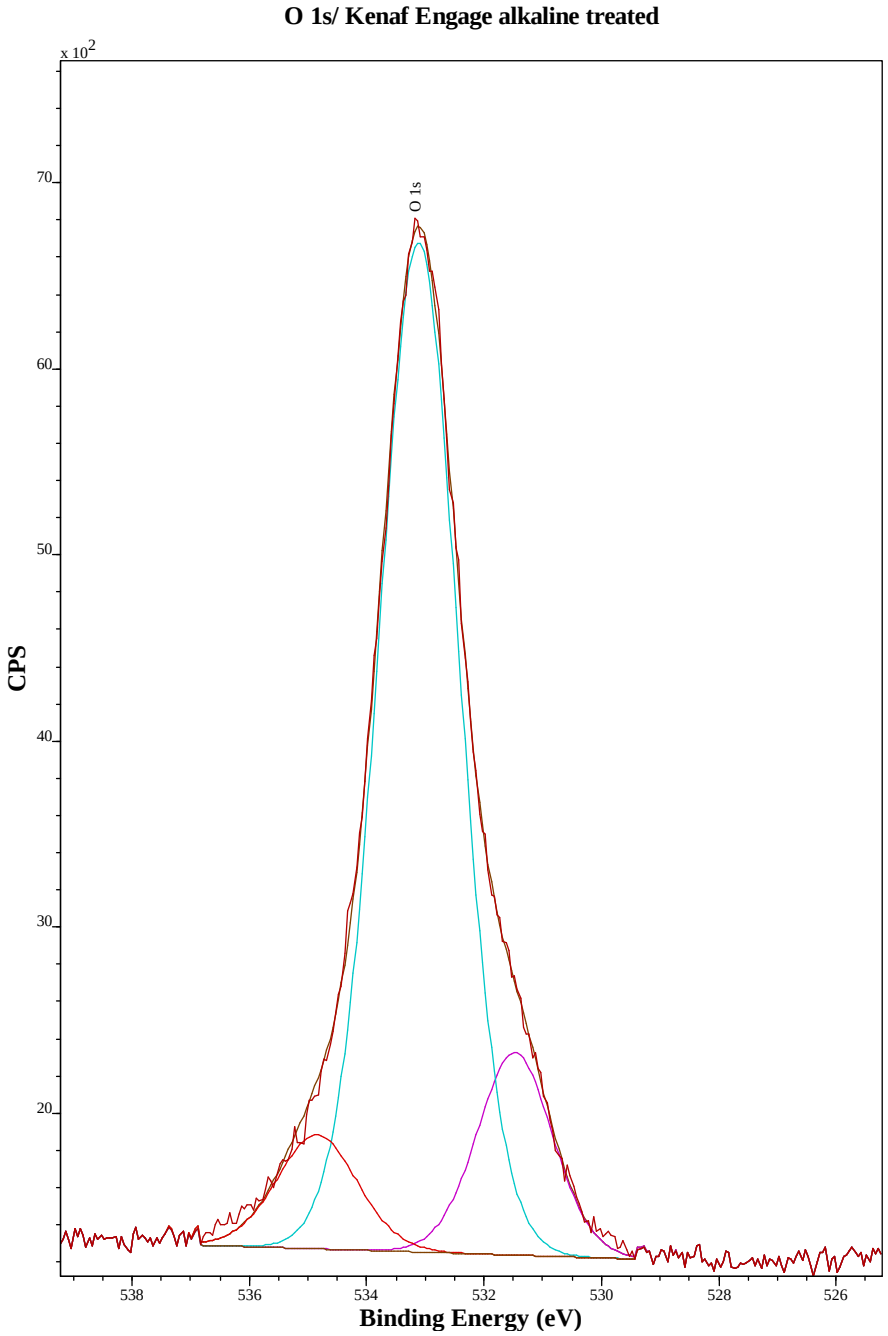

Figure 3.19: O1s spectra curve fitting for kenaf alkaline treated fibre sample

As shown in Figure 3.18, the C1s spectra was reconstructed with six peaks. Based on the C-C reference peak at 285 eV, the five other peaks were identified as follow:

- C1 peak at 285 eV was largely attributed to C-C bonds (reference peak). The binding energies of C=C and aromatic C are shifted only a small amount from that of C-C and so these are also present under 285 eV. Single carbon-carbon bonding does not exist in cellulose. Large C1s peak could account for the aromatic groups in lignins and for fatty acids that have a long carbon chain backbone. Certain types of carbohydrates also contain single carbon bonds. A small contribution from contamination on the sample surface should also be considered [Johansson et al., 2004].

- C2 peak at 286.4 eV could be either ether linkage C-O-C or hydroxyl C-OH, usually observed in the range 286.13 eV - 286.75 eV and 286.47 eV - 286.73 eV respectively. As mentioned previously, kenaf lignins have a majority of methoxy substitution and aryl ether linkage between the aromatic groups [Chakar and Ragauskas, 2004]. Poly(4- methoxystyrene) was taken as a reference model for the methoxy substitution with C1s at 286.4 eV and 286.8 eV (Beamson and Briggs [1992]). The monomer 4-methoxystyrene ($C_9H_{10}O$) is illustrated in Figure 3.20.

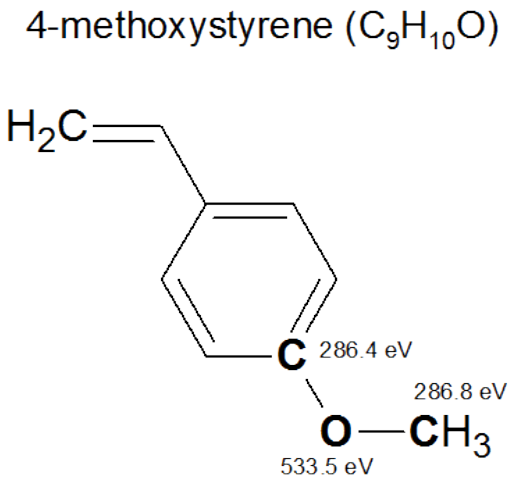

Figure 3.20: Binding Energies for Poly(4-methoxystyrene)

- C3 peak at 286.8 eV could be the ester group C*-O-C=O (286.12 eV - 286.98 eV). Aliphatic esters are present in pectins (carboxylic ester) and fatty acids. Lignins contain aromatic esters (ester substitution on the phenyl ring). Neto et al. [1996] found that kenaf hemicellulose was

particularly rich in xylan (xylan is a pentosan i.e. a carbohydrate with five C atoms) and uronic acids. Uronic acids, which contain both carbonyl and carboxyl acid groups, could also be present in soluble polysaccharides, for instance in pectins. Das et al. [1984] assumed that all the uronic acids on the xylan backbone are ester-bonded with lignins, forming a lignin-carbohydrate complex.

- C4 peak at 288.1 eV is typical from amide functional group N-C=O (287.97 eV - 288.59 eV). C1s peak at 288.1 eV is also O-C-O from cellulose but the O1s characteristic peaks from cellulose (532.9 eV and 533.5 eV) were missing (Figure 3.19), therefore C4 peak was assigned to N-C=O and C=O, most likely from pectins and proteins.

- C5 peak at 289.1 eV was attributed to the carbonyl bond in the ester group C-O-C*=O (288.64 eV - 289.23 eV).

- C6 peak at 290.3 eV could be attributed to carbonate (290.35 eV - 290.44 eV) but the O1s peaks characteristic from carbonate (532.4 eV and 533.9 eV) were not visible on the O1s spectra and the concentration was slightly higher than that of Ca observed on the spectra (0.2 at% to 0.4 at%) therefore the presence of $CaCO_3$ was unlikely. As mentioned in the previous section, Ca can also complex with pectins and form branched macromolecules [Sedan et al., 2007]. The latter are too complex to be identified and quantified by XPS. C6 peak could also result from satellite peaks arising from shake up processes that involve Pi-Pi* transition in aromatic groups [Clark et al., 1976, Morgan, 2014]. This phenomenon is likely to occur in the numerous phenyl rings in lignins [Dorris and Gray, 1978b].

- The oxygen spectra was peak fitted with a broad central peak at 533.1 eV and two auxiliary peaks at 531.5 eV and 534.8 eV (Figure 3.19). The broad peak was associated to ester bond in pectins and in the methoxy substitution, within the tolerance of 0.5 eV (see Figure 3.19). The low shoulder peak at 531.5 eV was attributed to the amide group (pectins) and carbonyl bond in ester group (pectins, lignins, fatty acids). The high shoulder peak at 534.8 eV could be from residual water in the fibre cells [Johansson et al., 1999]. This secondary peak has been observed previously by Truss et al. [2015] on hemp fibres.

- Nitrogen was curve fitted with a single peak at 400.2 eV. Nitrogen was attributed to amide N-C=O from pectins and proteins.

Cross-correlation of the elements was performed to validate the peak fitting model. Nitrogen was peak fitted with a single peak so it makes a good candidate to start the cross-correlation. Nitrogen appeared at 1.1 at%. The peaks related to the amide group in C1s and O1s should have similar concentration, so 1.1 at% was deduced from the total amount. The ester group and methoxy substitution were considered for cross-correlation following the same procedure. For better clarity, the calculations are reported in the table below:

Table 3.7: Binding energies and concentrations (at%) of kenaf fibres NaOH treated

Name	Pos. (eV)	At%	Amide group (at%)	Ester group (at%)	Methoxy substitution (at%)	Residual (at%)
O1s	531.48	4.2	4.2-1.1 = 3.1	3.1-2.1 = 1		1
O1s	533.12	22.1		22.1-2.1 = 20	20-12.3 = 7.7	7.7
O1s	534.85	2.5				2.5
N1s	400.2	1.1	Reference	/	/	/
C-C	285	27.1				27.1
C1s	286.43	17.3			17.3-12.3 = 5	5
C1s	286.83	14.4		14.4-2.1 = 12.3	Reference	/
C1s	288.11	8.4	8.4-1.1 = 7.3			7.3
C1s	289.13	2.1		Reference	/	/
C1s	290.29	0.8				0.8

Allocation of the residual amounts was not straightforward because the fibre surface consists of a complex mixture of polymers so the chemical environments of the atoms induce specific chemical shifts that may not be identifiable in the literature (usually based on pure organic samples). The residual O1s at 533.1 eV and C1s at 288.1 eV were in similar concentration of 7.7 at% and 7.3 at% respectively. These could not be precisely identified; it could not be cellulose as the O/C ratio did not match (1/1 in that case versus 2/1 in cellulose). It could be related to aliphatic C=O. The residual C1s at 286.43 eV (5 at%) could be attributed to ether bonds. This could be from fatty acids (see Figure 3.17). C1s at 290.3 eV could be due to Pi-Pi* transitions. O1s at 534.5 eV was attributed to residual water in the fibres (2.5 at%). Although it was not possible to identify all the chemical bonds due the complexity of the sample, the cross-correlations validated the peak fitting and the spectra analysis was considered as consistent.

These results are coherent with the previous findings from SEM and the XPS survey scans. SEM analysis suggested the fibre surface was rich in lignins and waxes with underneath a surface containing more cellulose, hemicellulose and pectins. The strong peaks associated with the functional groups (ester, methoxy substitution and Pi-Pi* shake-up) were also identified in the high resolution spectra. The strong C-C peak confirmed as well the presence of extractives. The high resolution scans also suggested the presence of pectins on the surface, or calcium complexed with pectins.

Once the peak fitting model validated for the reference sample, it was applied to the water washed fibre and the as received fibres. Figure 3.21 shows the C1s spectra of water washed kenaf fibres:

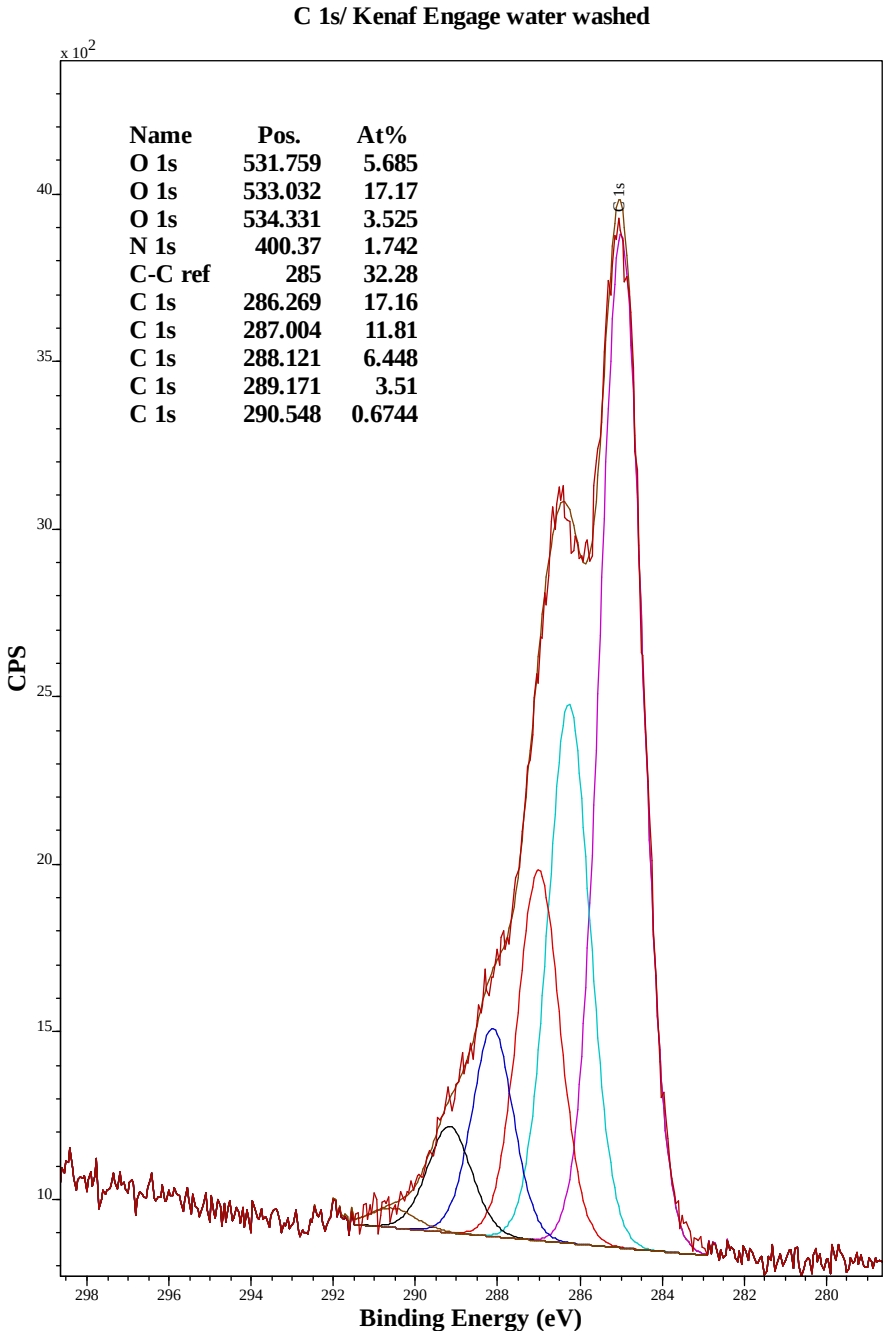

Figure 3.21: C1s spectra curve fitting for kenaf water washed fibre sample

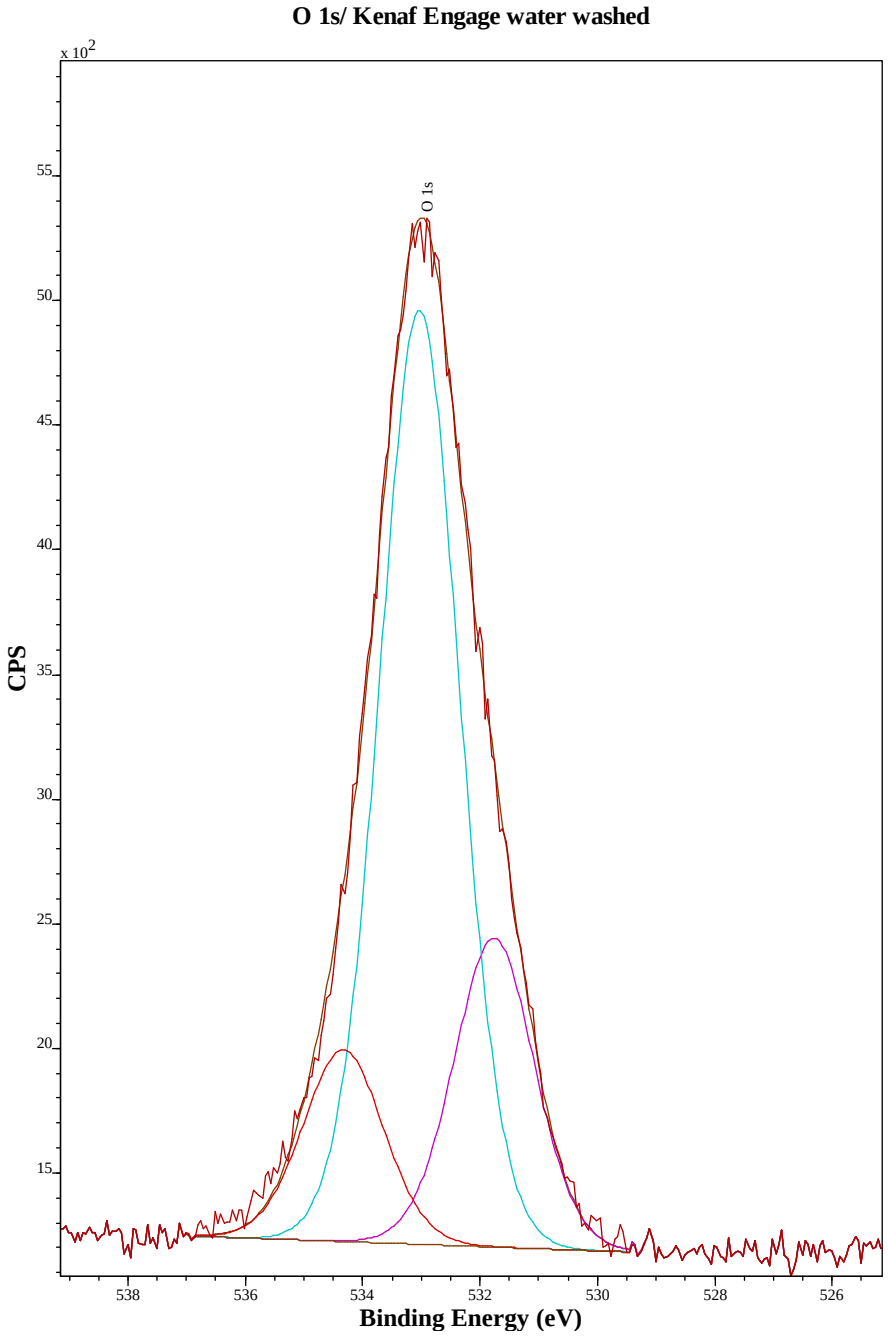

Figure 3.22: O1s spectra curve fitting for kenaf water washed fibre sample

Cross-correlation of the elements was performed in a similar way to the reference alkaline treated fibres. The details are summarised in Table 3.8:

TABLE 3.8: Binding energies and concentrations (at%) of kenaf fibres water washed

Name	Pos. (eV)	At%	Amide group (at%)	Ester group (at%)	Methoxy substitution (at%)	Residual (at%)
O1s	531.76	5.7	5.7-1.7 = 4	4-3.5 = 0.5		0.5
O1s	533.03	17.2		17.2-3.5 = 13.7	13.7-8.3 = 5.4	5.4
O1s	534.33	3.5				3.5
N1s	400.37	1.7	Reference	/	/	/
C-C	285	32.3				32.3
C1s	286.27	17.2			17.2-8.3 = 8.9	8.9
C1s	287.00	11.8		11.8-3.5 = 8.3	Reference	/
C1s	288.12	6.5	6.5-1.7 = 4.8			4.8
C1s	289.17	3.5		Reference	/	/
C1s	290.55	0.7				0.7

Similar to the analysis of the alkaline treated fibres, allocation of the residual amount is challenging due to the complex nature of the surface. The residual O1s at 533.03 eV and C1s at 288.12 eV were within the same concentration range of 5.4 at% and 4.8 at% respectively and were attributed to C=O, to be consistent with the previous model established in alkaline treated fibres. O1s at 534.33 eV was attributed to residual water in the fibre cells. The large C-C peak at 285 eV reflected a majority of single carbon bonds, or C=C or aromatic C within the multiple components. The residual C1s at 286.27 eV (8.9 at%) could be attributed to ether bonds. This could be from fatty acids indicating the presence of lignins (see Figure 3.17). Trace of the Pi-Pi* transitions were also observed in this spectra (0.7 at%).

These data were consistent with the SEM analysis and the XPS survey scans, which suggested a lignin rich surface poor in cellulose. The typical corresponding peaks (ester group, methoxy substitution, Pi-Pi* shake up) were visible on the XPS high resolution spectra. The peaks reflecting the presence of cellulose and hemicellulose on the surface (O1s at 533.03 eV and C1s at 288.12 eV) were in smaller concentrations than in the NaOH treated fibres (concentration of 5.4 at% and 4.8 at% vs. 7.7 at% and 7.3 at% respectively). This confirm the assumption that the alkaline treated fibre surface contained more cellulose than that of water washed fibres.

XPS high resolution scans also suggested that the surface contained more fatty acids than the alkaline treated fibre surface: the residual C1s at 286.27 eV (8.9 at%) were more important than in alkaline treated fibres (5 at% identified at 286.43 eV). This seems logical as NaOH is more efficient to remove fatty acid than water wash.

Finally, the spectra from kenaf as received were peak fitted and analysed (Figure 3.23 and Figure 3.24).

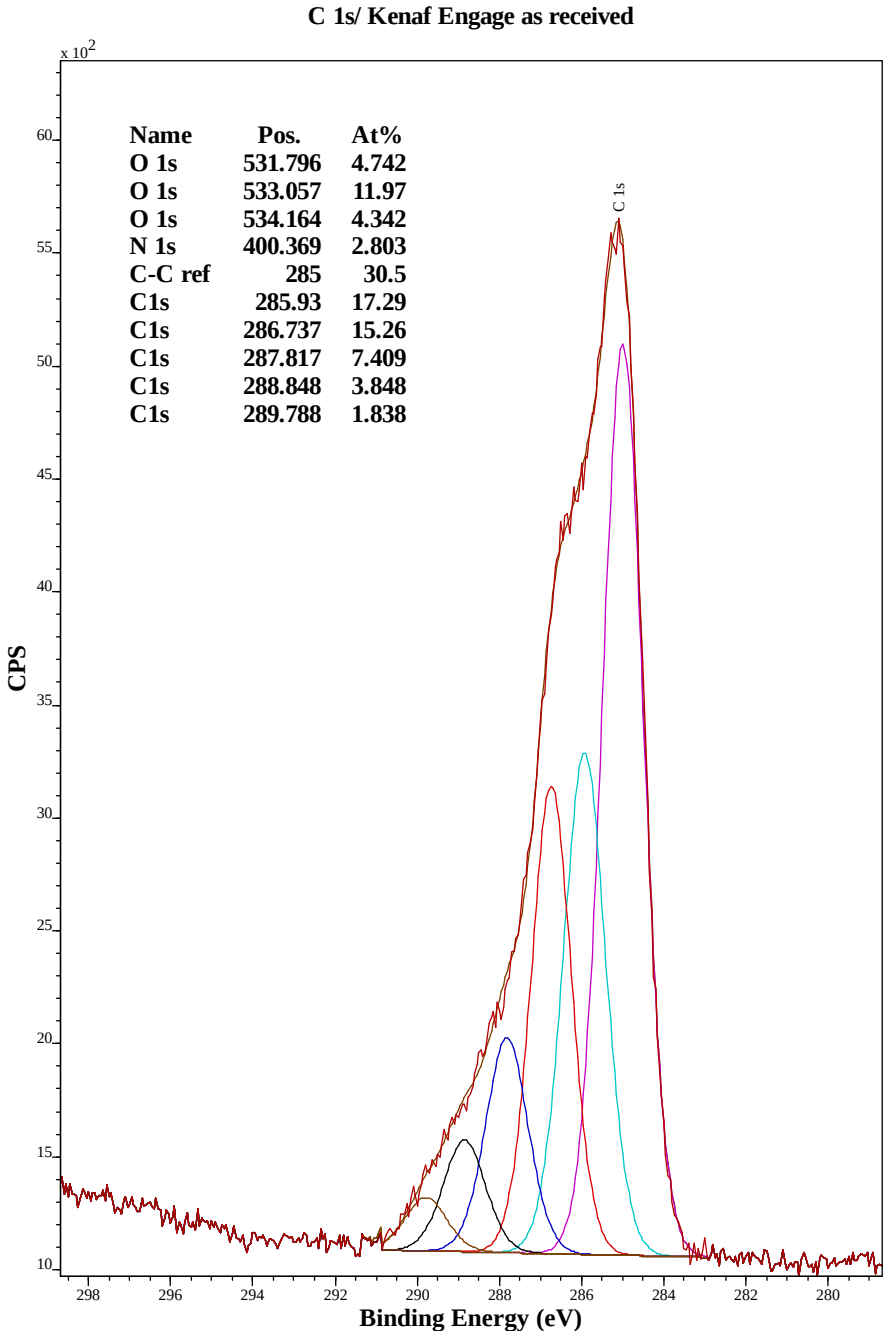

Figure 3.23: C1s spectra curve fitting for kenaf fibres as received

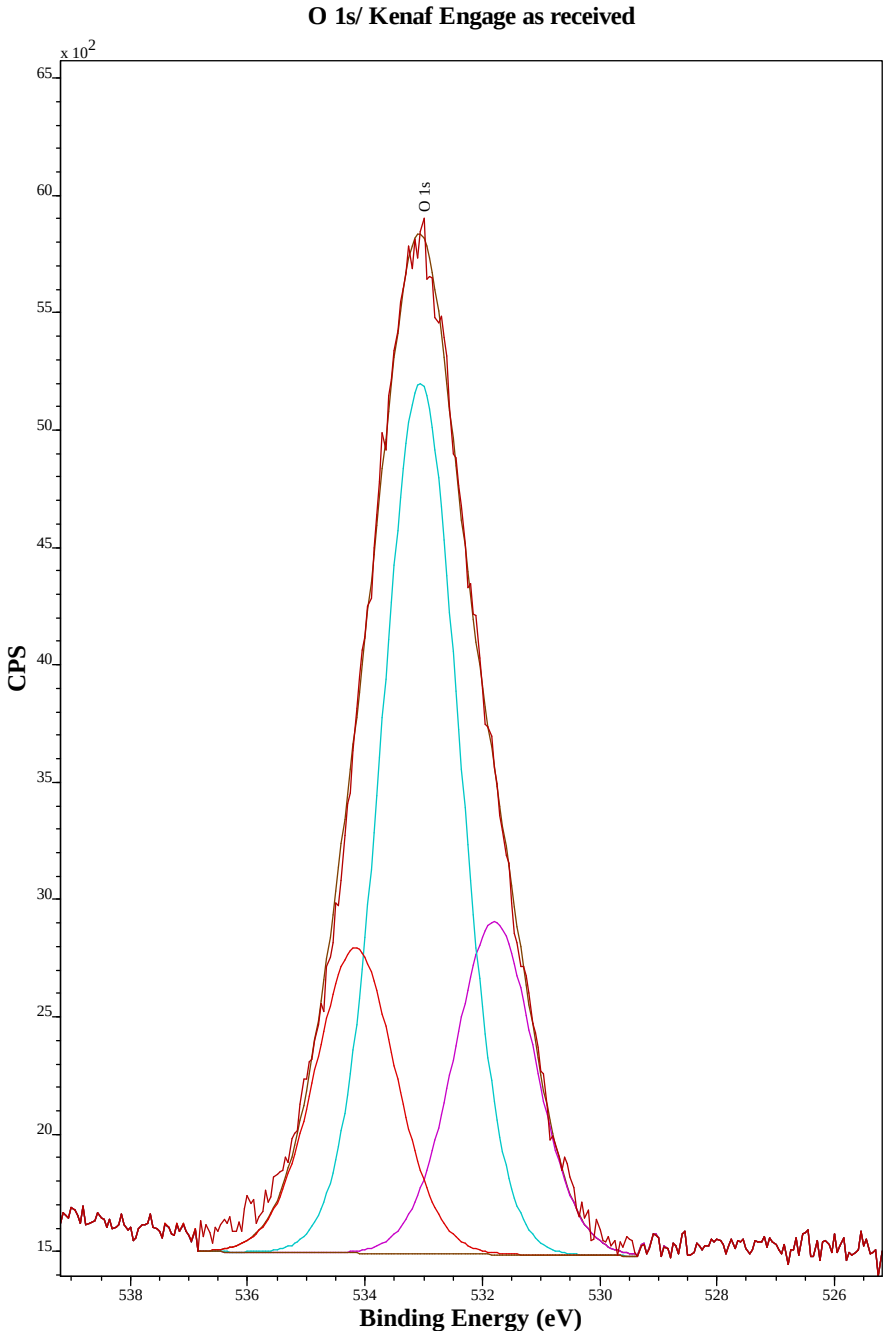

Figure 3.24: O1s spectra curve fitting for kenaf fibres as received

An attempt was performed to do cross-correlation of the elements following the same procedure as for the kenaf treated fibre samples but the peaks could not be specifically assigned to chemical groups because of the surface complexity. The spectra was fitted following the same constraints as for the other spectra and the residual standard deviation was 0.82 hence the curve fitting was assumed correct. However, the chemical shifts were different than those observed in the other samples and could not be identified either with typical binding energies referenced in the literature [Beamson and Briggs, 1992, Ratner and Castner, 2009]. The binding energies depend indeed on the specific environment where the chemical groups are located and, as shown earlier by SEM (see Figure 3.4 in section 2.1), the surface of kenaf fibres as received was a mixture of complex molecules therefore it was expected to observe slightly different shifts. Allocating the peak was too challenging considering the numerous polymeric species likely present on the surface and their complex molecular structure (lignins, extractives, oxygenated species etc.).

On the other hand, the trends were consistent with the SEM observations and the XPS survey scans. The strong C-C peak suggested the presence of long carbon chain from fatty acids and other extractives (see Figure 3.17). SEM analysis of the fibre surface revealed the presence of lignins, pectins and waxes as well as some epidermal tissues (Figure 3.4). Nitrogen was also more important than in the treated fibre spectra, suggesting more pectins and proteins on the fibre surface in the as received stage than in the treated fibres. These could result from the parenchyma cells in the epidermis/cuticle layer that are rich in pectins, as seen on the SEM images.

In conclusion, XPS analysis of bast fibres brought key complementary information to the SEM analysis. The survey scans showed that the O/C ratio of hemp and kenaf increased after treatment, which suggested a change in the fibre surface chemistry. This was further confirmed on the kenaf fibres with high resolution scans on carbon, oxygen and nitrogen. The experimental data confirmed that the water wash and alkaline treatment cleaned the fibre surface and removed most of the epidermal tissues. However, the treatments were too gentle to remove lignins and pectins and the fibres' surface remained rich in lignins and oxygenated species, and poor in cellulose. On the other hand, these treatments may have modified the bast fibre physical structure and the energetic site distribution, which play major roles in the physicochemical interactions between the fibre and the matrix. This will be discussed in the next chapter.

Chapter 4

Inverse Gas Chromatography on Natural Fibres

This chapter presents the research undertaken at the Composites Innovation Centre (CIC) in Winnipeg, Manitoba, as part of the ongoing collaboration with the Cooperative Research Centre for Advanced Composite Structures (CRC-ACS). The author was tasked to commission the inverse gas chromatograph system in the newly established FibreCITY facilities and successfully developed experimental procedures for characterisation of plant fibres by Inverse Gas Chromatography (IGC). Section 4.1 relates the method development to determine the specific surface area of natural fibres by IGC. This work has been published as: *Legras, A., et al. "Inverse gas chromatography for natural fibre characterisation: Identification of the critical parameters to determine the Brunauer–Emmett–Teller specific surface area."Journal of Chromatography A 1425 (2015): 273-279.* Section 4.2 presents a method to determine the surface energy profiles of plant fibres followed by application case studies.

Note: The paper has been formatted according to thesis requirements.

Chapter 4

4.1 Identification of the Critical Parameters to Determine the Brunauer-Emmett-Teller Specific Surface Area

4.1.1 Introduction

Bast fibres have been traditionally destined for the textile industry and this remains the primary application with constant innovations for clothing, technical textiles etc. However, the last decades have seen a significant trend to utilise natural fibres in other sectors, particularly the automotive industry [Ashori, 2008, Holbery and Houston, 2006, Karus and Kaup, 2002]. Natural fibres appeal to vehicle manufacturers with their excellent strength to weight ratio, low cost, low carbon footprint and availability. They are integrated into polymer matrices as filler or reinforcement elements for interior components [Huda et al., 2008, Marsh, 2003]. Biocomposites have also emerged as an alternative to wood plastic composites for building materials.

Diversification into novel applications places new demands on the fibre processing and properties. One of the major issues is that natural fibres are generally hydrophilic and consequently are inherently incompatible with hydrophobic commodity polymers. Natural fibres also suffer from considerable batch-to-batch heterogeneity and particularly dimensional variability, which directly affect the tensile properties. Natural fibre moisture sensitivity is another issue for the biocomposite durability.

The compatibility, dispersibility and reinforcement capability of natural fibres are related to the fibre surface energy and to its specific surface area. Bast fibres have a complex 3D microstructure with multiple membranes enclosing the lumen. The chemical composition and the molecular arrangement vary between the layers and depend on the fibre specie. The fibre location within the plant stem and the growth conditions also play a major role in the physico-chemical structure, creating fibres with unique and complex surfaces [Charlet et al., 2007, Satyanarayana et al., 2007]. Figure 4.1 illustrates the architecture of bast fibre bundles with cellulose microfibrils embedded into a matrix of hemicellulose and lignin. The outer layer also contains pectins, waxes and other extractives. The fibre surface chemistry, its adsorption

capacity as well as its wettability and dispersability in a matrix correlate with the fibre surface energy values and depend also on the accessible surface area. The surface energy provides information on the intermolecular forces that can occur at the fibre surface. These combine long range Van der Waals forces and short range chemical forces, also known as dispersive and polar forces respectively. The nature of these interactions and their intensity also depend on the accessible surface area.

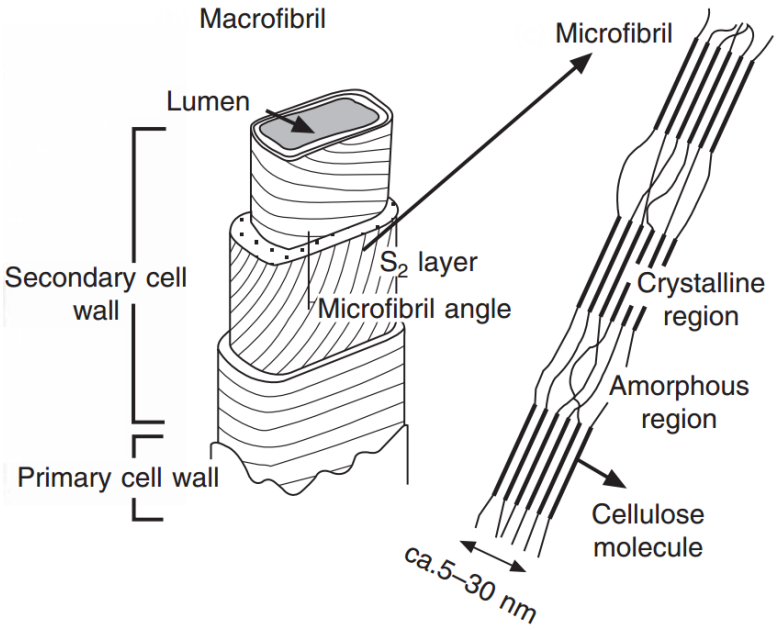

Figure 4.1: Structure of an elementary plant fibre showing the different layers and the orientation of the cellulose microfibrils (Adapted from Baillie [2004] and reproduced with authorisation of the author)

Traditional methods used to determine the fibre surface energy involve the measurement of contact angles. Various approaches reviewed by Williams [2015] and Heng et al. [2007] provide methods for measuring droplet angles to calculate the fibre surface tension. The most common are the Young model, the Fowkes and extended Fowkes (Owens & Wendt) approaches and the Van Oss et al. model [Heng et al., 2007]. Capillary rise, Wilhelmy plate and sessile drop are common methods and numerous studies have been published on natural fibres [Collins, 1947, Rong et al., 2002, Shen et al., 2004]. Although these techniques are excellent on flat surfaces, natural fibre's porous structure and heterogeneous surface properties challenge the accuracy and the validity of the experimental data. These methods are based on liquid-solid interactions where swelling and dissolution may occur and skew the data.

Chapter 4

Inverse Gas Chromatography is an alternative tool to study surface energies. IGC is based on solid-gas interactions and the affinity between gas probe molecules and the fibre surface molecules is quantified. It is a versatile technique to characterise samples of any shape, as long as the specimen can be packed in the column and molecular interactions can occur. IGC exists since the early 50s and it has been applied mostly to pharmaceutical industry [Mohammadi-Jam and Waters, 2014], for characterisation of zeolites [Aşkin and Bilgiç, 2005, Eva Díaz, 2004] and carbon nanostructures [Papirer et al., 1999] but IGC has not been well established yet for natural fibre characterisation. Most of the studies on natural fibres have been performed with home built equipment, using different solvents and various calculation procedures. The lack of information and details of experimental procedures make it difficult to compare and validate data. Moreover, the large variability of natural fibre properties and their complexity compared to synthesised and well designed man made materials means that a systematic study of the common procedures and models implemented in IGC is required to assess its capabilities as a technique to characterise natural fibre surfaces.

IGC requires the specific surface area to determine the surface energy, especially as this can depend on surface coverages. Usually, the specific surface area of a solid is determined by BET method which uses nitrogen sorption [Bismarck et al., 2002, Livingston, 1949] or krypton [Beebe et al., 1945, Rosenberg, 1956], for surfaces areas below 0.5 $m^2.g^{-1}$ where the nitrogen technique shows limitations [Sing, 2001]. These techniques involve extreme conditions of high vacuum at low temperature (77K) under which the fibre properties are likely to change and thus the BET surface area.

An alternative and preferred technique for measuring the BET surface area of low surface area natural fibres would be to use IGC at room temperature. This paper systematically studies the influence of various parameters that may affect the measured specific surface area using BET theory with IGC. On the basis of the results of this study, a procedure applicable to natural fibres is proposed.

BET theory

The BET theory was developed with nitrogen but is applicable to other gases such as those used in IGC. Five types of isotherms can occur depending on the adsorption scenario [Charmas

and Leboda, 2000, Thielmann, 2004]. The BET equation is applicable on isotherms type II and IV only, where there is a formation of a monolayer followed by multi-layers and further capillary condensation. The BET equation is given by:

$$\frac{P}{n(P_0 - P)} = \frac{C-1}{n_m C}(\frac{P}{P_0}) + \frac{1}{n_m C} \tag{4.1}$$

where P is the solvent partial pressure in the gas phase (Torr), P_0 the saturated solvent vapor pressure (Torr), n the amount of gas adsorbed ($Mol.g^{-1}$), n_m the monolayer capacity ($Mol.g^{-1}$) and C the BET constant. The BET equation fits the isotherm (type II or IV) over a specific range of equilibrium pressure P/P_0, usually for $0.05 < P/P_0 < 0.35$. The monolayer capacity n_m can be determined from the slope and intercept of the linearised BET equation fitted to the isotherm. The BET specific surface area ($m^2.g^{-1}$) is expressed as:

$$S_{BET} = aN_A n_m \tag{4.2}$$

with a the molecule cross section area, N_A the Avogadro Number and n_m the monolayer capacity. Since n_m and a are known, the specific surface area S_{BET} can be calculated.

4.1.2 Experimental procedure

4.1.2.1 Materials

Two types of bast fibres and one type of cellulose fibre were used in the study. The Canadian linseed flax (variety unknown) specimen was supplied by Composites Innovation Centre (CIC), Winnipeg, Manitoba (Canada). The fibres were not retted and have been mechanically decorticated by a lab scale scutching machine [Alcock et al., 2012]. Kenaf fibres (variety KK60) were provided by Engage Eco Products Co. Ltd. in Thailand. The fibres were locally ribbon retted, rinsed and dried before shipping. Both flax and kenaf samples were characterised in the

as-received conditions. BioMid® cellulose fibres were supplied by ENC International (South Korea). BioMid® is a 100% cellulose-based continuous filament produced from dry-jet-wet spinning process. The feedstock is a mixture of softwood and hardwood chips, a by-product from the wood pulp and paper industry. The cellulose is extracted from the biomass and then injected through a spinneret. Also, BioMid® structure is different from the bast fibres that have a "membrane" structure. BioMid® fibres are expected to be a pure cellulose sample and was considered as a reference for the study. The sample details are summarised in Table 4.1.

Table 4.1: Industrial fibre grades used for the study

Sample	Variety	Fibre processing
Cellulose	BioMid® (ENC International, South Korea)	Dry-jet-wet spinning process
Kenaf	KK60 (Thailand)	Water retting
Flax	Linseed flax (Canadian variety unknown)	Mechanical decortication by scutching

4.1.2.2 Methods

The strategy to study the influence of experimental parameters on the output BET value involved four criteria. The experimental approach is detailed in the following paragraphs and summarised in Table 4.2.

• Reproducibility within the column:

Various diffusion processes can drive the elutant molecule flow in a column packed with porous material. These scenarios depend on the column dimension, the sample porosity, the packing homogeneity and the flow rate [Thielmann, 2004]. Natural fibre pore widths range from micrometers down to a few nanometers [Arsène et al., 2013, Bledzki et al., 2005, Stone and Scallan, 1965] and so these exceed in size the elutant molecules (cross sectional area ca. 10 $Å^2$ to 100 $Å^2$ [Perry et al., 1997]). As a consequence, the free diffusion process dominates the molecule flow into the column: the gas probe molecules travel both in axial and longitudinal directions. As they elute, these likely encounter cavities and asperities where they will adsorb before complete elution. Whether this phenomenon occurs randomly and if it further affects the flow rate is questionable. Successive runs were performed on the same chromatography column

under identical experimental conditions to assess the reproducibility of the BET experiment. Note that this experiment is possible with inverse gas chromatography as the column can be used multiple times.

• Gas probe:

Various solvents can be used to run a BET experiment with IGC, the requirement being non-polar adsorbates where surface and no bulk sorption occurs. Octane, heptane and cyclohexane are common adsorbates. Whether the nature of the solvent affects the BET value of natural fibres or not has not been clarified so far and few authors specify which gas probe has been used to determine the specific surface area. For the sake of clarity and to know if data obtained from various solvents can be compared, the impact of the solvent choice on the output value was investigated. Among the common adsorbates used for the BET experiment, octane and cyclohexane were selected for two main reasons. The latter showed better retention peaks than other solvents, for instance, hexane and heptane had too low retention times. The second reason is that octane and cyclohexane differ in their molecular structure and chemical properties, which facilitates the observation of effects due to molecule geometry.

• Variability within a batch:

The variability of the BET specific surface area measured using octane was investigated within a batch of natural fibres. The specific surface area is expected to fluctuate as the diameter, porosity and the surface profile vary between fibres. Little information is currently available as to whether the specific surface area changes and to what extent. A chromatography column usually contains ca. a gram of fibres i.e. a relatively small amount of material. It is necessary to estimate how variable the BET value is for grading procedures.

• Sample packing:

Another variable rarely specified is the sample packing. Unlike powder particles, natural fibres can be packed in the column in multiple ways. For instance, post-processed fibres are usually chopped and well separated compared with fibres as received. Short and long fibres may behave differently in the inverse gas chromatography column. In this experiment, the fibres were cut

into “short”fibres of 2 cm length and compared with ”long” fibres of ca. 10 cm length (usual fibre length in a column of 4 mm internal diameter).

Table 4.2: Strategy to investigate the critical parameters for BET experiment

Criterion	Experimental Method
Reproducibility within the column	Repeat 3 runs per column
Gas probe	Run with octane and cyclohexane
Variability within a batch	Run 5 columns per batch
Sample packing	Pack the column with long (10 cm) and short (2 cm) fibres

All experiments were conducted with an Inverse Gas Chromatograph Surface Energy Analyser (IGC SEA) from Surface Measurement Systems (London, UK). This commercial equipment is set-up for pulse chromatography; a precise amount of adsorbate is transported by the carrier gas through the column containing the fibres. Adsorption followed by desorption occur at the fibre surface and an elution peak results. The configuration of the IGC SEA is schematised in Figure 4.2. The retention time was determined by a Flame Ionization Detector (FID) to benefit a high sensitivity compared to thermal conductivity detector [Mohammadi-Jam and Waters, 2014, Wang et al., 2013]. Silane-treated glass columns were filled with ca. 0.7 g to 1 g of fibres. The 4 mm internal diameter column was preferable for packing the fibres. To insert the fibres in a column, wax-free dental floss was tied to the end of the fibres and then pulled through the column. Once the fibres were in place, the dental floss was removed and the column was then plugged with silanised glass wool to avoid any contamination in the injection system. For the experiment with chopped fibres, the short fibres were introduced in the column using a funnel and then packed with a column packing device. The columns were then plugged as mentioned previously. The sample bed length was ca. 30 mm to minimise peak broadening due to free molecular diffusion in the column. Helium was the carrier gas and methane was the reference gas to determine the dead time, which represents the time necessary for a molecule to travel across the column without any interaction. Octane and cyclohexane were injected over a coverage range (n/n_m) within 0.01 to 0.44, the minima and maxima values depending on the sample mass. All experiments were carried out under the same conditions (30°C, 0% RH) with column conditioning for 1 hour (40°C, 0% RH) before the first injection only. The carrier gas flow rate was set up at 10 mL.min^{-1}.

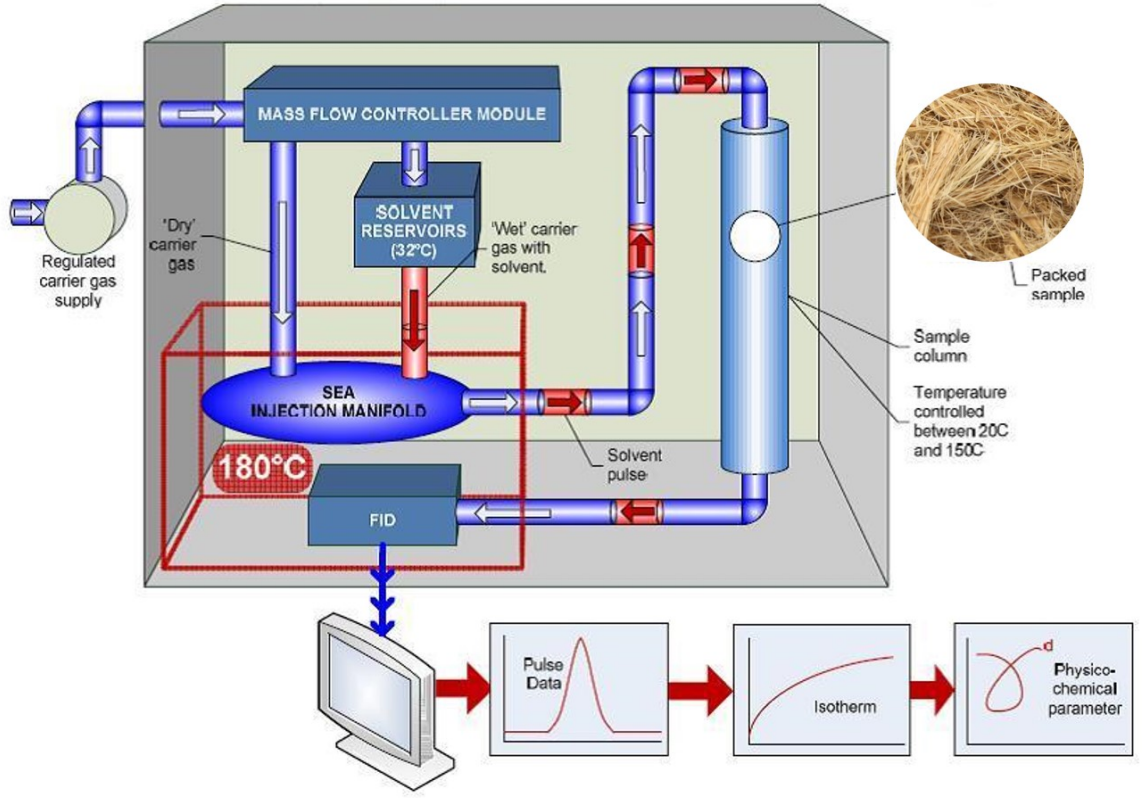

Figure 4.2: IGC Surface Energy Analyser set up (Modified image supplied by SMS).

The BET theory was applied to determine the specific surface area of the fibres according to the following procedure:

- The retention time was determined as the time corresponding to the peak centre of mass (CoM) rather than the time of the maximum FID signal. The peak CoM was preferred as most of the elution peaks were asymmetric.

- The solvent vapour pressure P_0 was calculated with the modified Antoine equation [Perry et al., 1997] described as:

$$P_0 = exp[C_1 + \frac{C_2}{T} + C_3 ln(T) + C_4 T^{C_5}] \tag{4.3}$$

with C_1, C_2, C_3, C_4 and C_5 constants specific to the solvent and T the temperature (K). P_0 is expressed in Pa.

- The linearised BET equation was fitted to the isotherms (amount adsorbed vs. relative pressure) in the range of $0.05 < P/P_0 < 0.35$. The range of calculation was adjusted so that $R^2 \geq 0.995$ with P/P_0 upper limit down to a minimum of 0.25 to get representative values.

4.1.3 Results and Discussions

4.1.3.1 Reproducibility within a column

Table 4.3 shows the repeatability of the BET experiment with octane on both bast fibres and on the BioMid® sample. In each case, all the runs were performed on the same column. An illustration of the data fitted to the linearised BET equation for the kenaf sample is given in Figure 4.3.

Table 4.3: Reproducibility BET experiment

BET Specific Surface Area (Octane) ($m^2.g^{-1}$) at 30°C and 0% RH					
Specimen	Run 1	Run 2	Run 3	**Mean**	Std (%)
BioMid®	0.546	0.545	0.543	**0.545**	0.1
Kenaf	0.503	0.494	0.501	**0.500**	0.5
Flax	1.373	1.423	1.440	**1.412**	3.5

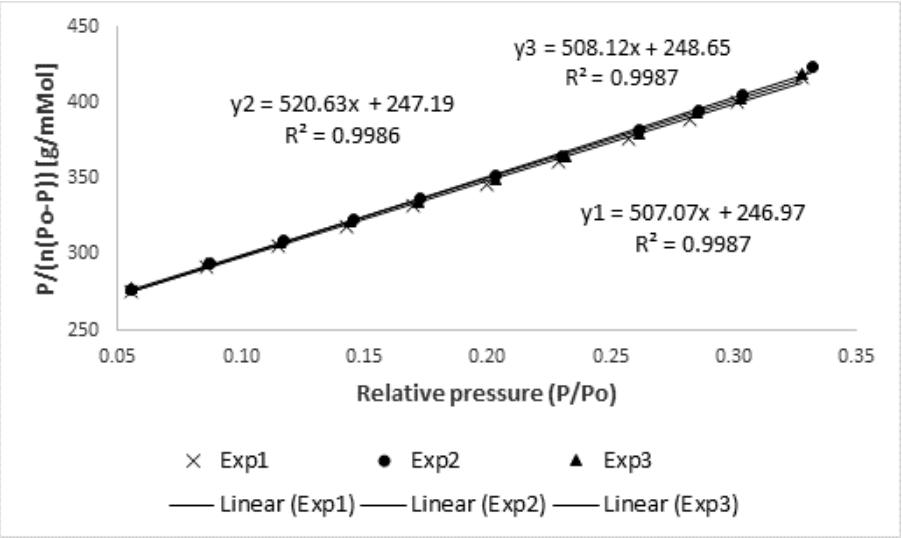

Figure 4.3: Plot of $P/n(P_0 - P)$ versus P/P_0 for successive runs on kenaf fibres.

With standard deviations less than 5% for all samples, the BET experiment showed excellent reproducibility. One run should suffice to determine the BET specific surface area of a fibre

specimen but it is suggested that two runs be completed to avoid any possible outlier. The BET surface area of BioMid® and kenaf fibres were similar (0.55 $m^2.g^{-1}$ and 0.50 $m^2.g^{-1}$) whilst the flax fibre showed tripled specific surface area (1.41 $m^2.g^{-1}$). This could be directly related to the surface roughness of the flax fibres. This batch has not been retted, which means that the microbial degradation process that helps separation of the fibres from non-fibrous tissues was omitted. Morrison and Andre [2005] and Akin et al. [1999] showed that insufficient retting leads to poor separation of the non-fibrous material (cuticle/epidermis and woody core) from the bast fibres. These remaining tissues tend to entangle with the fibres during next mechanical processing steps of scutching and hackling. In this study, the flax fibres were scutched without being retted and hence it was expected to observe numerous non-fibrous tissues spread on the surface. Optical microscope images (Figure 4.4) clearly showed that the flax fibres were covered with fragments of cuticle and epidermis tissues whereas the kenaf fibre surface appeared neat and clean, similar to the BioMid® fibres. The flax fibre surface roughness and heterogeneity accounted for a high BET surface area. BET surface areas of plant fibres were measured with IGC under similar conditions (30°C, 0% RH); Ashori et al. [2012] found to cotton fibres specific surface area of 0.75 $m^2.g^{-1}$ and Cordeiro et al. [2011b] obtained BET area values from bast fibres and other plant fibres that ranged from 0.10 $m^2.g^{-1}$ to 2.79 $m^2.g^{-1}$. BET specific surface areas were also reported on grass fibres with values between 0.81 $m^2.g^{-1}$ and 1.19 $m^2.g^{-1}$ [Cordeiro et al., 2012].

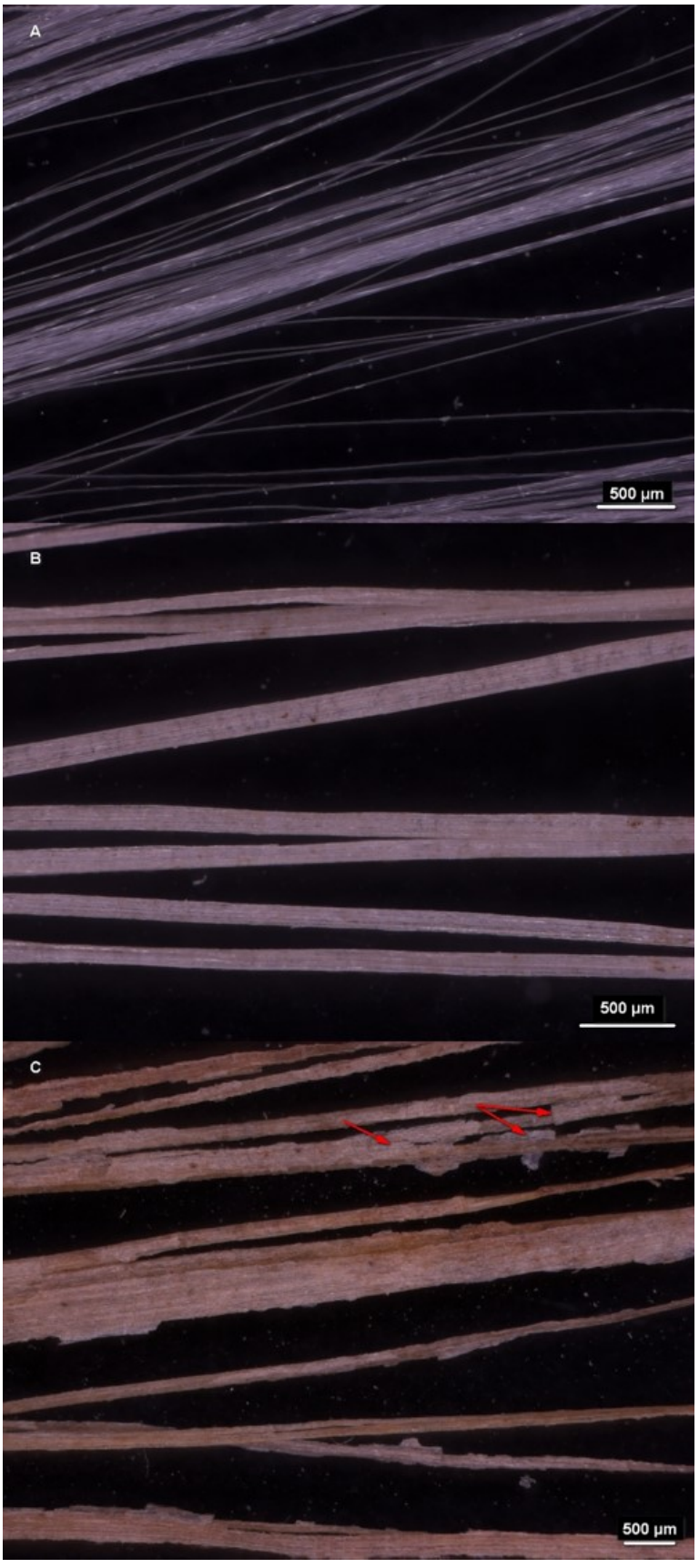

Figure 4.4: Optical microscope images of A) BioMid®, B) Kenaf and C) Flax fibre samples (Images obtained with an Axio Zoom.V16 microscope by CIC).

4.1.3.2 Solvent dependence

BET values calculated with different solvents are shown in Table 4.4. For each specimen, both octane and cyclohexane BET experiments were performed on the same sample column with a minimum of 2 runs. Both BioMid® and bast fibres showed a similar trend; BET values obtained with cyclohexane were lower than those obtained with octane. These results should be related to molecular orientation. Cyclohexane has predominantly a chair conformation whilst octane is linear, so the effect of molecular orientation is stronger in the latter. The average cross sections are $6.3 \times 10^{-19}\ m^2$ and $3.9 \times 10^{-19}\ m^2$ for octane and cyclohexane respectively, but octane width cross section is much smaller hence the molecules can access pores that are "invisible" for cyclohexane. This explains why BET values measured with octane are higher than those calculated with cyclohexane. The effect of molecular orientation and the consideration of uncertainties due to average "a" values for the calculation of surface energy have been previously discussed by Donnet et al. [1992] and Mukhopadhyay and Schreiber [1995].

Note that flax and kenaf fibres showed a large difference between octane and cyclohexane BET experiment compared to BioMid® sample (ca. 50% and 15% difference respectively). The BioMid® fibres were manufactured using a wet spinning process. These fibres are expected to be relatively homogeneous and to have relatively smooth surface even at the molecular level. Natural fibres on the other hand are known to be highly heterogeneous both physically and chemically (see Figure 4.1). Consequently, their surface might be expected to have asperities over a range of length scales down to the molecular level. Such features would amplify the effects of adsorbate orientation on the surface. The more linear octane molecule would have the ability to pack more densely on the surface giving a higher specific surface area while the cyclohexane molecule would pack less densely on the surface and generate lower measured specific surface areas. This is consistent with the observed results.

Table 4.4: Effect of adsorbate

		BET Specific Surface Area ($m^2.g^{-1}$)	
Specimen	Solvent	Mean	Std (%)
BioMid®	Octane	0.55	0.1
	Cyclohexane	0.47	0.2
Kenaf	Octane	0.50	0.5
	Cyclohexane	0.27	0.2
Flax	Octane	1.41	3.5
	Cyclohexane	0.75	0.3

4.1.3.3 Variability within a batch

As expected, the variability within the bast fibre batches was more pronounced than for the BioMid® fibres. As illustrated in Fig.4.5, the latter averaged 0.54 $m^2.g^{-1}$ and fell within 0.5 $m^2.g^{-1}$ and 0.58 $m^2.g^{-1}$ i.e. $\pm$ 7% variation. Bast fibre BET surface area values spread over wider range; between 1.22 $m^2.g^{-1}$ and 1.49 $m^2.g^{-1}$ for flax and 0.38 $m^2.g^{-1}$ to 0.63 $m^2.g^{-1}$ for kenaf batches, hence a variation of ca. $\pm$ 10% and $\pm$ 25% respectively. This was to be expected as natural materials have quite variable structure due to growth conditions, position within the plant, and damage during harvesting and processing. The range of BET surface areas reflects this phenomenon.

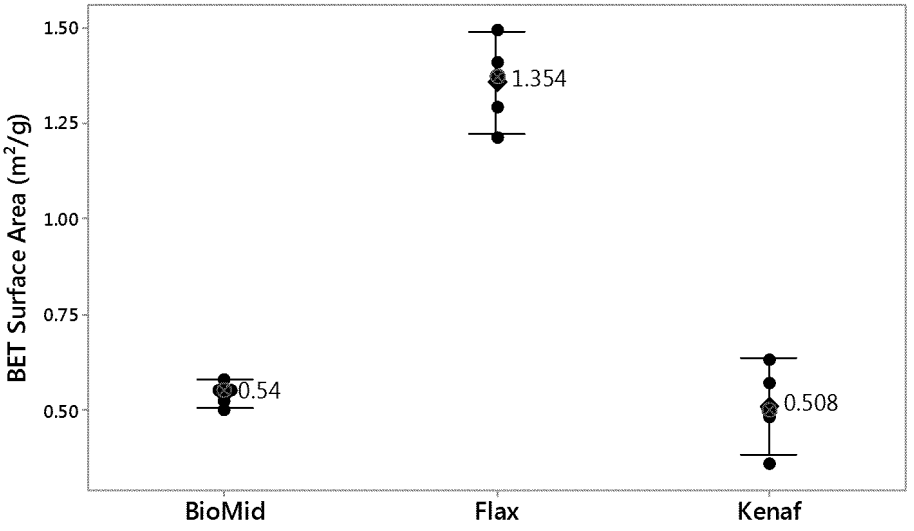

Figure 4.5: Individual value plots of the BET Surface Area ($m^2.g^{-1}$) with 95% Confidence Interval (CI).

4.1.3.4 Sample packing

Table 4.5 shows the effect of fibre length on the BET values. The ranges of variation for BioMid® (ca. +10%) and kenaf (ca. +20%) fibres agree well with the previous findings on the variability within a batch and the effect of fibre length could be considered negligible in that case. However, short flax fibres BET surface area values stepped outside the confidence interval (95% CI) with a variation of 20% i.e. chopping the fibres induced significant effects. The non consistency of these results could be related to the physico-chemical differencies between the fibres. As seen in Figure 4.4, both BioMid® and kenaf fibre surface were neat and homogeneous compared to the flax fibres that were unretted. Chopping the latter may have shredded the fibre ends, i.e. multiplied the accessible surface area. It may also have peeled off some of the cuticle/epidermis fragments and hence opened access to new surfaces that displayed different chemistries than the outer layer. Both phenomena likely generated new molecular interactions with the adsorbate.

TABLE 4.5: Effect of fibre length

		BET Specific Surface Area ($m^2.g^{-1}$)	
Specimen	Packing	Mean	Std (%)
BioMid® (Octane)	long	0.55	0.1
	short	0.59	0.4
Kenaf (Octane)	long	0.50	0.5
	short	0.42	0.1
Flax (Cyclohexane)	long	0.75	0.3
	short	0.92	1.5

4.1.4 Conclusions

The BET specific surface area of kenaf and flax fibres differed, with an average of 0.51 $m^2.g^{-1}$ vs. 1.35 $m^2.g^{-1}$ respectively and the kenaf fibres showed similar BET value to cellulose fibres (ca. 0.54 $m^2.g^{-1}$). The high specific area of flax, compared with kenaf and cellulose, was related to the fibre surface roughness. Bast fibres had larger batch-to-batch variability than synthesised cellulose fibres, which is a consequence of natural fibre structural irregularities and heterogeneous properties.

The BET values obtained by IGC SEA showed a noticeable dependence on the elutant properties. For all specimens, the specific surface areas calculated from octane measurements were higher than those from cyclohexane. This phenomenon is likely an effect of molecular orientation. Sample packing also affected the BET surface area values but no clear trend could be established. It is possible that chopping the unretted flax fibres either shredded the fibre ends or removed lightly adherent cuticle /epidermal material on the surface increasing the accessible surface area.

Based on these findings, the following protocol for determining the BET specific surface area of natural fibres by IGC is proposed:

• Pack the chromatography column with the sample as is. Chopping fibres may induce non negligible effects.

• Consider BET values obtained with the same solvent only for direct comparison.

• For accurate calculation, consider the linearised BET equation over a coverage range (n/n_m) so that the correlation factor $R^2 \geqslant 0.995$.

• Since repeatability is excellent (commercial equipment), two runs per column should be sufficient to ensure confident results, assuming none of the data is an outlier.

These experimental data highlight the structural heterogeneity between different species of bast fibres, in term of both chemical and physical singularities. Further data acquisition on natural fibres is necessary to strengthen these models and extend the database to get consistent references. However, the current results have demonstrated the potential of IGC for characterisation of natural fibre surfaces. The authors encourage the development of inverse gas chromatography for fibre grading as a complementary technique to traditional methods.

4.1.5 Acknowledgements

This study was undertaken as part of a collaboration between the Composites Innovation Centre (CIC) and the Cooperative Research Centre for Advanced Composites Structures Australia (CRC-ACS) research project, established and supported under the Australian Government's Cooperative Research Centre Program. The author acknowledge the CRC-ACS Project P1.1 team and the CIC for their access to equipment. The technical support from Surface Measurement Systems to develop the IGC experimental work is also gratefully acknowledged.

4.2 Surface Energy of Natural Fibres

In fibre reinforced composites, stress transfer between the fibres and the matrix largely depends on the adhesion mechanisms. These relate to the fibre physico-chemical properties, the surface roughness (mechanical interlocking at the interface) and more particularly to its surface energy [Heng et al., 2007]. In other words, surface energetics governs the fibre/matrix interactions. Chemical treatment and mechanical processing applied to modify the fibres' surface affect their surface energy. Quantification of the fibre surface energy should enable a better appreciation of the effect of modifications that occur at the fibre surface and to further optimise the fibre/matrix interactions.

This section introduces first the thermodynamics involved in the determination of surface energy by IGC, followed by a description of the experimental approach used in the study. The last part presents two application case studies on natural fibres: a comparison of the fibre surface energy between different species and an investigation on the effect of alkaline treatment on kenaf fibres' surface energy.

4.2.1 Theoretical background

4.2.1.1 Surface energy and adhesion mechanisms

By definition, the surface energy is "the energy required to form (or increase the surface by) a unit surface under reversible conditions"[Thielmann, 2004]. The surface molecules in a solid have higher energy than the bulk molecules and therefore tend to form bonds to lower their energetic state. The higher the surface energy, the more reactive the surface.

From a thermodynamic point of view, the concept of surface energy for a solid is analogous to the surface tension of a liquid. Inverse gas chromatography is based on thermodynamic interactions between an adsorbate (the gas probe injected in the column) and the adsorbent (the solid sample under study i.e. the natural fibre). In conditions of infinite dilution, adsorbate-adsorbate

interactions are negligible and the adsorption takes place in Henry's law region [Mukhopadhyay and Schreiber, 1995]. The Gibbs free energy of adsorption of the gas probe on the solid stationary phase is then given by :

$$\Delta G^{\circ}_{\text{ads}} = -RTln(V_n) + C \tag{4.4}$$

where $\Delta G^{\circ}_{\text{ads}}$ is the standard free energy of adsorption of the probe on the stationary phase (J.mole^{-1}), R is the gas constant (8.314 J.K^{-1}.mol^{-1}), T is the column temperature (K), V_n is the amount of carrier gas required to elute the injected volume of probe molecules through the column (m^3) and C a constant function of the chosen reference state (J.mole^{-1}).

In practice, the net retention volume V_n is measured from the flow rate in the column and is quantified by:

$$V_n = J.F(t_r - t_0)\frac{T}{273.15} \tag{4.5}$$

where J is the James-Martin gas compressibility correction factor, F is the gas volumetric flow rate (m^3.s^{-1}), t_r is the retention time (s) and t_0 is the dead time (s), which corresponds to the time required for the reference gas to elute. T is the column temperature (K).

On the other hand, the free energy of adsorption is related to the work of adhesion between the gas phase and the stationary phase by [Schultz et al., 1987]:

$$\Delta G^{\circ}_{\text{ads}} = -N.a.W_a \tag{4.6}$$

where N is Avogadro's number (Mol^{-1}), a is the molecular surface area of the probe (Å^2) and W_a the work of adhesion between the gas probe and the solid stationary phase (J.mole^{-1}).

According to Fowkes [1964], the work of adhesion between the adsorbent and the adsorbate can be described as the sum of the multiple intermolecular interactions involved:

$$W_a = \Sigma(\gamma^i) \tag{4.7}$$

where γ^i represent the energy components due to the dispersion (London) interactions, the orientation (Keesom) interactions also known as dipole-dipole interactions, the induction (Debye) interactions, the hydrogen bonding etc.

Van Oss et al. [1988] extended Fowkes' approach and isolated the acid-base contributions so that the work of adhesion between a solid phase (S) and a liquid phase (L) can be described as function of $\gamma_{S,L}^{LW}$ and $\gamma_{S,L}^{AB}$. $\gamma_{S,L}^{LW}$ represents the physical long range interactions; it includes the London-, Keesom- and Debye- interactions and is referred to as the Lifshitz- Van der Waals (LW) component. $\gamma_{S,L}^{AB}$ represents the chemical interactions; it includes both the Lewis acid-base interactions and the hydrogen bonding. $\gamma_{S,L}^{AB}$ is referred to as the Acid-Base (AB) energy component.

It is worth remembering that the acid-base component is of particular importance when considering natural fibres for biocomposite applications because the fibres are hydrophilic whereas the majority of thermoplastics are hydrophobic. For instance, hydrophobisation of the fibre surface (i.e. lowering the acid-base component) should improve the affinity with non-polar matrices. Determination of $\gamma_{S,L}^{AB}$ would provide key information on the efficiency of a fibre treatment to improve fibre/matrix affinity.

Note nomenclature: $\gamma_{S,L}^{LW}$ is commonly called dispersive component and $\gamma_{S,L}^{AB}$ is sometimes called specific component. For the sake of clarity, $\gamma_{S,L}^{LW}$ will be referred to as the dispersive component and $\gamma_{S,L}^{AB}$ will be referred to as the acid-base component.

4.2.1.2 Determination of the dispersive component of the fibre surface energy γ_S^{LW}

The dispersive component can be determined when the solvent injected through the column is non-polar (for instance, n-alkanes). When a non-polar adsorbate interacts with a polar solid surface, the interactions induced by the polar phase contribute to its free energy of cohesion but do not contribute to the free energy of adhesion between the non-polar and the polar phase [Dorris and Gray, 1979]. In other words, the dispersive interactions dominate at the interface and $\gamma_{S,L}^{AB}$ is negligible. Fowkes [1964] established that, in this condition, the work of adhesion equals twice the geometric mean of the dispersive components of the solid phase γ_S^{LW} and the liquid phase γ_L^{LW}:

$$W_{a_{S,L}} = 2(\gamma_S^{LW}\gamma_L^{LW})^{1/2} \tag{4.8}$$

Combining Eq. (4.4), (4.6) and (4.8):

$$RTln(V_n) = 2N.a.(\gamma_S^{LW})^{1/2}(\gamma_L^{LW})^{1/2} + constant \tag{4.9}$$

Assuming the relation $RTln(V_n)$ vs. $(\gamma_L^{LW})^{1/2}$ is linear, the dispersive component of the free surface energy of the fibre γ_S^{LW} can be deduced from the measurement of V_n [Mukhopadhyay and Schreiber, 1995]. The Schultz approach [Schultz et al., 1987] and the Dorris and Gray approach [Dorris and Gray, 1980] are commonly used to determine γ_S^{LW} from IGC measurement.

The Schultz approach represents $RTln(V_n)$ versus $a(\gamma_L^{LW})^{1/2}$ and therefore $\gamma_S^{LW} = (slope/2N)^2$, as represented in Figure 4.6a. This method has been questioned for two reasons. Firstly, the molecular surface area of the probe a is expected to vary with the different conformations of the molecule, which depend on the types of interactions with the solid surface. Secondly, the probe conformations may vary with the temperature and so does a [Mukhopadhyay and Schreiber, 1995].

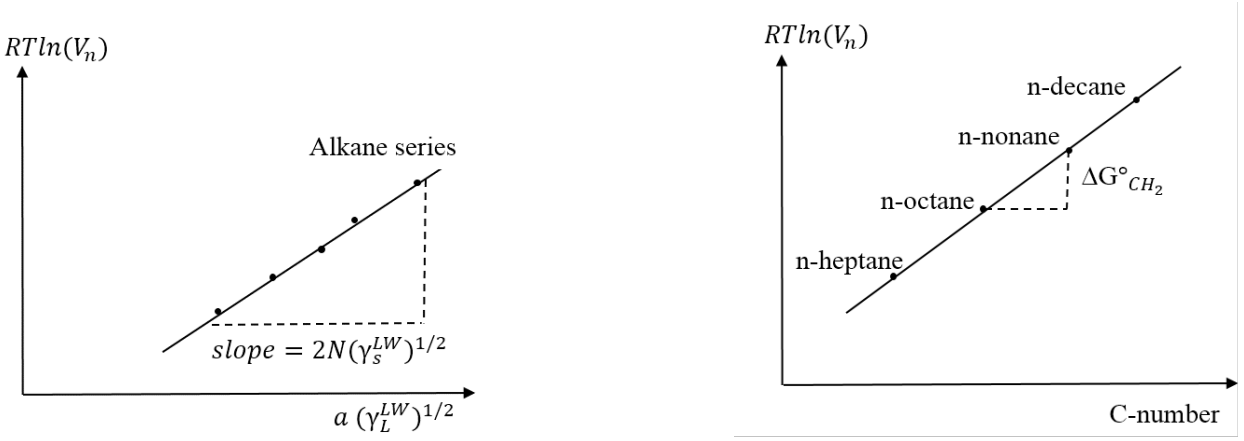

(a) (b)

Figure 4.6: Common approach to determine γ_S^{LW} (a) Schultz approach and (b) Dorris and Gray

Dorris and Gray [1980] proposed a method independent of the molecular area of the probe and that also includes the temperature. This approach considers the contribution of a single methylene group (-CH_2) to the free energy of adsorption in a series of two successive n-alkane probes (C_nH_{2n+2} and $C_{n+1}H_{2n+4}$), defined as $\Delta G^{\circ}_{CH_2}$ (see Figure 4.6b). For each alkane, Eq.(4.9) gives:

$$RTln(V_{n,C_nH_{2n+2}}) = 2N.a_{Ch2}.(\gamma_S^{LW})^{1/2}(\gamma^{LW}_{C_nH_{2n+2}})^{1/2} + constant \tag{4.10}$$

$$RTln(V_{n,C_{n+1}H_{2n+4}}) = 2N.a_{Ch2}.(\gamma_S^{LW})^{1/2}(\gamma^{LW}_{C_{n+1}H_{2n+4}})^{1/2} + constant \tag{4.11}$$

and therefore

$$\gamma_S^{LW} = \frac{\left[RTln\left(\frac{V_{n,C_{n+1}H_{2n+4}}}{V_{n,C_nH_{2n+2}}}\right)\right]^2}{4N^2.a^2_{Ch2}.\gamma^{LW}_{CH_2}} \tag{4.12}$$

with $\gamma^{LW}_{CH_2}$ the surface energy of a methylene group, which is defined at a given temperature T.

Both Schultz Lavielle and Dorris and Gray methods have shown good agreement [Mukhopadhyay and Schreiber, 1995] but the latter is more versatile and therefore usually preferred. Donnet et al. [1991] and Brendlé and Papirer [1997] developed alternative methods based on the polarisability of the gas probe and on the geometry of the probe respectively. These methods have been less frequently applied.

4.2.1.3 Determination of the acid-base component of the fibre surface energy γ_S^{AB}

When a polar probe elutes through the column, both dispersive and acid-base interactions occur at the fibre surface. The acid-base contribution $\Delta G^{\circ AB}_{\text{ads}}$ to the free surface energy $\Delta G^{\circ}_{\text{ads}}$ is deduced by comparison of the retention volume between a polar probe and an alkane (Figure 4.7). Various graphical methods have been developed to determine $\Delta G^{\circ AB}_{\text{ads}}$, namely the Schultz method (represented in Figure 4.7), the polarisation method [Dong et al., 1989], the Saint Flour and Papirer [1983] method and the Brookman and Sawyer [1968] method. These require the knowledge of distinct parameters and Panzer and Schreiber [1992] demonstrated that $\Delta G^{\circ}_{\text{AB}}$ was independent of the graphical method. Since then, the methods have been considered equivalent.

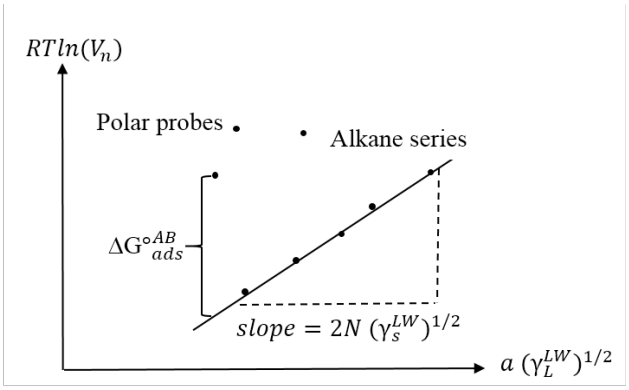

Figure 4.7: Determination of $\Delta G^{\circ AB}_{\text{ads}}$ with Schultz method

According to Van Oss et al. [1988], the acid-base free energy of interaction between two phases S, L in their condensed state can be described as:

$$\Delta G^{\circ AB}_{S,L} = -2(\gamma_S^+\gamma_L^-)^{1/2} - 2(\gamma_S^-\gamma_L^+)^{1/2} \tag{4.13}$$

where γ^+ represents the electron-acceptor parameter and γ^- the electron-donor parameter of the surface tension. These constituents are not additive and the total acid-base component of the surface tension is given by:

$$\gamma_S^{AB} = 2(\gamma_S^+ \gamma_S^-)^{1/2} \tag{4.14}$$

In practice, the experiment involves a series of n-alkanes to build the alkane reference line followed by injection of a mono polar acid probe $L1$ ($\gamma_{L1}^- = 0$) and a basic probe $L2$ ($\gamma_{L2}^+ = 0$). In these conditions, a system of two equations with two unknowns can be established from Eq.(4.13) to solve γ_S^{AB}. Two scales are commonly used for the surface tension components of the probes, which are based on the surface tension of water. The Van Oss scale considers the acid-base surface tension of water to be neutral ($\gamma_l^+ = \gamma_l^- = 25$ mJ.m^{-2}) where as the Della Volpe scale assumes that water is more acidic ($\gamma_l^+ = 10$ mJ.m^{-2} and $\gamma_l^- = 65$ mJ.m^{-2}) [Della Volpe and Siboni, 1997]. The latter has shown more accurate results than the Van Oss scale [Baley et al., 2006, Kondor et al., 2014, Thielmann, 2004].

Finally, the total surface energy of the fibre surface equals the sum of γ_S^{LW} and γ_S^{AB} as these components are additive [Van Oss et al., 1988]:

$$\gamma_S^{TOT} = \gamma_S^{LW} + \gamma_S^{AB} \tag{4.15}$$

4.2.2 Experimental procedure

IGC is usually performed at infinite dilution i.e. it involves very small amount of solvent, typically 10^{-6} to 10^{-5} Mol [Belgacem and Gandini, 1999]. In these conditions, only adsorbate-adsorbent interactions occur and adsorbate-adsorbate interactions are negligible: the retention volume V_n is independent of the amount of adsorbate injected in the column hence the isotherms are linear and Henry's law applies [Ylä-Mäihäniemi et al., 2008]. On the other hand, working at

infinite dilution implies preferential sampling because high energetic sites contribute more than low energetic sites and therefore the estimated dispersive component is in the upper range of the overall energetic sites [Mukhopadhyay and Schreiber, 1995]. In real solids, surface molecules have different energy levels due to chemical heterogeneity (surface groups, degree of crystallinity, impurites) and/or structural heterogeneity (porosity etc.). Therefore, the surface of real solids is energetically heterogeneous. This also explains why IGC data obtained at infinite dilution are often superior to those obtained by contact angle and other wet studies [Dove et al., 1996].

Ylä-Mäihäniemi et al. [2008] introduced a more realistic approach to the surface energy of solid samples and proposed a method to establish the surface energy profile by IGC experiment at finite concentration. The concept walk-through is summarised in Figure 4.8 and detailled in the following paragraphs.

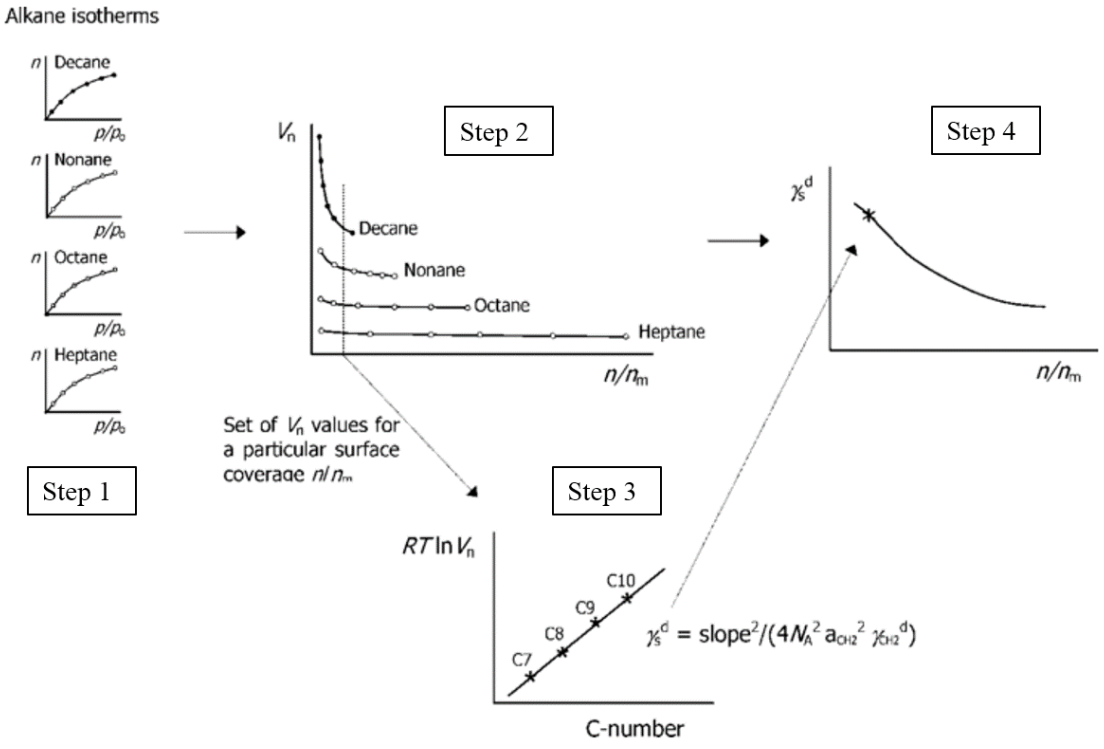

Figure 4.8: Overview of the calculation method to determine γ_S^{LW} (adapted from Ylä-Mäihäniemi et al. [2008])

• Step 1: Determination of alkane adsorption isotherms

Adsorption isotherms were obtained for a series of n-alkanes (three minimum, ideally four or five) at different surface coverages. The more data points obtained at different coverages, the better the precision of γ_S^{LW} profile. However, the injection range boundaries depend on the probe and on the sample specific surface area. A series of trial-and-error experiments with the natural fibre samples suggested that a minimum of six surface coverages from 0.6% up to 15% should be performed with the C7-C10 alkanes series (heptane, octane, nonane and decane). An example of isotherms obtained on kenaf fibres as received at 30°C and 0% RH is given in Figure 4.9.

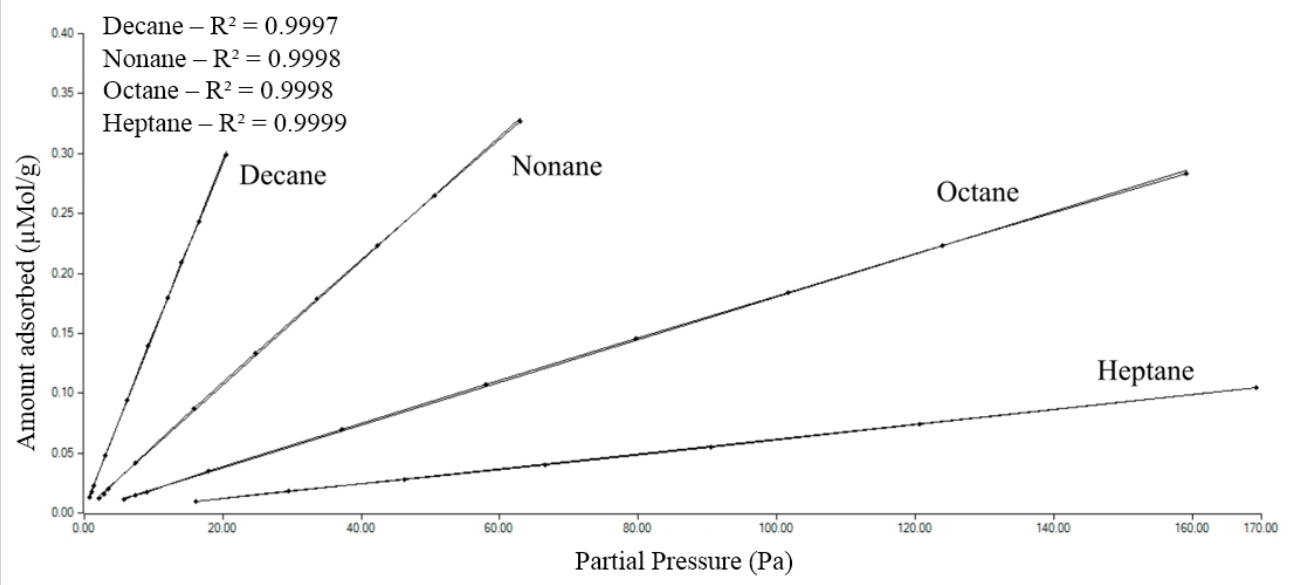

Figure 4.9: Alkane isotherms obtained with kenaf fibres as received (30°C, 0% RH)

• Step 2: Calculation of the retention volume for each solvent at the measured concentrations

For all samples, the conditions of linearity for the isotherms were satisfied ($R^2 \geq 0.999$) and therefore the classic methods established in infinite dilution [Dorris and Gray, 1980, Schultz et al., 1987] were assumed applicable. The retention volume V_n was calculated for each solvent injection according to Eq. (4.5) with the compression correction factor J determined by:

$$J = \frac{3}{2}\frac{[1-(P_i/P_a)^2]}{[1-(P_i/P_a)^3]} \tag{4.16}$$

where P_a is the atmospheric pressure (760 Torr) and P_i equals P_a plus the pressure drop in the column (Torr). The flow rate was 10 mL.min^{-1} and the dead time was measured with methane (average of four measurements). The monolayer capacity n_m was known for each alkane from the BET measurements and hence the actual surface coverage n/n_m was calculated. The retention volume V_n versus n/n_m was plotted for each solvent on the same graph:

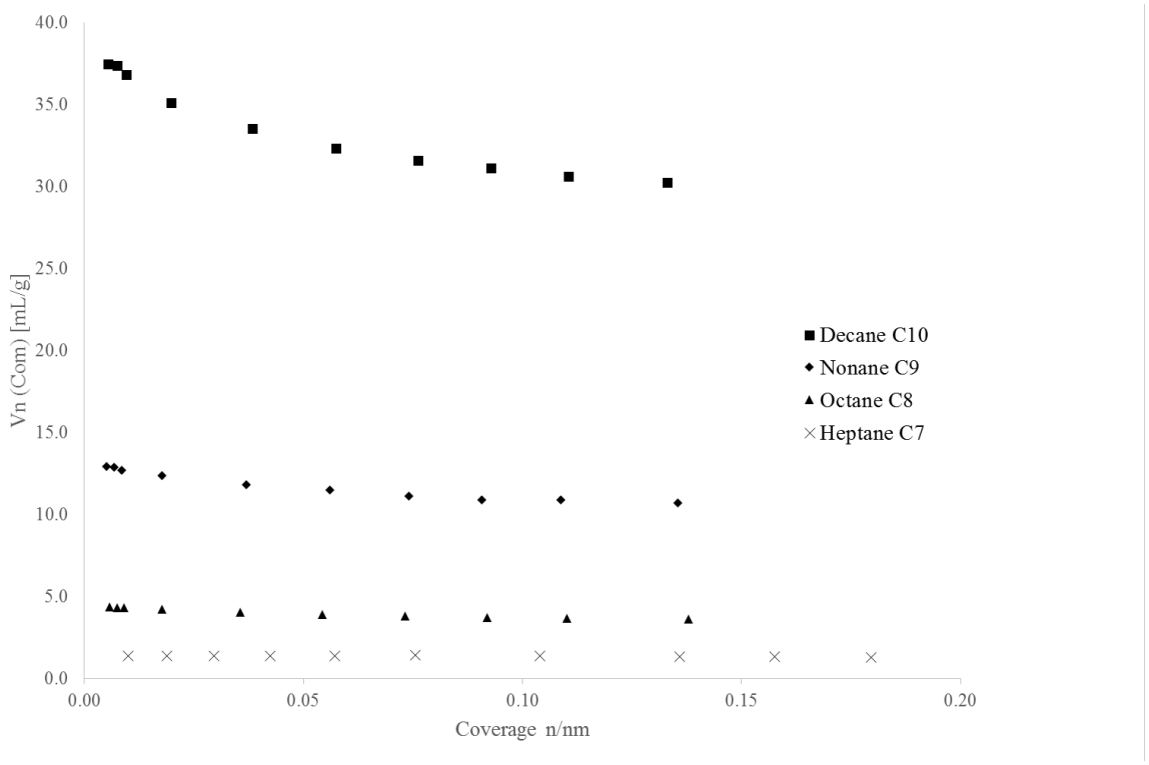

Figure 4.10: Retention volume of n-alkane series obtained with kenaf fibres as received (30°C, 0% RH)

• Step 3: Establish the alkane reference lines for a given surface coverage

The alkane reference line $RTln(V_n)$ vs. C-number was establish by interpolation of V_n from the curve V_n versus n/n_m at each target surface coverage. For all samples, the range of calculation was within 0.006 to 0.15. The n-alkane series for the kenaf fibres is illustrated in Figure 4.11:

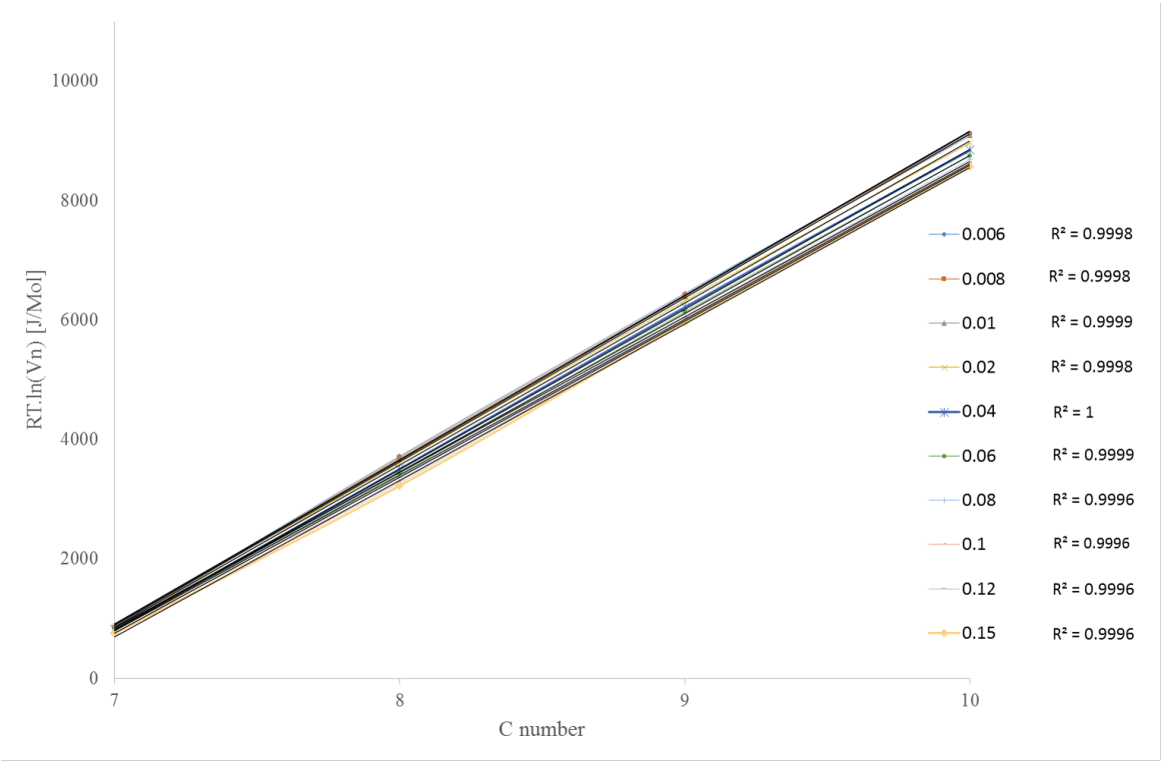

Figure 4.11: Alkane series obtained with kenaf fibres as received (30°C, 0% RH)

As seen in Figure 4.11 the conditions of linearity were satisfied for all reference lines. The condition $R^2 \geq 0.999$ was verified for all other samples.

• Step 4: Determination of γ_S^{LW}

For each coverage, γ_S^{LW} is calculated from the slope of the n-alkane reference line according to the Dorris and Gray method described previously:

$$\gamma_S^{LW} = \frac{slope^2}{4N^2.a_{Ch2}^2.\gamma_{CH_2}^{LW}} \tag{4.17}$$

with $a_{Ch2} = 0.06$ nm^2 [Jacob and Berg, 1994] and $\gamma_{CH_2}^{LW}$ value was estimated based on the surface tension of a linear polyethylene melt as a function of temperature T (°C) [Dorris and Gray, 1980]:

$$\gamma_{CH_2}^{LW} = 35.6 - 0.058(T - 20) \tag{4.18}$$

γ_S^{LW} values were obtained from Eq.(4.17) and Eq.(4.18) for each target surface coverage at a given temperature (30°C):

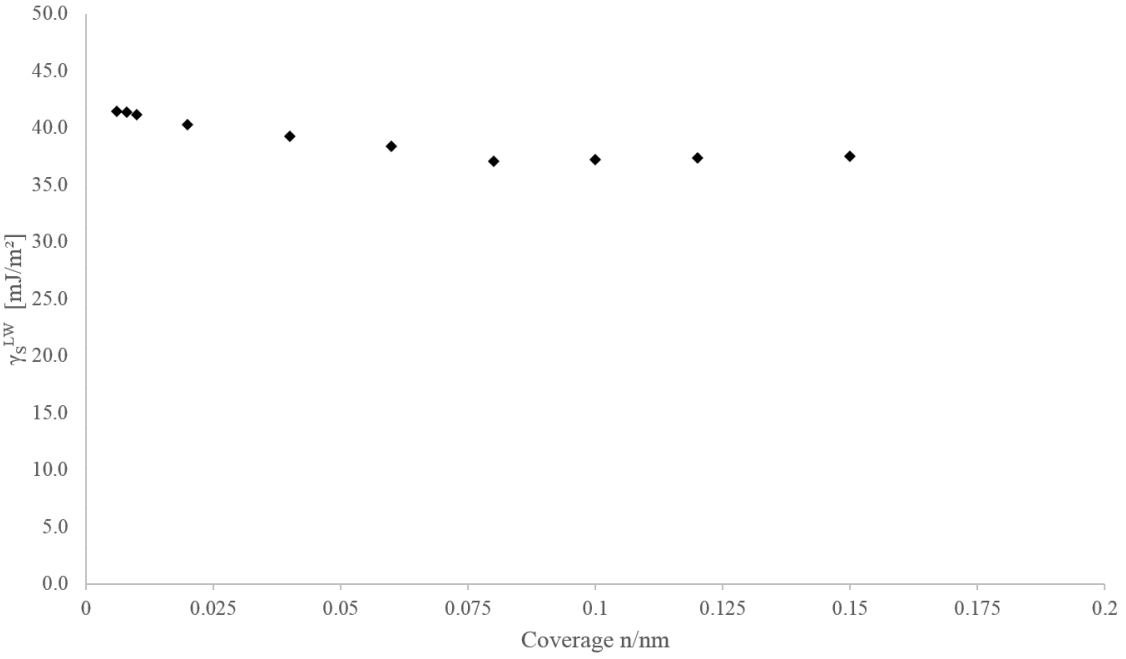

Figure 4.12: γ_S^{LW} profile of kenaf fibres as received obtained with Dorris and Gray method, peak CoM (30°C, 0% RH)

Extrapolation of γ_S^{LW} profile was obtained by regression with exponential decay in the form:

$$\gamma_S^{LW} = a.\exp\left[-b\left(\frac{n}{nm}\right)\right] + c \tag{4.19}$$

where a is the amplitude, b the decay constant and c the offset value. The γ_S^{LW} curve was extrapolated with MATLAB Curve Fitting Tool. Example of γ_S^{LW} profile for kenaf fibres as received:

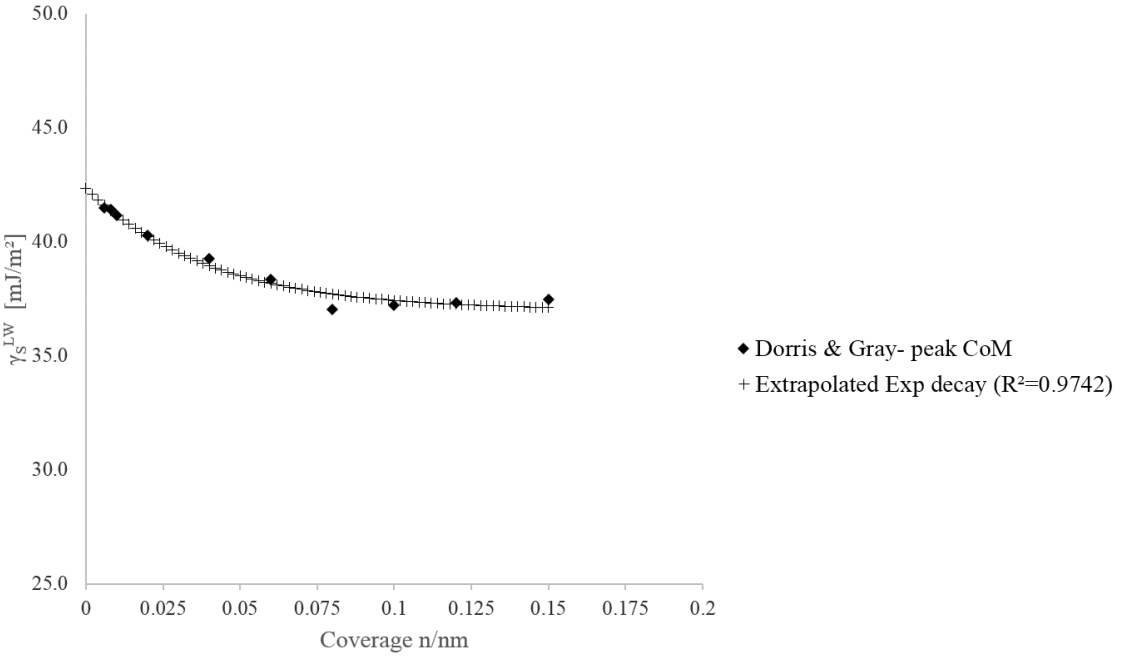

Figure 4.13: Extrapolation of γ_S^{LW} profile

Once γ_S^{LW} profile established, the dispersive surface energy distribution was obtained by integration of γ_S^{LW} over the coverage range (reported to 100%). This procedure is equivalent to a particle size distribution where γ_S^{LW} and the surface area increment represent the particle size and the frequency density respectively. A typical γ_S^{LW} distribution is shown below:

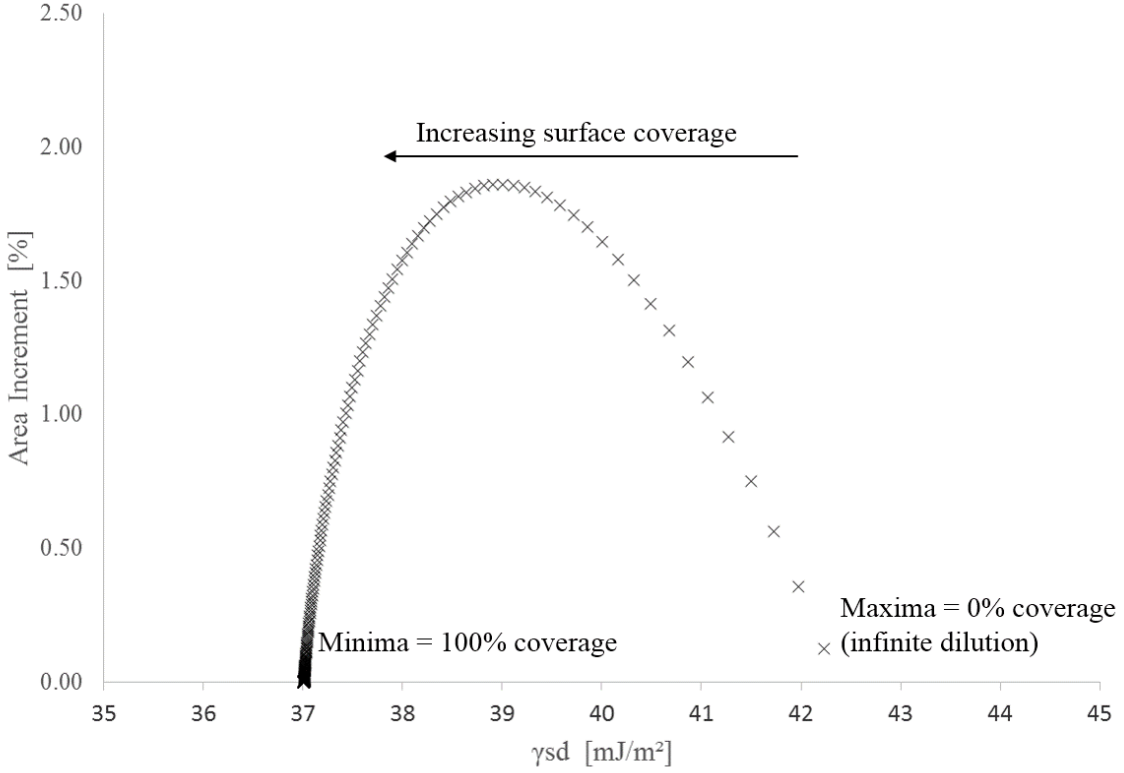

Figure 4.14: γ_S^{LW} distribution profile up to 100% coverage

Note that it is necessary to extrapolate γ_S^{LW} across the entire coverage (up to $n/n_m = 1$) to get a complete distribution curve (the area increment tends to zero when γ_S^{LW} tends to its lower limit). This also enables the superimposition of data obtained at different maximal coverages (up to 0.1, 0.12 etc.) to compare various samples.

γ_S^{AB} values were obtained by injection of mono polar probes (acid, base) at the same surface coverages as the alkanes and applying the Van Oss method (Eq. (4.13), Eq. (4.14)). The Della Volpe scale was chosen for the surface tension components of each polar probe. γ_S^{AB} profile and γ_S^{AB} distribution profile were then established following the same procedure as mentioned above. Finally, the total surface energy profile γ_S^{TOT} was established as the sum of both profiles (Eq. (4.15)).

4.2.3 Case studies

The first case study discusses the surface energy profiles of cellulose BioMid® fibres, linseed flax and kenaf KK60 fibres as received. The second experiment aims to investigate the effect of water wash and alkaline treatment on the fibre surface energy profile of kenaf fibres.

All IGC surface energy experiments were performed with the same conditions as that of the BET measurement (see paragraph 4.2.1). The columns were packed with ca. 1 g of fibres (about 10 cm long). Heptane (C7), octane (C8), nonane (C9) and decane (C10) were injected to build the alkane isotherms, dichloromethane and ethylacetate were injected as the mono polar acid probe and basic probe respectively. These probes were selected for calculation as they gave better elution peaks than other polar probes (chloroform, toluene). All solvents were of HPLC grade ($\geqslant$ 99.9%). Heptane, decane, dichloromethane and ethylacetate were supplied by Uniscience Laboratories (CAN). Octane and nonane were supplied by Sigma Aldrich (CAN). The solvents were injected over a coverage range within 0.006 to 0.15, the minima and maxima depending on the sample mass. The BET values obtained earlier were considered for the calculation of the coverage n/n_m. Data was collected with the SMS IGC Control Software and analysed with Cirrus Plus v.1.2.1.2. Note that the data was replicated manually using the method developed earlier and matched those obtained with the software, therefore the latter were extracted as is. Experimental conditions are summarised in Table 4.6.

Table 4.6: Experimental procedure for surface energy analysis

Samples	cellulose BioMid®, flax linseed, kenaf KK60
Solvents	reference: methane alkanes: heptane, octane, nonane, decane polar probes: dichloromethane, ethylacetate
Coverage	from 0.006 to 0.15
Column conditions	conditioning: 40°C, 0% RH for 1 h experiment: 30°C, 0% RH flow rate: 10 mL.min^{-1}
Calculation method	Dorris and Gray parameter: peak Centre of Mass (CoM) scale Della Volpe: dichloromethane: $\gamma_l^+ = 124.6$ mJ.m^{-2}, γ_l^- null ethylacetate: γ_l^+ null, $\gamma_l^- = 475.7$ mJ.m^{-2}

4.2.3.1 Surface energy profiles of natural fibres

Table 4.7: Surface energy components (mJ.m^{-2}) at 30°C, 0% RH

	γ_S^{LW}			γ_S^{AB}			γ_S^{TOT}			$\gamma_{Smean}^{AB}/\gamma_{Smean}^{TOT}$		
	Min	Max	Mean	Min	Max	Mean	Min	Max	Mean	Min	Max	Mean
BioMid®	40.7	42.8	41.1	3.8	4.3	3.9	44.5	47.1	45	0.08	0.09	0.09
Flax	38.6	41	39.1	6.6	8.3	6.9	45.3	49.4	46.1	0.15	0.17	0.15
Kenaf	37.7	43.6	38.8	11.1	18.4	12.5	48.9	62	51.3	0.23	0.3	0.24

Min value corresponds to maximal coverage ($n/n_m = 1$)

Max value corresponds to minimal coverage ($n/n_m = 0$), infinite dilution

Mean value corresponds to 50% coverage ($n/n_m = 50$)

The distribution profiles represent the surface energy heterogeneity in a similar manner to a population distribution profile: the wider the curve, the more heterogeneous the surface. γ_S^{LW} and γ_S^{AB} distribution profiles of the cellulose, flax and kenaf fibres are given in Figure 4.15a and Figure 4.15b respectively. The cellulose BioMid® fibre surface was the most homogeneous with dispersive energy values ranging from 40.7 mJ.m^{-2} to 42.8 mJ.m^{-2} and acid-base energy values comprised between 3.8 mJ.m^{-2} and 4.3 mJ.m^{-2}. This was expected as the BioMid® fibres were produced by spinning process and had a regular smooth surface. The flax fibre surface appeared more heterogeneous than the BioMid®, with 38.6 mJ.m^{-2} $\leqslant \gamma_S^{LW} \leqslant$ 41.0 mJ.m^{-2} and 6.6 mJ.m^{-2} $\leqslant \gamma_S^{AB} \leqslant$ 8.3 mJ.m^{-2}. The kenaf fibres showed the most heterogeneous surface with 37.7 mJ.m^{-2} $\leqslant \gamma_S^{LW} \leqslant$ 43.6 mJ.m^{-2} and 11.1 mJ.m^{-2} $\leqslant \gamma_S^{AB} \leqslant$ 18.4 mJ.m^{-2}.

The γ_S^{LW} profile trends suggested that the kenaf fibre surface contained active sites with energy levels spread more than those of flax fibre surface. The dispersive component heterogeneity could be due to porosity, defects and asperities on the kenaf fibres. Previously, SEM results highlighted that the kenaf and flax fibre surface topography clearly differed. The kenaf fibre surface was covered with patches of an amorphous mixture and the flax fibres were mostly covered by the epidermal/cuticle layer. Therefore, both surfaces likely contained different energetic sites with various energy levels. The kenaf fibres' surface likely contained a mixture of components which explains the large dispersion. A ranking based on the mean values (coverage of 50%) gives $\gamma_{Smean}^{LW}(kenaf) \leqslant \gamma_{Smean}^{LW}(flax) \leqslant \gamma_{Smean}^{LW}(BioMid®)$. The flax fibres were unretted and likely contained more waxy substances than the kenaf fibres (water retted), which could explain the higher dispersive energy values at higher coverages (waxes are highly non-polar).

The γ_S^{AB} distribution profile trends were similar to that of γ_S^{LW} (Figure 4.15b). As expected, BioMid® fibres were the least polar and the most homogeneous i.e. the few polar sites present on the fibres' surface had similar energy levels. Flax fibre surface contained polar groups of lower energy than that of kenaf fibre surface, which is consistent with the assumption that the former surface was rich in waxes and the kenaf fibres contained various polar components. Kenaf fibres' surface likely comprised more Lewis acid-base functional groups than that of flax, for instance lignins, pectins and extractives.

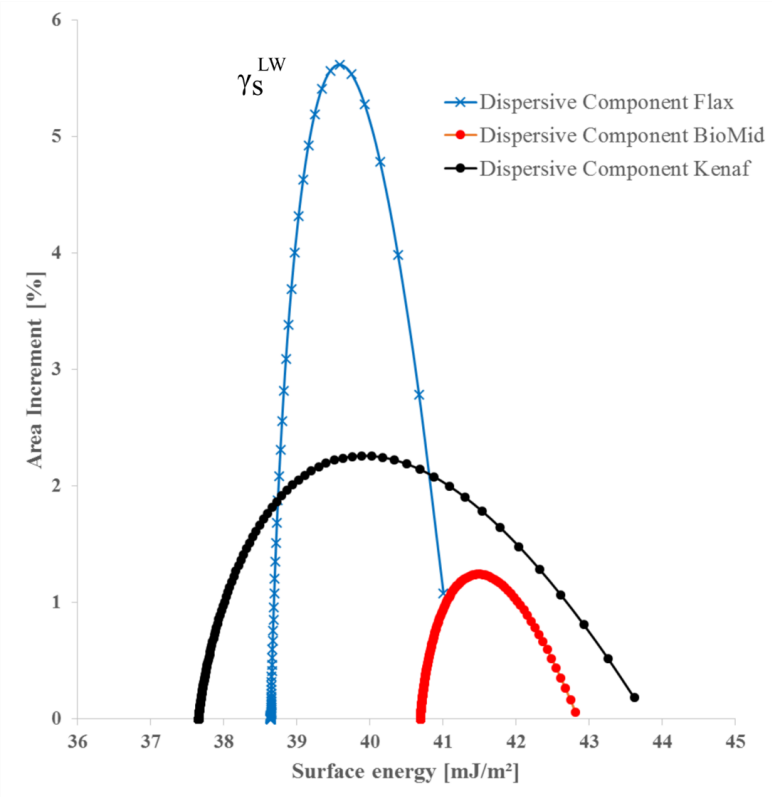

(a)

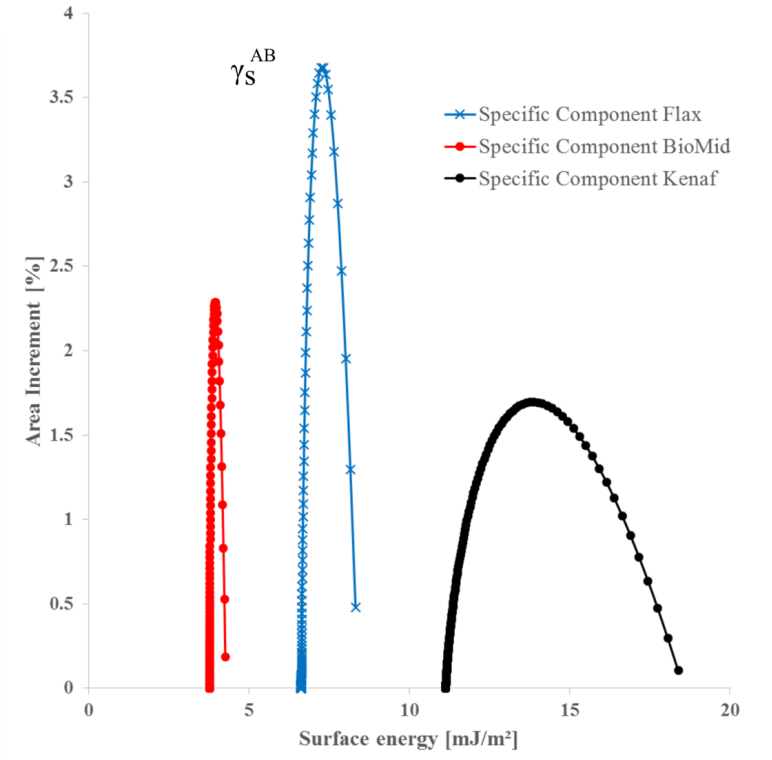

(b)

Figure 4.15: Distribution of the surface energy components: (a) γ_S^{LW} and (b) γ_S^{AB} distribution profiles for cellulose BioMid®, kenaf and linseed flax fibres

According to Eq.(4.15), addition of both distribution profiles gives the total surface energy distribution profiles (Figure 4.16). Logically, the trends were consistent with the components' distribution profiles; BioMid® fibres were the less reactive and had the most energetically homogeneous surface compared to bast fibres. A ranking based on the mean values gives $\gamma_{Smean}^{TOT}(BioMid^{®}) \leqslant \gamma_{Smean}^{TOT}(flax) \leqslant \gamma_{Smean}^{TOT}(kenaf)$ i.e. the kenaf fibre surface was the most reactive after the flax and the BioMid® fibre surface respectively. In addition, the acid-base energy component largely contributed to the total surface energy values of the bast fibres and in particular for the kenaf fibres. This can be expressed with the polarity indexed defined as $(\gamma_{Smean}^{AB}/\gamma_{Smean}^{TOT})$: kenaf fibres had highest polarity index (0.24) compared to flax and BioMid® fibres (0.15 and 0.09 respectively) (see Table 4.7).

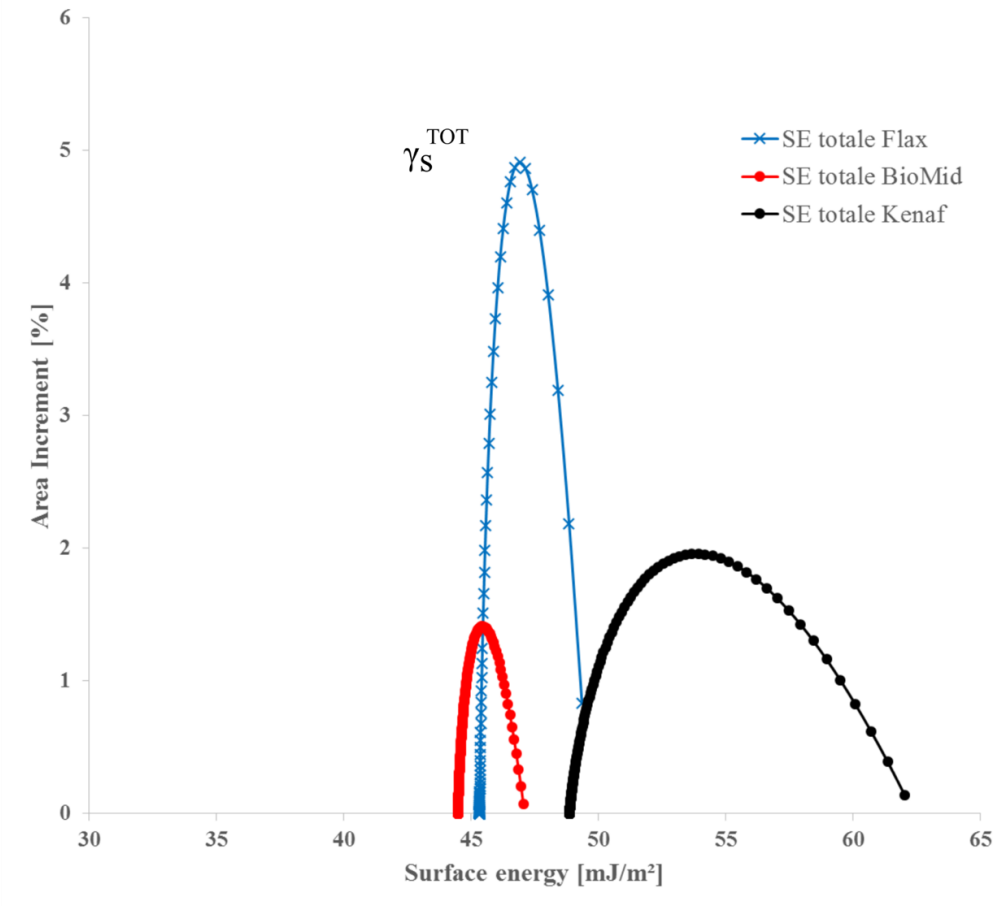

Figure 4.16: γ_S^{TOT} distribution profiles for cellulose BioMid®, kenaf and linseed flax fibres

It is worth noting that data interpretation based on energy values obtained at infinite dilution would be misleading. For instance, all energy components calculated at infinite dilution (energy values considered at 0% coverage) overestimate the mean values obtained at higher surface coverage (50% surface coverage). The surface energy values of BioMid® and flax fibres would be overestimated by 5% and 7% respectively and by more than 20% for the kenaf fibres. Ylä-Mäihäniemi et al. [2008] and Mukhopadhyay and Schreiber [1995] previously pointed out this weakness of traditional IGC experiments. In addition, values obtained at infinite dilution suggest that the kenaf fibres had highest dispersive energy component compared to the BioMid® and flax fibres, which differs from measurements at finite concentration. The latter provide a more accurate representation of the surface and these results highlight the necessity to perform IGC measurement at finite concentration.

4.2.3.2 Effect of chemical treatment on the fibre surface energy profile

TABLE 4.8: Surface energy components ($mJ.m^{-2}$) at 30°C, 0% RH

	γ_S^{LW}			γ_S^{AB}			γ_S^{TOT}			$\gamma_{Smean}^{AB}/\gamma_{Smean}^{TOT}$		
	Min	Max	Mean	Min	Max	Mean	Min	Max	Mean	Min	Max	Mean
Kenaf as received	37.6	43.6	38.8	11.1	18.4	12.5	48.9	62	51.3	0.23	0.3	0.24
Kenaf wash	39.5	41.7	39.9	9.2	13.9	10.1	48.8	55.6	50.1	0.19	0.25	0.20
Kenaf NaOH	39.8	43.1	40.4	7.2	12	8.1	47	55	48.5	0.15	0.22	0.17

Min value corresponds to maximal coverage ($n/n_m = 1$)

Max value corresponds to minimal coverage ($n/n_m = 0$), infinite dilution

Mean value corresponds to 50% coverage ($n/n_m = 50$)

The water wash and alkaline treatments changed both the distribution of the energetic sites and the energy levels of γ_S^{LW} and γ_S^{AB} and therefore of γ_S^{TOT} (Figure 4.17 and Figure 4.18). Both the water wash and alkaline treatments induced a shift to higher average γ_S^{LW} values suggesting that the kenaf fibre surface became more hydrophobic (Figure 4.17a). The evolution of γ_S^{LW} profile indicates an increase in number of high energetic sites and/or an increase in energy

levels of the active sites. This could be due to the removal of polar groups like pectins and extractives while increasing the cellulose and hemicellulose content on the fibre surface. Mills et al. [2008] and Mills [2009] previously observed an increase in γ_S^{LW} with increasing cellulose content. In addition, the water washed fibres had a smaller distribution of the dispersive energetic sites than the fibres as received, whilst alkaline treatment rendered the surface slightly more heterogeneous. The evolution of γ_S^{LW} distribution was consistent with the SEM analysis: the water washed fibres appeared smooth and regular whilst the alkaline treated fibres had a more heterogeneous surface with a visible pattern on the outer layer.

Logically, γ_S^{AB} profile shifted to lower values, as the surface became less polar (Figure 4.17b). The distribution of the polar active sites also diminished, suggesting a reduction in number of high polar sites and/or a decrease in energy levels of the polar active sites. As mentioned previously, both phenomena were likely to occur. At higher coverages, γ_S^{LW} values of kenaf water washed and kenaf alkaline treated fibres converged whereas the latter showed smaller γ_S^{AB} values than the water wash fibres. This suggested that the alkaline treatment induced a major change in the polar functional groups and affected to a smaller degree the dispersive energetic sites.

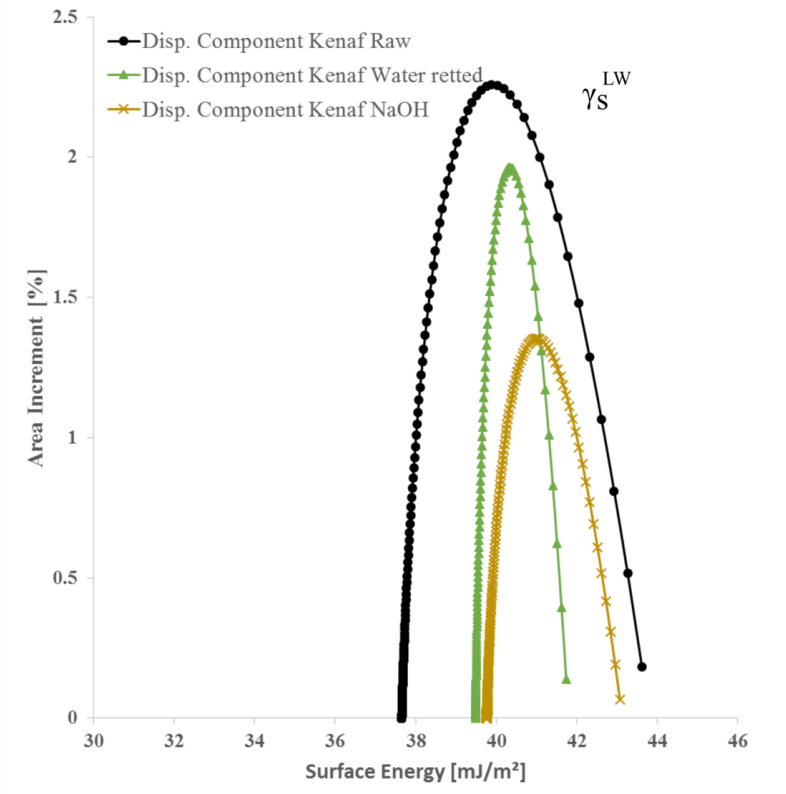

(a)

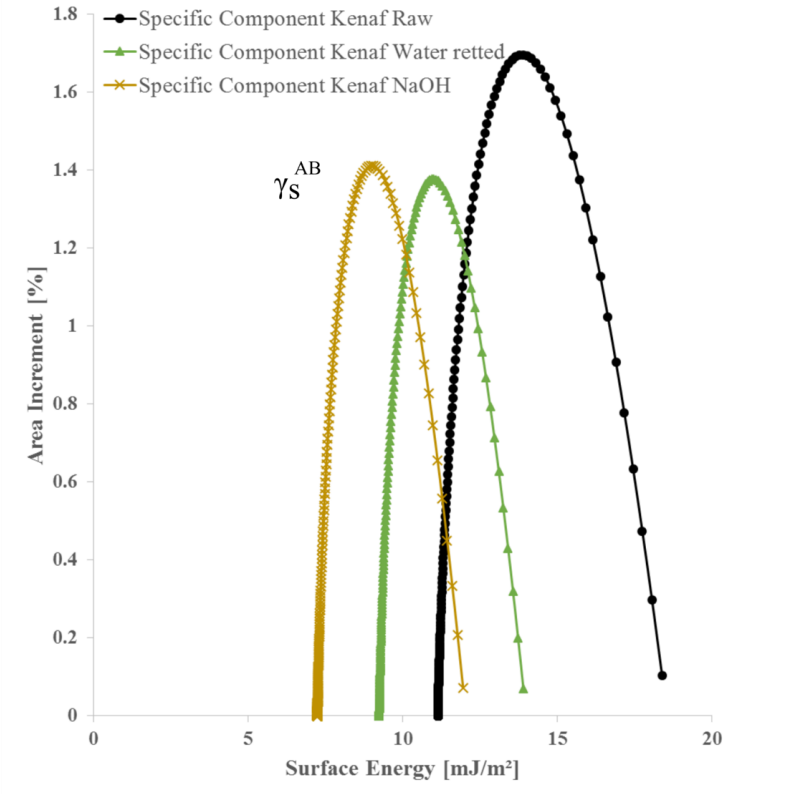

(b)

Figure 4.17: Effect of chemical treatment on (a) γ_S^{LW} and (b) γ_S^{AB}

Finally, a comparison of the γ_S^{TOT} distribution profiles highlights the overall effect of water wash and alkaline treatment on the surface energy profile (Figure 4.18). The water wash reduced the total surface energy values and the surface became more homogeneous. The alkaline treatment further decreased the total energy values but rendered the surface slightly more heterogeneous. Actually, the surface energy values were similar at high surface coverages: the kenaf as received, water washed and alkaline treated fibres had a γ_{Smin}^{TOT} = 48.9 mJ.m^{-2}, 48.8 mJ.m^{-2} and 47 mJ.m^{-2} respectively. This indicates that both treatments only slightly affected the overall surface energy of the fibres. On the other hand, the polarity index $\gamma_{Smean}^{AB}/\gamma_{Smean}^{TOT}$ showed that both treatments reduced the surface polarity: kenaf fibres as received had a polarity index of 0.24 compared to 0.20 and 0.17 for the water washed and alkaline treated fibres respectively (see Table 4.8).

As mentioned in the previous case study, a comparison based on measurements at infinite dilution would overestimate the surface energy values by 20% for the kenaf fibres as received (γ_{Sinf}^{TOT} = 62 mJ.m^{-2} and γ_{Smean}^{TOT} = 51.3 mJ.m^{-2}) and by ca. 10% for the kenaf water washed (γ_{Sinf}^{TOT} = 55.6 mJ.m^{-2} and γ_{Smean}^{TOT} = 50.1 mJ.m^{-2}) and alkaline treated (γ_{Sinf}^{TOT} = 55 mJ.m^{-2} and γ_{Smean}^{TOT} = 48.5 mJ.m^{-2}).

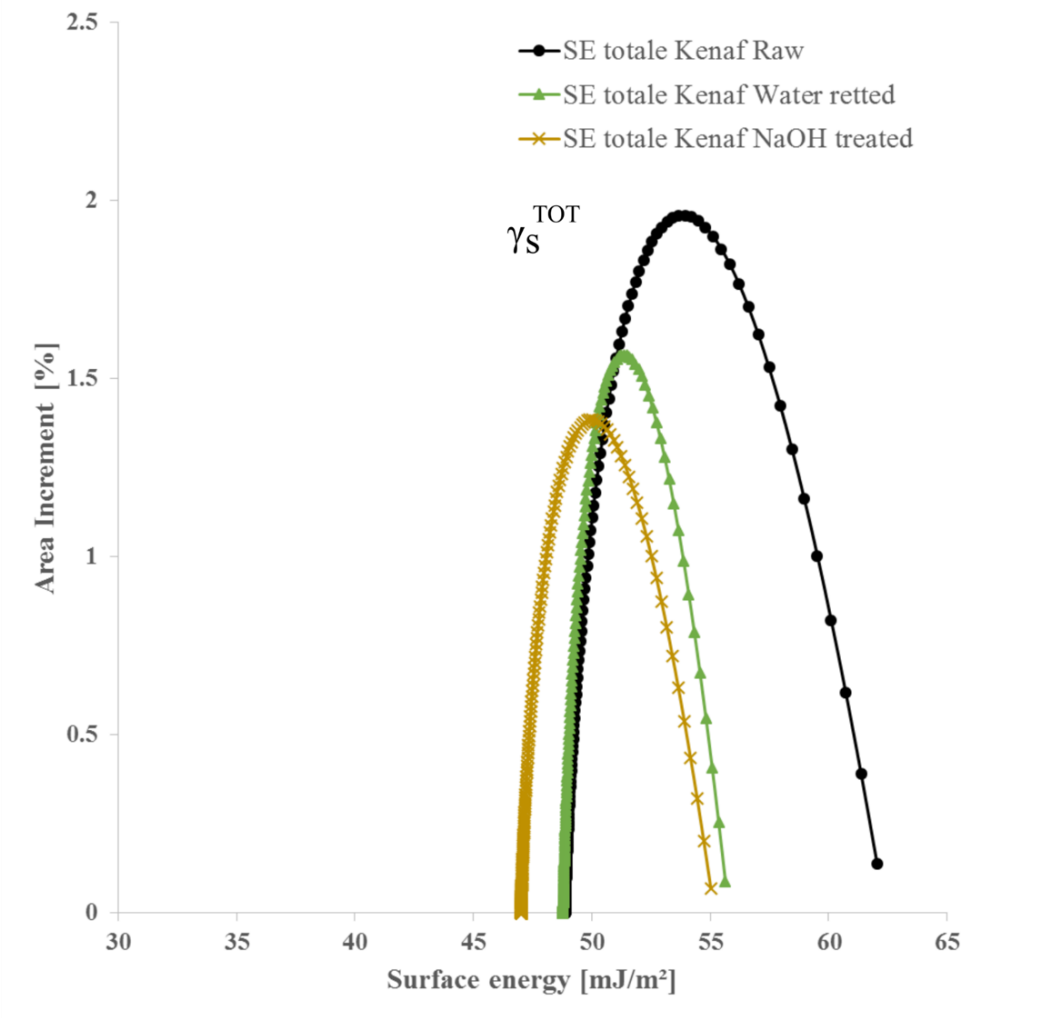

Figure 4.18: Effect of water wash and alkaline treatment on γ_S^{TOT} distribution profile of kenaf

4.3 Conclusions

• IGC is a promising technique to study the surface energy of natural fibres, but IGC applied to natural fibres is relatively recent therefore systematic studies need to be performed.

• In this study, the critical parameters to determine the BET surface area values were identified and a protocol applicable to natural fibres was proposed.

• While IGC traditionally involves infinite dilution, surface energy measurements were performed at finite concentration to obtain more realistic values. The surface energy distribution profiles of the dispersive and the acid-base components provided key complementary information to the overall surface energy profile of natural fibres and highlighted their specificity.

• Investigation of the effect of fibre treatment on the surface energy profiles of kenaf fibres provided new insights, in particular the change in polarity and the distribution of the energetic active sites. All results agreed well with the SEM and XPS analysis performed.

• IGC results showed that the alkaline treatment rendered the kenaf fibre surface less polar and more energetically homogeneous. Consequently, the latter is expected to increase the interfacial interactions with hydrophobic thermoplastics such as polypropylene, polyethylene and polyvinyl chloride.

Chapter 5

Optimisation of Extrusion Process for Biocomposites

The research presented in this chapter formed an integral part of the Cooperative Research Centre for Advanced Composite Structures (CRC-ACS), Project P1.1 "Plant Fibre Biocomposites". The first two sections give a brief synopsis of the CRC-ACS project and relevant research to provide the reader an appreciation on how the thesis fits within the overall project. The third section outlines the experimental approach used to design a series of extrusion trials, followed by the results with discussions. The chapter concludes with an overview of the extrusion trials performed with industrial partners.

5.1 Introduction

The aim of CRC-ACS P1.1 was to develop technology for increased adoption of plant fibre biocomposites, to provide information and guidelines to the Australian composites industry enabling them to increase usage of sustainable composites, and to develop new composites based on thermoset, thermoplastic and/or biopolymer matrices. Work package 2 "Enhanced Short Fibre Biocomposites", in which this project was integrated, had the aim to develop improved short-fibre natural fibre composites for applications in the building and construction sector and work towards the commercialisation of these materials by closing the existing gaps in the supply

chain. A primary focus was devoted to the development of a scalable supply chain where it was demonstrated that each processing step can be upscaled from laboratory to commercial scale. In that light, and with the aim to support a local fibre industry, three key industry partners joined the project. These included Engage Eco Product Co. Ltd, a well-established natural fibre producer in Thailand, Duromer, a speciality compounder in Sydney and Extrusion Technology International (ETI), a Brisbane based extrusion company specialised on commodity extrusions for the horticulture and building & construction sector. The main research partners participating in work relevant to extrusion and compound development are The University of Queensland and the University of Auckland. The Centre for Advanced Composite Materials (CACM) at the University of Auckland, directed by Prof. Debes Bhattacharyya, has a longstanding expertise in biocomposite materials, in particular the compounding and extrusion domain. Prior to the commencement of work related to this thesis, The University of Queensland had very limited experience in the field of natural fibre compounding and extrusion. Establishing this capability and proving the developed technology on an industrial size is seen as one of the major contributions of the project.

5.2 Preliminary Work

This section describes a summary of the research undertaken at the University of Auckland and The University of Queensland. Work performed at the University of Auckland helped guiding the research presented in this chapter. The work described in this section had little intellectual input form the author and is at this point only summarised to provide justification of the starting point of the here presented research. On the other hand, the experimental work undertaken at The University of Queensland on small scale extrusion was heavily influenced by the author, either as principle supervisor or associate supervisor of the students involved. Whilst the research was important in the overall context of the CRC-ACS project, it was decided that it did not form a core part of the thesis and therefore results are only briefly summarised. The results have been published elsewhere [Legras et al., a,b, Ziegelaar, 2013]. The lessons learned from this prior work, however, instructed the thesis work and is summarised in the Section 5.2.3.

5.2.1 Compound optimisation

Compounding work was undertaken by the University of Auckland with the aim to optimise the extrusion processes of short kenaf fibre biocomposites. A detailed summary of this research can be found in CRC-ACS report TR13053 [Rao and Bhattacharyya, 2013]. The experiment was carried out following the Taguchi approach (L9 fractional factorial) to study the effect of feeding location (Zone 1, Zone 2, Zone 3), fibre content (15 wt.%, 30 wt.%, 40 wt.%) and barrel temperature (190°C, 200°C, 210°C). Materials used were polypropylene grade Hopelen J-150 (injection moulding grade, melt flow rate 10 g.10 min^{-1} at 230°C) supplied by Lotte Chemical Corporation and maleic anhydride polypropylene (MAPP) from Clariant (Licocene PP MA 6452, fine grain). Compounding was carried out on a Brabender DSE 25 (40:1 L/D) with a dispenser to feed the polymer and a side feeder to introduce the fibres and MAPP (4 wt.% of the total composition) into the barrel. The screw design included four series of kneading blocs (Figure 5.1) and the screw speed was set up at 70 rpm. Once extruded, the compounds were pelletised and injection moulded into coupon specimens with an injection moulder (BOY 50A). Tensile results from this study are shown in Table 5.1.

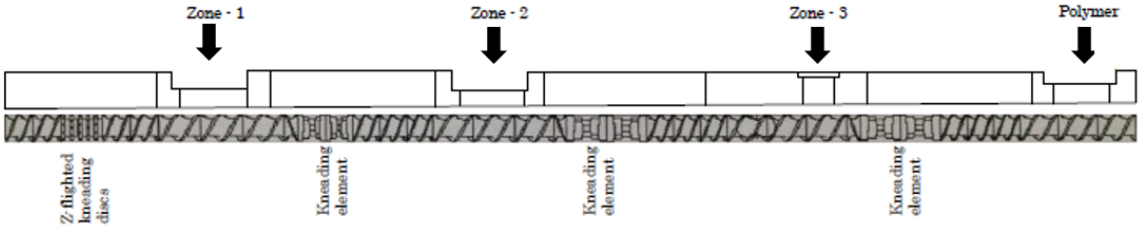

Figure 5.1: Screw configuration and feeding location on the twin-screw extruder Brabender DSE 25

TABLE 5.1: Tensile properties of kenaf/MAPP/PP composites (ASTM D638)

Run	Feeding zone	Barrel temperature (°C)	Fibre content (wt.%)	Average tensile strength (MPa)	Average Young's modulus (GPa)
1	Zone 2	200	15	34.3	3.1
2	Zone 1	190	15	33.6	2.9
3	Zone 3	210	15	38.3	4.2
4	Zone 2	190	30	39.7	4.0
5	Zone 1	210	30	37.9	3.9
6	Zone 1	200	40	38.9	4.2
7	Zone 3	200	30	40.5	4.3
8	Zone 3	190	40	48.2	6.5
9	Zone 2	210	40	41.6	5.5

Experimental data showed a clear trend towards the effect of fibre content on the compound properties, more particularly a strong positive correlation between the fibre load and the tensile properties. The maximum performance was obtained with rear feeding (Zone 3), 40 wt.% fibre content and low barrel temperature (190°C). Analysis of Variance (ANOVA) indicated that the dominant factors were fibre loading and feeding location. Surprisingly, the maximum performance was obtained with rear feeding, which questions the choice of downstream feeding as used in many extrusion experiments [Bengtsson et al., 2007, Santos et al., 2007]. The screw configuration used in these experiments could be classified as mild, therefore, although the residence time of the fibres was considerable, thermal degradation was limited thanks to low temperatures and low energy input all along the barrel.

Further work by the University of Auckland investigated the effect of polymer melt flow on compound properties [Sallih, 2015]. The polymer viscosity behaviour was found to be critical in the extrusion process. In particular, adding fibres into the polymer increased the viscosity hence reducing the melt processability. Therefore, it is advised to extrude polymers with high Melt Flow Index (MFI) in order to achieve efficient fibre wetting. On the other hand, polymers with low MFI offer better sag resistance and drawability due to their hight melt strength [Lau et al., 1998]. The purpose of the study was to characterise kenaf/MAPP/PP composite sheets while varying the die temperature and the MFI. Five PP grades were tested, with an MFI range

from 1.3 g.10 min^{-1} to 11 g.10 min^{-1}: HP555G (MFI 1.3), HA899J (MFI 2.5), HP400L (MFI 5.5), HP422M (MFI 8.5) and HP400N (MFI 11). The maximal tensile and flexural mechanical performance was obtained with the grade HP422M.

5.2.2 Effect of screw speed and screw design

A bench-top study was performed at The University of Queensland under supervision of the author. The study focused on the influence of processing parameters on the mechanical properties of kenaf/high density polyethylene (HDPE) compounds. Kenaf fibres were supplied by Ecofibre Industries Operations Pty Ltd and processed by high velocity air-mill (Aximill) prior to extrusion. Materials were HDPE grade Cotene 3925 (MFI 3.5 g.10min^{-1} at 190°C) supplied by ICO Polymers and ethylene-maleic anhydride copolymer (PEMA) (licocene PE MA 4351) supplied by Clariant. The fibres were added to the master batch PEMA (3 wt.%)/HDPE. L_9 fractional factorial was performed with a lab-scale co-rotating twin-screw extruder EuroLab XL16 (25:1 L/D). The Taguchi array involved three factors of three levels each: fibre loading (0 wt.%, 20 wt.%, 40 wt.%), screw speed (70 rpm, 100 rpm, 130 rpm) and various screw designs (soft, mild, aggressive). The screw mixing zones were altered to modulate the shear input to the melt flow using sequences of forward, neutral or rearward conveying elements (this will be explained later in section 5.3). The feeding system comprised a top-mounted vibration plate to feed the master batch and a Brabender volumetric side feeder to feed the fibres. The samples were waterjet cut from direct extrusion (strip die) into ASTM D638 type IV tensile coupons. Tensile data obtained are listed in Table 5.2.

TABLE 5.2: Tensile properties of kenaf/PEMA/HDPE composites (ASTM D638)

Run	Screw design	Screw speed (rpm)	Fibre content (wt.%)	Average tensile strength (MPa)	Average Young's modulus (GPa)
1	Aggressive	100	0	14.0	0.75
2	Aggressive	130	20	14.8	0.95
3	Aggressive	70	40	13.2	1.31
4	Mild	130	0	14.0	0.76
5	Mild	70	20	14.8	0.88
6	Mild	100	40	17.4	2.35
7	Soft	70	0	13.5	0.92
8	Soft	100	20	14.6	0.99
9	Soft	130	40	18.4	1.84

The efficacy of kenaf Aximilled fibres to improve the tensile modulus was considerable whilst the improvement in tensile strength was marginal: an increase of the Young's Modulus of up to 125% and up to 18% for the tensile strength with 40 wt.% fibre content was noted. This observation is often reported in the literature [Chevali and Ulven, 2012, Oksman et al., 2003, Puglia et al., 2008] and is thought to be due to the creation of defects during the extrusion process, particularly the introduction of porosity and surface heterogeneities. Introduction of porosity during compounding is a typical phenomenon for particle or fibre reinforced plastics that occurs with moisture release and polymer shrinkage at high cooling rate. Fibre bridging due to fibre feeding issues constitutes another plausible explanation for the low performance in tensile strength.

Statistical analysis with ANOVA methods showed a clear trend for the effect of the fibre content on the compound properties. In comparison, the relative efficacies of screw speed and the screw configuration to improve the composite performance were of secondary importance. The optimal configuration was then established based on the calculation of the signal-to-noise ratio for each variable. The major findings are presented in Table 5.3.

Table 5.3: Optimal configuration on Eurolab XL16 for kenaf/PEMA/HDPE composites

Design objective	Screw design	Screw speed (rpm)	Fibre content (wt.%)	Actual tensile properties
Maximum strength	Soft	130	40	Tensile strength: 18.4 MPa Young Modulus: 1.84 GPa
Maximum modulus	Mild	100	40	Tensile strength: 17.4 MPa Young Modulus: 2.35 GPa

As expected, the highest content (40 wt.%) of kenaf fibres lead to both highest tensile strength and elastic modulus. This is not the case for the other parameters; the screw speed and the screw design optimal configurations differ whether the target is to maximise the strength or the Youngs' modulus. This has also been observed in the literature [Alvarez and Vázquez, 2006, Gamon et al., 2013, Mano et al., 2010]. As shown in Table 5.3, there was a compromise between the screw speed and the screw design. A higher screw speed increases the amount of work put into the melt, thereby increasing the mixing intensity. An aggressive screw design induces high shear, hence increases the mixing but also leads to fibre attrition [Giles Jr et al., 2004]. Both screw speed and screw design are interdependent and it appears that there is not a optimum configuration for both strength and stiffness.

5.2.3 Lessons learned

5.2.3.1 Fibre feeding

The first and main lesson learned through the series of experiments performed as part of project CRC-ACS P 1.1 is the importance of feeding strategy. Feeding natural fibres in an extruder is more challenging than feeding synthetic fibres. Traditionally, reinforcement elements and polymer particles are fed as a master batch in compounding extrusion [Giles Jr et al., 2004]. However, feeding natural fibres mixed with the matrix as a master batch is difficult because the fibres have low density and tend to separate, leading to inhomogeneous distribution in the barrel. Also, fibres and polymer granules differ in size and hence do not mix easily. Side-feeding is a preferred option to adjust the feeding rates separately, and it enables the modulation of the feeding position. Natural fibres tend to bridge in the hopper which generates inconsistent feeding, obstruction in the barrel and therefore results in compounds with poor mechanical properties. Bridging is a common issue when feeding low density elements and in particular wood fibres and natural fibres.

Natural fibre pelletising prior to extrusion process has been recently investigated to palliate this issue (BioStruct project, Deutsche Bundesstiftung Umwelt project etc.). Following this approach, the development of a pelletising process for short kenaf fibres was undertaken as an undergraduate research project [Danks, 2014] at The University of Queensland. Natural fibre pellets were successfully produced with a lab pellet mill. The best consistency was achieved when adding 25 wt.% water content to the fibre prior to pelletising with the maximal vertical roller load, through a 6 mm diameter die hole plate. Further investigation was performed on the pellets drying behaviour in an oven and it was found that 70% of the additional water was removed after nine hours at 60°C. Validation tests were performed to feed fibre pellets with a Brabender volumetric side feeder. It was found that the fibre pellets fed more consistently than loose fibre feeding.

5.2.3.2 Up-scaling

The scale-up process was the second important aspect identified during the multiple extrusion trials performed. In biocomposite research, a majority of studies are undertaken with small to medium sized extruders and usually focus on one aspect rather than on the overall process. A complete production process also encompasses the management of material supply, storage, material preparation in large volumes and last but not least, extrusion on a large scale i.e. with large throughput. The scale-up process is challenging, particularly for research groups with limited facilities, but this procedure is *sine qua non* for commercialisation of short fibre biocomposites. It is necessary to study the feasibility of biocomposite extrusion at a large scale to identify the specific needs and issues that arise.

5.2.3.3 Fibre traceability from the field to the factory

Finally, fibre traceability is key for successful extrusion and product optimisation. Compared to typical synthetic fibres (E-glass, carbon fibres), handling large volumes of natural fibres requires better control when it comes to material supply and logistics. This is mainly due to the fact that plant fibres are natural materials, hence they exhibit a large variation in properties. Although the plant fibre microstructure is similar to the wood cell, the growth conditions, plant yield and post processing steps are completely different and only a few techniques can be transferred from the wood industry to the agro-fibre industry.

As discussed in the previous chapters, natural fibres have already a considerable "history" when they enter the compounding process. From the field to the factory, the fibres encounter multiple steps that impact the final properties [Akil et al., 2011, Summerscales et al., 2010]. For example, the bast fibre properties vary between genera and species, depend on the growing conditions (chemical input/weather conditions) and on the harvesting time and technique [Mediavilla et al., 2001]. The retting process and further treatment (chemical or mechanical) also impact the fibre properties [Paridah et al., 2011].

Most of the decisive factors are related to agronomy (plant variety, growing conditions) and the processing conditions (harvesting, retting, treatment). Also, natural fibres display considerable variance and there is currently little control over the "as received"sample properties. To better manage these uncertainties, a proper traceability scheme should be implemented so that industry and research entities obtain the maximum relevant information. It is suggested that each batch is accompanied with a record of the "fibre story"in order to adjust the post processing parameters (storage, fibre treatment, mechanical processing) i.e. to fully exploit the fibre potential. Case-by-case material preparation also facilitates the extrusion process (feeding strategy, control moisture content etc.) and maximises the fibre reinforcing effect.

A typical fibre record should provide at least the following information:

- Genera, specie (variety)
- Plantation location, growth conditions (chemical input)
- Retting process
- Post processing (chemical treatment, mechanical process)

5.3 Experimental Approach

The lessons learned from previous extrusion studies provided a new toolbox to run further trials en route to industrial commercialisation. A new design of experiment for biocomposite extrusion was performed at medium scale with well characterised bast fibres (Figure 5.2). The series of trials comprised direct extrusion and compounding followed by injection moulding.

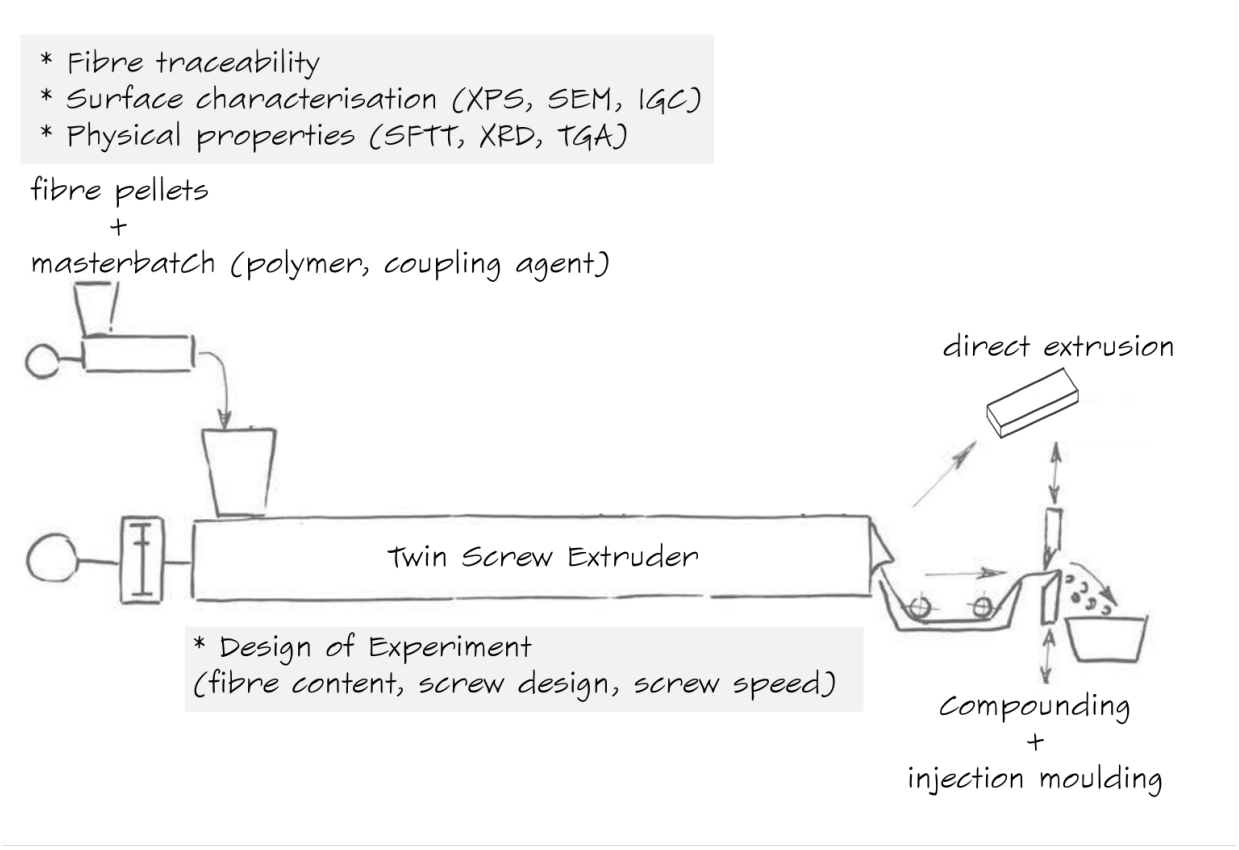

Figure 5.2: Experimental approach to optimise the extrusion process for short fibre biocomposites (image inspired by [Müssig and Haag, 2012])

5.3.1 Materials

The choice of materials was made according to the outcome and lessons learned from the previous studies. The fibres were supplied by Engage Eco Product Co. Ltd, the company grows kenaf locally and processes the plant stems on site to produce bast fibres, shives and leaves. According to the supplier, the crops are processed with environmentally-friendly technologies

and the products are dust and pesticide-free. The company supplies national and international customers from diverse industrial sectors (automotive, textile, construction, biocomposites, animal feed etc.). Therefore, the fibre source met all criteria identified previously: large and reliable supply, fibres produced and processed according to industrial standards with minimal chemical input in order to limit the overall carbon footprint and to obtain fibres as "green"as possible.

Engage Eco Product Co. Ltd grows the kenaf variety Khon Khaen 60 (KK60) from the specie *Hibiscus Cannabinus*. Kenaf KK60 is one of the most common varieties produced in Asia and Indonesia because of its high yield and high quality [Tahery et al., 2013]. The kenaf fibres were locally water retted and alkaline treated to maximise their mechanical performance and, in particular, to enhance the fibre/matrix interfacial interactions for biocomposite applications. A second batch of fibres that had been water retted and water washed was also supplied for comparison with the chemically treated fibres (see Table 3.2).

Polypropylene grade Moplen HP422M (MFI 8.5 g.10 min^{-1}, LyondellBasell) was selected based on the findings of Sallih [2015]. MAPP (Licocene PP MA 6452) was used as a coupling agent to improve the fibre/matrix adhesion. MAPP is a grafted copolymer that has been commonly used to enhance short fibre reinforced polypropylene compounds. It has been shown that addition of about 3 wt.% to 5 wt.% MAPP to the compound formulation improved the overall mechanical properties [Sallih, 2015]. Both the polypropylene and the coupling agent were fed in granulate form to match the size of fibre pellets (3 mm long). It is advisable to have a formulation with components of similar size to get good homogeneity and to maximise the mixing during processing [Giles Jr et al., 2004]. A summary of the materials used for the extrusion trials is provided in Table 5.4.

Table 5.4: Samples used for extrusion trials

Material	Specification	Supplier
Kenaf	Cultivar KK60	Engage Eco Product Co. Ltd.
Polypropylene	Moplen HP422M (MFI 8.5 g.10 min^{-1})	LyondellBasell Australia
Maleic anhydride polypropylene	Licocene PP MA6452 (7% maleic anhydride)	Clariant Germany

5.3.2 Fibre characterisation

Kenaf fibre surface properties have been characterised by SEM, XPS and IGC. These results were reported in the previous chapters and will only be briefly summarised in this section. The fibres were also characterised by Single Fibre Tensile Testing (SFTT) and X-Ray Diffraction (XRD) at the Composites Innovation Centre (Canada). In addition, Thermogravimetric Analysis (TGA) was performed at The University of Queensland. Finally, the fibre morphology and aspect ratio were determined with the HiRes Fibre Quality Analyser (FQA) developed by OpTest Equipment Inc. (Canada). These new results are briefly detailed in the following paragraphs and the overall characterisation results are summarised in Table 5.5 and Table 5.6.

TABLE 5.5: Characteristics of kenaf KK60 alkaline treated fibres

Characteristic	Technique	Findings
Surface morphology	SEM	Rough surface partially covered with an amorphous layer rich in lignins and waxes. The surface underneath likely contains cellulose, hemicellulose and pectins. Traces of extractives also visible on the surface.
Surface chemistry	XPS	O/C ratio of 0.44 suggests a surface rich in lignins and poor in cellulose. Specific peaks of the functional groups (ester group, methoxy substitution and Pi-Pi* shake up bands) confirm the presence of lignins, hemicellulose and pectins. Strong C-C peak confirms the presence of extractives.
Surface energy	IGC	BET specific surface area = 0.55 $m^2.g^{-1}$ Surface relatively energetically heterogeneous ranging from 47 $mJ.m^{-2}$ to 55 $mJ.m^{-2}$ with an average of 48.5 $mJ.m^{-2}$. Main contribution from dispersive interactions compared to polar sites. Polarity index (Dichloromethane/ Ethylactetate) = 0.17
Fibre dimensions	FQA	Fibre average length = 3.00 ± 1.79 mm Average aspect ratio = 75
Crystallinity [a]	XRD	Average crystallinity index = 45.4% (Cellulose I)
Thermal properties	TGA	Temperature of degradation 10 wt.% loss at 234°C and 20 wt.% loss at 287°C
Tensile properties [a]	SFTT	Youngs' Modulus = 36.6 ± 15.5 GPa Tensile strength = 528.2 ± 219.2 MPa Large standard deviation

[a] experiment performed on kenaf fibres as received

TABLE 5.6: Characteristics of kenaf KK60 water washed fibres

Characteristic	Technique	Findings
Surface morphology	SEM	Smooth and relatively homogeneous surface rich in lignins and waxes. Some inorganic materials loosely attached to the surface due to milling process.
Surface chemistry	XPS	O/C ratio of 0.34 suggests a surface containing predominantly lignins and poor in cellulose. Higher content of fatty acids and less cellulose than in NaOH treated fibres.
Surface energy	IGC	BET specific surface area = 0.80 $m^2.g^{-1}$ Surface relatively energetically heterogeneous ranging from 48.8 $mJ.m^{-2}$ to 55.6 $mJ.m^{-2}$ with an average of 50.1 $mJ.m^{-2}$. Main contribution from dispersive interactions compared to polar sites. Polarity index (Dichloromethane/ Ethylactetate) = 0.20
Fibre dimensions	FQA	Fibre average length = 2.78 ± 1.71 mm Average aspect ratio = 85
Crystallinity [a]	XRD	Average crystallinity index = 45.4% (Cellulose I)
Thermal properties	TGA	Temperature of degradation 10 wt.% loss at 258°C and 20 wt.% loss at 298°C
Tensile properties [a]	SFTT	Youngs' Modulus = 36.6 ± 15.5 GPa Tensile strength = 528.2 ± 219.2 MPa Large standard deviation

[a] experiment performed on kenaf fibres as received

5.3.2.1 Fibre length distribution

Alkaline treated fibres and water washed fibres were analysed with the HiRes FQA, a well-known commercial hydrodynamic equipment used in the pulp and paper industry to determine the fibre length distribution (TAPPI T271 and ISO 16065-1 standards). The system comprises a cytometric flow cell with a built-in analysis software and benefits from a circular polarised light to improve the measurement accuracy for the fibre length and shape. According to the

manufacturer, the HiRes FQA has a measurement sensitivity less than 1 μm per fibre and less than 0.1 μm per test [OpTest, 2010]. Average dimensions are given in Table 5.7 and fibre length distributions are provided in Figure 5.3.

Table 5.7: Fibre dimension measurements

Fibres	Average weighted length[a] L_W (mm)	Average width (μm)	Aspect ratio	Curl index	Kink index
Water washed	2.78 ± 1.71	32.7	85	0.132	0.885
NaOH treated	3.00 ± 1.79	39.9	75	0.164	1.264

[a] assumes constant coarsness

Water washed fibres and alkaline treated fibres had similar average weighted lengths of respectively 2.78 ± 1.71 and 3.00 ± 1.79 but the latter had a larger diameter and therefore the aspect ratio of water washed fibres was about 13% higher than that of NaOH treated fibres. The curvature index showed that the latter had slightly higher curvature (0.164 vs. 0.132) and contained almost double the number of kinks (abrupt change in the fibre curvature) than the water washed fibres. These differences in morphology will most likely affect the composite mechanical properties. This will be discussed later in the chapter.

Although both batches displayed similar average fibre length, the fibre length distributions were substantially different (Figure 5.3). The water washed fibre batch contained a large number of small fibres and a relatively homogeneous distribution of fibres between 0.8 mm and 4.5 mm length (Figure 5.3a). On the other hand, alkaline treated fibre distribution profile was closer to a normal distribution with most of the fibres of about 2 mm long (Figure 5.3b). This constitutes a major difference between both batches which may affect as well the composite properties.

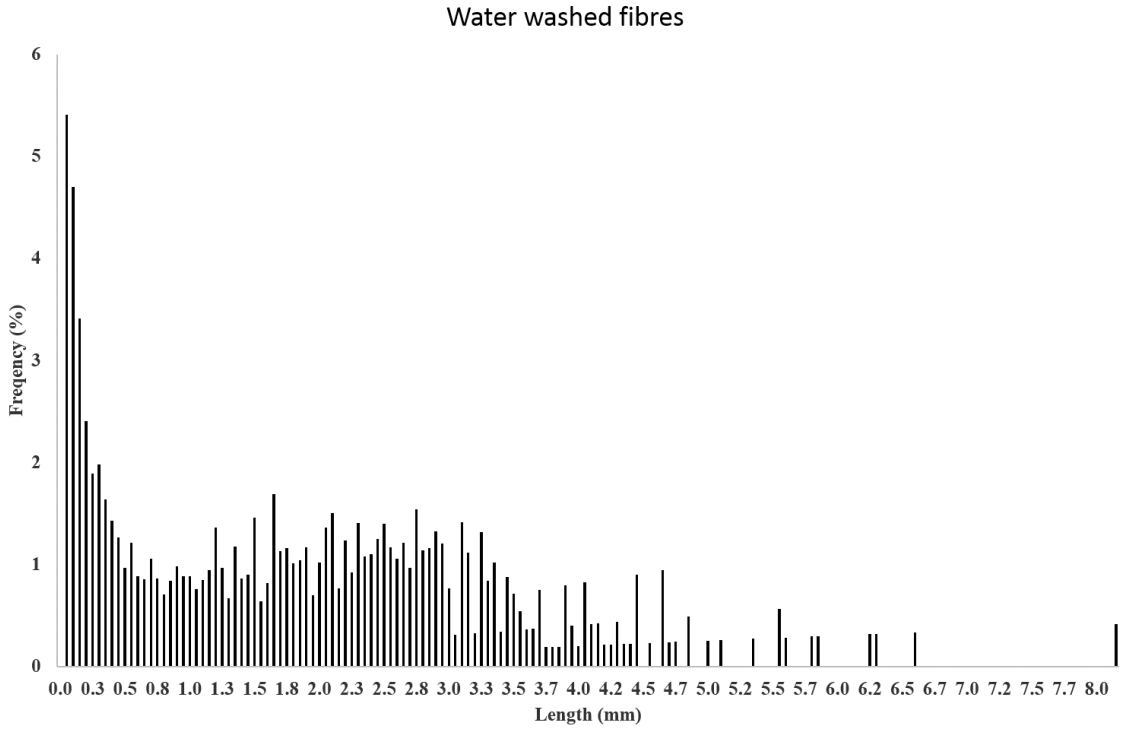

(a)

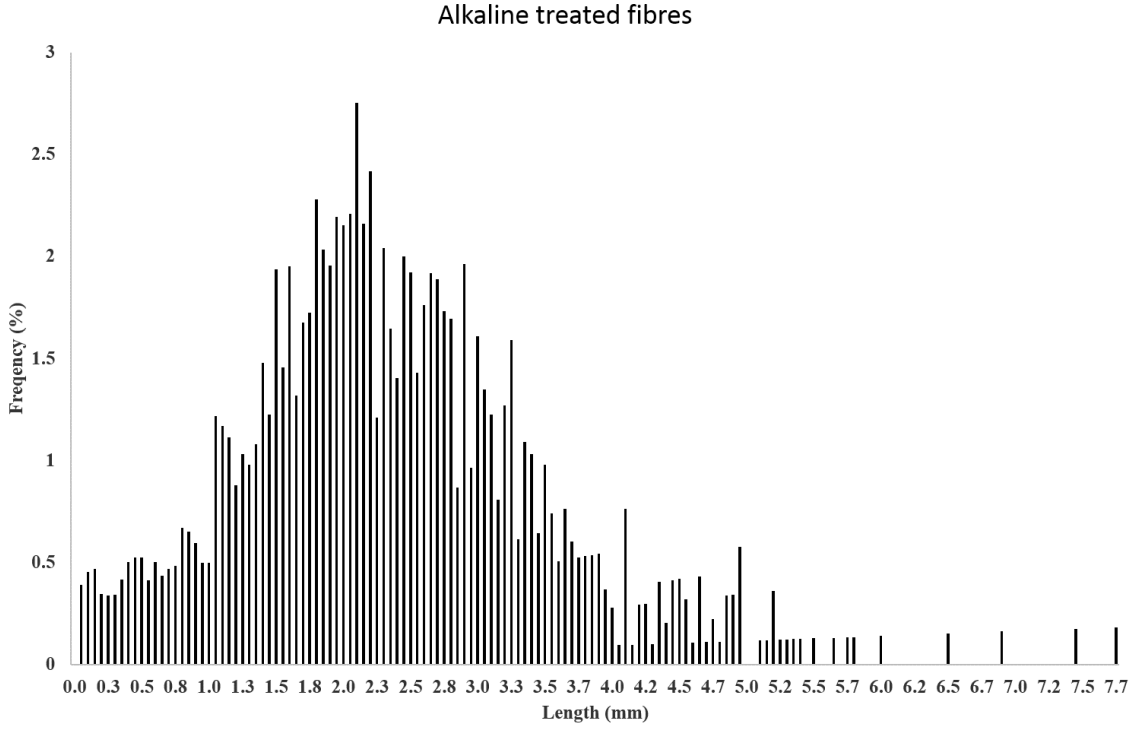

(b)

Figure 5.3: Fibre length distribution obtained with the HiRes FQA (a) water washed fibres and (b) alkaline treated fibres

5.3.2.2 XRD analysis

The fibres were analysed with an Agilent Technologies SuperNova A (Cu) X-ray diffractometer combined with an Atlas CCD area detector. The X-ray wavelength was 1.54 Å and the scan rate was 2 degrees per second. Data acquisition was performed with CrysAlisPro software. The background X-ray signal was obtained with no fibre in position in order to build the reference pattern. Five specimens of about 12 mm length were analysed and each data was averaged from three measurements along the fibre axis. Note that only the kenaf fibres as received were characterised because the alkaline treated and water washed fibre samples were non suitable for the XRD analysis (the single fibre strands were too short for the fixation system). Data analysis was performed with MATLAB and the Crystallinity Index (CI) was calculated from the XRD radial plot according to Segal's method [Segal et al., 1959]:

$$CI = \frac{I_{002} - I_{am}}{I_{002}} * 100 \tag{5.1}$$

where I_{002} is the maximum intensity of the 002 lattice diffraction (arbitrary units) and I_{am} is the intensity of diffraction at $2\theta = 18°$ (same units). I_{002} peak represents the interferences of native cellulose (cellulose I) and I_{am} that of amorphous cellulose. For the kenaf KK60 fibre sample (as received), I_{002} and I_{am} were identified at 22.15° and 18.4° respectively (Figure 5.4). The average CI index was estimated at 45.4% ± 0.7.

Although XRD analysis could not be performed on the water washed and alkaline treated fibres, the latter were expected to contained cellulose II due to the partial conversion of the cellulose crystal lattice from type I to type II during alkaline treatment [Gassan and Bledzki, 1999a, O'Sullivan, 1997]. Usually, bast fibres have their CI increased by alkaline treatment due to the removal of lignins and hemicellulose that enable better packing of the cellulose chains (see Section 3.1). For instance, the linseed flax and linen flax had their CI increased by respectively 9% and 11% after NaOh treatment (Figure 5.4). However, both alkaline treated and water washed kenaf fibres were hammer milled which may have slightly reduced their CI.

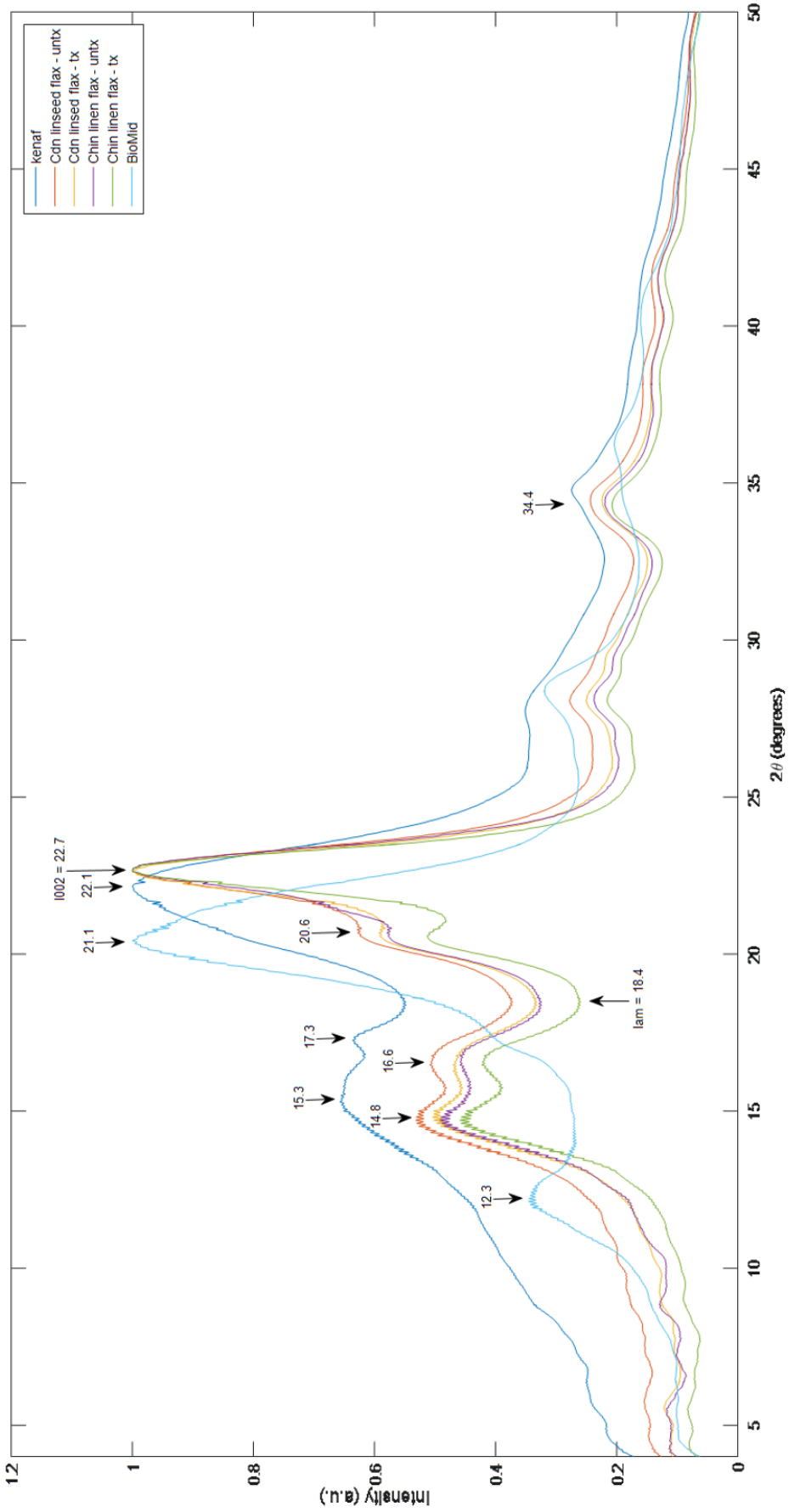

Figure 5.4: XRD radial plots (mean, normalized) (data kindly provided by CIC)

5.3.2.3 TGA analysis

TGA was performed with a Mettler Toledo TGA LF1600, at a heating rate of 10°C.min^{-1} up to 400°C in air. One sample of 6 ± 0.2 mg was tested per batch. The thermal degradation profiles are provided in Figure 5.5.

Table 5.8: TGA data

	Kenaf as received	Kenaf water washed	Kenaf alkaline treated
T 10 wt.% loss (°C)	262	258	234
T 20 wt.% loss (°C)	302	298	287
T 50 wt.% loss (°C)	344	342	342

A small weight loss was first observed between 50°C and 100°C, which corresponds to moisture release. The degradation temperature corresponding to 10 wt.% loss was similar for the as received and water washed fibres, at about 262°C and 258°C respectively (Table 5.8). Alkaline treated fibres started to degrade at slightly lower temperature (234°C) but the degradation rate was slower than that of the other samples (see Figure 5.5b). This suggested different degradation mechanisms occurring due to distinct physico-chemical properties, including the surface chemical composition. The difference in total weight loss between the samples was also due to the fibres' different chemical compositions (samples were normalised for calculation). From a processing point of view, all behaviours suggested that the fibres should not be exposed to temperatures more than 210°C to 230°C to avoid material degradation. The processing time, for instance, the residence time in the extruder and injection moulding system, may allow sufficient time for degradation processes to happen. It is therefore advised to keep the melt temperature under 200°C - 210°C to preserve the fibre integrity. Commercial grades of polypropylene have a Vicat softening point of 143°C - 164°C and a melting point of 161°C - 170°C (source CES Edupack 2012). PP grade Moplen HP422M Vicat softening point is at about 154°C therefore extrusion can be performed with little risk of fibre degradation.

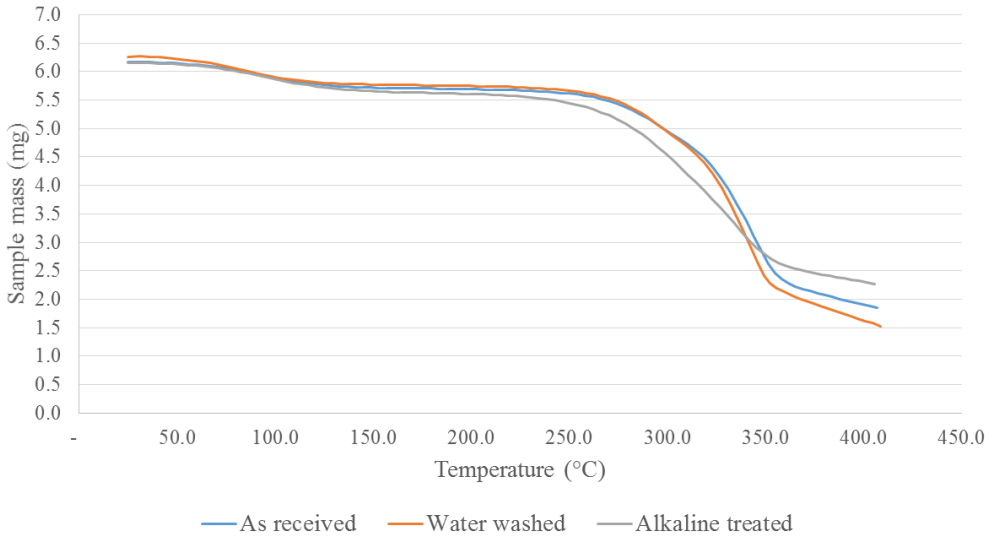

(a)

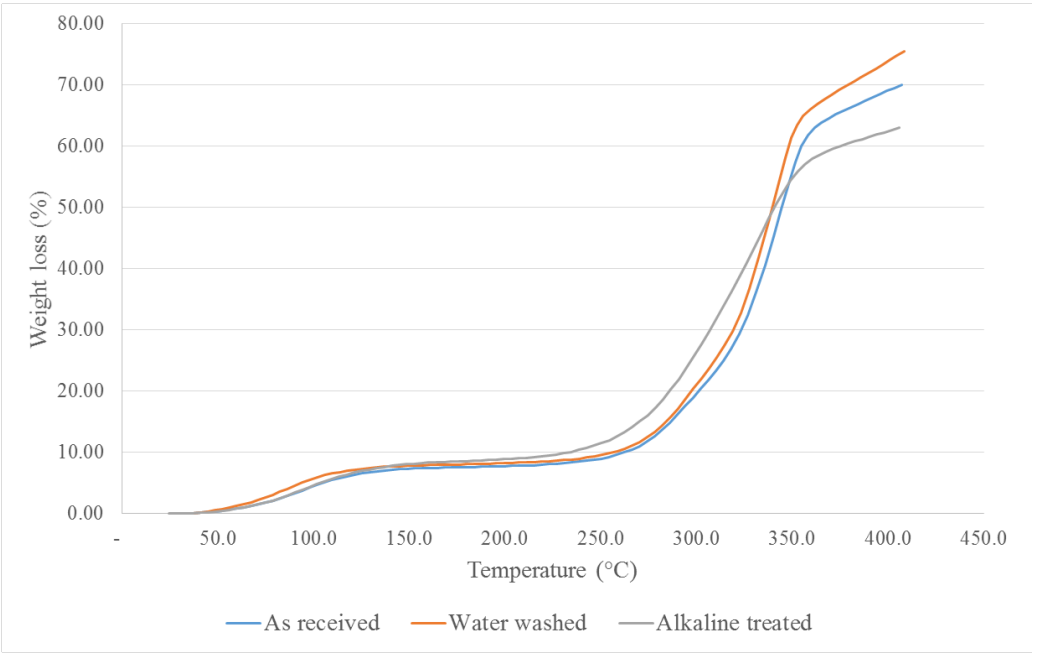

(b)

Figure 5.5: TGA curves (a) sample mass and (b) weight loss

5.3.2.4 Single Fibre Tensile Testing

Single fibre tensile testing was performed on a Dia-Stron system equipped with a linear extensometer LEX810 with a 20 N cell load and a high resolution dimensional measurement system FDAS770. The fibre gauge length was 12 mm. Only the kenaf fibres as received could be characterised because the alkaline treated and water washed fibre strands were too short for the fixation system. The cross sectional area, assumed to be an ellipse, was calculated based on three diameter measurements along the fibre axis. The strain rate was fixed to 0.0096 $mm.s^{-1}$ in order to meet the failure criteria from ASTM D2256 which assumes the fibre breaks within 20 $\pm$ 3 s. A cassette of 50 fibres was tested, among which 11 data-points were invalid and therefore omitted. The histograms of tensile data obtained are shown in Figure 5.6. Kenaf fibres had an average Young's Modulus of 36.6 $\pm$ 15.5 GPa and average tensile strength of 528.2 $\pm$ 219.2 MPa. The standard deviation was considerable as usually observed for natural fibres.

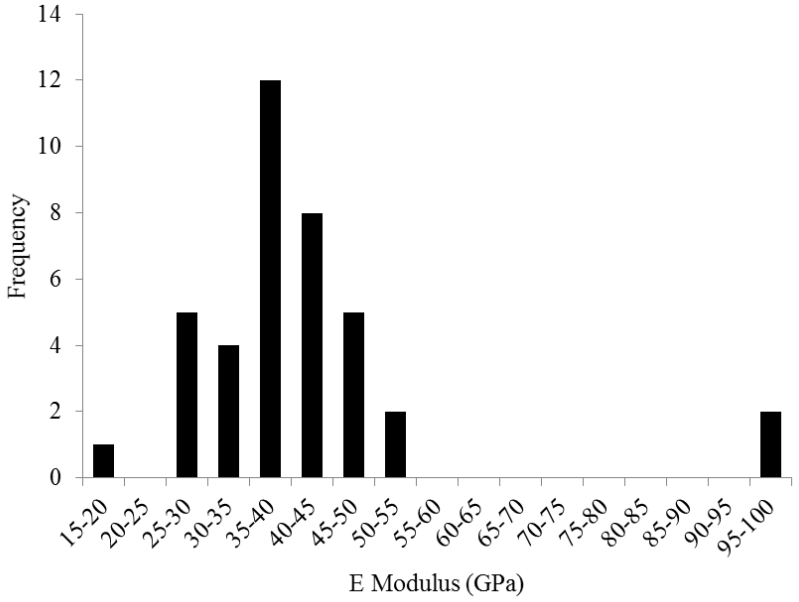

(a)

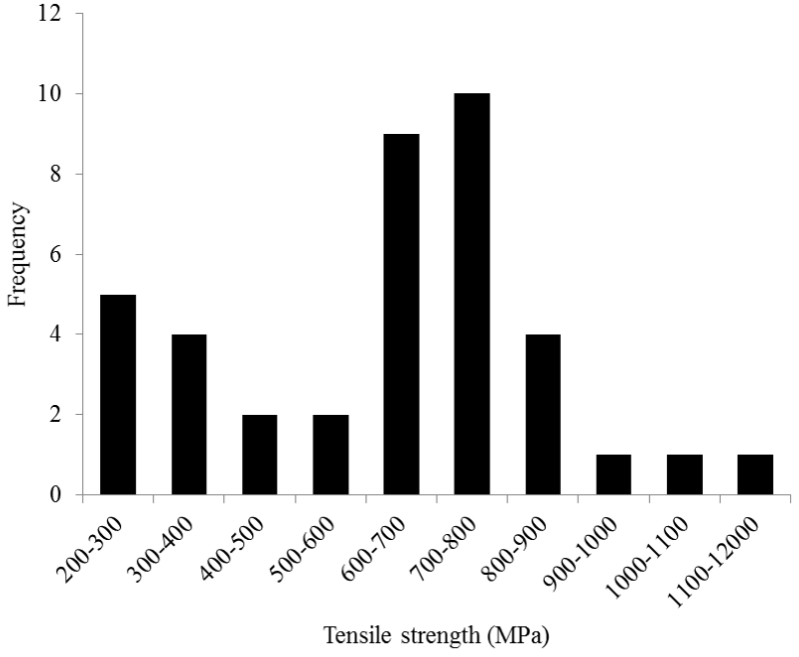

(b)

Figure 5.6: Histograms of tensile properties for a batch of kenaf fibres (39 elements): (a) Young's modulus and (b) tensile strength

5.3.3 Design of Experiment towards large scale compounding

Optimisation of the extrusion process was performed at a medium scale (40:1 L/D) to investigate which variables mostly affect the compound properties when extrusion is performed under "industrial" conditions. One of the main objectives was to investigate the effect of screw design. Screw configuration is key to obtaining adequate compound properties, in particular when adding particulates for polymer reinforcement. Careful design of the screw elements allows control of the melt pressure and the melt temperature in specific locations in order to obtain sufficient mixing without degrading the compound [Giles Jr et al., 2004]. Based on the guideline for extrusion published by Giles Jr et al. [2004], the following criteria were considered for short kenaf fibres reinforced polypropylene compounding on a twin-screw extruder:

• Polypropylene viscosity is very shear sensitive and less temperature sensitive. Therefore a high shear screw configuration was used to lower the viscosity and enhance the melt flow.

• Forward, neutral and rearward kneading elements were used to modulate the melt rheological properties as it progresses in the barrel. For instance, a rearward kneading block creates a melt seal which helps to completely melt the formulation before it moves downstream and it also prevents the air from passing through. Configuration of the kneading block sequences affects as well the residence time.

• Narrow kneading blocks were preferred to wide elements to provide efficient distributive mixing of the fibres and to limit dispersive mixing that would shorten the fibres.

• Large-pitch conveying elements were placed between mixing zones (high pressure areas) to create low pressure areas in order to avoid melt degradation due to overheating or too much shear.

Three screw designs were configured according to the above criteria in order to input a soft, mild or aggressive work into the melt flow. The soft screw design was based on a sequence of two single mixing zones located in the first half of the barrel that comprised forward elements only (M1-M2). The mild screw configuration involved a second sequence of kneading elements (M3) that included a melt seal. M3 was located in the last third section of the barrel, prior to compression zone towards the die. Finally, the most aggressive screw design comprised a third

mixing block with a melt seal (M4) located between M1-M2 and M3. Detailed configurations of the mixing zones are given in Table 5.9 and illustrated in Figure 5.7 with pressure profiles.

Table 5.9: Screw configurations used in the design of experiment

	Mixing Zones		
Screw design	M1-M2	M4	M3
Soft	F 30/5/30 C 90 mm F 30/5/30 F 60/5/30	/	/
Mild	F 30/5/30 C 90 mm F 30/5/30 F 60/5/30	/	F 30/5/30 N 90/5/30 R 30/5/30
Aggressive	F 30/5/30 C 90 mm F 30/5/30 F 60/5/30	F 30/5/30 N 90/5/30 F 60/5/30	F 30/5/30 N 90/5/30 R 30/5/30

C: conveying, F: forward, N: neutral, R: rearward

Sequence: stagger angle/number of elements/total block length

Small scale extrusion trials previously highlighted the dominant effect of fibre loading on the mechanical properties and therefore it was intended to assess as well the impact of fibre content at larger scale. On the other hand, screw speed was reported as a moderate factor on bench top extruders but the relative effect of screw speed may become a main factor at larger scale due to the interdependence of screw speed and screw design. Screw speed affects as well the residence time of the melt flow in the barrel. Therefore, the influence of screw speed on the compound resulting properties was also investigated.

Considering the multiple variables involved in the extrusion process, investigating the effect of each parameter separately would require a significant amount of time and resources. A full test matrix would consider all the possible situations that can occur with the factors and their different levels. An L9 fractional factorial was used to streamline the test matrix with three

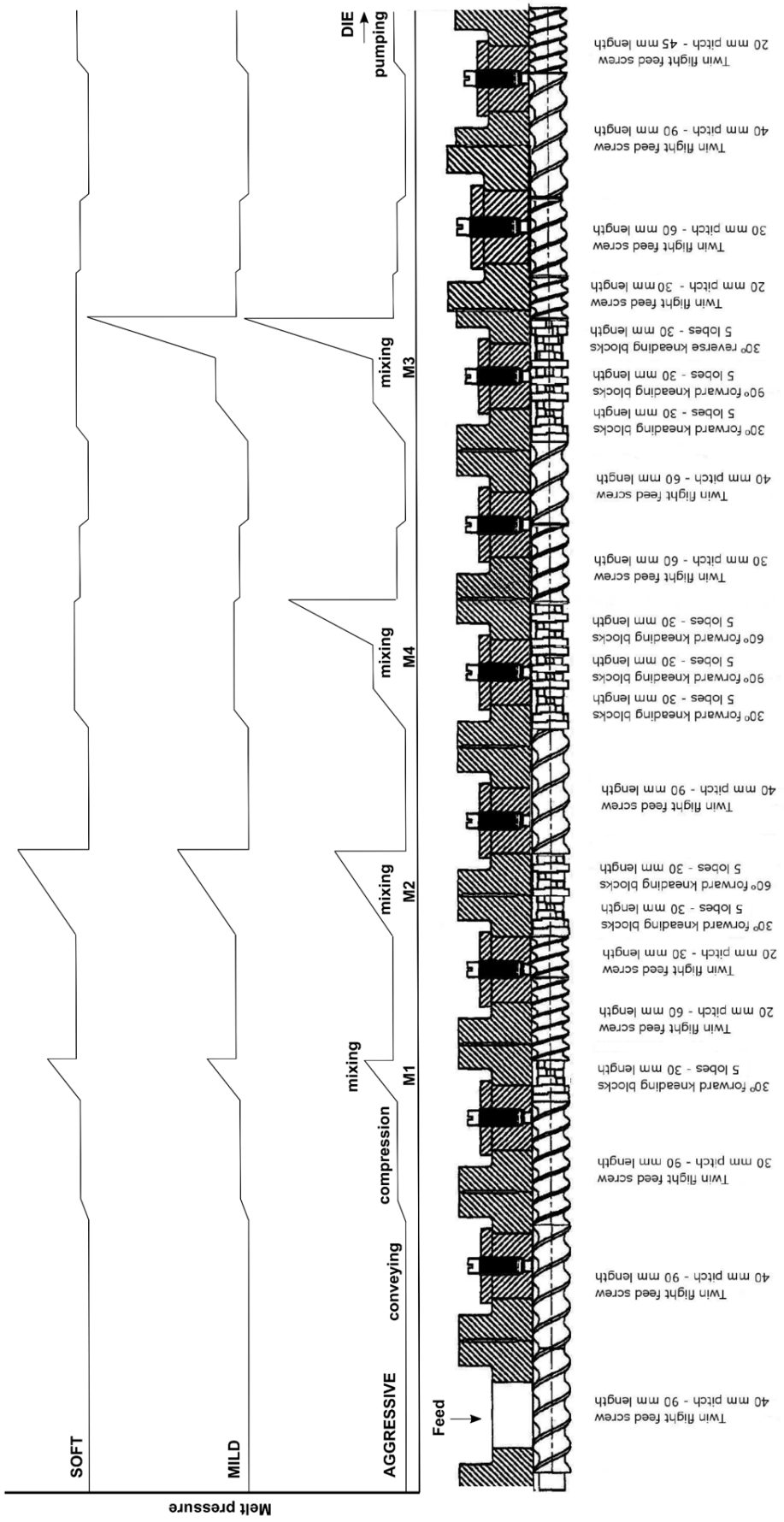

Figure 5.7: Screw design (aggressive configuration) and pressure profiles

factors at three level each: fibre load (0 wt.%, 20 wt.%, 40 wt.%), screw speed (80 rpm, 100 rpm, 130 rpm) and screw design (soft, mild, aggressive). The levels for fibre load and screw speed were based on the experience from previous experiments and on the extruder capability. The test matrix is provided in Table 5.10 and Table 5.11.

Table 5.10: Factors and levels used in the design of experiment

	Levels		
Factors	1	2	3
Screw design	soft	mild	aggressive
Screw speed (rpm)	80	100	130
Fibre load (wt.%)	0	20	40

Table 5.11: L9 fractional factorial used for large scale compounding

Trial	Screw design	Screw speed (rpm)	Fibre content (wt.%)
1	Aggressive	100	0
2	Aggressive	130	20
3	Aggressive	80	40
4	Mild	130	0
5	Mild	80	20
6	Mild	100	40
7	Soft	80	0
8	Soft	100	20
9	Soft	130	40

Extrusion trials were performed on a 27 mm co-rotating twin-screw extruder 40:1 L/D (ENTEK Emax). The barrel was 1080 mm and included ten individual heating zones (see Figure 5.7). Kenaf (KK60) alkaline treated fibres were pelletised into 3 mm diameter pellets and then dried overnight at 85°C prior to extrusion in an oven (Contherm Thermotec 2000). The fibre pellets were then mixed manually with the master batch MAPP (3wt.%)/PP and the formulation was fed into zone 1 with a gravimetric Brabender feeder. The latter was calibrated prior to extrusion to ensure the feeding rate was accurate and equal to 50 g.min^{-1}. The barrel temperature was set up for each trial as follow: zone 1 (feed) at 120 °C, zone 2-9 at 170°C/175°C, zone 10 at

175°C/180°C, zone 11 at 175°C/185°C and the die was not heated. Note that the extruder set-up did not include a venting zone to avoid protrusion of the melt due to the back flow. The melt was extruded through a strip die (30 mm x 4 mm) for direct extrusion and through a 3 x ∅3 mm rod die plate for compounding. The strips were water-jet cut into ASTM D638 type IV tensile coupons and tested with an Instron 5884 load frame and Bluehill software v.3 combined with an Instron Advanced Video Extensometer 2663 (gauge length 25 mm) at a crosshead speed of 5 $mm.min^{-1}$ and a 5 kN load cell. A minimum of five coupons were tested for each combination. The rod extrudates were cut into pellets with a granulator and injection moulded on a Babyplast 610P into ASTM D638 type IV at 170°C (the volume of material available was insufficient for a large scale injection moulding machine). Injection moulded specimens were tensile tested in similar conditions than the strip extrudates.

5.4 Results & Discussions

Tensile properties of the extruded compounds are given in Table 5.12 followed by discussions and statistical analysis with ANOVA methods.

TABLE 5.12: Tensile properties of kenaf/MAPP/PP composites (ASTM D638)

Trial	Screw design	Screw speed (rpm)	Fibre content (wt.%)	Tensile strength [range]* (MPa)	Young's modulus [range]* (GPa)
1	Aggressive	100	0	26.8 [22.0-29.2]	1.6 [1.4-1.9]
2	Aggressive	130	20	32.0 [32.4-34.4]	2.2 [2.1-2.2]
3	Aggressive	80	40	16.6 [12.3-34.4]	2.0 [1.7-2.5]
4	Mild	130	0	28.4 [27.6-29.5]	1.3 [1.1-1.5]
5	Mild	80	20	25.3 [22.0-27.0]	2.2 [2.1-2.3]
6	Mild	100	40	15.2 [9.8-17.2]	1.7 [1.5-1.9]
7	Soft	80	0	26.7 [25.6-27.8]	1.5 [1.2-1.9]
8	Soft	100	20	25.6 [23.6-27.8]	2.0 [1.8-2.4]
9	Soft	130	40	12.5 [10.9-14.3]	1.5 [1.3-1.7]

*Insufficient data to calculate the standard deviation

Comparing the average data from Table 5.12, adding kenaf fibres resulted in an increase the tensile modulus of up to 46% for 20 wt.% fibre content. On the other hand, the improvement in tensile strength was marginal with an increase of 17% only for 20 wt.% fibres and a reduction in tensile strength by almost 50% for 40 wt.% fibre load. These trends agreed with short fibre biocomposite mechanical behaviour and the tensile properties obtained fell well within the range of values typically published in literature but are considered to be on the lower end of the range (see Figure 2.3). This was likely due to porosity and/or poor interface. Micro computed tomography (CT) revealed considerable porosity in all specimens which confirms this hypothesis (see illustration later in Figure 5.11 and Figure 5.15). Porosity was most likely created from moisture release in the barrel that could not be completely evacuated because there was no vacuum port set up on the barrel or insufficient pressure in the die. However, the average tensile properties achieved with such large porosity suggest a great potential to obtain better mechanical properties if the compounds had lower porosity. Tensile testing of injection

moulded specimens from compounded pellets was performed to validate this assumption and the results will be discussed later.

ANOVA statistical analysis was performed to analyse the relative efficacy of the factors considered (screw design, screw speed and fibre content) and to determine the optimal extruder configuration for maximal mechanical performance.

5.4.1 Tensile modulus response

The response means for each control factor on the tensile modulus are given in Figure 5.8. The main effect plot showed different trends for all factors; screw speed and screw design have a pseudo linear response whereas the fibre content exhibits a local maxima at 20 wt.%. The amplitudes of the mean response showed that fibre loading has a main effect whilst screw speed and screw design affect to a lower degree the final response of the system. This is supported by the response table for means which shows that the variance induced by the fibre content is more than twice that of the screw speed and screw design (Table 5.13). The response table for signal-to-noise (S/N) ratios also suggested that fibre content was the most influential factor to maximise the S/N ratio for tensile modulus (Table 5.14).

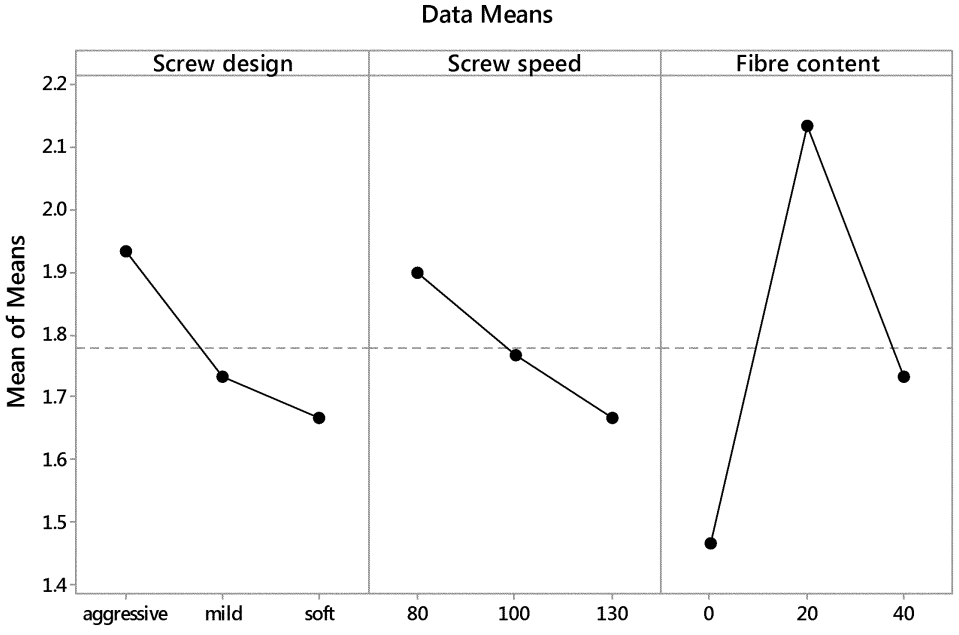

Figure 5.8: Main effect plot of elastic modulus (GPa)

Table 5.13: Response table for means showing the relative influence on each factor on tensile modulus

Level	Screw design	Screw speed	Fibre content
1	1.933	1.900	1.467
2	1.733	1.767	2.133
3	1.667	1.667	1.733
Delta	0.267	0.233	0.667
Rank	2	3	1

Table 5.14: Response table for signal-to-noise ratios for tensile modulus

Criterion: larger is better			
Level	Screw design	Screw speed	Fibre content
1	5.650	5.464	3.294
2	4.579	4.904	6.573
3	4.355	4.216	4.717
Delta	1.296	1.247	3.278
Rank	2	3	1

The relative importance of each control factor is illustrated in the Pareto chart below which shows that the fibre content represents over 57% of the total variability whilst screw design and screw speed contribute to circa 20% each.

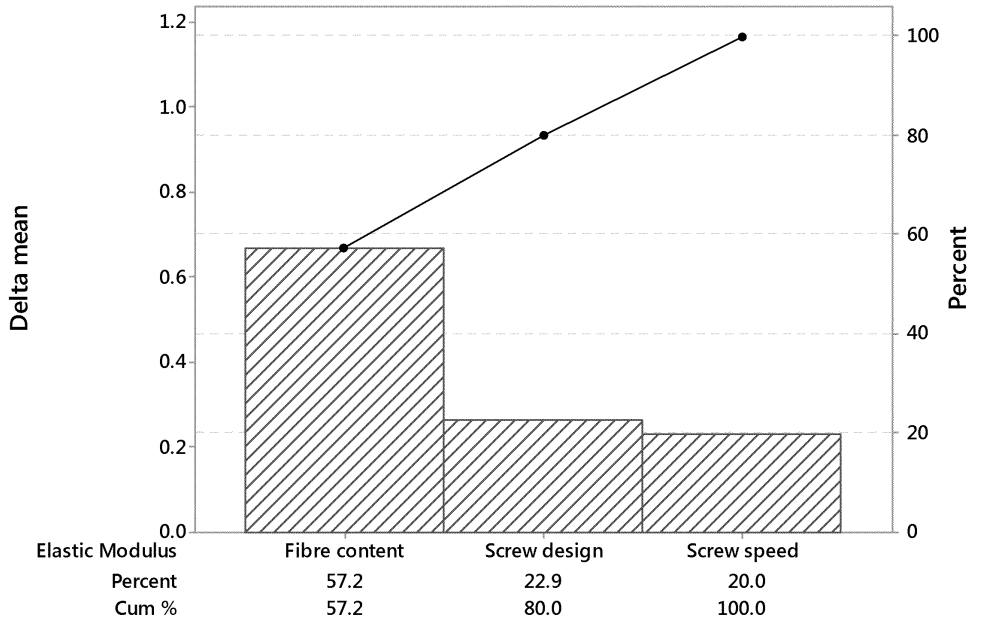

Figure 5.9: Pareto chart of elastic modulus (GPa)

ANOVA methods also enable the analysis of the interdependence of the variables in order to compare the relative strength of the effects across factors. The interaction plot for tensile modulus shows a significant interdependence between all factors and particularly between the screw speed and screw design (Figure 5.10). This was expected as the shear intensity depends on both factors. The non-linearity between the relative performance of screw speed and screw design suggests complex interactions. For instance, the tensile modulus obtained with the soft screw was inferior to that achieved with the mild and aggressive screws at low speed (80 rpm) but the trend reversed at 100 rpm. Poor performance at 80 rpm with the soft screw configuration could be due to insufficient mixing whilst at 100 rpm more shear was generated, optimising the rheological behaviour. However, the phenomenon was non-linear and the most aggressive screw gave the best results at higher screw speed. This was most likely due to the better consistency obtained with the aggressive screw compared to that obtained with the soft screw (Figure 5.11). This confirms that the melt seal helps preventing the air to pass through the last section of the barrel hence reducing porosity. On the other hand, screw speed and screw design interact to a smaller degree with the fibre content but the phenomenon is amplified at high fibre load. This can be related to the dominant effect of fibre content: the more the fibres,

the more the fibre properties affect the compound properties. A similar scenario was observed in the previous study on kenaf/PEMA/HDPE compounds [Ziegelaar, 2013].

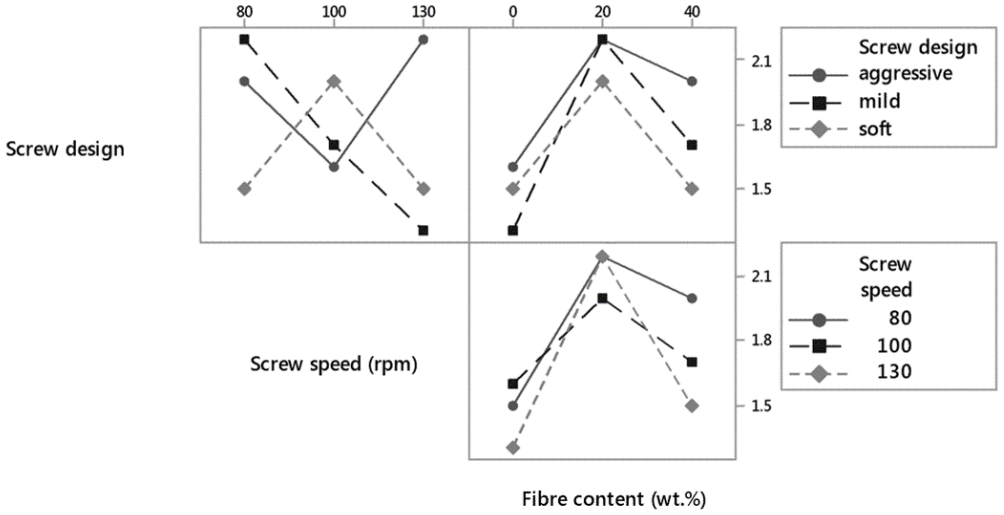

Figure 5.10: Interaction plot of elastic modulus (GPa)

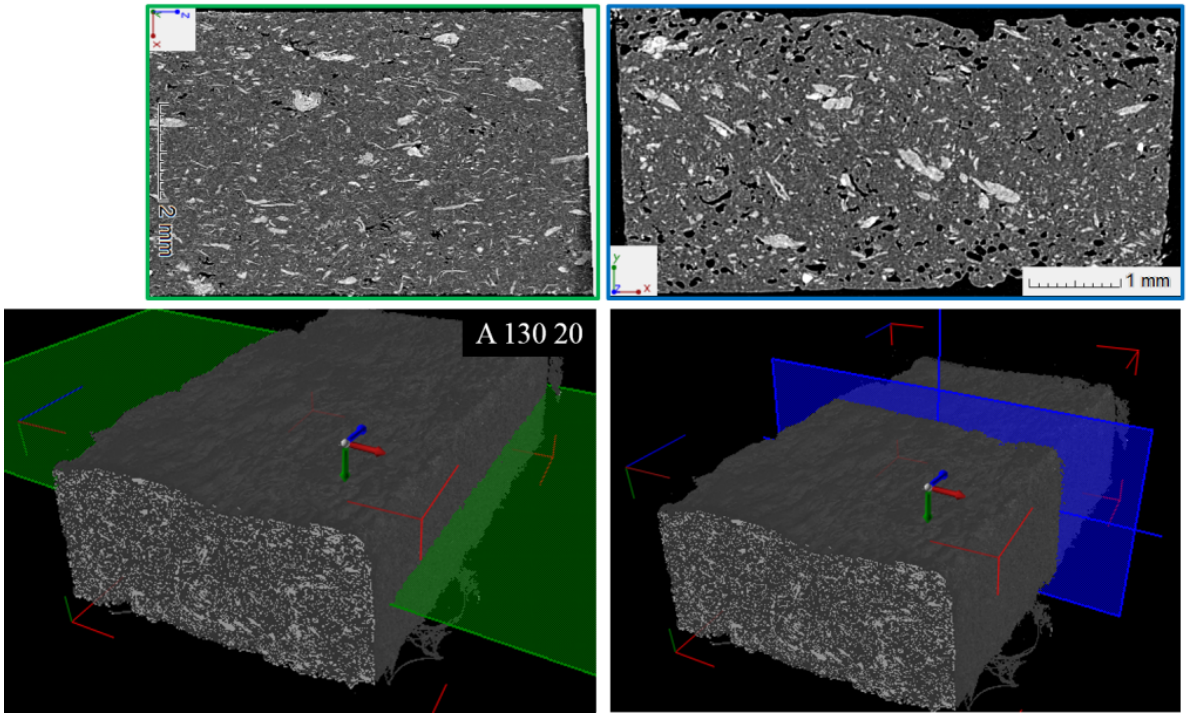

(a)

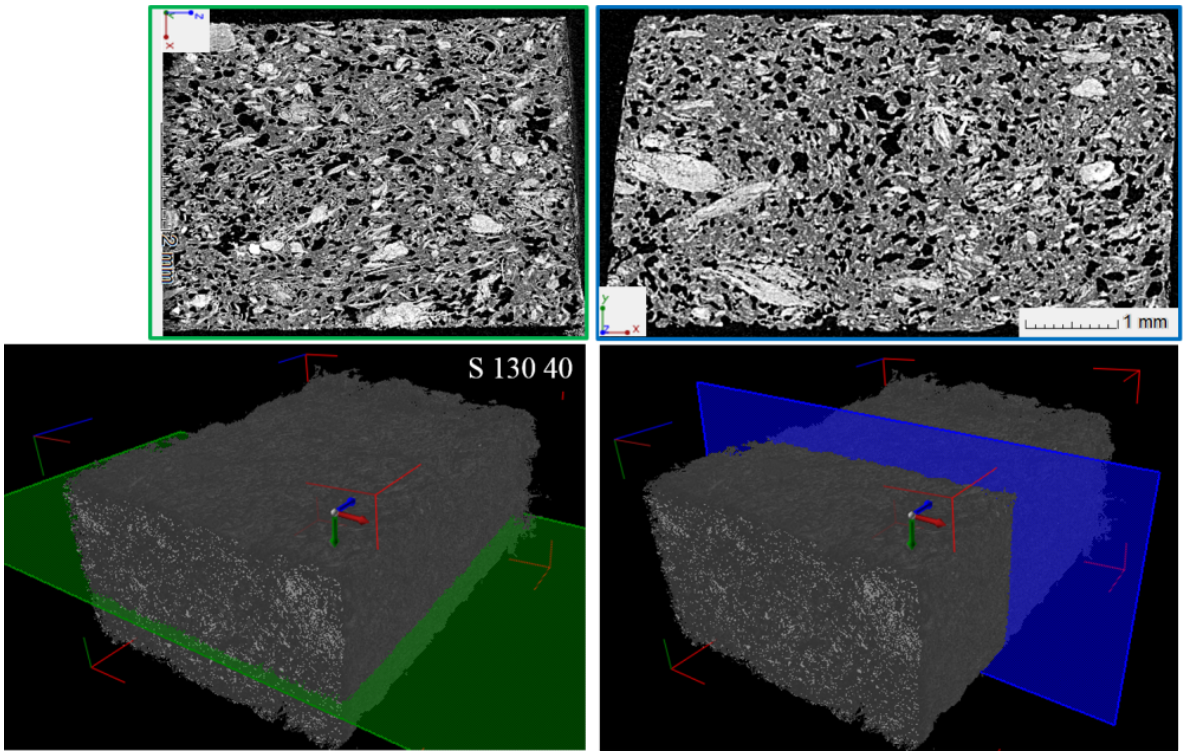

(b)

Figure 5.11: Volume rendering showing the porosity and fibre dispersion in kenaf/MAPP/PP compounds with (a) aggressive screw and (b) soft screw (Micro CT Images kindly provided by NDSU)

5.4.2 Tensile strength response

A similar approach was performed to analyse the effect of the control factors on the tensile strength. The response means for each control factor on the tensile strength are given in Figure 5.12. As for tensile modulus, fibre content appears as the most significant factor on the final response compared to screw speed and screw design. The latter shows a similar trend to that observed on tensile modulus with a positive correlation with shear intensity. On the other hand, screw speed displays a reverse trend with a negative correlation with increasing screw speed. The fibre content response peaks at 20 wt.% and drastically under-performs with higher fibre content. The main effect of fibre loading is quantified with the response table for means which shows that the variance induced by the fibre content is more than seven times that of the screw speed and more than three times that of the screw design (Table 5.15). The response table for S/N ratios also suggested that fibre content was the most influential factor to maximise the S/N ratio for tensile strength (Table 5.16).

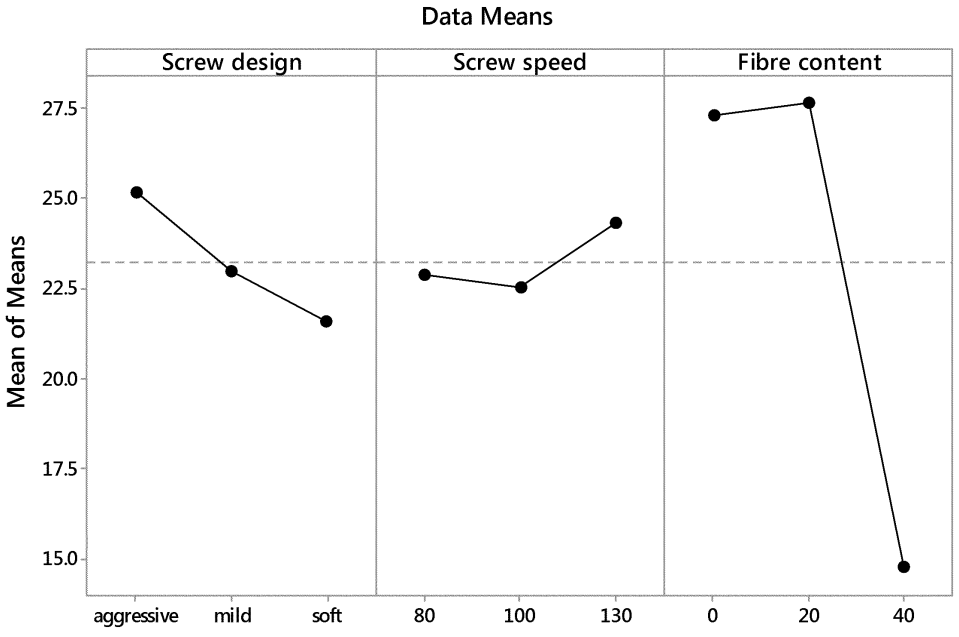

Figure 5.12: Main effect plot tensile strength (MPa)

TABLE 5.15: Response table for means showing the relative influence on each factor on tensile strength

Level	Screw design	Screw speed	Fibre content
1	25.13	22.87	27.30
2	22.97	22.53	27.63
3	21.60	24.30	14.77
Delta	3.53	1.77	12.87
Rank	2	3	1

TABLE 5.16: Response table for signal-to-noise ratios for tensile strength

Criterion: larger is better			
Level	Screw design	Screw speed	Fibre content
1	27.69	27.00	28.72
2	26.92	26.79	28.78
3	26.21	27.04	23.33
Delta	1.48	0.25	5.45
Rank	2	3	1

Finally, the relative importance of each control factor is illustrated in the Pareto chart below which shows that the fibre content represents over 70% of the total variability whilst screw design and screw speed contribute to circa 20% and 10% respectively. The relative efficacies are more heterogeneously distributed than for the tensile modulus (see Figure 5.9).

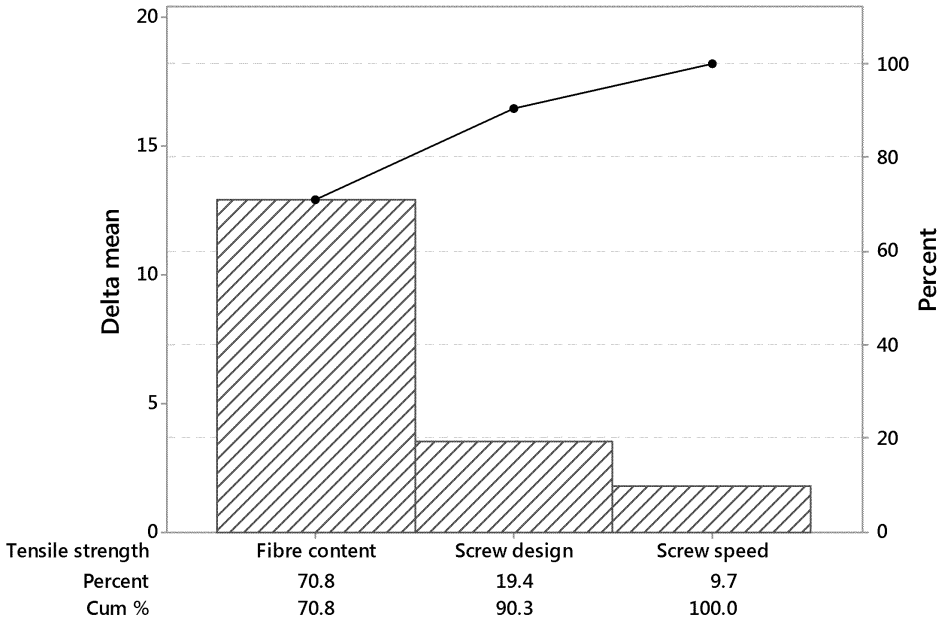

Figure 5.13: Pareto chart of tensile strength (MPa)

The interaction plot for tensile strength given in Figure 5.14 shows a significant interdependence between all factors and particularly between the screw speed and screw design, as observed previously for the elastic modulus (Figure 5.10). As for tensile modulus, the relative performance of screw speed and screw design were non linear and complex, with maximal performance obtained with high shear and high screw speed. Both the screw speed and screw design behaviours converged to low performance at higher fibre loading, which confirms the main effect of fibre content compared to the other factors. It suggested as well a poor interface independently of the fibre distribution.

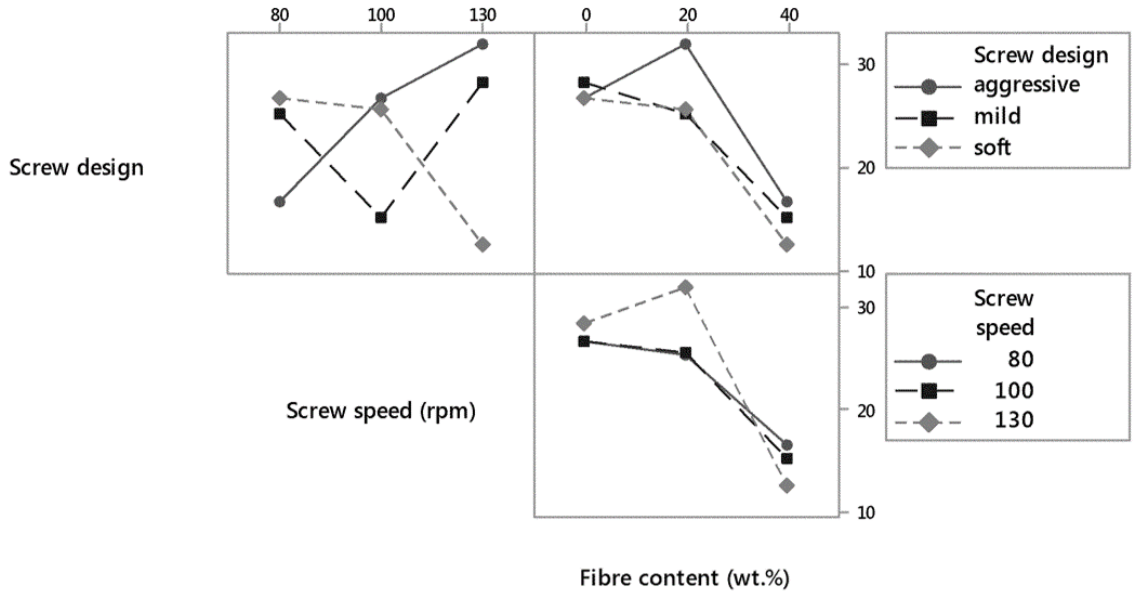

Figure 5.14: Interaction plot of tensile strength (MPa)

The optimal configuration to maximise the tensile properties of kenaf/MAPP/PP composites were deducted from the main effect plots and response tables. The optimal parameters to maximise the elastic modulus and the tensile strength differed (Table 5.17). Aggressive shear benefits both tensile modulus and tensile strength and is likely due to the melt seal effect that limits the porosity in the final compounds. More surprisingly, moderate fibre content is preferred to maximise the tensile properties. This could be due to a weak interface and poor distribution achieved in the current system. Further investigation on the interfacial properties and quantification of the fibre distribution would bring new information.

Interesting observations come out of the medium scale design of experiment when compared to previous observations on small scale studies (see section 5.2). ANOVA showed that fibre content was the main factor for both small and medium scales whilst screw speed and screw design affected to a moderate degree the overall properties. However, interaction plots revealed different trends and complex interdependence between screw speed and screw design. Aggressive screw design was preferred at medium scale to maximise the performance whereas soft and mild shear were found optimal on a small extruder. Fibre attrition in the barrel is less problematic on large L/D extruder as there is proportionally more free volume for the melt to flow and less contact with the walls and the screw flights compared to that of small L/D extruder. In both cases, high screw speed was required to maximise the tensile strength and medium to low

screw speed benefited the tensile modulus (Table 5.3, Table 5.17). This could be related to fibre length reduction that is limited at low screw speed and favoured at high screw speed. Finally, the optimal fibre content was estimated at 20 wt.% load on large extruder and 40 wt.% load on a smaller extruder in order to maximise the tensile properties. This inconsistency was due to the low performance obtained with 40 wt.% fibre load at medium scale, largely attributed to high porosity. Further optimisation is needed to confirm the trend observed at small scale.

Table 5.17: Optimal extuder configuration to maximise tensile properties

Design objective	Screw design	Screw speed (rpm)	Fibre content (wt.%)
Maximise tensile modulus	aggressive	80	20
Maximise tensile strength	aggressive	130	20

5.4.3 Effect of fibre treatment on tensile properties

Finally, a comparison study was performed to assess the effect of alkaline treatment. Two master batches containing water washed kenaf fibres and alkaline treated fibres were extruded under the same conditions as the design of experiment and the composites were tensile tested as extruded. Results are given in Table 5.18. Surprisingly, the biocomposites containing the water washed fibres performed better than the alkaline treated kenaf/MAPP/PP compounds: the tensile strength was about 25% higher and the elastic modulus approximately 20% higher. Overall, the properties obtained with the water washed fibres exceeded all those of composites characterised previously (see Table 5.12).

Table 5.18: Effect of fibre treatment on tensile properties of kenaf/MAPP/PP extruded composites (ASTM D638)

Treatment	Screw design	Screw speed (rpm)	Fibre content (wt.%)	Average tensile strength (MPa)	Average Young's modulus (GPa)
Water washed	Aggressive	100	20	31.4	2.5
NaOH treated	Aggressive	100	20	25.2	2.1

The micro CT images revealed that the kenaf water washed biocomposites had very few pores and the fibres were better dispersed compared to the alkaline treated kenaf biocomposites (Figure 5.15). In other words, water washed fibre pellets separated better than the alkaline treated fibre pellets. FQA analysis showed previously that alkaline fibres and water washed fibres had substantially different fibre length distribution (see Figure 5.3). It could also be related to the fibre surface properties that facilitated dispersion of the pellets into the melt. Alkaline and water washed fibres displayed dissimilar fibre surface properties and therefore different interfacial interactions occurred with the polymers in the melting process. TGA data showed no major difference in the fibre initial moisture content to explain the higher porosity obtained with alkaline treated fibres but the water washed fibres had slightly higher thermal resistance than the alkaline treated fibres (see Table 5.8), which would benefit their overall properties.

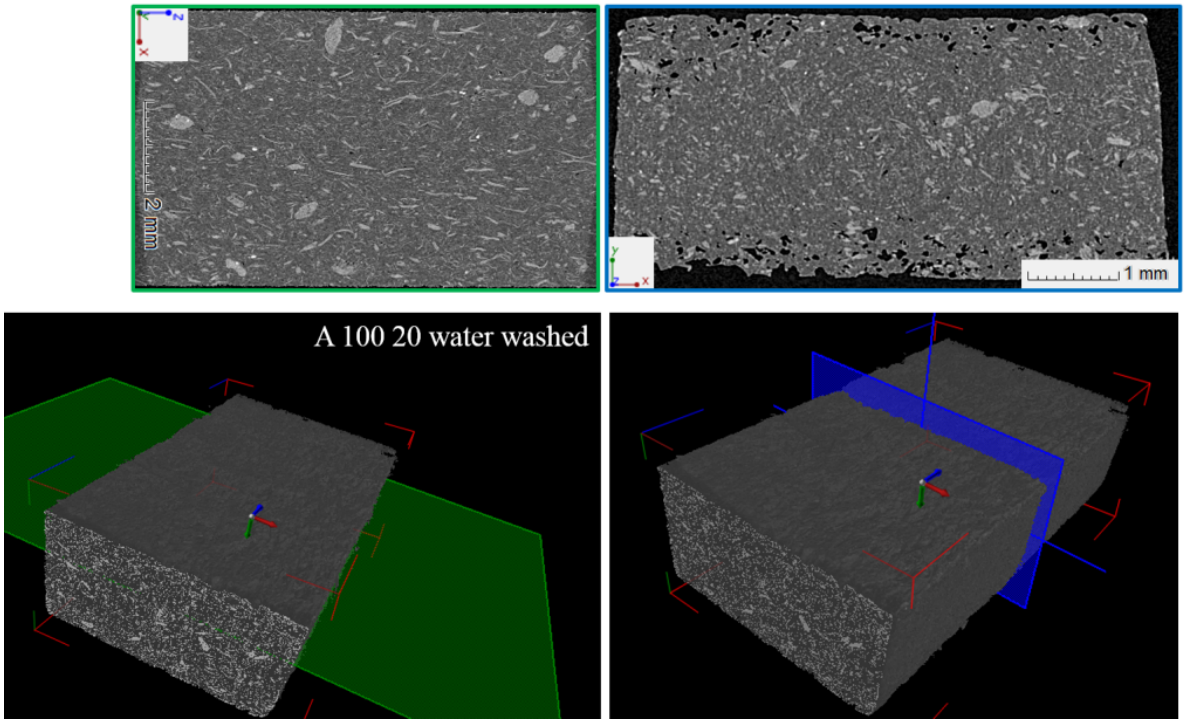

(a)

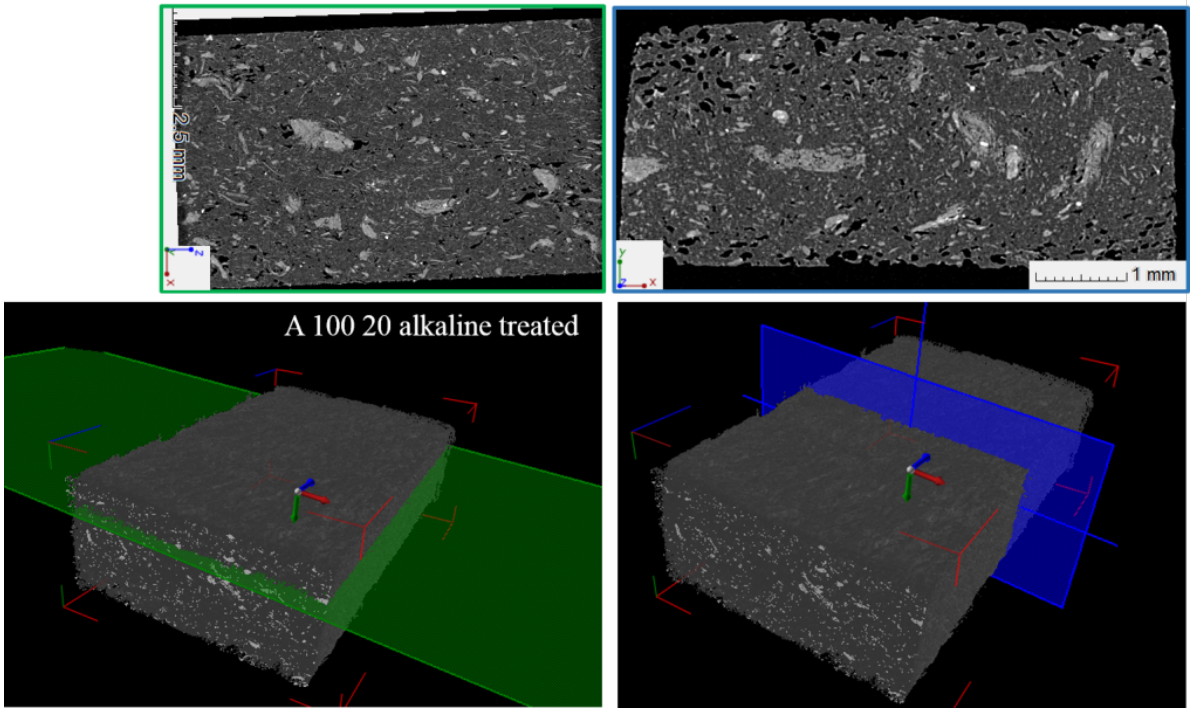

(b)

Figure 5.15: Volume rendering showing the porosity and fibre dispersion in (a) kenaf water washed fibres/MAPP/PP composites and (b) kenaf alkaline treated fibres/MAPP/PP composites (Micro CT Images kindly provided by NDSU)

5.4.4 Effect of injection moulding on tensile properties

In many cases, product manufacturing involves both compounding and injection moulding. Additional experiments were conducted in order to assess the effect of injection moulding on the tensile properties of extruded biocomposites. The materials used were the kenaf alkaline treated fibre pellets (∅3 mm), PP grade HP 422M and Licocene PP MA6452 (3 wt.% of total composition). Extrusion trials were performed on the medium scale extruder (ENTEK 40:1 L/D) with a rod die (3 x ∅3 mm) and the extrudates were pelletised with a granulator. The experimental conditions were similar to that of previous trials (see section 5.3.3). All samples were injection moulded on a Babyplast 610P into dogbone specimens (ISO 527-2:2012, type 1BA) at 175°C and tensile tested in similar conditions to the extruded samples (see section 5.3.3). A minimum of ten specimens were tested per batch. Details of the test matrix and results obtained are summarised in Table 5.19. A comparison between the samples as extruded and injection moulded is given in Figure 5.16.

Table 5.19: Tensile properties obtained after injection moulding

Trial	Extrusion set-up			Tensile properties	
	Screw design	Screw speed (rpm)	Fibre content (wt.%)	Tensile strength (MPa)	Elastic modulus (GPa)
HP 422M	soft	100	20	27.4 ± 0.3	1.4 ± 0.1
kenaf/MAPP/PP	soft	100	20	23.2 ± 2.3	2.4 ± 0.3
kenaf/MAPP/PP	aggressive	100	40	25.0 ± 1.0	2.7 ± 0.3

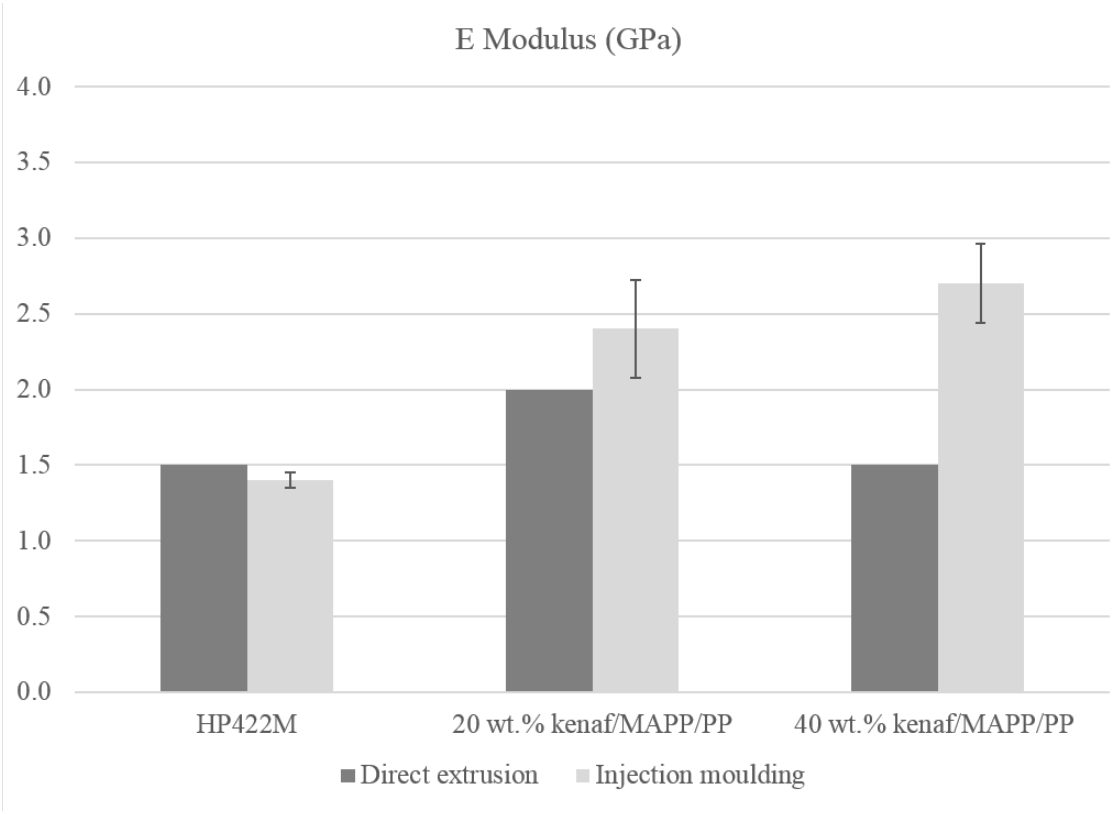

(a)

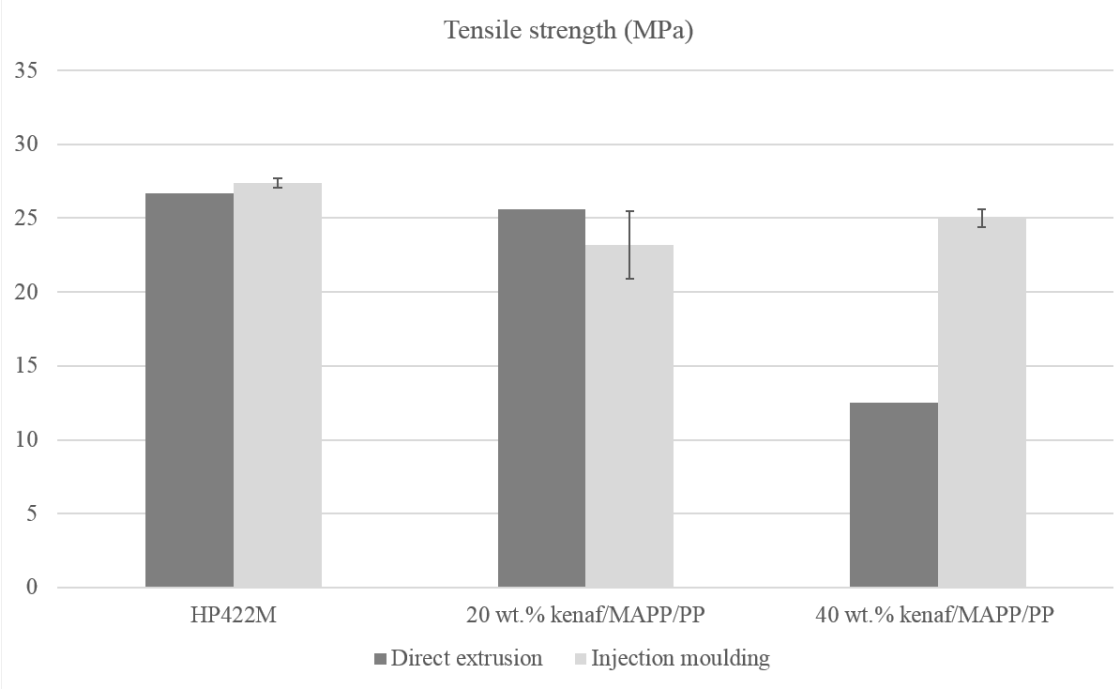

(b)

Figure 5.16: Tensile properties of compounds directly extruded vs. injection moulded (a) average tensile modulus (MPa) and (b) average tensile strength (GPa) *Note: error bars represent the standard deviation when it could be calculated*

Injection moulding had a negligible effect on the polypropylene samples; tensile strength increased by about 3% and the tensile modulus decreased by less than 7%. On the other hand, the injection moulded biocomposites displayed higher elastic modulus than those tested directly post extrusion and the effect amplified at higher fibre content: E modulus increased by 20% and by 100% for the 20 wt.% kenaf/MAPP/PP and 40 wt.% kenaf/MAPP/PP samples respectively (Figure 5.16a). This was most likely due to the loss in porosity during injection moulding, which may also have enabled better stress transfer from the matrix to the fibres.

The effect on the tensile strength was less consistent: the 20 wt.% kenaf/MAPP/PP samples showed slightly lower values (by about 10%) whereas that of 40 wt.% kenaf/MAPP/PP increased by 100% but still lower than the pure polymer. The lower tensile strength for 20 wt.% kenaf/MAPP/PP could result from a change in fibre orientation and fibre distribution due to injection moulding. On the other hand, at higher fibre load, the loss in porosity meant that injection moulding most likely compensated for this effect. This explains the increase in tensile strength for the 40 wt.% kenaf/MAPP/PP injection moulded composites compared to that of directly extruded composites (see Figure 5.11b).

When compared to polypropylene, the injection moulded biocomposites showed a considerable increase in elastic modulus whilst tensile strength hardly equalled that of polypropylene. This trend is similar to that generally observed on extruded biocomposites and highlights the real challenge for these materials that is to achieve acceptable tensile strength.

5.5 Industrial Trials

Based on the previous findings and with the experience gained through CRC-ACS P1.1 studies, extrusion trials were performed with two industrial partners on fully automated processing lines that included auxiliary equipment (water cooling bath, pullout assembly station, cutting station etc.). The trials are described in the following paragraphs.

5.5.1 Compounding of kenaf/MAPP/PP with Duromer

Kenaf alkaline treated fibre pellets (∅6 mm) were compounded with polypropylene grade Moplen HP400L (MFI 5 g.10 min^{-1}, LyondellBasell) and Licocene PP MA 6452 (5 wt.% of the total composition). The fibre load was 20 wt.% of the total composition. Extrusion trials were performed on a 72 mm co-rotating twin-screw extruder 45:1 L/D. The screw design included three mixing zones separated by conveying elements: one series of kneading blocks for polymer mixing, a second sequence of forward kneading blocks ("mild"mixing) and a third series of kneading blocks with a melt seal ("aggressive"mixing). A vacuum vent was set up after the last mixing zone followed by a pumping section towards the rod die (12 x ∅4 mm). PP and MAPP were fed separately in gravimetric feeders at the beginning of the barrel and the kenaf pellets were fed with a gravimetric side feeder after the first mixing zone. The latter were dried overnight in a drying hopper at 85°C prior to extrusion. The barrel temperature was set up at 180°C, the screw speed was 400 rpm and the total feeding rate was 250 $kg.h^{-1}$.

The polymers and kenaf pellets were fed consistently without bridging in the hopper and the extruded compound coming out of the die had an homogeneous texture. As a result, the composite melt was extruded continuously for about an hour with no issue. The compounded pellets were then injection moulded and tensile tested in the same conditions as the previous samples (see section 5.4.4). The results obtained are given in Table 5.20.

TABLE 5.20: Tensile properties obtained on industrial extrusion line with Duromer

Properties	HP 400L	20 wt.% kenaf/MAPP/PP
E modulus (GPa)	1.78 ± 0.1[a]	2.1 ± 0.3
Tensile strength (MPa)	36.0 ± 0.2[a]	23.1 ± 2.8

[a]data obtained by [Sallih, 2015]

Adding 20 wt.% kenaf to polypropylene increased by 17% the elastic modulus and decreased by ca. 35% the tensile strength (Table 5.20). These trends agreed well with the previous observations on medium scale extruder (see Figure 5.16). The loss in tensile strength was attributed to the biocomposite porosity that occurred despite the venting section (visual qualitative analysis).

5.5.2 Profile extrusion of kenaf/PVC compounded pellets with ETI

In a piece of work undertaken parallel to the project, industrial trials were organised with ETI to create a demonstration product. First, kenaf/Polyvinyl Chloride (PVC) pellets were compounded on the ENTEK extruder according to the lessons learned from the design of experiment. Kenaf alkaline treated fibre pellets (∅3 mm) were compounded with a commercial PVC formulation which contained additives, impact modifier, UV stabiliser etc. The screw was designed with one soft mixing zone (30/15/90 forward kneading blocks) in the first section of the barrel and a second series of kneading blocks that included a melt seal (F30/5/30 - F60/10/60 - R30/5/30) located at $2/3^{rd}$ of the barrel. The barrel temperature was set up at 170°C and the screw speed was 80 rpm. The kenaf pellets and PVC granulates were fed as a masterbatch at 2 kg.h^{-1} and extruded through a rod die (3 x ∅5 mm). The compounded pellets were then pelletised with a granulator.

The second processing stage consisted in extruding the kenaf/PVC compounded pellets through a profile used for a reflector guide post. This product was selected as it contained key features including angles, ridges and large flat sections. The biocomposite pellets were extruded on a large conical counterrotating twin-screw extruder (typical extruder for PVC profile extrusion). The barrel temperature was set up at 180°C, the screw speed was 7 r.min^{-1} and the feeding rate was synchronised at 7 r.min^{-1}. The composite melt was extruded continuously for an hour

without issue once the parameters adjusted on the auxiliary equipment. Coupon specimens were water-jet cut from the central section of the extruded profile and tensile tested in similar conditions to the previous samples. Tensile data obtained are summarised in Table 5.21.

TABLE 5.21: Tensile properties obtained on industrial extrusion line with ETI

Properties	PVC	20 wt.% kenaf/PVC
E modulus (GPa)	3.5 ± 0.2	4.8 ± 0.5
Tensile strength (MPa)	41.8 ± 0.7	35.5 ± 0.4

Adding 20 wt.% kenaf to PVC increased the elastic modulus by about 37% and slightly reduced the tensile strength by 15% (Table 5.21). These trends suggested that the two-stage manufacturing process (compounding + profile extrusion) benefited the composite properties. In particular, a visual assessment of the profile cross section revealed smaller porosity than that previously observed on the kenaf/MAPP/PP compounds.

Figure 5.17: First biocomposite profiles extruded in an Australian industry

5.6 Conclusions

The design of experiment performed at medium scale confirmed the findings from previous studies on bench top extruders and brought new insights on the feasibility of large scale biocomposite extrusion. Statistical analysis with ANOVA methods showed a significant interdependence between all factors and particularly between the screw speed and the screw design. At both scales, fibre content was the dominant factor for the tensile strength and elastic modulus whilst screw speed and screw design affected to a lower degree the tensile properties. Overall, the performance achieved agreed well with the general trends observed in literature. Considerable porosity revealed by Micro CT largely contributed to low tensile strength.

The series of experiments performed demonstrated the necessity to work with well characterised fibres as their surface properties and physical characteristics are determinant for the final composite properties. For instance, the alkaline treated fibre reinforced polypropylene composites under-performed compared to the water washed fibre polypropylene composites although the former had a surface more energetically homogeneous and less polar. It is assumed that the higher fibre aspect ratio of the water washed fibres and their homogeneous fibre length distribution largely contributed to increase the composite performance. Unfortunately, XRD and SFTT conventional set-ups were unsuitable for the characterisation of short processed fibres. Capability and methodology development are needed in the future to assess short fibre properties.

Injection moulding post compounding increased the Youngs' Modulus and slightly decreased the tensile strength of biocomposites whereas pure polypropylene compounds maintained their properties. This trend confirmed the challenge to achieve acceptable tensile strength in short fibre biocomposites.

The properties achieved on a medium scale extruder were similar to that obtained by Duromer on an industrial extrusion line. Such results demonstrate that the up-scaling process was successful and validated the development of biocomposites on a medium scale extruder prior to industrial extrusion line. Furthermore, fibre attrition and size effects are less problematic on a large L/D extruder compared to a small extruder where the kneading elements have similar dimension to the fibres.

Throughout the trials a significant amount of porosity was noticed in the extruded samples. This is an aspect which the project failed to overcome and has unfortunately resulted in mechanical properties lower than expected. Further work is required to overcome this issue, and the author believes that the two key areas that need to be addressed are the drying of the fibres prior to feeding and the development of screw configuration which allow moisture extraction by the use of alternating high/low pressure sections and vacuum venting. The industrial trials have shown that drying natural fibres is challenging on a industrial scale considering the high humidity in Queensland, the large volume of fibres to handle and the rapid moisture uptake of natural fibres. Whilst the porosity detected in the samples questions the industrial-usefulness of some of the results, the contribution of this thesis to the development of natural fibre compounding capability at The University of Queensland was immense. The methodology presented in this chapter and the lessons learned will undoubtedly be used to further optimise the extrusion process and produce better biocomposite materials.

Chapter 6

Conclusions & Recommendations

This thesis focused on key aspects of biocomposite development for industrial application that is the triad of natural fibre properties, the techniques for natural fibre grading and the extrusion process (Figure 6.1). The first objective was to characterise natural fibres with advanced surface techniques in order to resolve the chemistry and physical properties of the fibres' surface. This included the evaluation of existing techniques and capability development of inverse gas chromatography. The second main objective was to optimise the extrusion process for biocomposites and to study the feasibility of large volume production by up-scaling. Finally, this thesis aimed to establish a correlation between the fibre properties and the composite properties with respect to the fibres' surface characteristics and the processing variables. Chapter 3 showed the potential of the in-lens SEM technique to characterise natural fibre surface morphology and to obtain surface contrast mapping, which is limited with conventional SEM. XPS analysis has also been pushed further than a comparison based on the average composition, with peak fitting of high resolution spectra and systematic cross-correlation to ensure coherent data interpretation. Chapter 4 demonstrated the potential of IGC as a grading technique to investigate the surface energy of plant fibres, in particular, the effect of surface treatment on the energy profile and the surface polarity. Finally, a feasibility study for large scale production of short fibre biocomposites was performed via a series of design of experiments from laboratory scale up to industrial processing lines, and is reported in Chapter 5. This final chapter summarises the main messages delivered through the thesis followed by recommendations for future work.

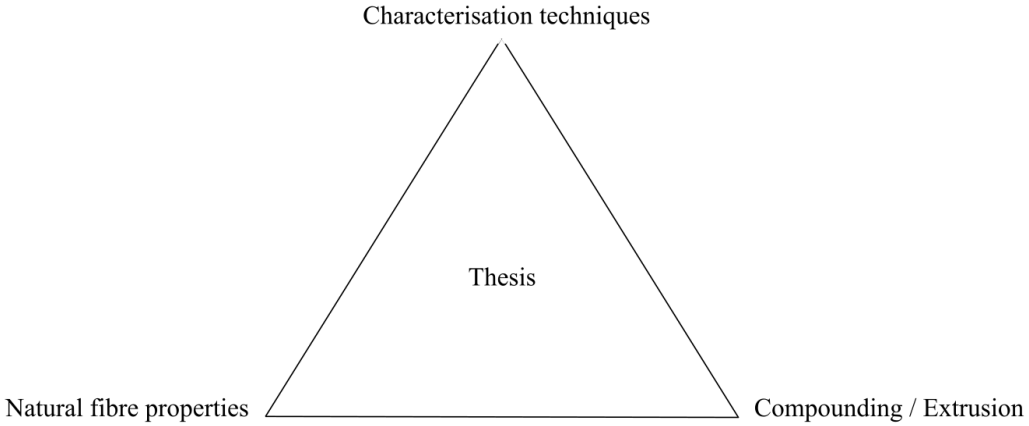

Figure 6.1: Triad of natural fibre properties, characterisation techniques and extrusion

6.1 Conclusions

Natural fibres challenge traditional characterisation techniques because of their complex physico-chemical structure and their large variability of properties. This demands a systematic study of the common procedures and models implemented in traditional techniques in order to assess their capabilities to characterise natural fibres. On the other hand, the variability of natural fibres fosters the development of new characterisation techniques.

• A series of experiments performed with the new generation of FE-SEM with TTL BSE detectors demonstrated the capability of obtaining good contrast between low atomic number polymeric species as well as fine topography of the very near surface. The SE and BSE images of flax and kenaf fibre samples showed clear evidence of the effect of chemical treatment on the fibre surface properties. Specific UED BSE images provided complementary information to interpret the physico-chemical mechanisms that occur on bast fibre surfaces during processing.

In particular, SE images of unretted flax fibres showed fibres with a rough surface containing multiple layers and partially fragmented due to scutching. The outer layer was coated with an amorphous mixture of organic materials such as lipids, pectins and extractives. BSE images revealed a clear contrast between the materials and a few bright spots that were most likely inorganic particles such as silicates. Alkaline treatment removed most of the cuticle/epidermis

outer layer and revealed kinks and nodes on single fibres' surface. Some patches scattered on the surface were most likely residual lignins.

Imaging of field retted kenaf fibres showed fibres covered with an amorphous layer and scattered with adhering particulates, likely organic compounds. Typical features of the epidermal tissues were also visible on the surface which suggested that water exposure solely was insufficient to remove lignins, pectins and waxes from the surface. BSE images confirmed that the surface contained mostly lignins and waxes, with traces of extractives non dissolved during field retting. The fibres appeared much cleaner and relatively smooth after water washing. SEI and BSE images revealed no major contrast except a few bright spots that were most likely inorganic materials deposited during the water washing or projected when the fibres were milled. Nature of the surface was similar to field retted fibres which was expected as both batches underwent water exposure only. Finally, alkaline treated fibres had a rough surface partially covered with an amorphous layer rich in lignins and waxes. Trace of extractives were still visible on the surface whilst the surface underneath contained more cellulose, hemicellulose and pectins.

• A set of bast fibres were further investigated by XPS to identify the nature of the compounds present on the fibres' surface and to quantify the elemental chemical composition. All fibres showed O/C ratios much lower than that of theoretical pure cellulose (O/C= 0.83) and that of bacterial cellulose (O/C = 0.73) that were used as a reference. Hemp fibres had an O/C of 0.32, kenaf fibres had O/C ratios of 0.26 and 0.28 and flax linseed had an O/C of 0.25 and flax linen of 0.15. Surprisingly, commercial synthesised cellulose fibres BioMid® displayed similar values with an average O/C of 0.31. Fibres subject to milling had their O/C ratio increased by ca. 35% that was assumed to be due to fibre breaking and defibrillation. Chemical treatment affected as well the surface chemistry. All specimens had an increased O/C of more than 50% on hemp fibres and up to 125% on flax fibres post alkaline treatment, which confirms the surfaces contained less amorphous substances such as lignins, pectins, waxes. However the O/C ratios were still much lower than the theoretical value of cellulose: hemp fibres had an O/C of 0.49 and kenaf 0.44 compared to 0.83 for pure cellulose. This agrees well with the SEM results that showed in both cases alkaline treated fibre surfaces were still rich in lignins and extractives.

Further analysis was performed with high resolution scans to identify the functional groups present on the kenaf fibre surface and to investigate the effect of alkaline treatment on the

surface chemistry. High resolution scans on carbon (C1s), oxygen (O1s) and nitrogen (N1s) confirmed that the very near surface of alkaline treated fibres was rich in lignins and poor in cellulose. Specific peaks of the functional groups present in lignins, hemicellulose and pectins were identified (ester group, methoxy substitutions and Pi-Pi* shake up bands). Strong C-C peaks confirmed the presence of lignins, waxes and extractives. On the other hand, the fibres contained proportionally more cellulose and hemicellulose than water washed fibres and fibres as received. The peaks' amplitude also suggested that the surface contained less fatty acids which was expected as NaOH was more efficient in removing fatty acids than water washing. The experimental data agrees well with SEM analysis and confirmed that the water wash and alkaline treatment cleaned the fibre surface and removed most of the epidermal tissues. However, the treatments were too gentle to remove lignins and pectins and the fibres' surface remained rich in lignins and oxygenated species, and poor in cellulose.

• IGC proved to be a promising technique for studying the surface energy of natural fibres. Because it is a relatively new technique for natural fibre characterisation, systematic studies needed to be performed. In this study, the critical parameters to determine the BET surface area values were identified and a protocol applicable to natural fibres was proposed. The BET specific surface area of kenaf and flax fibres differed, with an average of 0.51 $m^2.g^{-1}$ vs. 1.35 $m^2.g^{-1}$ respectively and the kenaf fibres showed similar BET value to cellulose fibres (ca. 0.54 $m^2.g^{-1}$). Bast fibres had larger batch-to-batch variability than synthesised cellulose fibres, which is a consequence of natural fibre structural irregularities and heterogeneous properties. The BET values obtained by IGC SEA showed a noticeable dependence on the elutant properties which was attributed to the effect of molecular orientation. Sample packing also affected the BET surface area values but no clear trend could be established.

Surface energy measurements were performed at finite concentration to obtain more realistic values than those obtained in infinite dilution. The surface energy distribution profiles of the dispersive and the acid-base components provided key complementary information to the overall surface energy profile of natural fibres and highlighted their specificity. For instance, γ_S^{LW} profiles showed that the kenaf fibres' surface contained active sites with energy levels spread more than those of flax and cellulose fibres' surface. In addition, $\gamma_{Smean}^{LW}(kenaf) \leqslant \gamma_{Smean}^{LW}(flax)$

$\leqslant \gamma_{Smean}^{LW}(BioMid^{®})$ which was coherent with the assumption that the unretted flax fibres contained more waxy substances than the field retted kenaf fibres. The γ_S^{AB} distribution profiles were similar to that of γ_S^{LW} with BioMid® fibres being the least polar and the most homogeneous. Flax fibre surface contained polar groups of lower energy than that of kenaf fibres which assumed that the latter comprised more Lewis acid-base functional groups, for instance, pectins, lignins and extractives. The acid-base energy component contribution to the total surface energy values was significant in particular for the kenaf fibres. The latter had a polarity index ($\gamma_{Smean}^{AB}/\gamma_{Smean}^{TOT}$) of 0.24 compared to 0.15 and 0.09 for flax and BioMid® fibres respectively.

Finally, investigation of the effect of fibre treatment on the surface energy profiles of kenaf fibres provided new insights, in particular the change in polarity and the distribution of the energetic active sites. Both the water wash and alkaline treatments induced a shift to higher average γ_S^{LW} values suggesting the fibres' surface became more hydrophobic. The evolution of γ_S^{LW} profiles indicated an increase in the number of high energetic sites and/or an increase in energy levels of the active sites. Logically, γ_S^{AB} profile shifted to lower values, as the surface became less polar. Both treatments only slightly affected the overall surface energy value of the fibres: γ_{Smin}^{TOT} = 48.9 mJ.m^{-2}, 48.8 mJ.m^{-2} and 47 mJ.m^{-2} for the kenaf as received, water washed and alkaline treated fibres respectively. However, the polarity index showed that both treatments reduced the surface polarity: kenaf fibres as received had a polarity index of 0.24 compared to 0.20 and 0.17 for the water retted and alkaline treated fibres respectively. Water wash and alkaline treatment also rendered the surface energetically more homogeneous than the fibres as received.

These experimental data highlight the structural heterogeneity between different species of bast fibres, in terms of both chemical and physical properties. Further data acquisition on natural fibres is necessary to strengthen these models and extend the database to get consistent references. However, the current results have demonstrated the potential of IGC for characterisation of natural fibre surfaces. Combined, XPS, in-lens SEM and IGC offer a unique complementarity to unravel natural fibre surface properties.

• Compounding short fibre biocomposites is challenging due to the multiple variables involved and the specific issues that arise when working with natural fibres. A series of experiments leading towards large scale processing have been performed and brought new insights on the feasibility of large scale biocomposite extrusion. Statistical analysis with ANOVA methods showed a significant interdependence between all factors and particularly between the screw speed and the screw design. At both bench top and medium scale, fibre content was the dominant factor for the tensile strength and elastic modulus whilst screw speed and screw design affected to a lower degree the tensile properties. The composites had higher tensile modulus than the pure polymer whilst the improvement in tensile strength was marginal. Injection moulding post compounding increased the composite Youngs' Modulus and slightly decreased their tensile strength. These trends agreed well with the published literature and confirmed the challenge to achieve acceptable tensile strength in short fibre biocomposites.

The series of experiments also demonstrated the necessity to work with well characterised fibres as their surface properties and physical characteristics determine the final composite properties. Fibre length distribution is important and may compromise the effect of fibre treatment. For instance, alkaline treated kenaf fibre reinforced polypropylene composites under-performed the water washed kenaf fibre polypropylene composites although the former had a surface more energetically homogeneous and less polar. It is assumed that the higher fibre aspect ratio of the water washed fibres and their homogeneous fibre length distribution largely contributed to increase the composite performance.

Finally, extrusion at industrial scale has been successfully performed and represents a major achievement of the thesis. However, a significant amount of porosity was noticed in the extruded samples throughout the trials and further work is required to overcome this issue. Whilst the porosity detected in the samples questions the industrial-usefulness of some of the results, the contribution of this thesis to the development of natural fibre compounding capability at The University of Queensland was immense. The methodology and the lessons learned will undoubtedly be used to further optimise the extrusion process and produce better biocomposite materials.

6.2 Recommendations

• Surface Characterisation

The multi-scale characterisation performed in this work demonstrated the complementarity of advanced surface characterisation techniques. The case studies presented brought new insights on bast fibre surface properties, in particular on the effect of alkaline treatment on the surface chemistry and energetic profile. Although the results were consistent and most of the hypothesis formulated could be confirmed through the thesis, several areas still need to be addressed.

Further experimental work with FE-SEM TTL should be performed to identify the nature of the amorphous substances on the fibre surface. A method developed by Fromm et al. [2003] that consists in staining the lignin with potassium permanganate $KMnO_4$ enables the detection of the presence of lignins on the fibre surface. $KMnO_4$ oxidises lignins and reduces the permanganate to MnO_2. Previous authors successfully labelled lignin with this technique [Day et al., 2005, Neto et al., 1996, Truss et al., 2015]. In addition, elemental analysis using Energy Dispersive X-Ray Spectroscopy (EDX) would help identifying the nature of the inorganic compounds.

The main challenge of XPS remains data interpretation. Peak fitting and cross-correlation enabled the identification of some of the functional groups present on the fibres' surface but some peaks remain unsolved. Whilst the complexity of peak fitting is typical of natural fibres and will unlikely be simplified in the future, building reference spectra could help identifying the specific functional groups. Recommendations for future work involve XPS analysis of the different types of lignins (H-lignin, S-lignin, G-lignin) from softwoods and hardwoods to build the respective XPS high resolution spectra. The spectra of pectins and plant waxes would also help differentiating some of the functional groups, however, these substances are more challenging to analyse due to sample preparation. Little work has been reported so far on these compounds.

Inverse Gas Chromatography is a versatile technique and a palette of experiments should be considered in a future work in order to extend the knowledge on surface energy of plant materials. In particular, evolution of the surface energy values with different conditions of temperature and humidity is of interest to better understand the fibre behaviour in the processing stage

and to improve fibre storage and conditioning. Investigation of the surface energy profiles of polymer matrices would enable the study of compatibility between plant fibres and matrices to be explored allowing optimisation of fibre/matrix systems. Finally, further research should be performed on natural fibres to extend the database and validate the preliminary findings presented in the thesis. In particular, the relevance of acid/base properties and the dependence of surface energy values on the solvents used.

• Compounding

Several areas still need to be addressed to optimise the extrusion process en route to industrial processing volumes. The next objective is to reduce porosity in the final product. It is also advisable to include in the formulation a fire retardant, a UV-stabiliser and other additives that would be necessarily added in commercial formulations such as impact modifiers etc. These components may change the rheological behaviour of the melt and therefore it is necessary to integrate them to the formulation as early as possible in the development phase.

Compound characterisation with Micro CT is a promising technique to investigate the fibre distribution, the fibre orientation and the fibre dispersion in extruded products. Quantification of these parameters and estimation of the total porosity constitute the next challenges for Micro CT technology. These involve the development of image numerical processing tools combined with volume rendering. Finally, evaluation of the long term performances is *sine qua non* of the feasibility study. These include durability and biodegradability as well as fire resistance. A series of design of experiments that integrate all the novelties aforementioned is the next step towards a real business case.

Bibliography

H. Akil, M. Omar, A. Mazuki, S. Safiee, Z. Ishak, and A. A. Bakar. Kenaf fiber reinforced composites: a review. *Materials & Design*, 32(8):4107–4121, 2011.

D. E. Akin. Linen most useful: perspectives on structure, chemistry, and enzymes for retting flax. *ISRN biotechnology*, 2012.

D. E. Akin, L. L. Rigsby, and W. Perkins. Quality properties of flax fibers retted with enzymes. *Textile research journal*, 69(10):747–753, 1999.

D. E. Akin, J. A. Foulk, R. B. Dodd, and D. D. McAlister. Enzyme-retting of flax and characterization of processed fibers. *Journal of Biotechnology*, 89(2):193–203, 2001.

M. Alcock, L. Van Loon, C. Karunakaran, S. Huo, S. Potter, and C. Ulven. High resolution characterisation of biofibre/resin interface bonds of thermoset composites through synchrotron illumination. *ECCM15, 15th European Conference on Composite Materials, Italy, 24-28 June 2012*, 2012.

A. Alemdar, H. Zhang, M. Sain, G. Cescutti, and J. Müssig. Determination of fiber size distributions of injection moulded polypropylene/natural fibers using x-ray microtomography. *Advanced Engineering Materials*, 10(1-2):126–130, 2008.

V. A. Alvarez and A. Vázquez. Influence of fiber chemical modification procedure on the mechanical properties and water absorption of materbi-y/sisal fiber composites. *Composites Part A: Applied Science and Manufacturing*, 37(10):1672–1680, 2006.

J. Anderson. Mechanical performance of thermoplastic matrix natural-fibre composites. *Properties and Performance of Natural-Fibre Composites*, page 402, 2008.

M. Andresen, L.-S. Johansson, B. S. Tanem, and P. Stenius. Properties and characterization of hydrophobized microfibrillated cellulose. *Cellulose*, 13(6):665–677, 2006. ISSN 0969-0239.

A. Arbelaiz, B. Fernandez, J. Ramos, A. Retegi, R. Llano-Ponte, and I. Mondragon. Mechanical properties of short flax fibre bundle/polypropylene composites: Influence of matrix/fibre modification, fibre content, water uptake and recycling. *Composites Science and Technology*, 65(10):1582–1592, 2005.

M. A. Arsène, K. Bilba, H. Savastano Junior, and K. Ghavami. Treatments of non-wood plant fibres used as reinforcement in composite materials. *Materials Research*, 16:903–923, 2013. ISSN 1516-1439.

K. Artyushkova. Art or black magic of curvefitting xps spectra. 2010.

S. Asahina, T. Togashi, O. Terasaki, S. Takami, T. Adschiri, M. Shibata, and N. Erdman. High-resolution low-voltage scanning electron microscope study of nanostructured materials. *Microsc. Analysis*, 26:S12–14, 2012.

A. Ashori. Wood-plastic composites as promising green-composites for automotive industries! *Bioresource Technology*, 99(11):4661 – 4667, 2008. ISSN 0960-8524. Exploring Horizons in Biotechnology: A Global Venture.

A. Ashori, M. Ornelas, S. Sheshmani, and N. Cordeiro. Influence of mild alkaline treatment on the cellulosic surfaces active sites. *Carbohydrate Polymers*, 88(4):1293–1298, 2012.

A. Aşkin and C. Bilgiç. Thermodynamics of adsorption of hydrocarbons on molecular sieves nay and cay by inverse gas chromatography. *Chemical Engineering Journal*, 112(1):159–165, 2005. ISSN 1385-8947.

B. G. Ayre, K. Stevens, K. D. Chapman, C. L. Webber, K. L. Dagnon, and N. A. D'Souza. Viscoelastic properties of kenaf bast fiber in relation to stem age. *Textile research journal*, 79(11):973–980, 2009.

C. Baillie. *Green Composites - Polymer Composites and the Environment*. Woodhead Publishing, 2004. ISBN 978-1-85573-739-6.

C. Baley. Analysis of the flax fibres tensile behaviour and analysis of the tensile stiffness increase. *Composites Part A: Applied Science and Manufacturing*, 33(7):939 – 948, 2002. ISSN 1359-835X.

C. Baley, F. Busnel, Y. Grohens, and O. Sire. Influence of chemical treatments on surface properties and adhesion of flax fibre–polyester resin. *Composites Part A: Applied Science and Manufacturing*, 37(10):1626–1637, 2006.

G. Beamson and D. Briggs. *High resolution XPS of organic polymers: the Scienta ESCA300 database, 1992*. 1992.

J. Beaugrand and F. Berzin. Lignocellulosic fiber reinforced composites: Influence of compounding conditions on defibrization and mechanical properties. *Journal of Applied Polymer Science*, 128(2):1227–1238, 2013.

R. A. Beebe, J. B. Beckwith, and J. M. Honig. The determination of small surface areas by krypton adsorption at low temperatures. *Journal of the American Chemical Society*, 67(9): 1554–1558, 1945.

M. Belgacem, G. Czeremuszkin, S. Sapieha, and A. Gandini. Surface characterization of cellulose fibres by xps and inverse gas chromatography. *Cellulose*, 2(3):145–157, 1995.

M. N. Belgacem and A. Gandini. Inverse gas chromatography as a tool to characterize dispersive and acid-base properties of the surface of fibers and powders. *Surfactant science series*, pages 41–124, 1999.

M. Bengtsson, M. Le Baillif, and K. Oksman. Extrusion and mechanical properties of highly filled cellulose fibre–polypropylene composites. *Composites Part A: Applied Science and Manufacturing*, 38(8):1922–1931, 2007.

A. Bismarck, A. K. Mohanty, I. Aranberri-Askargorta, S. Czapla, M. Misra, G. Hinrichsen, and J. Springer. Surface characterization of natural fibers; surface properties and the water up-take behavior of modified sisal and coir fibers. *Green chemistry*, 3(2):100–107, 2001.

A. Bismarck, I. Aranberri-Askargorta, J. Springer, T. Lampke, B. Wielage, A. Stamboulis, I. Shenderovich, and H.-H. Limbach. Surface characterization of flax, hemp and cellulose

fibers; surface properties and the water uptake behavior. *Polymer Composites*, 23(5):872–894, 2002. ISSN 1548-0569.

A. Bismarck, S. Mishra, and T. Lampke. Plant fibers as reinforcement for green composites, natural fibers, biopolymers and biocomposites, 2005.

A. Bledzki and J. Gassan. Composites reinforced with cellulose based fibres. *Progress in polymer science*, 24(2):221–274, 1999.

A. Bledzki, S. Reihmane, and J. Gassan. Properties and modification methods for vegetable fibers for natural fiber composites. *Journal of Applied Polymer Science*, 59(8):1329–1336, 1996.

A. Bledzki, H.-P. Fink, and K. Specht. Unidirectional hemp and flax ep-and pp-composites: Influence of defined fiber treatments. *Journal of Applied Polymer Science*, 93(5):2150–2156, 2004.

A. K. Bledzki, M. Letman, A. Viksne, and L. Rence. A comparison of compounding processes and wood type for wood fibre-pp composites. *Composites Part A: Applied Science and Manufacturing*, 36(6):789–797, 2005. ISSN 1359-835X.

D. H. Blount. Catalytic reaction of silicoformic acid, silicic acid and lignin, Sept. 27 1977. US Patent 4,051,115.

W. Bowyer and M. Bader. On the re-inforcement of thermoplastics by imperfectly aligned discontinuous fibres. *Journal of Materials Science*, 7(11):1315–1321, 1972.

E. Brendlé and E. Papirer. A new topological index for molecular probes used in inverse gas chromatography for the surface nanorugosity evaluation. *Journal of colloid and interface science*, 194(1):207–216, 1997.

D. Briggs and G. Beamson. Primary and secondary oxygen-induced c1s binding energy shifts in x-ray photoelectron spectroscopy of polymers. *Analytical chemistry*, 64(15):1729–1736, 1992.

D. J. Brookman and D. T. Sawyer. Specific interactions affecting gas chromatographic retention for modified alumina columns. *Analytical Chemistry*, 40(1):106–110, 1968.

O. S. Carneiro, J. A. Covas, and B. Vergnes. Experimental and theoretical study of twin-screw extrusion of polypropylene. *Journal of applied polymer science*, 78(7):1419–1430, 2000.

N. C. Carpita and D. M. Gibeaut. Structural models of primary cell walls in flowering plants: consistency of molecular structure with the physical properties of the walls during growth. *The Plant Journal*, 3(1):1–30, 1993.

F. S. Chakar and A. J. Ragauskas. Review of current and future softwood kraft lignin process chemistry. *Industrial Crops and Products*, 20(2):131–141, 2004.

K. Charlet, C. Baley, C. Morvan, J. Jernot, M. Gomina, and J. Bréard. Characteristics of hermès flax fibres as a function of their location in the stem and properties of the derived unidirectional composites. *Composites Part A: Applied Science and Manufacturing*, 38(8): 1912 – 1921, 2007. ISSN 1359-835X.

B. Charmas and R. Leboda. Effect of surface heterogeneity on adsorption on solid surfaces: Application of inverse gas chromatography in the studies of energetic heterogeneity of adsorbents. *Journal of Chromatography A*, 886:133–152, 2000. ISSN 0021-9673.

V. S. Chevali and C. A. Ulven. Effect of extrusion screw speed on biocomposite thermomechanical properties. *International Journal of Sustainable Engineering*, 5(1):38–46, 2012.

G. Chinga-Carrasco, O. Solheim, M. Lenes, and Å. Larsen. A method for estimating the fibre length in fibre-pla composites. *Journal of microscopy*, 250(1):15–20, 2013.

D. Clark, D. Adams, A. Dilks, J. Peeling, and H. Thomas. Some aspects of shake-up phenomena in some simple polymer systems. *Journal of Electron Spectroscopy and Related Phenomena*, 8(1):51–60, 1976. ISSN 0368-2048.

G. Collins. A surface tension method for measuring the perimeters of fibres and the contact angle of liquids against fibres. *Journal of the Textile Institute Transactions*, 38(2):T73–T77, 1947.

N. Cordeiro, C. Gouveia, and M. J. John. Investigation of surface properties of physico-chemically modified natural fibres using inverse gas chromatography. *Industrial Crops & Products*, 33(1):108–115, 2011a. ISSN 0926-6690.

N. Cordeiro, C. Gouveia, A. Moraes, and S. Amico. Natural fibers characterization by inverse gas chromatography. *Carbohydrate Polymers*, 84(1):110 – 117, 2011b. ISSN 0144-8617.

N. Cordeiro, M. Ornelas, A. Ashori, S. Sheshmani, and H. Norouzi. Investigation on the surface properties of chemically modified natural fibers using inverse gas chromatography. *Carbohydrate Polymers*, 87(4):2367–2375, 2012. ISSN 0144-8617.

D. J. Cosgrove. Assembly and enlargement of the primary cell wall in plants. *Annual review of cell and developmental biology*, 13(1):171–201, 1997.

H. Cox. The elasticity and strength of paper and other fibrous materials. *British journal of applied physics*, 3(3):72, 1952.

E. Csiszár, E. Fekete, A. Tóth, . Bandi, B. Koczka, and I. Sajó. Effect of particle size on the surface properties and morphology of ground flax. *Carbohydrate Polymers*, 94(2):927–933, 2013.

C. C. Curtis N. *Chemicals and Soils*. 1998.

M. Danks. Pelletising natural fibres for optimisation of a biocomposite extrusion process. Bachelor of Engineering thesis, The University of Queensland, 2014.

N. N. Das, S. C. Das, A. K. Sarkar, and A. K. Mukherjee. Lignin-xylan ester linkage in mesta fiber (hibiscus cannabinus). *Carbohydrate research*, 129:197–207, 1984.

A. Day, K. Ruel, G. Neutelings, D. Crônier, H. David, S. Hawkins, and B. Chabbert. Lignification in the flax stem: evidence for an unusual lignin in bast fibers. *Planta*, 222(2):234–245, 2005.

N. Defoirdt, S. Biswas, L. De Vriese, J. Van Acker, Q. Ahsan, L. Gorbatikh, A. Van Vuure, I. Verpoest, et al. Assessment of the tensile properties of coir, bamboo and jute fibre. *Composites Part A: applied science and manufacturing*, 41(5):588–595, 2010.

C. Della Volpe and S. Siboni. Some reflections on acid–base solid surface free energy theories. *Journal of Colloid and Interface Science*, 195(1):121–136, 1997.

D. B. Dittenber and H. V. GangaRao. Critical review of recent publications on use of natural composites in infrastructure. *Composites Part A: Applied Science and Manufacturing*, 43(8): 1419–1429, 2012.

G. Dolan. Bio-tribology of plant cell walls. Confirmation Report, School of Chemical Engineering, UQ, March 2014.

A. M. Donald. The use of environmental scanning electron microscopy for imaging wet and insulating materials. *Nature materials*, 2(8):511–516, 2003.

S. Dong, M. Brendle, and J. Donnet. Study of solid surface polarity by inverse gas chromatography at infinite dilution. *Chromatographia*, 28(9-10):469–472, 1989.

J. Donnet, S. Park, and H. Balard. Evaluation of specific interactions of solid surfaces by inverse gas chromatography. *Chromatographia*, 31(9-10):434–440, 1991.

J.-B. Donnet, R.-Y. Qin, and M.-J. Wang. A new approach for estimating the molecular areas of linear hydrocarbons and their derivatives. *Journal of colloid and interface science*, 153(2): 572–577, 1992.

G. Dorris and D. Gray. surface analysis of paper and wood fibres by esca. ii. surface composition of mechanical pulps. *Cellulose chemistry and technology*, 1978a.

G. M. Dorris and D. G. Gray. The surface analysis of paper and wood fibers by esca-electron spectroscopy for chemical analysis-i. applications to cellulose and lignin. *Cellulose Chemistry and Technology*, 12:9–23, 1978b.

G. M. Dorris and D. G. Gray. Adsorption, spreading pressure, and london force interactions of hydrocarbons on cellulose and wood fiber surfaces. *Journal of Colloid and Interface Science*, 71(1):93–106, 1979. ISSN 0021-9797.

G. M. Dorris and D. G. Gray. Adsorption of n-alkanes at zero surface coverage on cellulose paper and wood fibers. *Journal of Colloid and Interface Science*, 77(2):353–362, 1980.

J. Dove, G. Buckton, and C. Doherty. A comparison of two contact angle measurement methods and inverse gas chromatography to assess the surface energies of theophylline and caffeine. *International journal of pharmaceutics*, 138(2):199–206, 1996.

D. Dupeyre, M. Vignon, et al. Fibres from semi-retted hemp bundles by steam explosion treatment. *Biomass and Bioenergy*, 14(3):251–260, 1998.

A. Duval, A. Bourmaud, L. Augier, and C. Baley. Influence of the sampling area of the stem on the mechanical properties of hemp fibers. *Materials letters*, 65(4):797–800, 2011.

A. M. Edeerozey, H. M. Akil, A. Azhar, and M. Z. Ariffin. Chemical modification of kenaf fibers. *Materials Letters*, 61(10):2023–2025, 2007.

A. Espert, F. Vilaplana, and S. Karlsson. Comparison of water absorption in natural cellulosic fibres from wood and one-year crops in polypropylene composites and its influence on their mechanical properties. *Composites Part A: Applied science and manufacturing*, 35(11):1267–1276, 2004.

A. Etaati, S. Pather, Z. Fang, and H. Wang. The study of fibre/matrix bond strength in short hemp polypropylene composites from dynamic mechanical analysis. *Composites Part B: Engineering*, 62:19–28, 2014.

A. V. J. C. Eva Díaz, Salvador Ordóñez. Adsorption characterisation of different volatile organic compounds over alumina, zeolites and activated carbon using inverse gas chromatography. *Journal of chromatography A*, 1049(1):139–146, 2004.

O. Faruk, A. K. Bledzki, H.-P. Fink, and M. Sain. Biocomposites reinforced with natural fibers: 2000–2010. *Progress in Polymer Science*, 37(11):1552–1596, 2012.

J. M. Felix and P. Gatenholm. The nature of adhesion in composites of modified cellulose fibers and polypropylene. *Journal of Applied Polymer Science*, 42(3):609–620, 1991.

M. E. A. Fidelis, T. V. C. Pereira, O. d. F. M. Gomes, F. de Andrade Silva, and R. D. Toledo Filho. The effect of fiber morphology on the tensile strength of natural fibers. *Journal of Materials Research and Technology*, 2(2):149–157, 2013.

F. M. Fowkes. Attractive forces at interfaces. *Industrial & Engineering Chemistry*, 56(12): 40–52, 1964.

P. M. Froass, A. J. Ragauskas, and J. E. Jiang. Nmr studies part 3: Analysis of lignins from modern kraft pulping technologies. *Holzforschung-International Journal of the Biology, Chemistry, Physics and Technology of Wood*, 52(4):385–390, 1998.

J. Fromm, B. Rockel, S. Lautner, E. Windeisen, and G. Wanner. Lignin distribution in wood cell walls determined by tem and backscattered sem techniques. *Journal of structural biology*, 143(1):77–84, 2003.

S.-Y. Fu, B. Lauke, E. Mäder, C.-Y. Yue, and X. Hu. Tensile properties of short-glass-fiber-and short-carbon-fiber-reinforced polypropylene composites. *Composites Part A: Applied Science and Manufacturing*, 31(10):1117–1125, 2000.

J. A. F. Gamelas. The surface properties of cellulose and lignocellulosic materials assessed by inverse gas chromatography: a review. *Cellulose*, 20(6):2675–2693, 2013. ISSN 0969-0239.

G. Gamon, P. Evon, and L. Rigal. Twin-screw extrusion impact on natural fibre morphology and material properties in poly (lactic acid) based biocomposites. *Industrial Crops and Products*, 46:173–185, 2013.

J. Gassan and A. K. Bledzki. Alkali treatment of jute fibers: Relationship between structure and mechanical properties. *Journal of Applied Polymer Science*, 71(4):623–629, 1999a. ISSN 1097-4628.

J. Gassan and A. K. Bledzki. Possibilities for improving the mechanical properties of jute/epoxy composites by alkali treatment of fibres. *Composites Science and Technology*, 59(9):1303–1309, 1999b.

F. Gellerstedt and P. Gatenholm. Surface properties of lignocellulosic fibers bearing carboxylic groups. *Cellulose*, 6(2):103–121, 1999. ISSN 0969-0239.

J. George, M. Sreekala, and S. Thomas. A review on interface modification and characterization of natural fiber reinforced plastic composites. *Polymer Engineering & Science*, 41(9):1471–1485, 2001.

H. F. Giles Jr, E. M. Mount III, and J. R. Wagner Jr. *Extrusion: the definitive processing guide and handbook*. William Andrew, 2004.

K. Goda, M. Sreekala, A. Gomes, T. Kaji, and J. Ohgi. Improvement of plant based natural fibers for toughening green composites-effect of load application during mercerization of ramie fibers. *Composites Part A: Applied Science and Manufacturing*, 37(12):2213 – 2220, 2006. ISSN 1359-835X.

J. Goldstein, D. E. Newbury, P. Echlin, D. C. Joy, A. D. Romig Jr, C. E. Lyman, C. Fiori, and E. Lifshin. *Scanning electron microscopy and X-ray microanalysis: a text for biologists, materials scientists, and geologists*. Springer Science & Business Media, 2012.

T. Gorshkova, V. Salnikov, N. Pogodina, S. Chemikosova, E. Yablokova, A. Ulanov, M. Ageeva, J. Van Dam, and V. Lozovaya. Composition and distribution of cell wall phenolic compounds in flax (linum usitatissimum l.) stem tissues. *Annals of Botany*, 85(4):477–486, 2000.

A. H. Grigoriou and G. A. Ntalos. The potential use of ricinus communis l.(castor) stalks as a lignocellulosic resource for particleboards. *Industrial crops and products*, 13(3):209–218, 2001.

G. Guhados, W. Wan, and J. L. Hutter. Measurement of the elastic modulus of single bacterial cellulose fibers using atomic force microscopy. *Langmuir*, 21(14):6642–6646, 2005.

D. Gulati and M. Sain. Surface characteristics of untreated and modified hemp fibers. *Polymer Engineering & Science*, 46(3):269–273, 2006.

J. Gustafsson, L. Ciovica, and J. Peltonen. The ultrastructure of spruce kraft pulps studied by atomic force microscopy (afm) and x-ray photoelectron spectroscopy (xps). *Polymer*, 44(3): 661–670, 2003. ISSN 0032-3861.

A. Gutiérrez Suárez, G. Marques, J. Rencoret, and J. C. d. Río Andrade. Evaluation of the chemical composition of different non-woody plant fibers used for pulp and paper manufacturing. *The Open Agriculture Journal*, 101:93–101, 2010.

T. Hänninen, A. Thygesen, S. Mehmood, B. Madsen, and M. Hughes. Mechanical processing of bast fibres: The occurrence of damage and its effect on fibre structure. *Industrial Crops and Products*, 39:7–11, 2012.

J. He, Y. Tang, and S. Wang. Differences in morphological characteristics of bamboo fibres and other natural cellulose fibres: Studies on x-ray diffraction, solid state13c-cp/mas nmr, and second derivative ftir spectroscopy data. *Iranian Polymer Journal*, 16(12):807, 2007.

J. Y. Y. Heng, D. F. Pearse, F. Thielmann, T. Lampke, and A. Bismarck. Methods to determine surface energies of natural fibres: A review. *Composite Interfaces*, 14(7-9):581–604, 2007.

P. Herrera-Franco and A. Valadez-Gonzalez. A study of the mechanical properties of short natural-fiber reinforced composites. *Composites Part B: Engineering*, 36(8):597–608, 2005.

J. Holbery and D. Houston. Natural-fiber-reinforced polymer composites in automotive applications. *JOM*, 58(11):80–86, 2006. ISSN 1047-4838.

M. Huda, L. Drzal, D. Ray, A. Mohanty, and M. Misra. Natural-fibre composites in the automotive sector. *Properties and performance of natural-fibre composites*, pages 256–261, 2008.

M. Iguchi, S. Yamanaka, and A. Budhiono. Bacterial cellulose - a masterpiece of nature's arts. *Journal of Materials Science*, 35(2):261–270, 2000.

P. N. Jacob and J. C. Berg. Acid-base surface energy characterization of microcrystalline cellulose and two wood pulp fiber types using inverse gas chromatography. *Langmuir*, 10(9): 3086–3093, 1994.

L.-S. Johansson. Monitoring fibre surfaces with xps in papermaking processes. *Microchimica Acta*, 138(3-4):217–223, 2002.

L.-S. Johansson and J. Campbell. Reproducible xps on biopolymers: cellulose studies. *Surface and interface analysis*, 36(8):1018–1022, 2004.

L.-S. Johansson, J. Campbell, K. Koljonen, and P. Stenius. Evaluation of surface lignin on cellulose fibers with xps. *Applied Surface Science*, 144:92–95, 1999.

L.-S. Johansson, J. Campbell, K. Koljonen, M. Kleen, and J. Buchert. On surface distributions in natural cellulosic fibres. *Surface and interface analysis*, 36(8):706–710, 2004. ISSN 1096-9918.

M. J. John and R. D. Anandjiwala. Recent developments in chemical modification and characterization of natural fiber-reinforced composites. *Polymer composites*, 29(2):187, 2008.

D. C. Joy and C. S. Joy. Study of the dependence of e2 energies on sample chemistry. *Microscopy and Microanalysis*, 4(05):475–480, 1998.

D. P. Kamdem, H. Jiang, W. Cui, J. Freed, and L. M. Matuana. Properties of wood plastic composites made of recycled hdpe and wood flour from cca-treated wood removed from service. *Composites Part A: Applied Science and Manufacturing*, 35(3):347–355, 2004.

R. Karnani, M. Krishnan, and R. Narayan. Biofiber-reinforced polypropylene composites. *Polymer Engineering & Science*, 37(2):476–483, 1997.

M. Karus and M. Kaup. Natural fibres in the european automotive industry. *Journal of Industrial Hemp*, 7(1):119–131, 2002.

T. Keener, R. Stuart, and T. Brown. Maleated coupling agents for natural fibre composites. *Composites part A: applied science and manufacturing*, 35(3):357–362, 2004.

A. Keller. Compounding and mechanical properties of biodegradable hemp fibre composites. *Composites Science and Technology*, 63(9):1307–1316, 2003.

A. Kelly and a. W. Tyson. Tensile properties of fibre-reinforced metals: copper/tungsten and copper/molybdenum. *Journal of the Mechanics and Physics of Solids*, 13(6):329–350, 1965.

H. A. Khalil, M. Tehrani, Y. Davoudpour, A. H. Bhat, M. Jawaid, and A. Hassan. Natural fiber reinforced poly (vinyl chloride) composites: A review. *Journal of Reinforced Plastics and Composites*, 32(5):330–356, 2013.

K. Koljonen, M. Österberg, L.-S. Johansson, and P. Stenius. Surface chemistry and morphology of different mechanical pulps determined by esca and afm. *Colloids and Surfaces A: Physicochemical and Engineering Aspects*, 228(1):143–158, 2003.

A. Kondor, D. Williams, and D. Burnett. Determination of acid-base component of the surface energy by inverse gas chromatography. iGC SEA Application Note 227, Surface Measurement Systems, 2014.

L. Kroon-Batenburg and J. Kroon. The crystal and molecular structures of cellulose i and ii. *Glycoconjugate journal*, 14(5):677–690, 1997.

J. Laine, P. Stenius, G. Carlsson, and G. Ström. Surface characterization of unbleached kraft pulps by means of esca. *Cellulose*, 1(2):145–160, 1994. ISSN 0969-0239.

H. Lau, S. Bhattacharya, and G. Field. Melt strength of polypropylene: Its relevance to thermoforming. *Polymer Engineering and Science*, 38(11):1915, 1998.

A. Le Duigou, A. Bourmaud, E. Balnois, P. Davies, and C. Baley. Improving the interfacial properties between flax fibres and plla by a water fibre treatment and drying cycle. *Industrial Crops and Products*, 39:31–39, 2012.

M. Le Troëdec, A. Rachini, C. Peyratout, S. Rossignol, E. Max, O. Kaftan, A. Fery, and A. Smith. Influence of chemical treatments on adhesion properties of hemp fibres. *Journal of colloid and interface science*, 356(1):303–310, 2011.

H. L. Lee and P. Luner. Analysis of the adsorption of alkanes on high surface area cellulose by inverse gas chromatography. *Journal of Wood Chemistry and Technology*, 13(1):127–144, 1993. ISSN 0277-3813.

A. Lefeuvre, A. L. Duigou, A. Bourmaud, A. Kervoelen, C. Morvan, and C. Baley. Analysis of the role of the main constitutive polysaccharides in the flax fibre mechanical behaviour. *Industrial Crops and Products*, 76:1039 – 1048, 2015. ISSN 0926-6690.

A. Legras, R. W. Truss, C. Chaleat, and M. T. Heitzmann. A practical toolbox to overcome the multiple challenges of biocomposites extrusion. In *Composites Australia and CRC-ACS Conference 2015*, a.

A. Legras, R. W. Truss, S. Rao, D. Bhattacharyya, N. Soatthiyanon, A. Crosky, and M. T. Heitzmann. Optimisation of the twin-screw compounding process for short fibre biocomposites. In *Composites Australia and CRC-ACS Conference 2014*, b.

Y. Lei, Q. Wu, F. Yao, and Y. Xu. Preparation and properties of recycled hdpe/natural fiber composites. *Composites Part A: applied science and manufacturing*, 38(7):1664–1674, 2007.

X. Li, L. G. Tabil, and S. Panigrahi. Chemical treatments of natural fiber for use in natural fiber-reinforced composites: a review. *Journal of Polymers and the Environment*, 15(1): 25–33, 2007.

J. Liu. High-resolution and low-voltage fe-sem imaging and microanalysis in materials characterization. *Materials characterization*, 44(4):353–363, 2000.

W. Liu, A. K. Mohanty, P. Askeland, L. T. Drzal, and M. Misra. Influence of fiber surface treatment on properties of indian grass fiber reinforced soy protein based biocomposites. *Polymer*, 45(22):7589–7596, 2004.

H. Livingston. The cross-sectional areas of molecules adsorbed on solid surfaces. *Journal of colloid science*, 4(5):447–458, 1949.

J. Lu, P. Askeland, and L. T. Drzal. Surface modification of microfibrillated cellulose for epoxy composite applications. *Polymer*, 49(5):1285–1296, 2008.

B. Mano, J. Araújo, M. Spinacé, and M.-A. De Paoli. Polyolefin composites with curaua fibres: effect of the processing conditions on mechanical properties, morphology and fibres dimensions. *Composites Science and Technology*, 70(1):29–35, 2010.

S. D. Mansfield, H. Kim, F. Lu, and J. Ralph. Whole plant cell wall characterization using solution-state 2d nmr. *Nature protocols*, 7(9):1579–1589, 2012.

G. Marsh. Next step for automotive materials. *Materials Today*, 6(4):36 – 43, 2003. ISSN 1369-7021.

Á. T. Martínez, J. Rencoret, G. Marques, A. Gutiérrez, D. Ibarra, J. Jiménez-Barbero, and C. José. Monolignol acylation and lignin structure in some nonwoody plants: a 2d nmr study. *Phytochemistry*, 69(16):2831–2843, 2008.

M. Martins, L. Forato, L. Mattoso, and L. Colnago. A solid state 13 c high resolution nmr study of raw and chemically treated sisal fibers. *Carbohydrate polymers*, 64(1):127–133, 2006.

N. McIntyre, S. Sunder, D. Shoesmith, and F. Stanchell. Chemical information from xps—applications to the analysis of electrode surfaces. *Journal of Vacuum Science & Technology*, 18(3):714–721, 1981.

V. Mediavilla, M. Leupin, and A. Keller. Influence of the growth stage of industrial hemp on the yield formation in relation to certain fibre quality traits. *Industrial Crops and Products*, 13(1):49–56, 2001.

A. Miettinen, C. L. L. Hendriks, G. Chinga-Carrasco, E. K. Gamstedt, and M. Kataja. A non-destructive x-ray microtomography approach for measuring fibre length in short-fibre composites. *Composites Science and Technology*, 72(15):1901–1908, 2012.

D. Mikkelsen and M. Gidley. Formation of cellulose-based composites with hemicelluloses and pectins using gluconacetobacter fermentation. In Z. A. Popper, editor, *The Plant Cell Wall*, volume 715 of *Methods in Molecular Biology*, pages 197–208. Humana Press, 2011.

R. H. Mills. *Development of a Ligno-Cellulosic Polymeric and Reinforced Sheet Molding Compound (SMC)*. PhD thesis, The University of Maine, 2009.

R. H. Mills, D. J. Gardner, and R. Wimmer. Inverse gas chromatography for determining the dispersive surface free energy and acid–base interactions of sheet molding compound—part ii 14 ligno-cellulosic fiber types for possible composite reinforcement. *Journal of applied polymer science*, 110(6):3880–3888, 2008.

S. Mohammadi-Jam and K. E. Waters. Inverse gas chromatography applications: A review. *Advances in Colloid and Interface Science*, 212(0):21–44, 2014. ISSN 0001-8686.

A. Mohanty, M. Misra, and L. Drzal. Surface modifications of natural fibers and performance of the resulting biocomposites: an overview. *Composite Interfaces*, 8(5):313–343, 2001.

A. K. Mohanty, M. Misra, and L. T. Drzal. *Natural fibers, biopolymers, and biocomposites*. CRC Press, 2005.

S. Mohanty, S. Nayak, S. Verma, and S. Tripathy. Effect of mapp as a coupling agent on the performance of jute–pp composites. *Journal of reinforced plastics and composites*, 23(6): 625–637, 2004.

S. Mohanty, S. K. Verma, and S. K. Nayak. Dynamic mechanical and thermal properties of mape treated jute/hdpe composites. *Composites Science and Technology*, 66(3):538–547, 2006.

J. I. Morán, V. A. Alvarez, V. P. Cyras, and A. Vázquez. Extraction of cellulose and preparation of nanocellulose from sisal fibers. *Cellulose*, 15(1):149–159, 2008.

D. J. Morgan. X-ray photoelectron spectroscopy (xps): An introduction. *Cardiff Catalysis Institue*, 2014.

M. J. Morrison and A. G. Andre. Processing apparatus and methods, Jan. 14 2005. US Patent App. 10/586,194.

C. Morvan, C. Andème-Onzighi, R. Girault, D. S. Himmelsbach, A. Driouich, and D. E. Akin. Building flax fibres: more than one brick in the walls. *Plant physiology and biochemistry*, 41 (11):935–944, 2003.

A. Mukherjee, P. K. Ganguly, and D. Sur. Structural mechanics of jute: The effects of hemicellulose or lignin removal. *The Journal of The Textile Institute*, 84(3):348–353, 1993.

P. Mukherjee and K. Satyanarayana. Structure and properties of some vegetable fibres. *Journal of materials science*, 21(1):51–56, 1986.

P. Mukhopadhyay and H. Schreiber. Aspects of acid-base interactions and use of inverse gas chromatography. *Colloids and Surfaces A: Physicochemical and Engineering Aspects*, 100:47 – 71, 1995. ISSN 0927-7757.

R.-J. Müller. Biodegradability of polymers: Regulations and methods for testing. *Biopolymers Online*, 2005.

J. Müssig and K. Haag. Naturfaser pellet produktion- vorstellung der teschnischen analyse. Abschlussbericht, Hochschule Bremen, Juni 2012.

M. L. Nelson and R. T. O'Connor. Relation of certain infrared bands to cellulose crystallinity and crystal lattice type. part ii. a new infrared ratio for estimation of crystallinity in celluloses i and ii. *Journal of Applied Polymer Science*, 8(3):1325–1341, 1964a.

M. L. Nelson and R. T. O'Connor. Relation of certain infrared bands to cellulose crystallinity and crystal latticed type. part i. spectra of lattice types i, ii, iii and of amorphous cellulose. *Journal of applied polymer science*, 8(3):1311–1324, 1964b.

C. P. Neto, A. Seca, D. Fradinho, M. Coimbra, F. Domingues, D. Evtuguin, A. Silvestre, and J. Cavaleiro. Chemical composition and structural features of the macromolecular components of hibiscus cannabinus grown in portugal. *Industrial Crops and Products*, 5(3):189–196, 1996.

R. Newman and J. Hemmingson. Determination of the degree of cellulose crystallinity in wood by carbon-13 nuclear magnetic resonance spectroscopy. *Holzforschung-International Journal of the Biology, Chemistry, Physics and Technology of Wood*, 44(5):351–356, 1990.

S. Y. Oh, D. I. Yoo, Y. Shin, H. C. Kim, H. Y. Kim, Y. S. Chung, W. H. Park, and J. H. Youk. Crystalline structure analysis of cellulose treated with sodium hydroxide and carbon dioxide by means of x-ray diffraction and ftir spectroscopy. *Carbohydrate Research*, 340(15): 2376–2391, 2005a.

S. Y. Oh, D. I. Yoo, Y. Shin, and G. Seo. Ftir analysis of cellulose treated with sodium hydroxide and carbon dioxide. *Carbohydrate Research*, 340(3):417–428, 2005b.

K. Oksman, M. Skrifvars, and J. F. Selin. Natural fibres as reinforcement in polylactic acid (pla) composites. *Composites Science and Technology*, 63(9):1317–1324, 2003. ISSN 0266-3538.

OpTest. *HiRes Fiber Quality Analyzer Brochure*, 2010.

M. Östenson, H. Järund, G. Toriz, and P. Gatenholm. Determination of surface functional groups in lignocellulosic materials by chemical derivatization and esca analysis. *Cellulose*, 13 (2):157–170, 2006. ISSN 0969-0239.

A. C. O'Sullivan. Cellulose: the structure slowly unravels. *Cellulose*, 4(3):173–207, 1997. ISSN 0969-0239.

U. Panzer and H. P. Schreiber. On the evaluation of surface interactions by inverse gas chromatography. *Macromolecules*, 25(14):3633–3637, 1992.

E. Papirer, E. Brendle, F. Ozil, and H. Balard. Comparison of the surface properties of graphite, carbon black and fullerene samples, measured by inverse gas chromatography. *Carbon*, 37 (8):1265–1274, 1999.

M. T. Paridah, A. B. Basher, S. SaifulAzry, and Z. Ahmed. Retting process of some bast plant fibres and its effect on fibre quality: A review. *BioResources*, 6(4):5260–5281, 2011.

S. Park, J. O. Baker, M. E. Himmel, P. A. Parilla, and D. K. Johnson. Research cellulose crystallinity index: measurement techniques and their impact on interpreting cellulase performance. *Biotechnol Biofuels*, 3(10), 2010.

C. Pavithran, P. Mukherjee, M. Brahmakumar, and A. Damodaran. Impact properties of natural fibre composites. *Journal of Materials Science Letters*, 6(8):882–884, 1987. ISSN 0261-8028.

R. H. Perry, D. W. Green, and J. O. Maloney. *Perry s chemical engineers handbook*. McGraw Hill, New York, 1997.

K. Pickering. *Properties and performance of natural-fibre composites*. Elsevier, 2008.

A. Pietak, S. Korte, E. Tan, A. Downard, and M. P. Staiger. Atomic force microscopy characterization of the surface wettability of natural fibres. *Applied Surface Science*, 253(7): 3627–3635, 2007.

M. Pommet, J. Juntaro, J. Y. Heng, A. Mantalaris, A. F. Lee, K. Wilson, G. Kalinka, M. S. Shaffer, and A. Bismarck. Surface modification of natural fibers using bacteria: depositing bacterial cellulose onto natural fibers to create hierarchical fiber reinforced nanocomposites. *Biomacromolecules*, 9(6):1643–1651, 2008.

M. Preisner, W. Wojtasik, A. Kulma, M. Żuk, and J. Szopa. Flax fiber. *Kirk-Othmer Encyclopedia of Chemical Technology*, 2014.

D. Puglia, A. Terenzi, S. E. Barbosa, and J. M. Kenny. Polypropylene-natural fibre composites. analysis of fibre structure modification during compounding and its influence on the final properties. *Composite Interfaces*, 15(2-3):111–129, 2008.

M. R. Rahman, M. Hasan, M. M. Huque, and M. N. Islam. Physico-mechanical properties of jute fiber reinforced polypropylene composites. *Journal of Reinforced Plastics and Composites*, 29(3):445–455, 2010.

J. Ralph, R. D. Hatfield, F. Lu, J. H. Grabber, H. G. Jung, J. S. Han, and S. A. Ralph. Kenaf's amazing lignin. In *Proceedings of the 8th International Symposium on Wood and Pulping Chemistry, Helsinki. Finland*, volume 2, page 125, 1995.

E. C. Ramires and E. Frollini. Tannin–phenolic resins: synthesis, characterization, and application as matrix in biobased composites reinforced with sisal fibers. *Composites Part B: Engineering*, 43(7):2851–2860, 2012.

A. Rana, A. Mandal, and S. Bandyopadhyay. Short jute fiber reinforced polypropylene composites: effect of compatibiliser, impact modifier and fiber loading. *Composites Science and Technology*, 63(6):801–806, 2003.

S. Rao and D. Bhattacharyya. Pre-extrusion compounding and analysis. Technical report, CRC-ACS, TR13053, 2013.

R. Rasch, A. Stricher, and R. W. Truss. Energy filtered low voltage "in lens detector" sem and xps of natural fiber surfaces. *Journal of Applied Polymer Science*, 131(9), 2014.

B. D. Ratner and D. G. Castner. Electron spectroscopy for chemical analysis. *Surface Analysis-The Principal Techniques, 2nd Edition*, pages 47–112, 2009.

D. Ray, B. K. Sarkar, A. Rana, and N. R. Bose. The mechanical properties of vinylester resin matrix composites reinforced with alkali-treated jute fibres. *Composites Part A: applied science and manufacturing*, 32(1):119–127, 2001.

M. Z. Rong, M. Q. Zhang, Y. Liu, H. M. Yan, G. C. Yang, and H. M. Zeng. Interfacial interaction in sisal/epoxy composites and its influence on impact performance. *Polymer composites*, 23 (2):182–192, 2002.

A. J. Rosenberg. Rapid, precise measurements of krypton adsorption and the surface area of coarse particles. *Journal of the American Chemical Society*, 78(13):2929–2934, 1956.

W. Rudzinski and D. H. Everett. *Adsorption of gases on heterogeneous surfaces*. Academic Press, 2012.

C. Saint Flour and E. Papirer. Gas-solid chromatography: a quick method of estimating surface free energy variations induced by the treatment of short glass fibers. *Journal of Colloid and Interface Science*, 91(1):69–75, 1983.

T. Sakai, T. Sakamoto, J. Hallaert, and E. J. Vandamme. Pectin, pectinase and protopectinase: production, properties, and applications. *Advances in applied microbiology*, 39:213, 1993.

N. Sallih. Manufacturing and evaluation of kenaf/ polypropylene honeycombe cores. The University of Auckland, Unpublished thesis, 2015.

P. A. Santos, M. A. Spinacé, K. K. Fermoselli, and M.-A. De Paoli. Polyamide-6/vegetal fiber composite prepared by extrusion and injection molding. *Composites Part A: Applied Science and Manufacturing*, 38(12):2404–2411, 2007.

R. B. Santos, P. Hart, H. Jameel, and H.-m. Chang. Wood based lignin reactions important to the biorefinery and pulp and paper industries. *BioResources*, 8(1):1456–1477, 2013.

K. Satyanarayana, J. Guimarães, and F. Wypych. Studies on lignocellulosic fibers of brazil. part i: Source, production, morphology, properties and applications. *Composites Part A: Applied Science and Manufacturing*, 38(7):1694 – 1709, 2007. ISSN 1359-835X.

K. G. Satyanarayana, G. G. Arizaga, and F. Wypych. Biodegradable composites based on lignocellulosic fibers—an overview. *Progress in Polymer Science*, 34(9):982–1021, 2009.

J. Schultz, L. Lavielle, and C. Martin. The role of the interface in carbon fibre-epoxy composites. *The Journal of Adhesion*, 23(1):45–60, 1987.

A. M. Seca, J. A. Cavaleiro, F. M. Domingues, A. J. Silvestre, D. Evtuguin, and C. Pascoal Neto. Structural characterization of the bark and core lignins from kenaf (hibiscus cannabinus). *Journal of Agricultural and Food Chemistry*, 46(8):3100–3108, 1998.

D. Sedan, C. Pagnoux, T. Chotard, A. Smith, D. Lejolly, V. Gloaguen, and P. Krausz. Effect of calcium rich and alkaline solutions on the chemical behaviour of hemp fibres. *Journal of Materials Science*, 42(22):9336–9342, 2007.

L. Segal, J. Creely, A. Martin, and C. Conrad. An empirical method for estimating the degree of crystallinity of native cellulose using the x-ray diffractometer. *Textile Research Journal*, 29(10):786–794, 1959.

N. Sgriccia, M. Hawley, and M. Misra. Characterization of natural fiber surfaces and natural fiber composites. *Composites Part A: Applied Science and Manufacturing*, 39(10):1632–1637, 2008.

H. S. Sharma, T. W. Fraser, D. McCall, N. Shields, and G. Lyons. Fine structure of chemically modified flax fibre. *The Journal of The Textile Institute*, 86(4):539–548, 1995.

H. Shen, S. Nutt, and D. Hull. Direct observation and measurement of fiber architecture in short fiber-polymer composite foam through micro-ct imaging. *Composites Science and Technology*, 64(13):2113–2120, 2004.

B. Siaotong, L. Tabil, S. Panigrahi, and W. Crerar. Extrusion compounding of flax-fiber-reinforced polyethylene composites: Effects of fiber content and extrusion parameters. *Journal of Natural Fibers*, 7(4):289–306, 2010.

K. Sing. The use of nitrogen adsorption for the characterisation of porous materials. *Colloids and Surfaces A: Physicochemical and Engineering Aspects*, 187:3–9, 2001.

L. Sobczak, R. W. Lang, and A. Haider. Polypropylene composites with natural fibers and wood–general mechanical property profiles. *Composites Science and Technology*, 72(5):550–557, 2012.

N. Sombatsompop and M. Panapoy. Effect of screw rotating speed on polymer melt temperature profiles in twin screw extruder. *Journal of materials science*, 35(24):6131–6137, 2000.

M. Sreekala, M. Kumaran, S. Joseph, M. Jacob, and S. Thomas. Oil palm fibre reinforced phenol formaldehyde composites: influence of fibre surface modifications on the mechanical performance. *Applied Composite Materials*, 7(5-6):295–329, 2000.

P. Sriamornsak. Chemistry of pectin and its pharmaceutical uses: A review. *Silpakorn University International Journal*, 3(1-2):206–228, 2003.

S. Stock. X-ray microtomography of materials. *International Materials Reviews*, 44(4):141–164, 1999.

J. E. Stone and A. M. Scallan. Effect of component removal upon the porous structure of the cell wall of wood. *Journal of Polymer Science Part C: Polymer Symposia*, 11(1):13–25, 1965. ISSN 1935-3065.

A. Stricher. Natural fibres composites, chemical modification of fibres' surface to improve fibre/ matrix interactions. Technical report, The University of Queensland, 2012.

T. Stuart, Q. Liu, M. Hughes, R. McCall, H. Sharma, and A. Norton. Structural biocomposites from flax—part i: Effect of bio-technical fibre modification on composite properties. *Composites Part A: Applied Science and Manufacturing*, 37(3):393–404, 2006.

J. Summerscales, N. P. Dissanayake, A. S. Virk, and W. Hall. A review of bast fibres and their composites. part 1–fibres as reinforcements. *Composites Part A: Applied Science and Manufacturing*, 41(10):1329–1335, 2010.

Y. Tahery, N. Shukor, H. Abdul-Hamid, et al. Growth characteristics and biomass production of kenaf. *African Journal of Biotechnology*, 10(63):13756–13761, 2013.

F. Thielmann. Introduction into the characterisation of porous materials by inverse gas chromatography. *Journal of Chromatography A*, 1037:115–123, 2004. ISSN 0021-9673.

J. Thomason and M. Vlug. Influence of fibre length and concentration on the properties of glass fibre-reinforced polypropylene: 1. tensile and flexural modulus. *Composites Part A: Applied science and manufacturing*, 27(6):477–484, 1996.

A. Thumm and A. R. Dickson. The influence of fibre length and damage on the mechanical performance of polypropylene/wood pulp composites. *Composites Part A: Applied Science and Manufacturing*, 46:45–52, 2013.

M. M. Thwe and K. Liao. Durability of bamboo-glass fiber reinforced polymer matrix hybrid composites. *Composites Science and Technology*, 63(3):375–387, 2003.

R. W. Truss, B. Wood, and R. Rasch. Quantitative surface analysis of hemp fibers using xps, conventional and low voltage in-lens sem. *Journal of Applied Polymer Science*, 2015.

J. Trygg and P. Fardim. Enhancement of cellulose dissolution in water-based solvent via ethanol–hydrochloric acid pretreatment. *Cellulose*, 18(4):987–994, 2011.

V. Tserki, N. Zafeiropoulos, F. Simon, and C. Panayiotou. A study of the effect of acetylation and propionylation surface treatments on natural fibres. *Composites Part A: applied science and manufacturing*, 36(8):1110–1118, 2005.

M. A. Tshabalala. Determination of the acid-base characteristics of lignocellulosic surfaces by inverse gas chromatography. *Journal of applied polymer science*, 65(5):1013–1020, 1997.

W. T. Y. Tze, M. E. P. Walinder, and D. J. Gardner. Inverse gas chromatography for studying interaction of materials used for cellulose fiber/polymer composites. *Journal of Adhesion Science and Technology*, 20(8):743–743, 2006. ISSN 0169-4243.

S. Ugbolue. Structure/property relationships in textile fibres. *Textile Progress*, 20(4):1–43, 1990.

A. Valadez-Gonzalez, J. Cervantes-Uc, R. Olayo, and P. Herrera-Franco. Chemical modification of henequen fibers with an organosilane coupling agent. *Composites Part B: Engineering*, 30 (3):321–331, 1999.

C. Van Oss, R. Good, and M. Chaudhury. Additive and nonadditive surface tension components and the interpretation of contact angles. *Langmuir*, 4(4):884–891, 1988.

T. Villmow, B. Kretzschmar, and P. Pötschke. Influence of screw configuration, residence time, and specific mechanical energy in twin-screw extrusion of polycaprolactone/multi-walled carbon nanotube composites. *Composites Science and Technology*, 70(14):2045–2055, 2010.

A. S. Virk, W. Hall, and J. Summerscales. Multiple data set (mds) weak-link scaling analysis of jute fibres. *Composites Part A: Applied Science and Manufacturing*, 40(11):1764–1771, 2009.

A. S. Virk, W. Hall, and J. Summerscales. Failure strain as the key design criterion for fracture of natural fibre composites. *Composites Science and Technology*, 70(6):995–999, 2010.

P. Wambua, J. Ivens, and I. Verpoest. Natural fibres: can they replace glass in fibre reinforced plastics? *Composites Science and Technology*, 63(9):1259 – 1264, 2003. ISSN 0266-3538. Eco-Composites.

W. Wang, Q. Hua, Y. Sha, D. Wu, S. Zheng, and B. Liu. Surface properties of solid materials measured by modified inverse gas chromatography. *Talanta*, 112:69–72, 2013.

Y. Wang, F.-B. Chen, and K.-C. Wu. Twin-screw extrusion compounding of polypropylene/organoclay nanocomposites modified by maleated polypropylenes. *Journal of applied polymer science*, 93(1):100–112, 2004.

J. O. Warwicker and P. Hallam. 6-the effect of alkaline and acid swelling agents on the mechanical properties of cotton fibres. *The Journal of The Textile Institute*, 61(2):61–76, 1970.

D. Williams. Inverse gas chromatography. *Characterisation of Composite Materials. London, UK: Butterworth-Heinemann*, pages 80–104, 1994.

D. Williams. Particle engineering in pharmaceutical solids processing: surface energy considerations. *Current pharmaceutical design*, 21(19):2677–2694, 2015.

Y. Xie, C. A. Hill, Z. Xiao, H. Militz, and C. Mai. Silane coupling agents used for natural fiber/polymer composites: A review. *Composites Part A: Applied Science and Manufacturing*, 41(7):806–819, 2010.

Y. Xu, Q. Wu, Y. Lei, F. Yao, and Q. Zhang. Natural fiber reinforced poly(vinyl chloride) composites: Effect of fiber type and impact modifier. *Journal of Polymers and the Environment*, 16(4):250–257, 2008. ISSN 1566-2543.

H. Yang, R. Yan, H. Chen, D. H. Lee, and C. Zheng. Characteristics of hemicellulose, cellulose and lignin pyrolysis. *Fuel*, 86(12):1781–1788, 2007.

P. P. Ylä-Mäihäniemi, J. Y. Y. Heng, F. Thielmann, and D. R. Williams. Inverse gas chromatographic method for measuring the dispersive surface energy distribution for particulates. *Langmuir : the ACS journal of surfaces and colloids*, 24(17):9551–9557, 2008. ISSN 0743-7463.

N. Zafeiropoulos, D. Williams, C. Baillie, and F. Matthews. Engineering and characterisation of the interface in flax fibre/polypropylene composite materials. part i. development and investigation of surface treatments. *Composites part A: applied science and manufacturing*, 33(8):1083–1093, 2002.

N. E. Zafeiropoulos, P. E. Vickers, C. A. Baillie, and J. F. Watts. An experimental investigation of modified and unmodified flax fibres with xps, tof-sims and atr-ftir. *Journal of Materials Science*, 38(19):3903–3914, 2003. ISSN 0022-2461.

S. H. Zeronian, H. Kawabata, and K. W. Alger. Factors affecting the tensile properties of nonmercerized and mercerized cotton fibers. *Textile Research Journal*, 60(3):179–183, 1990.

Z.-X. Zhang, C. Gao, Z. X. Xin, and J. K. Kim. Effects of extruder parameters and silica on physico-mechanical and foaming properties of pp/wood-fiber composites. *Composites Part B: Engineering*, 43(4):2047–2057, 2012.

Y.-T. Zheng, D.-R. Cao, D.-S. Wang, and J.-J. Chen. Study on the interface modification of bagasse fibre and the mechanical properties of its composite with pvc. *Composites part A: applied science and manufacturing*, 38(1):20–25, 2007.

B. Ziegelaar. An investigation of the effects of extrusion parameters on the mechanical properties of natural fibre composites. Bachelor of Engineering thesis, The University of Queensland, 2013.

R. Zuluaga, J. L. Putaux, J. Cruz, J. Vélez, I. Mondragon, and P. Gañán. Cellulose microfibrils from banana rachis: Effect of alkaline treatments on structural and morphological features. *Carbohydrate Polymers*, 76(1):51–59, 2009.

Appendix A

Tensile properties of natural fibres: reference data

Source	Materials				Manufacture		Composite properties			
Author	Fibres	Matrix	Fibre treatment	Coupling agent	Fibre content (wt%)	Processing	Tensile strength (MPa)	E modulus (GPa)	Impact energy	
Bengtsson et al. 2007	Cellulose	PP	bleached sulfite cellulose fibres		40	Extrusion + compression moulding	33.3		256.2	J/m
					50		29.9		163.4	
					60		24.9		134.8	
				MAPP 3wt%	40		43.2		182	
					50		49.7		175	
					60		50.8		173.5	
			bleached kraft cellulose fibres	MAPP 3wt%	40		31.7		191.3	
					50		32.6		182.5	
					60		25.2		129.6	
					40		43.2		211	
					50		51.6		153.2	
					60		47.9		182.1	
					0		29.4			
Bledzki et al. 2005	Hardwood fibres Lignocel	PP			50	Extrusion + compression moulding	18	0.9		
						Two-roll mill + compression moulding	22	0.75		
						High speed mixer + compression moulding	15	0.8		
				MAPP 5wt%		Extrusion + compression moulding	25	1.2		
						Two-roll mill + compression moulding				
						High speed mixer + compression moulding	22	1		
Facca et al. 2006	Hemp	HDPE			0	Mixing + compression moulding		1		
					10			1.9		
					20			2.5		
					30			3		
					40			3.5		
					50			5		
					60			6.3		
	Hardwood flour A				10			1.5		
					20			1.6		
					30			2.1		
					40			2.4		
					50			2.8		
					60			3.9		
	Hardwood flour B				10			1.5		
					20			1.6		
					30			2.1		
					40			2.6		
					50			2.8		
					60			3.9		
Karnani et al. 1997	Kenaf	PP			0	Extrusion + injection moulding	28.4	1.2	42.1	J/m
					20		26.9	2.7	43.8	
					40		27.1	2.8	39.9	
					60		27.4	3.0	33.4	
				MAPP 2wt%	20		32.7	2.9	47.6	
					40		41.2	3.4	41.4	
					60		53.8	4.1	38.7	
				MAPP 5wt%	20		38.1	3.2	50.1	
					40		49.4	4.3	43.9	
					60		61.2	5.1	39.2	
			silane		20		42.5	3.3	54.6	

Figure A.1: Literature review on biocomposite properties (1)

Lei et al. 2007	Bagasse	RHDPE			0	Compression moulding	32.6		12.3	kJ/m²
					30		21.4		4.9	
				MAPE 1.5 wt%			30.6		5.7	
				MAPE 3.0 wt%			29.8		5.9	
				MAPE 4.5 wt%			27.2		5.82	
	Pine flour						23.5		6.1	
				MAPE 10.6 wt%			32.6		5.87	
				MAPE 1.2 wt%			32.6		6.74	
				MAPE 1.8 wt%			34.9		6.67	
				MAPE 2.4 wt%			36.1		6.09	
Li et al. 2009	Flax	LLDPE			0	Twin-screw extrusion	13.5			
			no treatment		10		13.8			
			alkali				13.9			
			silane				14			
		HDPE			0		19.5			
			no treatment		10		20.1			
			alkali				20.4			
			silane				20.5			
		LLDPE	no treatment		0		13.3			
					10		14.2			
					20		15.5			
					30		17			
Mano et al. 2010	Curaua	HDPE			20	Twin-screw extrusion + injection moulding	28 max value	2.4max		
							24 min value	2.0min		
		PP					31 max	3.4max		
							27min	3.1min		
Mohanty et al. 2006	Jute	HDPE			0	Mixing + compression moulding	20.82		32.57	J/m
					10		23.47		40.82	
					15		25.68		46.73	
					30		27.24		51.28	
					45		22		45.8	
				MAPE 0.5%	30		36.44		56.23	
				MAPE 1%			40.14		65.69	
				MAPE 2%			37.10		63.33	
Rana et al. 2003	Jute	PP		MAPP 1wt% + impact modifier	30	Mixing + injection moulding	27-39	3.4-3.8	182-187/ 34-58	un-notched /notched J/m
					40		31-43	4-5.5	183-194/ 38-64	
					50		28-44	4.5-6.3	185-210/ 41-82	
Wambua et al. 2003	Kenaf	PP			30	Compression moulding	26		13	kJ/m²
					40		30	6.8	14	
					50		35		23	
	Coir				40		10	1.3	22	
	Hemp						52	6.8	25	
	Jute						30	3.5	15	
	Sisal						30	5.3	27	

Figure A.2: Literature review on biocomposite properties (2)

Appendix A.

1. M. Bengtsson, M. Le Baillif, and K. Oksman, *Extrusion and mechanical properties of highly filled cellulose fibre–polypropylene composites*, Composites Part A: Applied Science and Manufacturing, 38 (8):1922-1931, 2007. ISSN 1359-835X.

2. A. K. Bledzki, M. Letman, A. Viksne and L. Rence, *A comparison of compounding processes and wood type for wood fibre-PP composites*, Composites Part A: Applied Science and Manufacturing, 36 (6):789-797, 2005. ISSN 1359-835X.

3. A. G. Facca, M. T. Kortschot and N. Yang, *Predicting the elastic modulus of natural fibre reinforced thermoplastics*, Composites Part A: Applied Science and Manufacturing, 37 (10):1660-1671, 2006. ISSN 1359-835X.

4. R. Karnani, M. Krishnan and R. Narayan, *Biofiber reinforced polypropylene composites*, Polymer Engineering & Science, 37 (2):476-483, 1997. ISSN 1548-2634.

5. Y. Lei, Q. Wu, F. Yao and Y. Xu, *Preparation and properties of recycled HDPE/natural fiber composites*, Composites Part A: applied science and manufacturing, 38 (7):1664-1674, 2007. ISSN 1359-835X.

6. X. Li, S. Panigrahi and L. G. Tabil, *A study on flax fiber-reinforced polyethylene biocomposites*, Applied Engineering in Agriculture, 25 (4):525-531, 2009. ISSN 0883-8542.

7. B. Mano, J. R. Araujo, M. A. S. Spinace and M. -A. De Paoli, *Polyolefin composites with curaua fibres: Effect of the processing conditions on mechanical properties, morphology and fibres dimensions*, Composites Science and Technology, 70 (1):29-35, 2010. ISSN 0266-3538.

8. S. Mohanty, S. K. Verma and S. K. Nayak, *Dynamic mechanical and thermal properties of MAPE treated jute/HDPE composites*, Composites Science and Technology, 66 (3-4):538-547, 2006. ISSN 0266-3538.

9. A. K. Rana, A. Mandal and S. Bandyopadhyay, *Short jute fiber reinforced polypropylene composites: effect of compatibiliser, impact modifier and fiber loading*,Composites Science and Technology, 63 (6):801-806, 2003. ISSN 0266-3538.

Appendix A.

10. P. Wambua, J. Ivens and I. Verpoest, *Natural fibres: can they replace glass in fibre reinforced plastics?*, Composites Science and Technology, 63 (9):1259-1264, 2003. ISSN 0266-3538.